A Study of the Coupling between Morphodynamics and Energy Metabolism in Macrophages

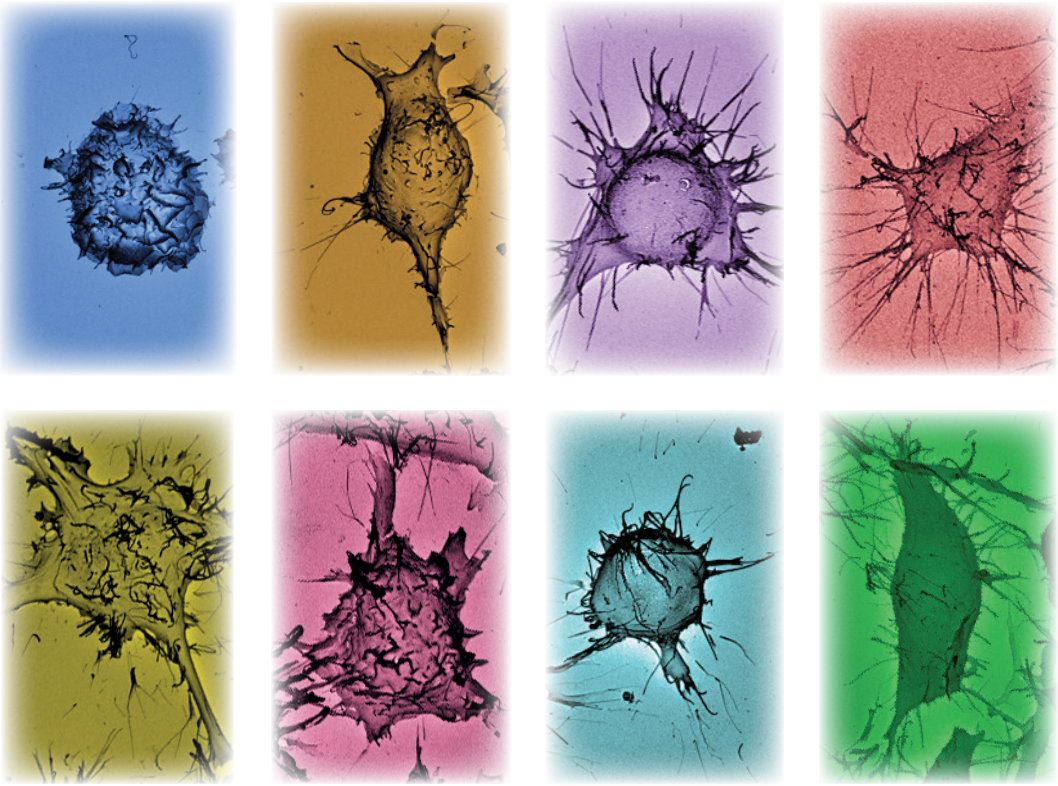

Gerda Venter - van Helden

A Study of the Coupling between Morphodynamics and Energy Metabolism in Macrophages

The research described in this thesis was performed at the Department of Cell Biology, Radboud Institute for Molecular Life Sciences, Radboud University Medical Centre, Nijmegen, The Netherlands

ISBN 978-94-6259-312-1

Cover: Top images from left to right: Maf-DKO cell, RAW 264.7 cell, RAW 264.7 cell with inhibited CK-B-activity, RAW 264.7 cell with inhibited OXPHOS
Bottom images from left to right: RAW 264.7 cell under low glucose conditions, RAW 264.7 cell with inhibited glycolysis, RAW 264.7 cell in the absence of glucose, RAW 264.7 cell with reduced NAD^+ synthesis

Cover design and layout: Evette Del Vecchio

Printed by Ipskamp Drukkers, Enschede, The Netherlands

A Study of the Coupling between Morphodynamics and Energy Metabolism in Macrophages

Proefschrift

ter verkrijgen van de graad van doctor
aan de Radboud Universiteit Nijmegen
op gezag van de rector magnificus prof. mr. S.C.J.J. Kortmann,
volgens besluit van het college van decanen
in het openbaar te verdedigen op 10 oktober 2014
om 12.30 uur precies
door

Gerda Venter – van Helden

geboren op 11 april 1982
te Krugersdorp, Zuid-Afrika

Promotor
Prof. dr. B. Wieringa

Copromotor
Dr. J. A. M. Fransen

Manuscriptcommissie
Prof. dr. G. Adema (voorzitter)
Dr. F. N. Van Leeuwen
Prof. dr. A. Heerschap

Aan hem die door de kracht die in ons werkt bij machte is oneindig veel meer te doen dan wij vragen of denken, aan hem komt de eer toe

(Ef. 3:20-21; Nieuwe Bijbelvertaling)

Table of contents

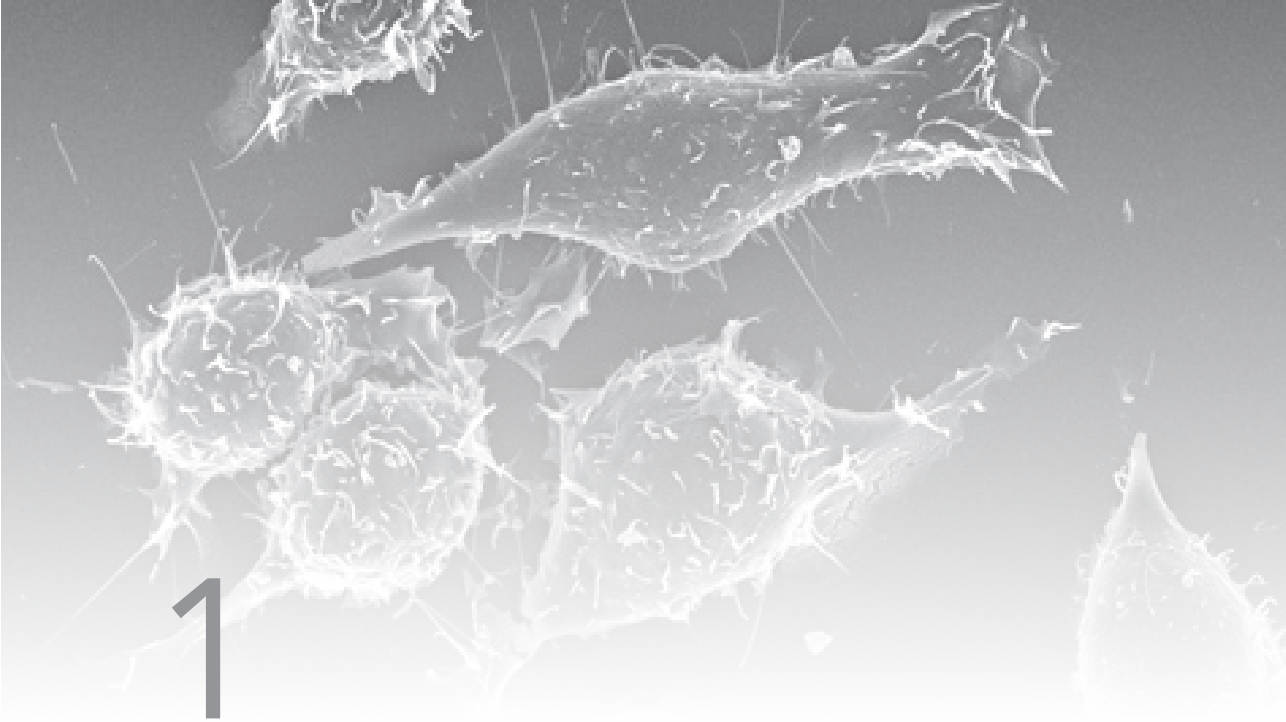

1

Introduction

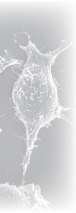

Introduction

The shape of animal cells is determined and maintained by the formation of an intracellular scaffold of protein polymers, called the cytoskeleton. Three different groups of polymers contribute to form the cytoskeleton: microtubules, intermediate filaments, and actin filaments. In this chapter (and throughout the thesis), only the latter will be discussed.

Rapid adjustment of cell morphology, mediated by dynamic reorganization of the cortical actin filament network, facilitates the functional activities of many cell types. Remodeling of the actin cytoskeleton also underlies some mechanisms of disease progression, e.g. cancer cell metastasis. The organization of the actin cytoskeleton in healthy or transformed cells is, thereby, influenced by numerous cues from the extracellular environment of the cell, e.g. interaction with the extracellular matrix, cytokines, growth factors, and nutrient availability. In addition, reorganization of the actin cytoskeleton strongly depends on efficient ATP-supply and perhaps other aspects of energy-redox metabolism.

This complex regulation is especially relevant for the migratory and adhesive capacity of macrophages, which live throughout tissues under dramatically different physiological conditions and are involved in immune surveillance, phagocytosis, wound healing, tissue homeostasis and, modulation of tumor cell growth and invasion. This work focuses on the link between remodeling of the actin cytoskeleton and metabolism, with special attention directed toward the morphodynamic behavior of these cells.

1. The actin cytoskeleton

1.1 Actin polymerization

Actin (together with myosin) was discovered during the 1940's in muscle but soon thereafter also in other cells [1]. The monomers of this 42 kDa protein are called globular (G-) actin and can spontaneously assemble to form double helical filamentous (F-) actin [1, 2]. Polymerization starts with unfavorable dimer formation (nucleation), followed by the formation of a stable trimer and rapid elongation of the actin filament [3]. Since the subunits all point in the same direction, actin filaments are polarized, containing a "pointed" end and a "barbed" end. Although association and dissociation of G-actin can occur on both ends, filament elongation mainly occurs at the barbed end while disassembly is mostly associated with the pointed end. Since nucleation is unfavorable, actin nucleation factors are required to overcome this first step. Three classes of actin nucleating factors are known: Arp2/3-complex, formins, and Spire proteins. Regulation of actin polymerization by Arp2/3 and

formins are the best studied and has been extensively reviewed by Pollard [4]. While formins produce unbranched filaments for actin bundles that are found in filopodia, the Arp2/3 complex forms branched filaments which push forward the leading edge of migrating cells. The Arp2/3 complex consists of seven polypeptides, ARPC1-5, Arp2, and Arp3, and has to be activated by nucleation promoting factors (NPFs) before it can give rise to new actin filaments. These NPFs include, amongst others, WASp, Scar/WAVE proteins, WIP, N-WASp, and cortactin proteins. In turn, NPFs are regulated by Rho-family GTPases (Figure 1 and paragraph 1.3 below) and contain three short functional segments, the verprolin (V-), connecting (C-), and acidic (A-) motifs, through which interaction with monomeric actin and the Arp2/3 complex is established. The V- and C-motifs interact simultaneously with actin, while the CA-

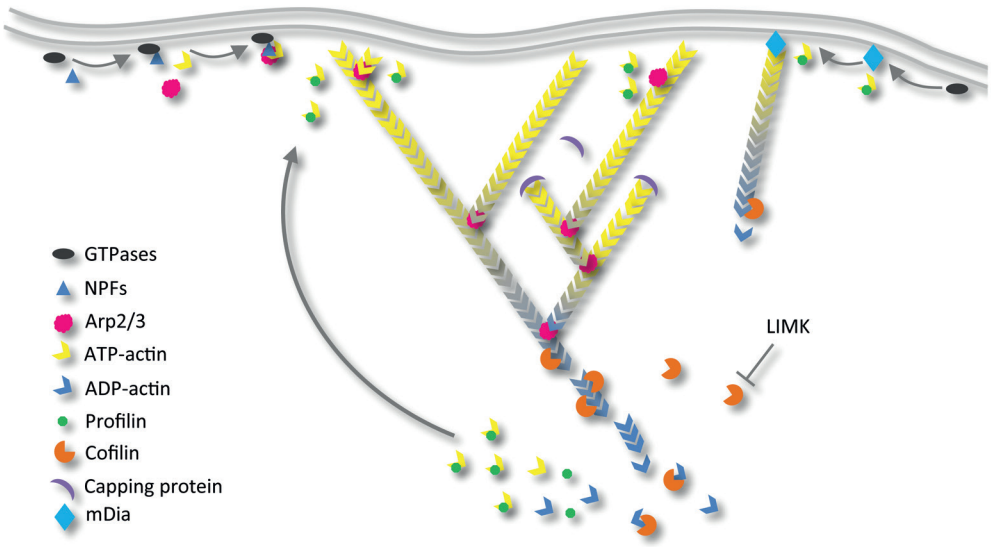

Figure 1. Regulation of actin polymerization. *Activation of receptors by extracellular stimuli induces signaling pathways that lead to the activation of Rho-family GTPases. NPFs (nucleation promoting factors) are activated by GTPases and facilitate the interaction between Arp2/3 and the first actin monomer of the daughter/branch filament. Elongation of the filament occurs at the barbed end of the filament, until elongation is terminated by binding of a capping protein. Filament growth at the barbed end pushes the membrane forward. Within the filament, ATP on the actin monomers is hydrolyzed (yellow subunits become grey) after which the inorganic phosphate is released (grey subunits become blue). ADF/Cofilin promotes the release of the phosphate from actin, severs actin filaments, and promotes the dissociation of ADP-actin from actin filaments. Phosphorylation of cofilin by LIMK inactivates cofilin and leads to stabilization of actin filaments. Profilin facilitates the exchange of ADP for ATP on the free actin monomers (blue subunits become yellow), so that they can be incorporated at the barbed end of a new actin filament. GTPases also activate formins like mDia which nucleate unbranched actin filaments. Formins remain attached to the barbed end while new actin monomers are incorporated during filament growth. (Adapted from Pollard and Cooper [1], Pollard [4], Pollard and Borisy [5]; see also references in the main text).*

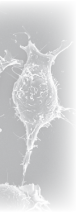

motif interacts with the Arp2/3 complex, thereby bringing together the first subunit of the daughter filament and the Arp2/3 complex. During filament elongation, the Arp2/3 complex stays associated at the pointed end while new subunits are being added to the barbed end until the elongation is terminated by binding of a capping protein. Of importance for this thesis study is that both Arp 2 and 3 contain nucleotide binding sites and occupation of this site by ATP increases the affinity of the Arp2/3 complex for the VCA-domains of NPFs. Hydrolysis of the ATP on Arp2 and 3 contributes to dissociation of the complex from the actin network and promotes network disassembly [6].

Formins (e.g. mDia1 and mDia2) are single-polypeptide, multi-domain proteins that form dimers via their formin homolog 2 (FH-2) domains. Their FH-1 domains contain a proline-rich sequence which associates with the actin monomer-binding protein, profilin, thereby enhancing the elongation efficiency of the actin filament. During elongation, the FH-2 domain stays associated with the barbed end of the filament (Figure 1) but how actin subunits are inserted between the formin and the barbed end is not exactly clear [2, 4]. Formins are regulated by autoinhibition through intramolecular interaction between the N-terminal Rho-GTPase binding domain (GBD) and the C-terminal Dia autoinhibitory domain (DAD) [7]. Rho-family GTPases relieve this autoinhibition by binding to the GBD and displacing the C-terminus of the formin molecule.

Actin polymerization further involves the subsequent binding, hydrolysis, and release of ATP-molecules on the actin subunits. Monomeric G-actin contains a nucleotide binding site which is almost exclusively associated with ATP. Shortly after incorporation into an actin filament, the ATP is hydrolyzed in two sequential steps: ATP-F-actin → ADP-P_i-F-actin → ADP-F-actin + P_i. The release of inorganic phosphate is the slowest step of the reaction, yielding ADP-P_i-F-actin, the major intermediate in actin polymerization [8]. Dissociation of the phosphate causes a conformational change in the actin subunits [9], rendering ADP-F-actin susceptible for disassembly by regulatory proteins (see 1.3 below). After the release of ADP-G-actin from the pointed end, ADP is substituted for ATP. The small actin monomer-binding protein profilin catalyzes this exchange and directs the incorporation of newly formed ATP-G-actin onto free barbed ends (Figure 1). This 'flow' of actin monomers from the barbed to the pointed end of the filament is known as treadmilling and signifies the universal mechanism that drives actin dynamics in eukaryotes [10].

1.2. Cell morphodynamics

Polymerized actin filaments provide internal mechanical support, tracks for movement of intracellular cargo, and force to drive cell movements [1]. Dynamic remodeling of the actin network forms the basis of the morphological adaptations that

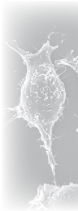

motile cells undergo in order to crawl, adhere, engulf particles, or probe their environment. These processes are collectively referred to as cell *morphodynamics* or *morphodynamic processes* through the remainder of the thesis.

Cell motility is a defining characteristic of animal cells and involved in a number of physiological and pathophysiological processes. These include immune cell migration to search and destroy pathogens, migration of cells during embryonic development, migration of cancer cells during metastasis and tissue invasion, nerve cell migration and formation of cellular processes to reach their targets, and tissue development and wound healing [1, 5]. The crawling motility of cells is signified by a cycle of four steps: (1) protrusion of the leading edge, (2) adhesion to the substratum, (3) retraction of the rear, and (4) de-adhesion [5]. The surface-attached, sheet-like membrane protrusion that is formed during the first step is called the lamellipodium and results from the assembly of a network of actin filaments underneath the cell membrane. These filaments are orientated with their barbed ends to the plasma membrane, pushing the membrane forward as actin monomers are added to the growing filament [2]. Although some evidence has been provided that long, unbranched, overlapping filaments are abundant in the lamellipodium [11, 12], dendritically branched actin filaments are believed to be the dominant structural component in these structures[2, 13].

The intracellular actin cytoskeleton interacts with the extracellular matrix (ECM) through four different adhesive structures: focal adhesions and complexes, invadopodia, and podosomes. Focal adhesions are large adhesion contacts that are anchored to the ECM and the end of tangentially oriented actin stress fibers inside the cell via trans-membrane receptors of the integrin family. Adhesion complexes are smaller and found at the tips of protrusions such as filopodia and lamellipodia [14]. Invadopodia are actin rich membrane protrusions comprising a core of actin filament bundles growing out perpendicular to the plasma membrane from a branched actin filament basis[15]. These structures are formed by invasive cancer cells and serve to degrade to ECM during migration. Many cells, especially osteoclasts and macrophages, form adhesion structures on their ventral[a] side that are called podosomes. These consist of bundles of actin filaments that form the core perpendicular to the substratum, surrounded by a multimeric protein complex of integrins and integrin-associated proteins (talin, vinculin, paxilin), and an actin cloud of radial actin filaments that lie parallel to the substratum. Podosomes are dynamic structures that assemble and disassemble and have a lifespan of 2-4 minutes [15].

Cells can form thin finger-like membrane protrusions, called filopodia, through which they probe the extracellular environment for adhesion sites or foreign matter [16, 17]. Filopodia contain parallel bundles of 10-30 actin filaments with their

[a] ventral – refers to the bottom (adhesive side) of a cell in a 2D environment

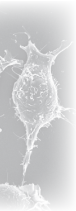

barbed ends oriented towards the plasma membrane, and are adhered to the substratum or another cell. Their assembly entails filament nucleation, sustained barbed end growth along the length of the protrusion, and filament bundling by fascin proteins [2]. Membrane ruffles are another type of sheet-like actin-dependent membrane protrusions and differ from lamellipodia in that they do not attach to the substratum at all. They either form at the leading edge of a motile cell from where they move backward (peripheral ruffles), or assemble on the dorsal[b] surface and constrict into a circular structure before they disappear again (circular dorsal ruffles), thereby affecting receptor internalization and possibly macropinocytosis [2], a process highly active in macrophages.

The structures described above are commonly present in many different cell types. One actin-rich cellular structure that is not so common and only found in certain cell types (particularly neutrophils and macrophages), is the phagocytic cup. Phagocytosis is the internalization of particles > 0.5 μm that may include inorganic material, cell debris, micro-organisms, and necrotic and apoptotic cells. Receptors on the cell surface recognize and bind these particles, triggering the activation of Rho GTPases and leading to actin polymerization underneath the plasma membrane[18, 19]. This results in the formation of membrane protrusions that surround and, eventually, enclose the particle for internalization. Although the mechanism of phagocytosis (see 2.3 below) has been studied intensively the morphology of the actin filaments forming the phagocytic cup is still not known [2].

A distinct feature of the phagocytic cup is that it is locally formed at a specific site on the cell periphery (where contact is established with an extracellular particle) and its formation is locally triggered and regulated. Another example of the significance of local formation and function of actin-rich protrusive structures is the small, actin rich protrusions formed by neuronal cells. These structures are called dendritic spines and are found on neuronal dendrites that form the postsynaptic part of most excitatory synapses and are major sites of information processing and storage in the brain. The size and morphology of the spines depend on local actin dynamics and determine synaptic activity [20].

Other structures that comprise actin and myosin filaments include the cytokinetic contractile ring in dividing cells which pinches the mother cell in two, actin cables for transport of organelles, and stress fibers (contractile actomyosin bundles) that play a role in cell adhesion and morphogenesis [1, 21]. Finally, cells can also form protrusive membrane structures that are devoid of polymerized actin. These structures are called membrane blebs and are formed when the plasma membrane locally detaches from the actin cortex due to actomyosin contraction of the cortex. The hydrostatic pressure from the cytoplasm then pushes the membrane outwards

[b] dorsal – refers to the top (non-adhesive side) of a cell in a 2D environment

causing it to expand. When expansion of the membrane slows down, the actin cortex is reassembled underneath the bleb membrane, myosin is recruited, and the bleb is retracted again [22, 23]. In order to precisely control the assembly and disassembly of all these structures, cells are equipped with a multitude of actin binding proteins (ABPs) which, in concert with Rho-family GTPases, cellular redox state, pH, and posttranslational modification of actin, regulate actin dynamics.

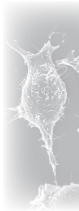

1.3. Regulation of actin dynamics

Rho-family GTPases

The nucleation of actin is triggered by Ras-related GTP-binding proteins of the Rho-family, including Rho, Rac, and Cdc42 [24]. Formin autoinhibition has been shown to be (partially) relieved by binding of Rho to its GBD [7, 25, 26]. The NPFs WASp and WAVE mediate the activation of the Arp2/3 complex via direct interaction with Cdc42 and Rac, respectively. Similar to formins, WASp and N-WASp are controlled by intramolecular interaction of a GBD with the C-motif, causing autoinhibition. Rho-family GTPases in cooperation with phosphatidylinositol 4,5-biphosphate (PIP_2), release this autoinhibition by binding to GBD and replacing the VCA-domain which can then interact with actin and the Arp2/3 complex [4]. The WAVE-complex is activated by binding to Rac and to acidic phospholipids (PIP_3) in the cell membrane, and phosphorylation of the WAVE complex [24]. The distinct signaling pathways, regulated by Rho, Rac, and Cdc42 respectively, link activation of plasma membrane receptors to the formation of the specific actin-based cellular structures described above. Stress fibers, for example, are regulated by Rho, lamellipodia and membrane ruffles by Rac, while filopodia are regulated by Cdc42 [27-29]. However, cross-talk does exist between Rho GTPases, as has been shown for Cdc42 and Rac in integrin-dependent adhesion and spreading in NIH3T3 cells [30]. The activation of Rho GTPases is regulated locally [31-34] and the timing and location of activation differs between the various GTPases. This differential regulation of GTPases has been visualized, for example, during cell protrusion [35], FcγR-mediated phagocytosis [36], and neurite outgrowth [37], and coordinates the rearrangement of the actin cytoskeleton and the cell membrane.

Actin-binding proteins

Once actin filaments have been formed, they can be modified by interaction with specific actin-binding proteins (ABPs) to match the specific requirements of the cell. Filament elongation is terminated by the binding of capping proteins (e.g. CapG/C and Hsp70) to filament barbed ends. This involves the degradation of polyphosphoinositides at the barbed end and activation of the capping proteins by Ca^{2+} or phosphorylation [38]. Filaments can also be severed or cut to expose fresh barbed

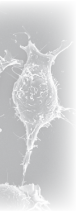

ends for polymerization. Severing proteins include the gelsolin-family of ABPs which disrupt the interaction between actin subunits in response to Ca^{2+} and tyrosine phosphorylation [39] and cofilin. Stabilization, cross-linking, and bundling of filaments is achieved by interaction with tropomyosin, filamin, α-actinin, fascin, and dynamin1/cortactin complexes, amongst others [3, 40-42]. These proteins are responsible for the formation of actin filament bundles that are found in filopodia but also for the formation of actin filament scaffolds underneath the plasma membrane in protrusive structures. While polymerization mainly occurs at the barbed end, filament disassembly and monomer recycling is mainly associated with the pointed end. Here, members of the ADF/cofilin-family of proteins bind to the actin filament, causing the filament to twist. This leads to changes in the thermodynamic stability of the filament and subsequent dissociation of actin subunits. The activity of ADF/cofilin is regulated by phosphorylation, phosphoinositides, acidity, and interaction with other proteins [3, 43, 44]. After actin monomers are released from the pointed end of filaments, they are bound by a number of actin monomer-binding proteins which regulate the size, location, and dynamics of the monomer pool [43]. Thymosin β-4 and twinfilin inhibit actin polymerization and nucleotide exchange on actin monomers, while profilin promotes it. Another protein, Srv2/CAP (cyclase-associated protein), recycles ADF/cofilin for another round of depolymerization and makes actin monomers again available for polymerization.

ROS, pH, phosphorylation, and arginylation

Actin dynamics are further influenced by changes in cellular redox status, pH, and posttranslational modification of ABPs or of actin itself. Oxidation alters the physiochemical properties of actin and can thereby adversely affect actin polymerization [45]. In addition, the activity of two actin depolymerizing proteins is regulated in a redox-dependent fashion. In *Drosophila*, Mical has been shown to associate with Sema-bound plexin and disassemble actin in a redox reaction with NADPH as co-enzyme [46]. The other protein, cofilin, is activated through dephosphorylation by slingshot-1L (SSH-1L) which is in turn activated by reactive oxygen species (ROS) [47]. Cofilin activity is additionally controlled by local changes in cellular pH. This is established through modulation of the inhibitory phosphoinositide binding to cofilin, where an increase in pH is associated with reduced binding and, thus, increased cofilin activity [48]. On the other hand, low pH has been shown to induce the actin severing activity of gelsolin [49]. Very recently, actin filament nucleation and elongation have been shown to be enhanced at acidic pH, reaching a maximum close to the iso-electric point of actin, suggesting an important role for electrostatic forces between actin subunits in filament formation [50]. As mentioned in the foregoing text, ABPs are often phosphorylated or dephosphorylated in order to regulate their activity in actin

filament assembly and disassembly. In addition, actin itself can be phosphorylated, as has been shown in *Dictyostelium* [51]. Phosphorylation of Tyr-53 causes allosteric modification of the nucleotide binding-cleft conformation, reducing the rate of nucleotide exchange on actin [52, 53]. Finally, β-actin is N-terminally arginylated and arginylation seems to be important for normal actin polymerization and filament structure, as well as interaction with several ABPs [54, 55].

1.4. Actomyosin contractility

The interaction of actin with myosin is responsible for the movement of cells. Myosins are motorproteins that convert chemical energy into mechanical energy, thereby generating force and movement [56]. Together, the myosins form a huge superfamily of proteins, which are categorized in 18 different classes, based on phylogenetic analysis of their head (i.e. motor) domains. Some of the best known myosins belong to class II and are main cytoskeletal components for the generation of cellular traction force, a process that is ATP-dependent. In the absence of ATP, the head of the myosin molecule is bound to actin. This activates the ATPase activity of the myosin head. Upon binding of ATP to myosin, the myosin-actin complex dissociates. Hydrolysis of the ATP induces a conformational change in the myosin molecule that causes the head to change position. In this state the myosin head can bind again to the actin filament at a different position. Binding of myosin to actin results in the release of the hydrolysis products ADP and Pi, which in turn causes the myosin head to return to its original position, thereby sliding the actin filament in one direction (the so-called “power stroke”) [56].

Myosin II has been implicated in a number of morphodynamic processes, including phagocytosis [57, 58] and shown to regulate the activity of the Rho-family GTPases Rac 1 and Cdc42 [59]. However, other unconventional myosins have also been shown to be involved in phagocytosis and protrusion formation, for example myosin I, V, IX and X [57, 60-63]. While myosin II is mostly responsible for the contraction of actin filaments, the most important role of other myosins is to power the directed transport of protrusion components towards the cell membrane, and to mediate the adhesion of actin filaments to the inner leaflet of the plasma membrane.

Our current knowledge on the mechanisms and regulation of actin dynamics is based on studies of different processes in many different cell types. Although these cells share certain commonalities, they may also be quite unique in their morphodynamic behavior. Stress fibers, for example, are formed by many cell types in culture but are especially prominent in fibroblasts [21], while cancer cells like glioblastoma cells are highly motile and typically form lamellipodia and invadiopodia to

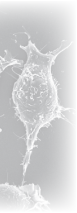

mediate migration [64]. Cells of the immune system exhibit again another unique type of morphodynamic behavior [65]. In order to fulfill their function in immunity and tissue homeostasis, macrophages, for example, have to undergo extensive morphodynamic changes which rely on proper regulation of actin cytoskeletal reorganization.

2. Macrophages

2.1. Origin, distribution, and polarization

Macrophages are mediators of the immune system that provide a first line of defense against pathogens and help to maintain steady-state tissue homeostasis by eliminating foreign matter and apoptotic cells via phagocytosis and secreting cytokines and growth factors [66-68]. They are derived from peripheral blood mononuclear cells (PBMCs) which develop from a common haematopoietic stem cell (HSC) in the bone marrow. The HSC gives rise to myeloid progenitor cells called granulocyte/macrophage colony-forming units (CFU-GM) which in turn give rise to monoblasts, pro-monocytes, and finally monocytes which are released from the bone marrow into the blood [67, 68]. Monocytes undergo differentiation after entering the surrounding tissue in the steady state or in response to inflammatory signals, giving rise to macrophages. Recent work by several groups has now also provided evidence for self-renewal of macrophages formed from embryonic progenitors independent of haematopoetic stem cells, via proliferation of cell populations that are already prenatally established in various tissues [69-79]. These new findings suggest that two subsets of tissue macrophages can be distinguished: those of bone marrow-dependent and -independent origin [80].

Macrophages are present in all tissues and can undergo tissue-specific differentiation. This leads to the generation of specific macrophages of the bone (osteoclasts), the alveoli, the central nervous system (microglial cells), connective tissue (histiocytes), the gastrointestinal tract, the liver (Kupffer cells), the spleen, the peritoneum, the eye (intraocular macrophages), the lymph nodes (subcapsular sinusoidal and medullary macrophages), and tumor associated macrophages (TAMs)[66, 68]. When macrophages encounter foreign material (e.g. bacterial products like lipopolysaccharide (LPS)) or are exposed to stimuli like inflammatory cytokines (IFN-g, TNF, or IL-4) and immunoglobulin G (IgG) immune complexes they gain specific functional properties and become polarized [81]. Mills et al. [82] were the first to observe that macrophages obtain a different activation state when exposed to cytokines from lymphocytes of the Th1 immune response and those of the Th2 immune response and classified these macrophages as “M1” and “M2”, respectively. However, since M2 macrophages make up a very heterogeneous group of cells, Mosser and Edwards [68] suggested that this group be further divided in “Wound healing”

and “Regulatory” macrophages based on their fundamental function. The identification of a third polarization state has been accepted in the field and macrophages are now broadly classified as classically activated (M1), alternatively activated (M2 or M2a), and regulatory macrophages (M2b&c) [83-85]. However, after differentiation macrophages retain plasticity and further adapt their functional phenotype in response to microenvironmental cues [86]. Therefore, “polarization of macrophage function should be viewed as an operationally useful, simplified, conceptual framework describing a continuum of diverse functional states” [81].

2.2. Macrophage function

Macrophages constantly survey their environment for signs of tissue injury, dying cells, toxic materials, or invading organisms [66]. When these signals are detected by phagocytosis or by surface receptors, macrophages may activate a response in other immune cells, like lymphocytes. Following infection or injury, macrophages can also assume an immune suppressive role, in order to restore tissue homeostasis. Whether macrophages take on a pro-inflammatory, anti-inflammatory, tissue remodeling, or regulatory phenotype depends on the environmental cues they encounter and the corresponding polarization state they obtain.

Classically activated (M1) macrophages emerge in response to interferon γ (IFNγ) and tumor necrosis factor (TNF) and products associated with bacterial pathogens (e.g. LPS). These cells have enhanced microbicidal and tumoricidal activity through the production of nitric oxide (NO) and phagocytosis of bacteria and tumor cells. In addition, they produce pro-inflammatory cytokines (e.g. IL-1, IL-6, and IL-23) and are involved in the stimulation of other immune cells [66, 68].

Alternatively activated (M2) macrophages develop in response to IL-13 and IL-4 [87] and are involved in wound healing, tissue remodeling, and angiogenesis. IL-4 is one of the first innate signals released during tissue injury and triggers the production of extracellular matrix (ECM) by stimulating arginase-mediated conversion of arginine to ornithine which is a precursor of polyamines and collagen [68]. Growth factors that are secreted by these macrophages include transforming growth factor β1 (TGFβ1) and platelet derived growth factor (PDGF), which promote fibroblast differentiation into myofibroblasts and stimulate the synthesis of interstitial fibrilar collagens [88]. M2 macrophages additionally have a immunoregulatory role by antagonizing toxic M1 responses, and suppressing inflammation and antitumor immunity [84]. Although TAMs in the early stages of cancer have a M1 phenotype, TAMs from solid metastatic tumors obtain a suppressive M2 phenotype due to changes in the tumor microenvironment and thereby contribute to tumor progression [66, 68].

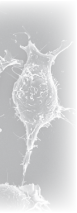

Finally, regulatory macrophages are characterized by the production of high levels of the immune-suppressive cytokine IL-10 in response to a combination of two stimuli, e.g. a TLR agonist in the presence of IgG immune complexes. These macrophages have a role in suppressing antimicrobial immunity, for example in the gut, but they can also arise during the later stages of adaptive immune responses to dampen the immune response and limit inflammation [68, 84].

2.3. Macrophage morphodynamics

Of all macrophage effector functions, their occupation as professional phagocytes stands central. Their ability to internalize relatively large (>0.5 µm) particles is vital to the host for the clearance of pathogens, dead erythrocytes, apoptotic cells, and debris generated during tissue remodeling. Through these processes macrophages fulfill their primary function in host defense and maintaining tissue homeostasis. Surveillance and phagocytosis efficiency relies on the ability to adhere, migrate, and produce cell surface protrusions, processes that involve active cell shape changes and depend on dynamic actin remodeling underneath the plasma membrane [2, 65].

Macrophage migration

After extravasation of monocytes into target tissues, the differentiated macrophages may undergo further directed migration (chemotaxis) in response to chemoattractants, like chemokines and bacterial peptides. Macrophages can migrate by squeezing through pores (amoeboid mode) or by adhering to and degrading the ECM (mesenchymal mode) [89]. At first, the density of the ECM was thought to determine the migration mode, but more recently Cougoule et al.[90] have shown that all macrophages can use the amoeboid migration mode, but only M2 polarized cells can adopt a mesenchymal migration mode. Instead of large, stable adhesion structures linked to actin stress fibers, macrophages form small, short lived point contacts, focal complexes and podosomes for traction [89, 91]. Podosomes have been implicated in cell migration and ECM degradation [92] and in line with this Cougoule et al.[90] demonstrated that mesenchymal migration of M2 macrophages correlates with the formation of podosome rosettes and degradation of the ECM by these cells. Inflammatory M1 macrophages formed podosomes with increased lifetimes and did not migrate at all, confirming much earlier observations [93]. Similar to other cells, migrating macrophages extend a lamellipodium at the front which depends on actin polymerization [65]. Point contacts are most strikingly formed in the leading lamellipodium of migrating macrophages, along with scattered focal complexes at the peripheral region [89]. Detachment of the uropod at the rear of the cell involves actomyosin contraction and is regulated by RhoA [65].

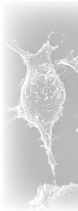

Phagocytosis

Macrophages continuously probe their environment through the formation of protrusive actin-dependent membrane structures. These structures include filopodia and membrane ruffles and facilitate the binding of foreign molecules [17, 94, 95]. Formation of these structures are driven by Rho-family GTPases and require $PI(4,5)P_2$ and $PI(3,4,5)P_3$ [96]. Macrophages may encounter and bind foreign molecules via different receptors on their cell surface. These include pattern recognition receptors (PRRs) that recognize pathogen-associated molecular patterns (PAMPs), scavenger receptors that recognize phosphatidylserine on apoptotic cells, Fc-receptors and complement receptors that recognize, respectively, immunoglobulins and complement molecules on opsonized pathogens [18]. Binding and activation of these receptors stimulate the phagocytic uptake of a particle via specific signaling pathways. The Fcγ-receptor (FcγR) and complement receptor 3 (CR3) are the best studied and mediate two distinct mechanisms of phagocytic uptake [97] (Figure 2A,B). Particles that are opsonized with IgG are bound by the Fc-domain of FcγR. Ligand binding leads to receptor clustering and phosphorylation of the cytoplasmic ITAM (Ig gene family tyrosine activation motive) on the receptor by Src-family protein tyrosine kinases. This leads to docking and phosphorylation (activation) of Syk on ITAM and the initiation of transcriptional activity, actin remodeling, and release of inflammatory mediators [18]. Actin polymerization is triggered by the recruitment of Cdc42 and Nck, which bind and activate WASp/N-WASp to stimulate Arp2/3 [36, 98, 99]. Growing actin filaments underneath the plasma membrane causes receptor-guided advance of the membrane over the particle surface, enclosing it in a "zipper-like" fashion [100] and yielding a continuous F-actin cup [97, 101].

Unlike FcRs, complement receptors require an additional stimulus to internalize a particle after binding [102]. Examples are PKC-activators like phorbol myristate acetate (PMA) [103] and LPS. Activation of CR3 leads to clustering of the receptor which is required for particle binding, and the association of its cytoplasmic domain to cytoskeletal proteins, like α-actinins [98]. Complement-opsonized particle binding activates RhoA, which in turn activates ROCK. Actin polymerization is then triggered by recruitment and activation of mDia (downstream target of ROCK) [104] and the ROCK/myosin II mediated recruitment of Arp2/3 complex [58]. In some cells the formation of a CR3-phagosome may resemble the "zippering" model, but in macrophages the phagosome forms as a depression in the cell surface, consisting of discrete patches of actin and other cytoskeletal proteins[100].

Closure of the phagosome is triggered by the PI3K-mediated conversion of $PI(4,5)P_2$ to $PI(3,4,5)P_3$ [98] and followed by the disassembly of actin filaments. Depolymerization of the actin cage around the phagosome is essential to allow fusion with digestive enzyme-containing lysosomes. Hydrolysis of $PI(4,5)P_2$ from the

phagosomal membrane have been shown to be involved in the disassembly of the actin network and completion of phagocytosis [105], although the inactivation of the Rho GTPases that induce actin polymerization also seem to play a role [106].

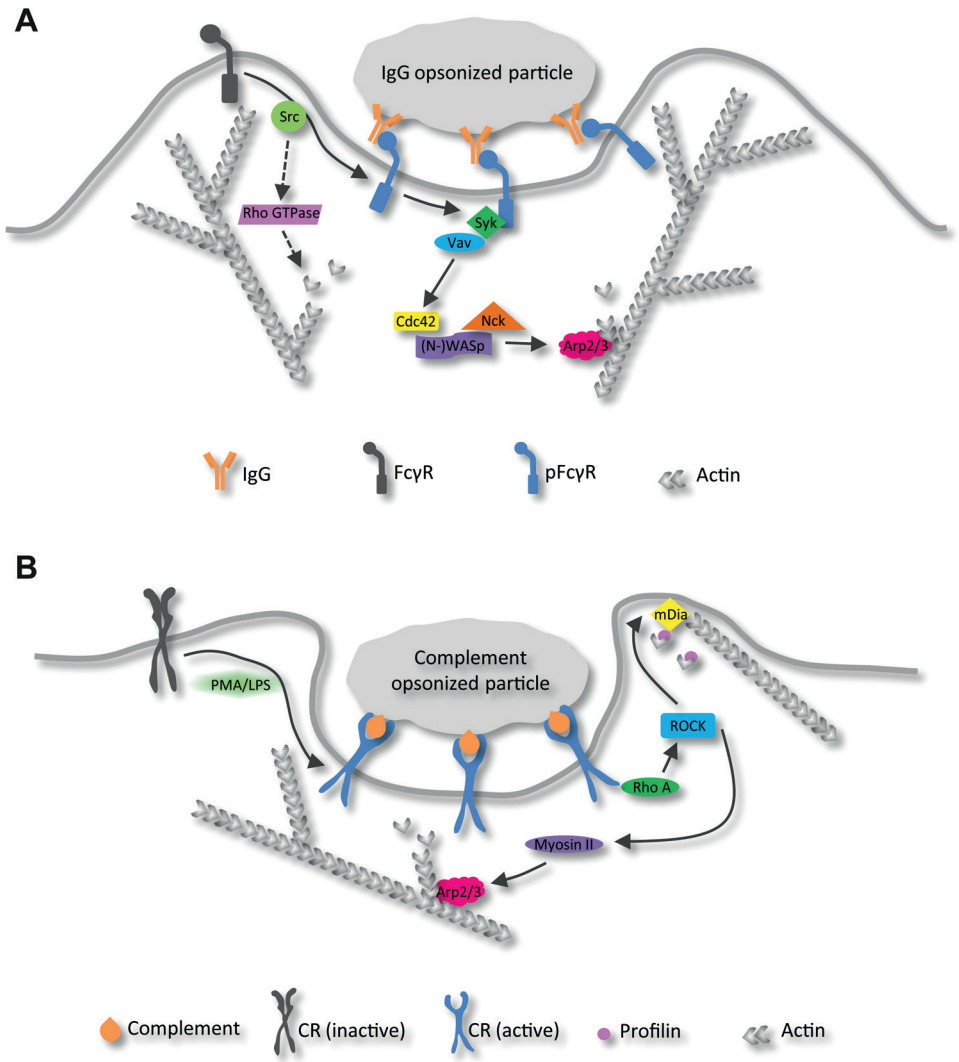

Figure 2. Mechanisms of phagocytosis in macrophages. *(A) Particles opsonized with IgG are bound by Fcγ-receptors on the cell surface. This leads to clustering and activation of the receptors and the initation of signaling pathways that ultimately result in polymerization of actin filaments. (B) Complement opsonized particles are recognized by the complement receptor. For internalization to take place, the CR has to be activated by an additional stimulus (e.g. LPS or PMA). This results in the initiation of GTPase-mediated signaling to the actin cytoskeleton. FcγR, Fcγ-receptor; pFcγR, phosphorylated (activated) Fcγ-receptor; CR, complement receptor.*

Macropinocytosis

Another process characteristic of macrophages is macropinocytosis. This process involves the uptake of extracellular fluid through relatively large vacuoles that are formed by membrane ruffles that close back against the plasma membrane. Like phagocytosis, macropinocytosis is actin-dependent, although no receptor-binding is involved. Macropinocytosis enables macrophages to sample the surrounding fluid for nutrients and pathogens [107, 108].

Given the nature and diversity of processes that support their biological roles, macrophages can be best classified as morphodynamically hyperactive cells. The constant remodeling of the actin cytoskeleton that drives this activity may place considerable pressure on the cellular energy demand in these cells [109, 110].

3. Cell metabolism

3.1. The cellular energy currency: ATP

Adenosine triphosphate (ATP) is a high energy compound that serves as energy shuttle within living cells. The production of ATP comprises the addition of a high-energy phosphoryl group to adenosine diphosphate (ADP) and is catalyzed by pyruvate kinase and phosphoglycerate kinase during glycolysis, and by ATP synthase during OXPHOS (see 3.2 below). ATP-consumption does not involve cleavage of the molecule but only hydrolysis of the phosphate group at the gamma-position to yield ADP and P_i (inorganic phosphate). Hydrolysis of ATP is highly exergonic, releasing 31 kJ/mol of chemical energy [111]. In some metabolic reactions ATP may be hydrolyzed into adenosine monophosphate (AMP) and pyrophosphate (PP_i). In order to recycle ATP from AMP, the adenine nucleotides may be interconverted via an enzyme called adenylate kinase as follows:

$$AMP + ATP \rightarrow 2\ ADP$$

Cell viability and functionality strongly depends on sufficient energy (ATP) supply to drive cellular processes and on the availability of biosynthetic material to provide building blocks for macromolecule synthesis. In order to supply this ATP and biosynthetic material, carbohydrates, proteins, and lipids are taken up from the extracellular environment or acquired from intracellular stores, and broken down (catabolized) or converted through different 'processing' pathways comprising a series of enzyme driven biochemical reactions that are all interconnected to form a complex metabolic network (Figure 3).

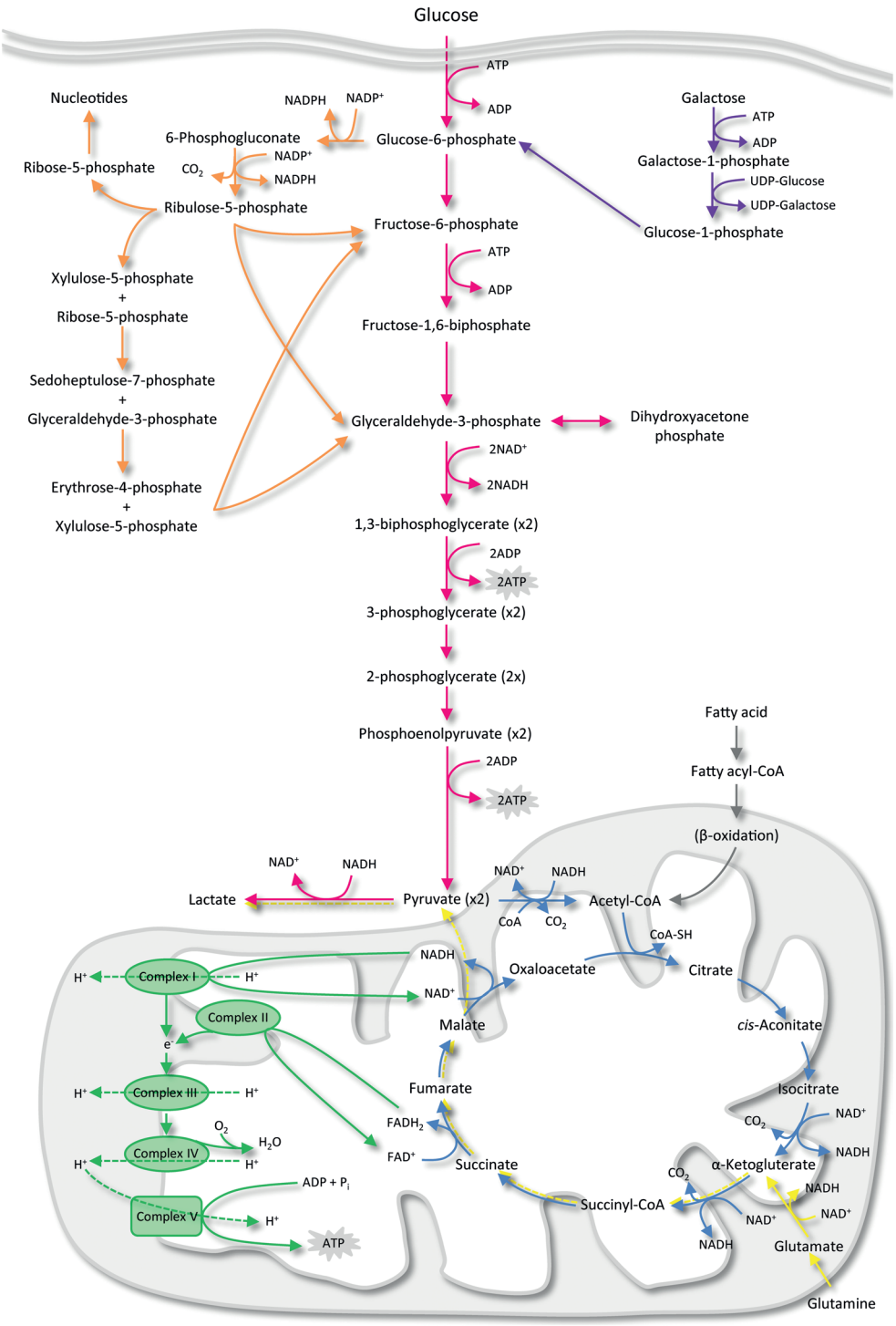
Glucose
ATP
ADP
Nucleotides
NADPH
NADP+
6-Phosphogluconate
Glucose-6-phosphate
Galactose
ATP
ADP
Galactose-1-phosphate
UDP-Glucose
UDP-Galactose
Glucose-1-phosphate
Ribose-5-phosphate
CO2
NADP+
NADPH
Ribulose-5-phosphate
Fructose-6-phosphate
ATP
ADP
Xylulose-5-phosphate
+
Ribose-5-phosphate
Fructose-1,6-biphosphate
Sedoheptulose-7-phosphate
+
Glyceraldehyde-3-phosphate
Glyceraldehyde-3-phosphate
Dihydroxyacetone phosphate
2NAD+
2NADH
Erythrose-4-phosphate
+
Xylulose-5-phosphate
1,3-biphosphoglycerate (x2)
2ADP
2ATP
3-phosphoglycerate (x2)
2-phosphoglycerate (2x)
Phosphoenolpyruvate (x2)
2ADP
2ATP
Fatty acid
Fatty acyl-CoA
(β-oxidation)
NAD+
NADH
Lactate
Pyruvate (x2)
NAD+
NADH
CoA
CO2
Acetyl-CoA
CoA-SH
NADH
Oxaloacetate
Citrate
H+
Complex I
H+
NAD+
Malate
cis-Aconitate
Complex II
e-
H+
Complex III
H+
Fumarate
Isocitrate
CO2
NAD+
O2
H2O
FADH2
NADH
H+
Complex IV
H+
FAD+
Succinate
CO2
α-Ketogluterate
ADP + Pi
NADH
Succinyl-CoA
Complex V
H+
NAD+
NAD+
NADH
Glutamate
ATP
Glutamine

Figure 3. Cellular metabolism. *Glucose is taken up by the cell through GLUT and catabolized through glycolysis (pink arrows). The product of the first step in glycolysis (glucose-6-phosphate) may also enter the pentose phosphate pathway (PPP; orange arrows) to produce NADPH. Intermediates from the PPP may re-enter the glycolytic pathway to be further broken down. Other hexose sugars, like galactose, also enter the glycolytic pathway (purple arrows). However, the breakdown of galactose via glycolysis doesn't yield any net ATP. Therefore, the cell is forced to rely exclusively on mitochondrial-derived ATP[112, 113]. The end-product of glycolysis (pyruvate) can either be converted into lactate or be transported into the mitochondrion where it is converted into acetyl-CoA. Acetyl-CoA enters the TCA-cycle (blue arrows) where the electron carriers NADH and $FADH_2$ are produced. Electrons from NADH and $FADH_2$ are transferred to the complexes of the electron transport chain (green arrows) and which results in the production of ATP. The carbon skeletons of amino acids (e.g. glutamine) may enter the TCA-cycle at various points (e.g. as α-Ketoglutarate; yellow arrows) in order to contribute to cellular ATP production. Cells may also utilize fatty acid for ATP production through β-oxidation (grey arrows) [114].*

3.2. Cellular energy-redox reactions and catabolic/anabolic metabolism

Glycolysis

The pathway of carbohydrate catabolism starts with the breakdown of six-carbon sugars via glycolysis (Figure 3). This pathway is active under aerobic as well as anaerobic conditions and utilizes glucose as its main substrate [111]. Glucose is imported by the cell via special glucose transporters. Two classes of glucose transporters exist: the Na^+-dependent glucose co-transporters (SGLT family) and the facilitative Na^+-independent sugar transporters (GLUT family) [115, 116]. SGLT utilizes the Na^+-electrochemical gradient provided by the Na^+/K^+ ATPase pump to transport glucose into cells against its concentration gradient, while GLUT utilizes the diffusion gradient of glucose (and other sugars such as galactose) across plasma membranes. In the cytosol, glucose is converted into pyruvate (a three-carbon keto-acid) via a series of reactions forming the glycolytic pathway [111]. In addition to pyruvate, the glycolytic breakdown of glucose yields two ATP molecules, directly providing chemical energy for the fuelling of cellular reactions, and two reduced nicotinamide adenine dinucleotide (NADH) molecules, serving as electron carriers. Although glycolysis is essential for ATP production, it also provides biosynthetic material via intermediates of the pathway, e.g. for nucleotide, amino acid, and lipid synthesis. Under anaerobic conditions, most of the formed pyruvate is turned into lactate together with the recycling of NADH to its oxidized from, NAD^+, which can then be reused as co-factor and electron acceptor in the earlier glycolytic reactions (Figure 3). Under aerobic conditions, pyruvate is transported from the cytosol into the mitochondria via a specific mitochondrial pyruvate carrier (MPC1/MPC2 complex) in the inner mitochondrial membrane [117, 118]. Here, it is oxidized to a metabolically active two-carbon fragment, acetyl-coenzyme A (acetyl-CoA), that undergoes further oxidation in the tricarboxylic acid (TCA) cycle [111].

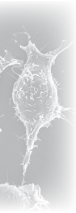

The TCA-cycle and OXPHOS

In the TCA-cycle all catabolic pathways merge into one path for oxidative metabolism. Simple carbon compounds from carbohydrate, protein, and lipid breakdown enter the TCA-cycle and are oxidized to CO_2. Under exceptional circumstances also reversal of the reaction sequence (with α-ketoglutarate converted to citrate) is possible [119]. This is important for lipid synthesis and proliferation of cancer cells under hypoxia and may also be relevant for macrophage survival and function. In the forward mode, in four consecutive oxidative reactions of the TCA-cycle, reduced electron carriers are generated, producing three NADH and one $FADH_2$ (reduced flavin adenine dinucleotide) molecules (Figure 3). Together with the NADH derived from glycolysis, which have to be shuttled across the mitochondrial membrane (see 3.3), these electron carriers donate electrons to the complexes of the electron transport chain (ETC) situated in the inner mitochondrial membrane. As the electrons are transferred from one complex to another, protons are pumped from the matrix across the inner mitochondrial membrane into the intermembrane space, thereby generating a proton gradient across the inner membrane and establishing an electric potential. At the last complex of the ETC, the F_0F_1 complex, complex V or ATP synthase, protons flow back to the matrix and the gradient is discharged, releasing energy and driving the synthesis of ATP from ADP and P_i. The last electron acceptor in the chain is molecular oxygen, thereby producing H_20 (Figure 3). This production of ATP via the ETC is called oxidative phosphorylation (OXPHOS) [111].

Amino acid metabolism: Glutaminolysis

The pyruvate-acetyl-CoA reaction is not the only entry point into the TCA-cycle. When amino acid availability exceeds the need for protein synthesis, the cell degrades the excess nitrogen and metabolizes the carbon skeletons in the TCA-cycle [111]. Depending on the amino acid, the carbon skeletons may enter the TCA-cycle either as pyruvate, acetyl-CoA, α-ketoglutarate, succinate, fumurate, or oxaloacetate. Thus, proteins - when broken down into amino acids - can contribute significantly to the energetic requirements of the cell. Glutamine is the most abundant amino acid in blood plasma [120] and is imported by cells via amino acid transporters in the plasma membrane [121]. In proliferating cells, it contributes to essentially all the main metabolic tasks of the cell. It is involved in bioenergetics, defense against oxidative stress, and the production of macromolecules [122]. The γ-nitrogen of glutamine is used for nucleotide and hexosamine synthesis while its conversion into glutamate by glutaminase is essential for the synthesis of other amino acids and glutathione (GSH), as well as its entry into the TCA-cycle via α-ketoglutarate (Figure 3), and the production of reduced nicotinamide adenine dinucleotide phosphate (NADPH) from its oxidized form ($NADP^+$) via the malate-pyruvate conversion by ma-

lic enzyme [122]. Under conditions when glucose is limiting, glutamine metabolism through the TCA-cycle may provide an alternative energy-generating pathway [123]. In addition, cells may use the reductive metabolism of α-ketoglutarate to synthesize acetyl-CoA for lipid synthesis, especially during hypoxia or when mitochondrial respiration is disturbed [124, 125].

β-oxidation

Lipids that are synthesized intracellularly can either be stored in the form of triacylglycerol (TG) or used, for example, in membrane synthesis. Under conditions of high energy demand, TGs are mobilized and hydrolyzed to yield glycerol and three fatty acids. Glycerol may serve as gluconeogenic substrate, yielding glucose, or can enter glycolysis while FAs are imported into the mitochondria via the carnitine acyltransferase-system and catabolized to acetyl-CoA via β-oxidation, releasing reduced electron carriers (NADH and $FADH_2$) along the way [111] (Figure 3).

The pentose phosphate pathway

As mentioned above, glycolysis may also contribute to biosynthesis (anabolism) of various cellular compounds. One essential anabolic pathway that is linked to the catabolism of glucose is the pentose phosphate pathway (PPP). The product of the first reaction in glycolysis, glucose-6-phosphate (G6P), forms the starting substrate of the PPP and is used to provide NADPH for reductive biosynthesis and protection against oxidative stress, and ribose-5-phosphate (R5P) for nucleotide and nucleic acid synthesis [111] (Figure 3). The PPP comprises an oxidative and a nonoxidative branch. The first three reactions of the pathway forms the oxidative branch and in two of these NADPH is produced from the reduction of $NADP^+$. In the nonoxidative branch, some ribulose-5-phosphate (Ru5P) from the oxidative phase is converted into R5P. However, if the cell doesn't require large quantities of R5P for nucleotide synthesis, Ru5P may have other fates (see Figure 3). If the primary need of the cell is reducing molecules, fructose phosphates formed towards the end of the pathway are reconverted to G6P for reoxidation in the oxidative phase. Ru5P may also be used for energy production by being reconverted to glycolysis through the formation of fructose-6-phosphate (F6P) and glyceraldehyde-3-phosphate (G3P) thereby providing pyruvate to enter the TCA-cycle [111].

3.3. Pyridine nucleotide co-factors and redox couples: NAD(P) and NAD(P)H

Mitochondrial ATP production via OXPHOS involves the transfer of electrons between complexes I to IV of the ETC with molecular oxygen as the final acceptor. As

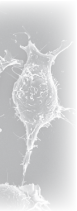

explained in 3.2 above, these electrons are derived from dehydrogenase reactions of glycolysis and the TCA-cycle, transferred to NAD^+, and carried to the mitochondria as NADH. In addition to their role in cellular energy production, the two redox couples NAD^+/NADH and $NADP^+$/NADPH buffer the redox state of the cell by accepting and donating electrons during oxidation and reduction reactions, respectively. NAD^+ can be synthesized *de novo* from the essential amino acid tryptophan, although most of the cellular NAD^+ in mammalian cells comes from salvage pathways using the NAD^+ precursors nicotinic acid (NA), nicotinamide (NAM), or nicotinamide riboside (NR) as starting substrates [126] (Figure 4). Tryptophan is first converted into N-formylkynurenine either by indolamine 2,3-dioxygenase (IDO) or tryptophan 2,3-dioxygenase (TDO), which is then converted into α-amino-β-carboxymuconate-ε-semialdehyde (ACMS) in four separate reaction steps. ACMS can undergo spontaneous cyclization to form quinolinic acid which is transformed into nicotinic acid mononucleotide (NAMN) by quinolinate phosphoribosyltransferase (QPRT). Subsequently, NAMN is converted into nicotinic acid adenine dinucleotide (NAAD) by NAM mononucleotide adenylyltransferase (NMNAT), which is finally converted into NAD^+ by glutamine-dependent NAD synthase (NADS). Salvage synthesis from NA starts with the formation of NAMN by nicotinic acid phosphoribosyltransferase (NAPRT) which then enters the *de novo* pathway. The other two salvage pathways involve conversion of NAM and NR to nicotinamide mononucleotide (NMN) by nicotinamide phosphoribosyltransferase (NAMPT) and nicotinamide riboside kinase (NRK), respectively. NMN is then finally converted into NAD^+ by NMNAT[126]. NAD^+ is the precursor for the other three pyridine nucleotides, NADH, $NADP^+$, and NADPH. Its reduced form, NADH, is produced in reactions catalyzed by dehydrogenases while $NADP^+$ is synthesized through the phosphorylation of NAD^+ by NAD kinase (NADK). $NADP^+$ is subsequently and very quickly reduced to NADPH [127] via the PPP, via malic enzyme catalyzed reactions, or by the mitochondrial energy-linked transhydrogenase (or complex VI of the ETC). Thus, cellular NADP(H) (i.e. $NADP^+$ and NADPH) occurs mostly as NADPH, while cellular NAD(H) (i.e. NAD^+ and NADH) occurs mainly in the oxidized form, i.e. NAD^+.

Within the cell, NAD(H) and NADP(H) are heavily compartmentalized and not able to freely move across membranes. *De novo* as well as salvage NAD^+ synthesis occurs mainly in the cytosol. However, mitochondria may have the ability to synthesize and maintain their own NAD through NMNAT3 and NMN derived from the cytosol [128]. The transfer of reducing equivalents across the mitochondrial membrane, therefore, involves specific redox shuttles: the 2-oxoglutarate/isocitrate redox shuttle in the case of NADP(H), and the malate-aspartate and α-glycerophosphate shuttles for NAD(H) [126]. Furthermore, recent literature also suggest separate NAD(P)(H) pools for other organelles such as the Golgi-complex and the endoplasmic reticulum [129].

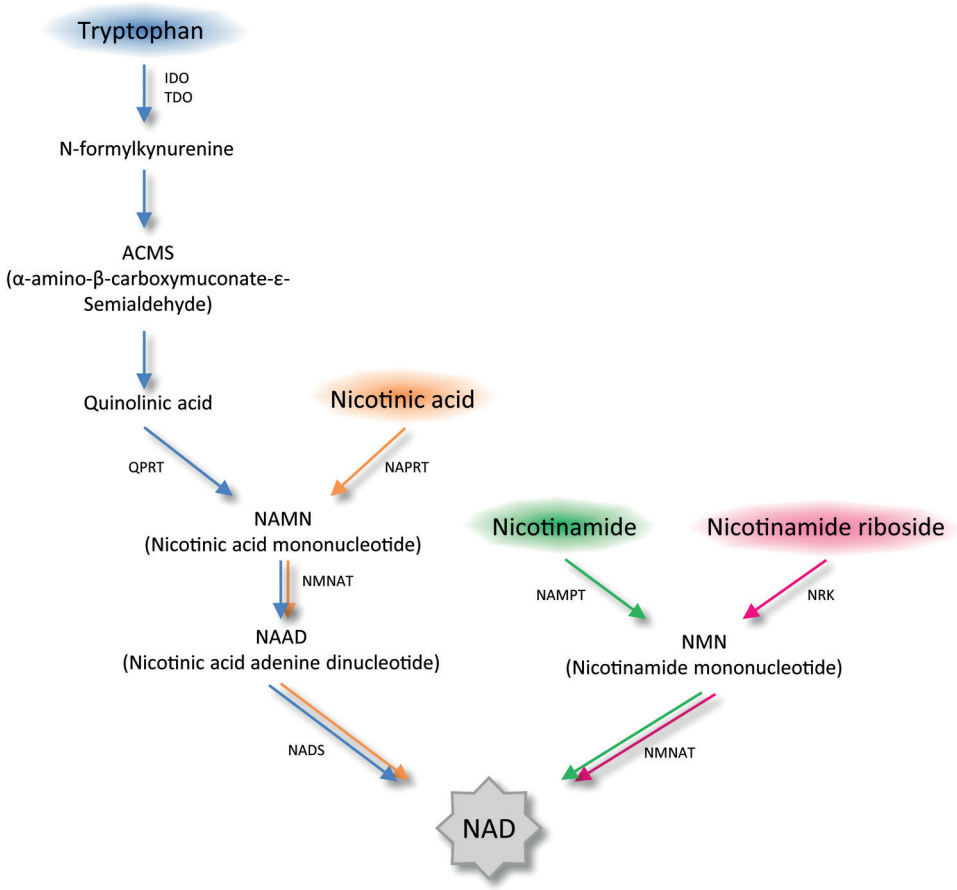

Figure 4. *De novo* and salvage synthesis pathways of NAD^+ in mammalian cells. *NAD^+ can be synthesized de novo from the essential amino acid tryptophan, although most of the cellular NAD^+ in mammalian cells comes from salvage pathways using the NAD^+ precursors nicotinic acid (NA), nicotinamide (NAM), or nicotinamide riboside (NR) as starting substrates. Salvage synthesis from NA starts with the formation of NAMN by nicotinic acid phosphoribosyltransferase (NAPRT) which then enters the de novo pathway. The other two salvage pathways involve conversion of NAM and NR to nicotinamide mononucleotide (NMN) by nicotinamide phosphoribosyltransferase (NAMPT) and nicotinamide riboside kinase(NRK), respectively. NMN is then finally converted into NAD^+ by NMNAT* [126].

NADP(H) plays a major role as co-enzyme in cellular electron transfer reactions. During reductive anabolic reactions, such as fatty acid and steroid biosynthesis, NADPH is the electron donor. It also contributes to DNA synthesis since it is involved in the reduction of ribonucleotides to deoxyribonucleotides by ribonucleotide reductase. Detoxification of xenobiotics by cytochrome P-450 enzymes in the liver depends on continuous re-reduction by NADPH-dependent cytochrome P450 reductases in order to regenerate these enzymes. Another important function of NADPH is the regeneration of anti-oxidant systems, for example, the regenera-

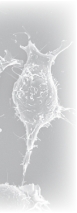

tion of GSH from GSSG through the action of glutathione reductase [130]. Last but not least, NADPH is involved in the production of ROS and the regulation of pH via NADPH oxidases, which has first been identified in phagocytes but is known to be also present in other cells [130, 131].

Since its discovery as cofactor and electron carrier in cellular energy metabolism, NAD^+'s cellular functions have been expanded to include roles in gene regulation, Ca^{2+}-homeostasis, cell signaling, and immunological reactions [132]. In these settings, NAD^+ is no longer a redox molecule that can be recycled via transfer of electrons, but acts as substrate for certain enzymes that are able to physically cleave NAD^+. Among these NAD^+-consuming enzymes are sirtuins, poly-ADP-ribose-polymerases (PARP), and CD38, which have been shown to regulate cytokine secretion, DNA repair, gene expression, and Ca^{2+}-mobilization [126, 132, 133]. Regulation and maintenance of cellular NAD levels are, therefore, of utmost importance for (immune) cell viability and function. In this regard, NAMPT-mediated NAD^+-synthesis, the main pathway for NAD^+-regeneration, has been shown to be essential in T-lymphocytes [134], as well as monocytes and macrophages [135-137], thereby directly linking cellular metabolism and the immune response.

3.4. Intracellular ATP storage and transfer: the creatine kinase/phosphocreatine energy circuit

The ATP produced from glycolysis or OXPHOS can have two fates: it either has to be transported to those regions in the cell where it is hydrolyzed, or it should be stored until the cell requires extra energy. In order to achieve this, cells (especially those with a high energy demand) are equipped with a special energy storage and transport system: the creatine kinase/phosphocreatine (CK/PCr) energy circuit [138]. The circuit comprises a chain of reversible reactions, catalyzed by creatine kinase (CK), through which a high energy phosphoryl group is transferred between ATP and creatine (Cr) or ADP and phosphocreatine (PCr):

$$PCr^{2-} + MgADP^{-} + H^{+} \leftrightarrow MgATP^{2-} + Cr$$

Creatine is either synthesized endogenously or derived from dietary products, such as fish and meat. Biosynthesis of creatine involves the formation of guanidinoacetate (GAA) in the kidney, which is transported through the blood and methylated to form creatine in the liver [139]. Creatine is then released into the blood for uptake by cells with a high energy demand via the specific creatine transporter [140]. Intracellularly, it is converted to metabolically inert PCr by CK to such an extent that two thirds of the total Cr pool is phosphorylated. In this way, the cell can store up to ten times the amount of energy in the ATP-pool. If cells with a high energy demand would simply maintain a high cellular [ATP] instead of building up a PCr

energy store, the accumulation of ADP + P_i and liberation of H^+ upon ATP hydrolysis would largely inhibit ATPases [141].

Creatine kinase has a number of tissue- and cell-specific isoforms with defined subcellular locations [138]. Cytosolic CK isoforms include ubiquitous brain-type CK (CK-B) and sarcomeric muscle-type CK (CK-M) which form homo- or heterodimers and may be present as soluble enzyme (CK-c), or be specifically associated with ATP-consuming processes (CK-a), such as myofibrillar acto-myosin ATPases [142], or be coupled to glycolysis (CK-g; [143]). Presently, it is not known how the intracellular localization of these different CK's are determined. One possibility could be differential post-translational modification of the enzyme. CK-g is coupled to glycolytic enzymes that are either involved in ATP-generation (e.g. pyruvate kinase), or with phosphofructokinase (PFK), the main regulatory glycolytic enzyme [143, 144]. In this way, they prevent negative feedback inhibition of PFK by immediate removal of ATP, and at the same time replete the PCr pool. Mitochondrial CK (mtCK) isoforms also include a ubiquitous and a sarcomeric enzyme. MtCK is a homo-octamer and functionally coupled to OXPHOS either via the adenine nucleotide translocator (ANT) alone which catalyzes the antiport of ATP vs ADP across the inner mitochondrial membrane, or via ANT and voltage-dependent ion channel (VDAC) which is situated in the outer mitochondrial membrane and facilitates the export of ATP into the cytosol [145]. Thus, ATP synthesized in the mitochondrial matrix by F_0F_1- ATPase is transported across the inner membrane via ANT in exchange for ADP and exported into the cytosol directly via VDAC or after being converted into PCr.

The CK/PCr circuit, therefore, connects sites of ATP production (glycolysis or OXPHOS) with subcellular sites of ATP utilization (ATPases) without the need for ATP or ADP to diffuse back and forth [141] (Figure 5). This is of great advantage to the cell since the diffusion rates of ATP and especially ADP is much lower than that of Cr and PCr [146]. In addition, the CK/PCr system provides an immediately available temporal energy buffer and regulates metabolism through the net liberation of P_i between ATPase- and CK-reactions, resulting in the stabilization of cellular [ATP] at approximately 3-5 mM [141].

Macrophages contain primarily the CK-B isoform, the expression of which is upregulated during monocyte differentiation into macrophages together with their ability to import creatine via the transmembrane creatine transporter [147]. Creatine kinase is activated in macrophages after LPS treatment [148, 149] but whether CK is differentially expressed in M1 and M2 macrophages is not known. Since macrophages cannot synthesize creatine themselves, the size of the intracellular PCr pool is directly proportional to the creatine concentration of the culture medium *in vitro* [150]. During phagocytosis, cellular ATP remains fairly stable while [PCr] decreases by 40-50%, indicating that the energy consumed during phagocytosis is largely

replenished by CK via PCr [151]. Moreover, the early stages of complement-opsonized particle adhesion and internalization are characterized by the local accumulation of CK-B at the phagocytic cup, where it is also involved in the recruitment of actin molecules [152]. The CK/PCr system, therefore, plays a significant role when immediate ATP-supply is required in macrophages.

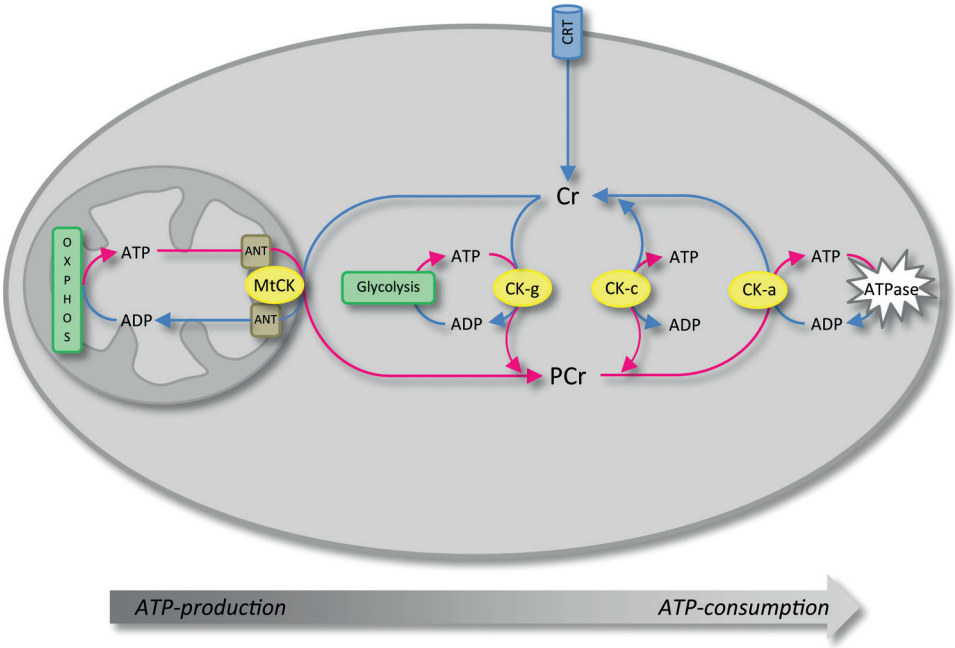

Figure 5. The CK/PCr system for intracellular ATP transfer and temporal and spatial energy buffering. *Creatine is transported across the cell membrane via the creatine transporter (CRT). Cytosolic CK (CK-c) regulates intracellular PCr/Cr and ATP/ADP ratios. CK coupled to glycolytic enzymes (CK-g) accepts ATP produced by glycolysis, while ATP from oxidative phosphorylation (OXPHOS) is accepted by mitochondrial CK (mtCK), which - in turn - is coupled to the adenine nucleotide translocator (ANT). CK may also be associated with specific sites of ATP consumption (CK-a), for example ATP-gated ion pumps. The CK/PCr circuit, therefore, connects sites of ATP production (glycolysis or OXPHOS) with subcellular sites of ATP utilization (ATPases) without the need for ATP or ADP to diffuse back and forth. (Adapted from Wallimann et al. [141])*

3.5. Metabolism and macrophage polarization state

Carbohydrate metabolism

Recent literature has revealed that macrophage differentiation and polarization strongly influences macrophage metabolism [153]. Also the reciprocal relationship, i.e. that metabolism determines differentiation state may be true [154]. When combined, these observations imply that macrophage metabolic state may be just as hetero-

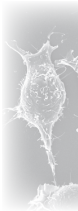

geneous and complex as their polarization phenotype. During the early studies on macrophage metabolism, this was not (fully) acknowledged and general conclusions were drawn from experiments performed on macrophages with different origins and activation/polarization status. A significant number of studies have been performed using thioglycollate elicited mouse peritoneal macrophages (TEPMs) which appear - at least partially - polarized towards a M2 phenotype [155, 156]. These TEPMs consume three times more oxygen than resident peritoneal macrophages [157]. Nonetheless, carbohydrate metabolism in all macrophages is fundamentally glycolytic [158]. Monocytes acquire a glycolytic metabolism as they differentiate into macrophages *in vitro* [159], although a concomitant increase in aerobic metabolism (mitochondrial mass and cytochrome oxidase activity) has also been described under aerobic conditions [160, 161]. Upon polarization, macrophage metabolism is altered to shape the new activation state and to meet the specific requirements for performing effector functions such as phagocytosis, cytokine secretion, ROS production, and ECM synthesis [153]. After polarization, the largest amount (95%) of all glucose consumed by macrophages remains converted into lactate [158] instead of being oxidized via the TCA-cycle and OXPHOS, even under aerobic conditions. In this regard, macrophage metabolism closely resembles that of cancer cells where this phenomenon is termed the “Warburg phenotype”.

Glucose is imported by macrophages via different GLUT isoforms. The expression of GLUT isoforms seems to be dependent on species, origin (primary cells or cell lines), and differentiation and polarization state. THP-1 cells (human monocytic cell line) express GLUT1,3, and 4 and upon differentiation into macrophages upregulate GLUT3 and 5 expression [162]. In primary human blood monocytes GLUT1 is expressed and upregulated during differentiation into macrophages [159], while RAW 264.7 cells (murine macrophage cell line) mainly express GLUT3 [163]. Stimulation with LPS (driving M1 polarization) causes an upregulation of GLUT isoform expression, leading to elevated influx of glucose [164, 165]. This is accompanied by an increase in glycolysis gene expression and glycolytic flux to lactate [154, 158]. The molecular basis of this upregulation in glycolysis involves a switch in the expression of liver-type phosphofructokinase (L-type PFK2) in resting TEPMs to the more active ubiquitous PFK2 (uPFK2) in M1 TEPMs [158]. This causes a nine times rise in PFK2 activity and five times increase in fructose-2,6-bisphosphate levels. In contrast, IL-4/IL-13 stimulation, which drives M2 polarization, causes no alteration in PFK2 expression and has only mild metabolic effects.

The increased rate of gene transcription and synthesis of macromolecules during macrophage activation increases the bioenergetic demand but also the need for anabolic intermediates. Accordingly, the activity of the pentose phosphate pathway (PPP) is increased in LPS-stimulated M1 macrophages and a substantial portion of

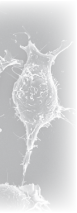

glucose-derived carbon is routed into the PPP [154]. Increased PPP activity switches these cells to a reductive mode with elevated levels of reduced glutathione (GSH) and NADH. Concomitantly, the oxygen consumption rate and expression of OXPHOS genes are downregulated in classically activated macrophages [154, 158]. In contrast, IL-4 stimulated M2 cells exhibit an upregulation in TCA-cycle genes [158] and mitochondrial biogenesis [166] and adapt a more oxidative mode with lower GSH levels [167] and increased superoxide production [168].

Lipid metabolism

Although glucose is the main energy producing substrate in macrophages, these cells are also able to derive cellular energy from fatty acid (FA) oxidation. They are equipped with intracellular triglyceride lipase (TGL) [169, 170] but also produce and secrete lipoprotein lipase (LPL) [171-174]. These enzymes release FAs through the hydrolysis of intracellular triacylglycerol (TG) stores or through the hydrolysis of exogenously supplied lipoproteins, respectively. LPL activity and fatty acid uptake and oxidation are inhibited in M1 and upregulated in M2 macrophages [166, 175, 176]. TEPMs, which are partially M2 polarized, relatedly express a substantial amount of adipose TGL (ATGL). In the absence of ATGL (by double knockout), TEPMs accumulate TG-rich droplets, reducing the availability of FAs for β-oxidation, and have decreased ATP levels even while glucose is sufficiently available [177]. Under conditions where glucose is limiting, LPL-catalyzed hydrolysis of exogenously supplied lipoproteins have been shown to provide energy for (M2 polarized) macrophages during periods of intense metabolic activity (e.g. phagocytosis) [178]. However, the presence of FAs does not suppress normal glucose or glutamine utilization when this is sufficiently available [179]. Macrophages probably first esterify and convert internalized FAs into TGs before hydrolysis by ATGL and transport into the mitochondria for β-oxidation [177]. The largest fraction of oxidized FAs is incorporated into phospholipids and TAGs both in TEPMs and unstimulated peritoneal macrophages [179, 180]. Apart from supplying energy, lipid metabolism, therefore, also regulate membrane fluidity which is a determining factor in macrophage adhesion and phagocytosis [153, 181]. Since the saturation status of fatty acids determines membrane fluidity, saturated and unsaturated FAs differentially affect phagocytosis in macrophages: saturated FAs, like palmitic acid, inhibit phagocytosis, while unsaturated FAs, like oleic acid, stimulate phagocytosis [180, 181].

Amino acid metabolism

Macrophages, and immune cells in general, consume relatively large amounts of glutamine [182]. Polarization state does not seem to affect glutamine utilization or glutamate production within the first 12 hours of activation [158]. However, a minor

increase in glutamine consumption has been observed in LPS stimulated mouse peritoneal macrophages (resident and Bacillus Calmette–Guerin (BCG) activated) later, after 24 and/or 48 hours [183]. As mentioned in 3.2 above, glutamine can be converted to lactate in a reaction pathway that involves the production of NADPH by malic enzyme. Increased NADPH-production may be beneficial to LPS-stimulated (M1) macrophages, since NADPH is required for the production of ROS via NADPH oxidase (NOX) during the oxidative burst, the production of nitric oxide (NO) by inducible nitric oxide synthase (iNOS), and as co-factor in anabolic reactions (e.g. cytokine production, and DNA and RNA synthesis) [184]. The production of NO involves the conversion of another amino acid, arginine, into citrulline and NO by iNOS. Glutamine itself may also contribute to NO production by being converted into arginine first. However, this has only been shown for macrophages cultured in the absence of extracellular arginine [183].

Although arginine, therefore, plays a role in M1 activation, its metabolism through arginase 1 is upregulated in mouse M2 macrophages and not in M1 cells [153]. Alternatively activated (M2) mouse macrophages metabolize L-Arg into ornithine and urea thereby contributing to polyamine production for collagen synthesis, cell proliferation, and tissue remodeling [185]. It is not clear whether arginine metabolism is also differentially regulated in human M2 macrophages.

Another amino acid with a notable role in immunometabolism is tryptophan. This essential amino acid is the starting substrate for *de novo* biosynthesis of NAD^+ (see 3.3 above). The first enzyme of this pathway, IDO, is downregulated by IL-4 but upregulated upon IFNγ or LPS stimulation in monocytes and macrophages [186, 187], resulting in increased tryptophan utilization. NAD^+ has been implicated in the regulation of inflammatory cytokine production in macrophages and in the modulation of immune function [133, 135, 136, 188] in addition to its role as metabolic cofactor. *De novo* NAD^+-synthesis from tryptophan may, therefore, have a role in the immune function of M1 macrophages. The above examples illustrate that also aspects of amino acid metabolism and polarization state of macrophages are clearly - and probably reciprocally - coupled.

3.6. Regulation of macrophage metabolism and polarization

PPAR

The adaptation of macrophage metabolism that accompanies the change in polarization state is determined by a number of regulating molecules that control the shift between oxidative and reductive metabolism. Peroxisome proliferator-activated receptors (PPARs) are the master regulators of lipid metabolism. Of the three isoforms, PPARγ and PPARδ play a central role in macrophage polarization, while

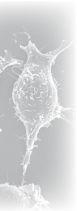

PPARα's role is more trivial [189]. TEPMs as well as IL-4 activated resident mouse peritoneal macrophages and human peripheral blood monocytes have increased PPARγ mRNA and protein synthesis [190]. PPARγ orchestrates the changes in lipid metabolism that accompanies M2 polarization and is required for the acquisition and maintenance of alternative activation [156, 189, 191]. In addition to the induction of β-oxidation and mitochondrial biogenesis, PPARγ directly regulates the ability of IL-4 to activate the arginase I promoter and increases arginase I mRNA levels, and mediates IL-4-induced expression of CD36 which may function as scavenger receptor for oxidized low density lipoprotein (LDL) or apoptotic cells [156, 190]. PPARδ, on the other hand, coordinates the immunologic effector functions of alternative activation which include suppression of the inflammatory response [189].

HIF-1α and HIF-2α

A second regulatory molecule of macrophage metabolic state is hypoxia-inducible factor alpha (HIF-α). Two isoforms of this transcription factor, HIF-1α and HIF-2α, are differentially activated in M1 and M2 polarized macrophages and influence metabolism distinctly [155]. HIF-1α mRNA expression is increased during classical activation by LPS and INFγ, while HIF-2α mRNA expression is significantly repressed [155, 158]. HIF-1α regulates NO production and glycolytic pathways that promote the effector response of M1 macrophages by induction of the iNOS gene and glycolysis-related genes [192]. Alternative activation by IL-4 and IL-13, on the other hand, has almost no effect on HIF-1α mRNA while HIF-2α mRNA is significantly increased [155]. This is also true for TEPMs. HIF-2α activation is essential for arginase I induction in M2 macrophages (even under normoxia) and the suppression of NO synthesis in these cells but is not required for the hypoxic induction of HIF-1α target genes, e.g. GLUT 1 and LDH-A. A remarkable difference between HIF-1α and HIF-2α activation is that HIF-1α increases rapidly in response to classical activators, while HIF-2α responds slowly to alternative activators and has a longer half-life, reflecting their respective roles in transient, acute phase reactions or in long-term responses of inflammation resolution and restoration of homeostasis [155]. Further study of this topic in macrophages is surely needed as HIF-1 may also be involved in regulating glutamate metabolism and lipid synthesis by controlling the direction (forward/reverse) of the TCA-cycle at the α-ketoglutarate dehydrogenase step [119].

c-MYC

Downstream of HIF and upstream of PPARγ, the transcription factor c-MYC regulates macrophage polarization by controlling the induction of 45% of the genes associated with alternative activation[193]. Upon stimulation with IL-4 or other M2-stimuli, c-MYC expression and translocation to the nucleus is induced, leading to

upregulation of the STAT6/ PPARγ signaling axis which is required for alternative activation [156, 193]. c-MYC is also expressed in TAMs, stimulating their pro-tumoral program, and thereby enhancing cancer progression [194]. In mouse embryonic fibroblasts and cancer cells MYC has been shown to promote glutaminolysis and its inhibition by HIF-1α and FOXO proteins negatively regulates mitochondrial biogenesis and O_2-consumption [195-197]. In contrast, HIF-2α increases MYC activity [198], thereby positively regulating mitochondrial function. Although it has not been directly demonstrated, inhibition and activation of MYC by HIF-1α and HIF-2α may have the same metabolic consequences in M1 and M2 macrophages.

KLF4

Krüppel-like factor 4 (KLF4), a member of the KLF subfamily of the zinc finger class of DNA-binding transcriptional regulators has also been shown to regulate macrophage polarization and the accompanying adaptations in metabolism [199]. Its expression is induced in M2 macrophages where it cooperates with STAT6 to induce a M2-genetic program. In M1 macrophages KLF4 expression is repressed and KLF4 loss induces a M1 phenotype, comprising increased pro-inflammatory gene expression, enhanced bactericidal activity, and increased glycolytic flux.

p53 and TAp73

Very recently, the tumor suppressor p53 has been shown to influence macrophage polarization state and contribute to tumor suppression non-cell-autonomously [200]. p53 expression promotes cellular senescence involving stable cell cycle arrest and secretion of factors that promote an anti-tumor tissue microenvironment and drive the classical activation of macrophages. In contrast, proliferating p53 deficient cells secrete factors that promote the alternative activation and hence also tumorigenesis. Wild type p53 promotes mitochondrial function and suppresses anaerobic metabolism [201]. However, p53 is mutated in many different types of cancer [202] and therefor also influence cancer cell metabolism. Another member of the p53 family, Tap73, has also very recently been identified as a modulator of the macrophage phenotype. Absence of TAp73 maintains a M1 phenotype while suppressing M2 polarization and hence resolution of inflammation [203].

CARKL

Also quite recently, carbohydrate kinase-like protein (CARKL) has been identified as a novel regulatory molecule which orchestrates pro- and anti-inflammatory immune responses in macrophages through metabolic control [154]. CARKL catalyzes the production of sedoheptulose-7-phosphate (S7P), an intermediate of the pentose phosphate pathway (PPP; Figure 3)). Upon LPS treatment, CARKL is rapidly down-

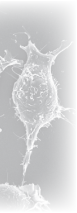

regulated in mice and humans, *in vitro* and *in vivo*. This downregulation occurs in synchronization with the induction of IL-6 and TNFα and is required for proper classical activation. CARKL-loss promotes the rerouting of glucose from aerobic to anaerobic metabolism, similar to LPS-induction. Moreover, CARKL-loss causes a marked potentiation of LPS-stimulated TNFα, IL-6, and IL-10 response. Therefore, a reduction in CARKL can induce a mild M1-phenotype in macrophages. In contrast, CARKL is mildly increased during alternative activation. Similar to IL-4 stimulation, overexpression of CARKL blocks the production of a number of LPS-induced cytokines, e.g. TNFα, IL-6, IL-1α, IL-β, and CxCL2, while M2-related molecules are upregulated, such as Mrc-1. CARKL, therefore, seems to sensitize macrophages to M2 polarization. During LPS stimulation, PPP activity is increased and accompanied by an increase in NADH and GSH levels. However, when CARKL-overexpressing cells are stimulated with LPS, there is a reduction in NADH but not NAD^+ levels, increasing the NAD^+/NADH ratio, as well as a reduction in the GSH/GSSG ratio. CARKL, therefore, acts as an important metabolic catalyst for maintaining cellular redox state during activation [154].

4. Coupling between the actin cytoskeleton and cell metabolism

Macrophage polarization is not only recognized by substantial adaptations in metabolic activity, but is also accompanied by distinctive alterations in the arrangement of the actin cytoskeleton. The formation of cellular protrusions and podosomes as well as the ability to spread are differently affected when macrophages obtain a M1 or M2 polarization state [90, 204, 205], raising the question whether coupling also exists between macrophage metabolism and morphodynamic behavior.

ATP is involved in, and affects, many different facets of actin dynamics. As outlined in more detail above, binding of ATP to actin monomers determines actin filament properties [9, 206] and influences binding of ABPs, while hydrolysis of this ATP by non-muscle myosin ATPase is involved in force generation for contraction [207]. In addition, ATP binding and hydrolysis on the Arp2/3 complex influence actin filament branch formation and stability [4, 6] (see 1.1 above). Furthermore, since GTP levels are tightly linked to ATP levels, the normal function of the Rho GTPases that regulate actin polymerization is also under the influence of cellular [ATP] [208]. When cellular ATP is depleted, actin filaments are stabilized by decreasing actin-ATP hydrolysis, thereby reducing ATP-consumption [209, 210]. This leads to the aggregation of actin filaments that in turn sensitizes the cells to apoptosis [211].

Several studies have suggested that morphodynamic processes are driven by local ATP-supply. For example, when ATP-supply via the adenylate kinase system is experimentally targeted to focal contacts in mouse embryonic fibroblasts, motility

and spreading is enhanced [212]. In addition, glycolytic enzymes (especially GAPDH and aldolase) have been shown to associate with the actin cytoskeleton [213-215] and to be enriched at sites of dynamic actin remodeling, such as pseudopodia [216, 217] and lamellipodia [218], promoting cell motility.

Apart from supplying ATP, cell metabolism is also an important regulator of cellular pH (via the production of lactate and H^+) [219] and redox status (via ROS production and supplying reducing molecules such as NADPH). As mentioned in 1.3, actin itself, as well as several ABPs involved in actin filament assembly and disassembly (for example cofilin), is regulated by these factors.

Based on the cumulative evidence mentioned in this chapter and a constant stream of new findings there is no doubt that the metabolic state of the cell is an important regulator of the morphodynamic behavior of the cell. However, we should also realize that this is a relatively new area of interest, and many details on the metabo-morphodynamic coupling are still not known.

5. Aim and outline of the thesis

The aim of this thesis was, therefore, to investigate this coupling in more detail, focusing on the relationship between actin dynamics and cellular energy metabolism in macrophages. The two macrophage lineages (RAW 264.7 and Maf-DKO) that were used during our investigation were first compared with respect to their actin-based morphology, phagocytic activity, proliferation, and carbohydrate metabolism in chapter 2. New insights regarding the mechanism of CK-B-mediated ATP supply at subcellular sites of actin polymerization were obtained from the results described in chapter 3. In chapter 4 the importance of glucose for actin-based morphodynamic processes such as membrane protrusion formation and phagocytosis was investigated, and in chapter 5 a regulatory role for NAD^+ (the key metabolite in cellular redox regulation) in macrophage morphodynamics was identified. Finally, the major findings of chapters 2 to 5 are discussed in a broader context in chapter 6.

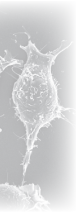

References

1. Pollard, T.D. & Cooper, J.A. Actin, a Central Player in Cell Shape and Movement. *Science* **326**, 1208-1212 (2009).
2. Chhabra, E.S. & Higgs, H.N. The many faces of actin: matching assembly factors with cellular structures. *Nat. Cell Biol.* **9**, 1110-1121 (2007).
3. Dos Remedios, C.G. *et al.* Actin Binding Proteins: Regulation of Cytoskeletal Microfilaments. *Physiol. Rev.* **83**, 433-473 (2003).
4. Pollard, T.D. Regulation of Actin Filament Assembly by Arp2/3 Complex and Formins. *Annu. Rev. Biophys. Biomol. Struct.* **36**, 451-477 (2007).
5. Pollard, T.D. & Borisy, G.G. Cellular motility driven by assembly and disassembly of actin filaments. *Cell* **112**, 453-465 (2003).
6. Ingerman, E., Hsiao, J.Y. & Mullins, R.D. Arp2/3 complex ATP hydrolysis promotes lamellipodial actin network disassembly but is dispensable for assembly. *J. Cell Biol.* **200**, 619-633 (2013).
7. Li, F. & Higgs, H.N. The Mouse Formin mDia1 Is a Potent Actin Nucleation Factor Regulated by Autoinhibition. *Curr. Biol.* **13**, 1335-1340 (2003).
8. Carlier, M.F. & Pantaloni, D. Direct evidence for ADP-Pi-F-actin as the major intermediate in ATP-actin polymerization. Rate of dissociation of Pi from actin filaments. *Biochemistry (Mosc).* **25**, 7789-7792 (1986).
9. Pfaendtner, J., Branduardi, D., Parrinello, M., Pollard, T.D. & Voth, G.A. Nucleotide-dependent conformational states of actin. *Proc. Natl. Acad. Sci. U. S. A.* **106**, 12723-12728 (2009).
10. Carlier, M.-F. & Pantaloni, D., Vol. 282 23005-230092007).
11. Urban, E., Jacob, S., Nemethova, M., Resch, G.P. & Small, J.V. Electron tomography reveals unbranched networks of actin filaments in lamellipodia. *Nat. Cell Biol.* **12**, 429-435 (2010).
12. Small, J.V., Winkler, C., Vinzenz, M. & Schmeiser, C. Reply: Visualizing branched actin filaments in lamellipodia by electron tomography. *Nat. Cell Biol.* **13**, 1013 (2011).
13. Yang, C. & Svitkina, T. Visualizing branched actin filaments in lamellipodia by electron tomography. *Nat. Cell Biol.* **13**, 1012-1013 (2011).
14. Petit, V. & Thiery, J.-P. Focal adhesions: Structure and dynamics. *Biol. Cell* **92**, 477-494 (2000).
15. Albiges-Rizo, C., Destaing, O., Fourcade, B., Planus, E. & Block, M.R. Actin machinery and mechanosensitivity in invadopodia, podosomes and focal adhesions. *J. Cell Sci.* **122**, 3037-3049 (2009).
16. Galbraith, C.G., Yamada, K.M. & Galbraith, J.A. Polymerizing Actin Fibers Position Integrins Primed to Probe for Adhesion Sites. *Science* **315**, 992-995 (2007).
17. Kress, H. *et al.* Filopodia act as phagocytic tentacles and pull with discrete steps and a load-dependent velocity. *Proc. Natl. Acad. Sci. U. S. A.* **104**, 11633-11638 (2007).
18. Aderem, A. & Underhill, D.M. Mechanisms of phagocytosis in macrophages. *Annu. Rev. Immunol.* **17**, 593-623 (1999).
19. Cougoule, C., Wiedemann, A., Lim, J. & Caron, E. Phagocytosis, an alternative model system for the study of cell adhesion. *Semin. Cell Dev. Biol.* **15**, 679-689 (2004).
20. Hotulainen, P. & Hoogenraad, C.C. Actin in dendritic spines: connecting dynamics to function. *J. Cell Biol.* **189**, 619-629 (2010).
21. Tojkander, S., Gateva, G. & Lappalainen, P. Actin stress fibers - assembly, dynamics and biological roles. *J. Cell Sci.* **125**, 1855-1864 (2012).
22. Charras, G. & Paluch, E. Blebs lead the way: how to migrate without lamellipodia. *Nat. Rev. Mol. Cell Biol.* **9**, 730-736 (2008).
23. Charras, G.T. A short history of blebbing. *J. Microsc.* **231**, 466-478 (2008).
24. Groves, J.T. & Kuriyan, J. Molecular mechanisms in signal transduction at the membrane. *Nat. Struct. Mol. Biol.* **17**, 659-665 (2010).
25. Watanabe, N., Kato, T., Fujita, A., Ishizaki, T. & Narumiya, S. Cooperation between mDia1 and ROCK in Rho-induced actin reorganization. *Nat. Cell Biol.* **1**, 136-143 (1999).
26. Li, F. & Higgs, H.N. Dissecting Requirements for Auto-inhibition of Actin Nucleation by the Formin, mDia1. *J. Biol. Chem.* **280**, 6986-6992 (2005).
27. Ridley, A.J. & Hall, A. The small GTP-binding protein rho regulates the assembly of focal adhesions and actin stress fibers in response to growth factors. *Cell* **70**, 389-399 (1992).
28. Ridley, A.J., Paterson, H.F., Johnston, C.L., Diekmann, D. & Hall, A. The small GTP-binding protein rac regulates growth factor-induced membrane ruffling. *Cell* **70**, 401-410 (1992).
29. Nobes, C.D. & Hall, A. Rho, Rac, and Cdc42 GTPases regulate the assembly of multimolecular focal complexes associated with actin stress fibers, lamellipodia, and filopodia. *Cell* **81**, 53-62 (1995).
30. Price, L.S., Leng, J., Schwartz, M.A. & Bokoch, G.M. Activation of Rac and Cdc42 by Integrins Mediates Cell Spreading. *Mol. Biol. Cell* **9**, 1863-1871 (1998).

31. Kraynov, V.S. *et al.* Localized Rac Activation Dynamics Visualized in Living Cells. *Science* **290**, 333-337 (2000).
32. Nalbant, P., Hodgson, L., Kraynov, V., Toutchkine, A. & Hahn, K.M. Activation of Endogenous Cdc42 Visualized in Living Cells. *Science* **305**, 1615-1619 (2004).
33. Kurokawa, K. & Matsuda, M. Localized RhoA Activation as a Requirement for the Induction of Membrane Ruffling. *Mol. Biol. Cell* **16**, 4294-4303 (2005).
34. Pertz, O., Hodgson, L., Klemke, R.L. & Hahn, K.M. Spatiotemporal dynamics of RhoA activity in migrating cells. *Nature* **440**, 1069-1072 (2006).
35. Machacek, M. *et al.* Coordination of Rho GTPase activities during cell protrusion. *Nature* **461**, 99-103 (2009).
36. Hoppe, A.D. & Swanson, J.A. Cdc42, Rac1, and Rac2 Display Distinct Patterns of Activation during Phagocytosis. *Mol. Biol. Cell* **15**, 3509-3519 (2004).
37. Picard, M. *et al.* Spatial and temporal activation of the small GTPases RhoA and Rac1 by the netrin-1 receptor UNC5a during neurite outgrowth. *Cell. Signal.* **21**, 1961-1973 (2009).
38. Stossel, T.P., Fenteany, G. & Hartwig, J.H. Cell surface actin remodeling. *J. Cell Sci.* **119**, 3261-3264 (2006).
39. Silacci, P. *et al.* Gelsolin superfamily proteins: key regulators of cellular functions. *Cell. Mol. Life Sci.* **61**, 2614-2623 (2004).
40. Stossel, T.P. *et al.* Filamins as integrators of cell mechanics and signalling. *Nat. Rev. Mol. Cell Biol.* **2**, 138-145 (2001).
41. Courson, D.S. & Rock, R.S. Actin Cross-link Assembly and Disassembly Mechanics for α-Actinin and Fascin. *J. Biol. Chem.* **285**, 26350-26357 (2010).
42. Yamada, H. *et al.* Stabilization of Actin Bundles by a Dynamin 1/Cortactin Ring Complex Is Necessary for Growth Cone Filopodia. *J. Neurosci.* **33**, 4514-4526 (2013).
43. Paavilainen, V.O., Bertling, E., Falck, S. & Lappalainen, P. Regulation of cytoskeletal dynamics by actin-monomer-binding proteins. *Trends Cell Biol.* **14**, 386-394 (2004).
44. Sumi, T., Matsumoto, K., Takai, Y. & Nakamura, T. Cofilin Phosphorylation and Actin Cytoskeletal Dynamics Regulated by Rho- and Cdc42-Activated Lim-Kinase 2. *J. Cell Biol.* **147**, 1519-1532 (1999).
45. Dalle-Donne, I., Rossi, R., Milzani, A., Di Simplicio, P. & Colombo, R. The actin cytoskeleton response to oxidants: from small heat shock protein phosphorylation to changes in the redox state of actin itself. *Free Radic. Biol. Med.* **31**, 1624-1632 (2001).
46. Hung, R.-J., Pak, C.W. & Terman, J.R. Direct Redox Regulation of F-Actin Assembly and Disassembly by Mical. *Science* **334**, 1710-1713 (2011).
47. Kim, J.-S., Huang, T.Y. & Bokoch, G.M. Reactive Oxygen Species Regulate a Slingshot-Cofilin Activation Pathway. *Mol. Biol. Cell* **20**, 2650-2660 (2009).
48. Frantz, C. *et al.* Cofilin is a pH sensor for actin free barbed end formation: role of phosphoinositide binding. *J. Cell Biol.* **183**, 865-879 (2008).
49. Garg, R., Peddada, N., Sagar, A., Nihalani, D. & Ashish Visual Insight into How Low pH Alone Can Induce Actin-severing Ability in Gelsolin under Calcium-free Conditions. *J. Biol. Chem.* **286**, 20387-20397 (2011).
50. Crevenna, A.H. *et al.* Electrostatics control actin filament nucleation and elongation kinetics. *J. Biol. Chem.* **288**, 12102-12113 (2013).
51. Liu, X., Shu, S., Hong, M.-S.S., Levine, R.L. & Korn, E.D. Phosphorylation of actin Tyr-53 inhibits filament nucleation and elongation and destabilizes filaments. *Proc. Natl. Acad. Sci. U. S. A.* **103**, 13694-13699 (2006).
52. Liu, X., Shu, S., Hong, M.-S.S., Yu, B. & Korn, E.D. Mutation of Actin Tyr-53 Alters the Conformations of the DNase I-binding Loop and the Nucleotide-binding Cleft. *J. Biol. Chem.* **285**, 9729-9739 (2010).
53. Baek, K. *et al.* Modulation of actin structure and function by phosphorylation of Tyr-53 and profilin binding. *Proc. Natl. Acad. Sci. U. S. A.* **105**, 11748-11753 (2008).
54. Saha, S. *et al.* Arginylation Regulates Intracellular Actin Polymer Level by Modulating Actin Properties and Binding of Capping and Severing Proteins. *Mol. Biol. Cell* **21**, 1350-1361 (2010).
55. Karakozova, M. *et al.* Arginylation of ß-Actin Regulates Actin Cytoskeleton and Cell Motility. *Science* **313**, 192-196 (2006).
56. Cooper, G. in The Cell: A Molecular Approach, Edn. 2nd (Sinauer Associates, Sunderland (MA); 2000).
57. Araki, N. Role of microtubules and myosins in Fc gamma receptor-mediated phagocytosis. *Front. Biosci.* **11**, 1479-1490 (2006).
58. Olazabal, I.M. *et al.* Rho-Kinase and Myosin-II Control Phagocytic Cup Formation during CR, but Not FcgammaR, Phagocytosis. *Curr. Biol.* **12**, 1413-1418 (2002).
59. Lee, C.-S., Choi, C.-K., Shin, E.-Y., Schwartz, M.A. & Kim, E.-G. Myosin II directly binds and inhibits Dbl family guanine nucleotide exchange factors: a possible link to Rho family GTPases. *J. Cell Biol.* **190**, 663-674 (2010).
60. Swanson, J. *et al.* A contractile activity that closes phagosomes in macrophages. *J. Cell Sci.* **112**, 307 - 316 (1999).
61. Diakonova, M., Bokoch, G. & Swanson, J.A. Dynamics of Cytoskeletal Proteins during Fcγ Receptor-mediated Phagocytosis in Macrophages. *Mol. Biol. Cell* **13**, 402-411 (2002).
62. Cox, D. *et al.* Myosin X is a downstream effector of PI(3)K during phagocytosis. *Nat. Cell Biol.* **4**, 469-477

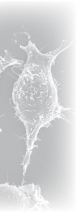

(2002).
63. Dart, A.E., Tollis, S., Bright, M.D., Frankel, G. & Endres, R.G. The motor protein myosin 1G functions in FcγR-mediated phagocytosis. *J. Cell Sci.* **125**, 6020-6029 (2012).
64. Weaver, A. Invadopodia: Specialized Cell Structures for Cancer Invasion. *Clin. Exp. Metastasis* **23**, 97-105 (2006).
65. Vicente-Manzanares, M. & Sanchez-Madrid, F. Role of the cytoskeleton during leukocyte responses. *Nat. Rev. Immunol.* **4**, 110-122 (2004).
66. Murray, P.J. & Wynn, T.A. Protective and pathogenic functions of macrophage subsets. *Nat. Rev. Immunol.* **11**, 14 (2011).
67. Geissmann, F. *et al.* Development of Monocytes, Macrophages, and Dendritic Cells. *Science* **327**, 656-661 (2010).
68. Mosser, D.M. & Edwards, J.P. Exploring the full spectrum of macrophage activation. *Nat. Rev. Immunol.* **8**, 958 (2008).
69. Davies, L.C. *et al.* A quantifiable proliferative burst of tissue macrophages restores homeostatic macrophage populations after acute inflammation. *Eur. J. Immunol.* **41**, 2155-2164 (2011).
70. Yona, S. *et al.* Fate Mapping Reveals Origins and Dynamics of Monocytes and Tissue Macrophages under Homeostasis. *Immunity* **38**, 79-91 (2013).
71. Hashimoto, D. *et al.* Tissue-Resident Macrophages Self-Maintain Locally throughout Adult Life with Minimal Contribution from Circulating Monocytes. *Immunity* **38**, 792-804 (2013).
72. Jenkins, S.J. *et al.* Local Macrophage Proliferation, Rather than Recruitment from the Blood, Is a Signature of TH2 Inflammation. *Science* **332**, 1284-1288 (2011).
73. Jenkins, S.J. *et al.* IL-4 directly signals tissue-resident macrophages to proliferate beyond homeostatic levels controlled by CSF-1. *J. Exp. Med.* **210**, 2477-2491 (2013).
74. Chorro, L. *et al.* Langerhans cell (LC) proliferation mediates neonatal development, homeostasis, and inflammation-associated expansion of the epidermal LC network. *J. Exp. Med.* **206**, 3089-3100 (2009).
75. Schulz, C. *et al.* A Lineage of Myeloid Cells Independent of Myb and Hematopoietic Stem Cells. *Science* **336**, 86-90 (2012).
76. Murphy, J., Summer, R., Wilson, A.A., Kotton, D.N. & Fine, A. The Prolonged Life-Span of Alveolar Macrophages. *Am. J. Respir. Cell Mol. Biol.* **38**, 380-385 (2008).
77. Ajami, B., Bennett, J.L., Krieger, C., Tetzlaff, W. & Rossi, F.M.V. Local self-renewal can sustain CNS microglia maintenance and function throughout adult life. *Nat. Neurosci.* **10**, 1538-1543 (2007).
78. Kanitakis, J., Petruzzo, P. & Dubernard, J.-M. Turnover of Epidermal Langerhans' Cells. *N. Engl. J. Med.* **351**, 2661-2662 (2004).
79. Sieweke, M.H. & Allen, J.E. Beyond Stem Cells: Self-Renewal of Differentiated Macrophages. *Science* **342** (2013).
80. Davies, L.C., Jenkins, S.J., Allen, J.E. & Taylor, P.R. Tissue-resident macrophages. *Nat. Immunol.* **14**, 986-995 (2013).
81. Mantovani, A., Sica, A. & Locati, M. Macrophage Polarization Comes of Age. *Immunity* **23**, 344-346 (2005).
82. Mills, C.D., Kincaid, K., Alt, J.M., Heilman, M.J. & Hill, A.M. M-1/M-2 Macrophages and the Th1/Th2 Paradigm. *J. Immunol.* **164**, 6166-6173 (2000).
83. Cassetta, L., Cassol, E. & Poli, G. Macrophage Polarization in Health and Disease. *ScientificWorldJournal* **11**, 12 (2011).
84. Galli, S.J., Borregaard, N. & Wynn, T.A. Phenotypic and functional plasticity of cells of innate immunity: macrophages, mast cells and neutrophils. *Nat. Immunol.* **12**, 1035-1044 (2011).
85. Mantovani, A. *et al.* The chemokine system in diverse forms of macrophage activation and polarization. *Trends Immunol.* **25**, 677-686 (2004).
86. Stout, R.D. *et al.* Macrophages Sequentially Change Their Functional Phenotype in Response to Changes in Microenvironmental Influences. *J. Immunol.* **175**, 342-349 (2005).
87. Gordon, S. Alternative activation of macrophages. *Nat. Rev. Immunol.* **3**, 23-35 (2003).
88. Wynn, T.A. & Barron, L. Macrophages: Master Regulators of Inflammation and Fibrosis. *Semin. Liver Dis.* **30**, 245-257 (2010).
89. Pixley, F.J. Macrophage Migration and Its Regulation by CSF-1. *Int. J. Cell Biol.* **2012**, 501962 (2012).
90. Cougoule, C. *et al.* Blood leukocytes and macrophages of various phenotypes have distinct abilities to form podosomes and to migrate in 3D environments. *Eur. J. Cell Biol.* **91**, 938-949 (2012).
91. Linder, S., Hufner, K., Wintergerst, U. & Aepfelbacher, M. Microtubule-dependent formation of podosomal adhesion structures in primary human macrophages. *J. Cell Sci.* **113**, 4165-4176 (2000).
92. Linder, S. The matrix corroded: podosomes and invadopodia in extracellular matrix degradation. *Trends Cell Biol.* **17**, 107-117 (2007).
93. Bianco, C., Götze, O. & Cohn, Z.A. Regulation of macrophage migration by products of the complement system. *Proc. Natl. Acad. Sci. U. S. A.* **76**, 888-891 (1979).

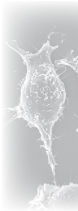

94. Vonna, L., Wiedemann, A., Aepfelbacher, M. & Sackmann, E. Micromechanics of filopodia mediated capture of pathogens by macrophages. *Eur. Biophys. J.* **36**, 145-151 (2007).
95. Patel, P.C. & Harrison, R.E. Membrane Ruffles Capture C3bi-opsonized Particles in Activated Macrophages. *Mol. Biol. Cell* **19**, 4628-4639 (2008).
96. Flannagan, R.S., Harrison, R.E., Yip, C.M., Jaqaman, K. & Grinstein, S. Dynamic macrophage "probing" is required for the efficient capture of phagocytic targets. *J. Cell Biol.* **191**, 1205-1218 (2010).
97. Caron, E. & Hall, A. Identification of Two Distinct Mechanisms of Phagocytosis Controlled by Different Rho GTPases. *Science* **282**, 1717-1721 (1998).
98. May, R.C. & Machesky, L.M. Phagocytosis and the actin cytoskeleton. *J. Cell Sci.* **114**, 1061-1077 (2001).
99. Dart, A.E., Donnelly, S.K., Holden, D.W., Way, M. & Caron, E. Nck and Cdc42 co-operate to recruit N-WASP to promote FcγR-mediated phagocytosis. *J. Cell Sci.* **125**, 2825-2830 (2012).
100. Swanson, J. Shaping cups into phagosomes and macropinosomes. *Nat. Rev. Mol. Cell Biol.* **9**, 639 - 649 (2008).
101. Allen, L. & Aderem, A. Molecular definition of distinct cytoskeletal structures involved in complement- and Fc receptor-mediated phagocytosis in macrophages. *J. Exp. Med.* **184**, 627 - 637 (1996).
102. Bianco, C., Griffin, F.M. & Silverstein, S.C. Studies of the macrophage complement receptor. Alteration of receptor function upon macrophage activation. *J. Exp. Med.* **141**, 1278-1290 (1975).
103. Wright, S.D. & Meyer, B.C. Phorbol esters cause sequential activation and deactivation of complement receptors on polymorphonuclear leukocytes. *J. Immunol.* **136**, 1759-1764 (1986).
104. Colucci-Guyon, E. *et al.* A Role for Mammalian Diaphanous-Related Formins in Complement Receptor (CR3)-Mediated Phagocytosis in Macrophages. *Curr. Biol.* **15**, 2007-2012 (2005).
105. Scott, C.C. *et al.* Phosphatidylinositol-4,5-bisphosphate hydrolysis directs actin remodeling during phagocytosis. *J. Cell Biol.* **169**, 139-149 (2005).
106. Beemiller, P. *et al.* A Cdc42 Activation Cycle Coordinated by PI 3-Kinase during Fc Receptor-mediated Phagocytosis. *Mol. Biol. Cell* **21**, 470-480 (2010).
107. Swanson, J.A. & Watts, C. Macropinocytosis. *Trends Cell Biol.* **5**, 424-428 (1995).
108. Kerr, M.C. & Teasdale, R.D. Defining macropinocytosis. *Traffic* **10**, 364-371 (2009).
109. Daniel, J.L., Molish, I.R., Robkin, L. & Holmsen, H. Nucleotide exchange between cytosolic ATP and F-actin-bound ADP may be a major energy-utilizing process in unstimulated platelets. *Eur. J. Biochem.* **156**, 677-683 (1986).
110. Culic, O., Gruwel, M.L. & Schrader, J. Energy turnover of vascular endothelial cells. *Am. J. Physiol.* **273**, C205-C213 (1997).
111. Mathews, C.K., van Holde, K.E. & Ahern, K.G. *Biochemistry*, Edn. 3. (Benjamin/Cummings, San Francisco; 1999).
112. Rossignol, R. *et al.* Energy Substrate Modulates Mitochondrial Structure and Oxidative Capacity in Cancer Cells. *Cancer Res.* **64**, 985-993 (2004).
113. Marroquin, L.D., Hynes, J., Dykens, J.A., Jamieson, J.D. & Will, Y. Circumventing the Crabtree Effect: Replacing Media Glucose with Galactose Increases Susceptibility of HepG2 Cells to Mitochondrial Toxicants. *Toxicol. Sci.* **97**, 539-547 (2007).
114. Salway, J. *Metabolism at a glance*, Edn. 3rd. (Blackwell Publishing, Oxford; 2004).
115. Wood, I.S. & Trayhurn, P. Glucose transporters (GLUT and SGLT): expanded families of sugar transport proteins. *Br. J. Nutr.* **89**, 3-9 (2003).
116. Elsas, L.J. & Longo, N. Glucose Transporters. *Annu. Rev. Med.* **43**, 377-393 (1992).
117. Bricker, D.K. *et al.* A Mitochondrial Pyruvate Carrier Required for Pyruvate Uptake in Yeast, Drosophila, and Humans. *Science* **337**, 96-100 (2012).
118. Herzig, S. *et al.* Identification and Functional Expression of the Mitochondrial Pyruvate Carrier. *Science* **337**, 93-96 (2012).
119. Sun, R.C. & Denko, N.C. Hypoxic regulation of glutamine metabolism through HIF1 and SIAH2 supports lipid synthesis that is necessary for tumor growth. *Cell Metab.* **19**, 285-292 (2014).
120. Aoki, T.T., Brennan, M.F., Müller, W.A. & Cahill jr, G.F. Amino acid levels across normal forearm muscle: Whole blood vs. plasma. *Adv. Enzyme Regul.* **12**, 157-165 (1974).
121. Bode, B.P. Recent Molecular Advances in Mammalian Glutamine Transport. *J. Nutr.* **131**, 2475S-2485S (2001).
122. DeBerardinis, R.J. & Cheng, T. Q's next: the diverse functions of glutamine in metabolism, cell biology and cancer. *Oncogene* **29**, 313-324 (2009).
123. Le, A. *et al.* Glucose-Independent Glutamine Metabolism via TCA Cycling for Proliferation and Survival in B Cells. *Cell Metab.* **15**, 110-121 (2012).
124. Metallo, C.M. *et al.* Reductive glutamine metabolism by IDH1 mediates lipogenesis under hypoxia. *Nature* **481**, 380-384 (2012).
125. Anastasiou, D. & Cantley, L.C. Breathless cancer cells get fat on glutamine. *Cell Res.* **22**, 443-446 (2012).
126. Houtkooper, R.H., Canto, C., Wanders, R.J. & Auwerx, J. The Secret Life of NAD+: An Old Metabolite Controlling New Metabolic Signaling Pathways. *Endocr. Rev.* **31**, 194-223 (2010).

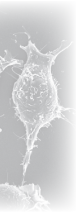

127. Pollak, N., Niere, M. & Ziegler, M. NAD Kinase Levels Control the NADPH Concentration in Human Cells. *J. Biol. Chem.* **282**, 33562-33571 (2007).
128. Nikiforov, A., Doelle, C., Niere, M. & Ziegler, M. Pathways and subcellular compartmentation of NAD biosynthesis in human cells: From entry of extracellular precursors to mitochondrial NAD generation. *J Biol Chem* (2011).
129. Dölle, C., Niere, M., Lohndal, E. & Ziegler, M. Visualization of subcellular NAD pools and intra-organellar protein localization by poly-ADP-ribose formation. *Cell. Mol. Life Sci.* **67**, 433-443 (2010).
130. Agledal, L., Niere, M. & Ziegler, M. The phosphate makes a difference: cellular functions of NADP. *Redox Rep.* **15**, 2-10 (2010).
131. Jankowski, A. & Grinstein, S. Modulation of the Cytosolic and Phagosomal pH by the NADPH Oxidase. *Antioxid. Redox Signal.* **4**, 61-68 (2002).
132. Ying, W. NAD+/NADH and NADP+/NADPH in Cellular Functions and Cell Death: Regulation and Biological Consequences. *Antioxid. Redox Signal.* **10**, 179-206 (2008).
133. Grahnert, A. *et al.* NAD+: a modulator of immune functions. *Innate Immun.* (2010).
134. Bruzzone, S. *et al.* Catastrophic NAD^+ Depletion in Activated T Lymphocytes through Nampt Inhibition Reduces Demyelination and Disability in EAE. *PLoS ONE* **4**, e7897 (2009).
135. Busso, N. *et al.* Pharmacological Inhibition of Nicotinamide Phosphoribosyltransferase/Visfatin Enzymatic Activity Identifies a New Inflammatory Pathway Linked to NAD. *PLoS ONE* **3**, e2267 (2008).
136. Van Gool, F. *et al.* Intracellular NAD levels regulate tumor necrosis factor protein synthesis in a sirtuin-dependent manner. *Nat. Med.* **15**, 206-210 (2009).
137. Schilling, E. *et al.* Inhibition of nicotinamide phosphoribosyltransferase modifies LPS-induced inflammatory responses of human monocytes. *Innate Immun.* **0**, 1-13 (2011).
138. Wallimann, T., Wyss, M., Brdiczka, D., Nicolay, K. & Eppenberger, H.M. Intracellular compartmentation, structure and function of creatine kinase isoenzymes in tissues with high and fluctuating energy demands: the 'phosphocreatine circuit' for cellular energy homeostasis. *Biochem. J.* **281**, 21-40 (1992).
139. Wyss, M. & Kaddurah-Daouk, R. Creatine and Creatinine Metabolism. *Physiol. Rev.* **80**, 1107-1213 (2000).
140. Speer, O. *et al.* Creatine transporters: a reappraisal. *Mol. Cell. Biochem.* **256-257**, 407-424 (2004).
141. Wallimann, T., Tokarska-Schlattner, M. & Schlattner, U. The creatine kinase system and pleiotropic effects of creatine. *Amino Acids* **40**, 1271-1296 (2011).
142. Wallimann, T., Schlösser, T. & Eppenberger, H.M. Function of M-line-bound creatine kinase as intramyofibrillar ATP regenerator at the receiving end of the phosphorylcreatine shuttle in muscle. *J. Biol. Chem.* **259**, 5238-5246 (1984).
143. Kraft, T., Hornemann, T., Stolz, M., Nier, V. & Wallimann, T. Coupling of creatine kinase to glycolytic enzymes at the sarcomeric I-band of skeletal muscle: a biochemical study in situ. *J. Muscle Res. Cell Motil.* **21**, 691-703 (2000).
144. Dillon, P.F. & Clark, J.F. The theory of diazymes and functional coupling of pyruvate kinase and creatine kinase. *J. Theor. Biol.* **143**, 275-284 (1990).
145. Schlattner, U., Tokarska-Schlattner, M. & Wallimann, T. Mitochondrial creatine kinase in human health and disease. *Biochim. Biophys. Acta* **1762**, 164-180 (2006).
146. Yoshizaki, K., Watari, H. & Radda, G.K. Role of phosphocreatine in energy transport in skeletal muscle of bullfrog studied by 31P-NMR. *Biochim. Biophys. Acta* **1051**, 144-150 (1990).
147. Loike, J.D., Kozler, V.F. & Silverstein, S.C. Creatine kinase expression and creatine phosphate accumulation are developmentally regulated during differentiation of mouse and human monocytes. *J. Exp. Med.* **159**, 746-757 (1984).
148. Weintz, G. *et al.* The phosphoproteome of toll-like receptor-activated macrophages. *Mol Syst Biol* **6** (2010).
149. Nau, G.J. *et al.* Human macrophage activation programs induced by bacterial pathogens. *Proc. Natl. Acad. Sci. U. S. A.* **99**, 1503-1508 (2002).
150. Loike, J.D., Somes, M. & Silverstein, S.C. Creatine uptake, metabolism, and efflux in human monocytes and macrophages. *Am. J. Physiol.* **251**, C128-135 (1986).
151. Loike, J.D., Kozler, V.F. & Silverstein, S.C. Increased ATP and creatine phosphate turnover in phagocytosing mouse peritoneal macrophages. *J. Biol. Chem.* **254**, 9558-9564. (1979).
152. Kuiper, J.W.P. *et al.* Creatine Kinase–Mediated ATP Supply Fuels Actin-Based Events in Phagocytosis. *PLoS Biol.* **6**, e51 (2008).
153. Biswas, Subhra K. & Mantovani, A. Orchestration of Metabolism by Macrophages. *Cell Metab.* **15**, 432-437 (2012).
154. Haschemi, A. *et al.* The Sedoheptulose Kinase CARKL Directs Macrophage Polarization through Control of Glucose Metabolism. *Cell Metab.* **15**, 813-826 (2012).
155. Takeda, N. *et al.* Differential activation and antagonistic function of HIF-α isoforms in macrophages are essential for NO homeostasis. *Genes Dev.* **24**, 491-501 (2010).
156. Odegaard, J.I. *et al.* Macrophage-specific PPARγ controls alternative activation and improves insulin resis-

tance. *Nature* **447**, 1116-1120 (2007).
157. Cohen, M.S., Ryan, J.L. & Root, R.K. The oxidative metabolism of thioglycollate-elicited mouse peritoneal macrophages: the relationship between oxygen, superoxide and hydrogen peroxide and the effect of monolayer formation. *J. Immunol.* **127**, 1007-1011 (1981).
158. Rodríguez-Prados, J.-C. *et al.* Substrate Fate in Activated Macrophages: A Comparison between Innate, Classic, and Alternative Activation. *J. Immunol.* **185**, 605-614 (2010).
159. Roiniotis, J. *et al.* Hypoxia Prolongs Monocyte/Macrophage Survival and Enhanced Glycolysis Is Associated with Their Maturation under Aerobic Conditions. *J. Immunol.* **182**, 7974-7981 (2009).
160. Simon, L.M., Axline, S.G., Horn, B.R. & Robin, E.D. Adaptations of energy metabolism in the cultivated macrophage. *J. Exp. Med.* **138**, 1413-1425 (1973).
161. Bennett, W.E. & Cohn, Z.A. The isolation and selected properties of blood monocytes. *J. Exp. Med.* **123**, 145-160 (1966).
162. Fu, Y., Maianu, L., Melbert, B.R. & Garvey, W.T. Facilitative glucose transporter gene expression in human lymphocytes, monocytes, and macrophages: a role for GLUT isoforms 1, 3, and 5 in the immune response and foam cell formation. *Blood Cells. Mol. Dis.* **32**, 182-190 (2004).
163. Ahmed, N., Kansara, M. & Berridge, M.V. Acute regulation of glucose transport in a monocyte-macrophage cell line: Glut-3 affinity for glucose is enhanced during the respiratory burst. *Biochem. J.* **327**, 369-375 (1997).
164. Fukuzumi, M., Shinomiya, H., Shimizu, Y., Ohishi, K. & Utsumi, S. Endotoxin-induced enhancement of glucose influx into murine peritoneal macrophages via GLUT1. *Infect. Immun.* **64**, 108-112 (1996).
165. Maratou, E. *et al.* Glucose transporter expression on the plasma membrane of resting and activated white blood cells. *Eur. J. Clin. Invest.* **37**, 282-290 (2007).
166. Vats, D. *et al.* Oxidative metabolism and PGC-1β attenuate macrophage-mediated inflammation. *Cell Metab.* **4**, 13-24 (2006).
167. Murata, Y., Shimamura, T. & Hamuro, J. The polarization of Th1/Th2 balance is dependent on the intracellular thiol redox status of macrophages due to the distinctive cytokine production. *Int. Immunol.* **14**, 201-212 (2002).
168. Zhang, Y. *et al.* ROS play a critical role in the differentiation of alternatively activated macrophages and the occurrence of tumor-associated macrophages. *Cell Res.* **23**, 898-914 (2013).
169. Small, C.A., Rogers, M.P., Goodacre, J.A. & Yeaman, S.J. Phosphorylation and activation of hormone-sensitive lipase in isolated macrophages. *FEBS Lett.* **279**, 323-326 (1991).
170. Goldberg, D.I. & Khoo, J.C. Secretion of the lysosomal acid triacylglycerol hydrolase precursor by J774 Macrophages. *Biochim. Biophys. Acta* **960**, 200-209 (1988).
171. Stray, N., Letnes, H. & Blomhoff, J.P. Intracellular regulation of lipoprotein lipase in human monocyte-derived macrophages. *Biochim. Biophys. Acta* **1045**, 280-284 (1990).
172. Mahoney, E.M., Khoo, J.C. & Steinberg, D. Lipoprotein lipase secretion by human monocytes and rabbit alveolar macrophages in culture. *Proc. Natl. Acad. Sci. U. S. A.* **79**, 1639-1642 (1982).
173. Chait, A., Iverius, P.H. & Brunzell, J.D. Lipoprotein lipase secretion by human monocyte-derived macrophages. *J. Clin. Invest.* **69**, 490-493 (1982).
174. Khoo, J.C., Mahoney, E.M. & Witztum, J.L. Secretion of lipoprotein lipase by macrophages in culture. *J. Biol. Chem.* **256**, 7105-7108 (1981).
175. Domin, W.S., Chait, A. & Deeb, S.S. Transcriptional activation of the lipoprotein lipase gene in macrophages by dexamethasone. *Biochemistry (Mosc).* **30**, 2570-2574 (1991).
176. Hill, M.R. *et al.* Lipopolysaccharide regulation of lipoprotein lipase expression in murine macrophages. *Infect. Immun.* **63**, 858-864 (1995).
177. Chandak, P.G. *et al.* Efficient Phagocytosis Requires Triacylglycerol Hydrolysis by Adipose Triglyceride Lipase. *J. Biol. Chem.* **285**, 20192-20201 (2010).
178. Yin, B. *et al.* Lipoprotein lipase regulates Fc receptor-mediated phagocytosis by macrophages maintained in glucose-deficient medium. *J. Clin. Invest.* **100**, 649-657 (1997).
179. Newsholme, P. & Newsholme, E.A. Rates of utilization of glucose, glutamine and oleate and formation of end-products by mouse peritoneal macrophages in culture. *Biochem. J.* **261**, 211-218 (1989).
180. Lokesh, B.R. & Wrann, M. Incorporation of palmitic acid or oleic acid into macrophage membrane lipids exerts differential effects on the function of normal mouse peritoneal macrophages. *Biochim. Biophys. Acta* **792**, 141-148 (1984).
181. Calder, P.C., Bond, J.A., Harvey, D.J., Gordon, S. & Newsholme, E.A. Uptake and incorporation of saturated and unsaturated fatty acids into macrophage lipids and their effect upon macrophage adhesion and phagocytosis. *Biochem. J.* **269**, 807-814 (1990).
182. Newsholme, P. *et al.* Glutamine metabolism by lymphocytes, macrophages, and neutrophils: its importance in health and disease. *J.Nutr. Biochem.* **10**, 316-324 (1999).
183. Murphy, C. & Newsholme, P. Importance of glutamine metabolism in murine macrophages and human monocytes to L-arginine biosynthesis and rates of nitrite or urea production. *Clin. Sci.* **95**, 397-407 (1998).

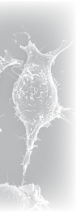

184. Newsholme, P. Why Is l-Glutamine Metabolism Important to Cells of the Immune System in Health, Postinjury, Surgery or Infection? *J. Nutr.* **131**, 2515S-2522S (2001).
185. Kreider, T., Anthony, R.M., Urban Jr, J.F. & Gause, W.C. Alternatively activated macrophages in helminth infections. *Curr. Opin. Immunol.* **19**, 448-453 (2007).
186. Carlin, J.M., Borden, E.C., Sondel, P.M. & Byrne, G.I. Interferon-induced indoleamine 2,3-dioxygenase activity in human mononuclear phagocytes. *J. Leukoc. Biol.* **45**, 29-34 (1989).
187. Musso, T., Gusella, G.L., Brooks, A., Longo, D.L. & Varesio, L. Interleukin-4 inhibits indoleamine 2,3-dioxygenase expression in human monocytes. *Blood* **83**, 1408-1411 (1994).
188. Moffett, J.R. & Namboodiri, M.A.A. Tryptophan and the immune response. *Immunol. Cell Biol.* **81**, 247-265 (2003).
189. Odegaard, J.I. & Chawla, A. Alternative Macrophage Activation and Metabolism. *Annu. Rev. Pathol.* **6**, 275-297 (2010).
190. Huang, J.T. *et al.* Interleukin-4-dependent production of PPARg ligands in macrophages by 12/15-lipoxygenase. *Nature* **400**, 378-382 (1999).
191. Chawla, A. Control of Macrophage Activation and Function by PPARs. *Circ. Res.* **106**, 1559-1569 (2010).
192. Cramer, T. *et al.* HIF-1a Is Essential for Myeloid Cell-Mediated Inflammation. *Cell* **112**, 645-657 (2003).
193. Pello, O.M. *et al.* Role of c-MYC in alternative activation of human macrophages and tumor-associated macrophage biology. *Blood* **119**, 411-421 (2012).
194. Pello, O.M. *et al. In Vivo* Inhibition of c-MYC in Myeloid Cells Impairs Tumor-Associated Macrophage Maturation and Pro-Tumoral Activities. *PLoS ONE* **7**, e45399 (2012).
195. Wise, D.R. *et al.* Myc regulates a transcriptional program that stimulates mitochondrial glutaminolysis and leads to glutamine addiction. *Proc. Natl. Acad. Sci. U. S. A.* **105**, 18782-18787 (2008).
196. Zhang, H. *et al.* HIF-1 Inhibits Mitochondrial Biogenesis and Cellular Respiration in VHL-Deficient Renal Cell Carcinoma by Repression of C-MYC Activity. *Cancer Cell* **11**, 407-420 (2007).
197. Peck, B., Ferber, E.C. & Schulze, A. Antagonism between FOXO and MYC regulates cellular powerhouse. *Front. Oncol.* **3**, 96 (2013).
198. Keith, B., Johnson, R.S. & Simon, M.C. HIF1a and HIF2a: sibling rivalry in hypoxic tumour growth and progression. *Nat. Rev. Cancer* **12**, 9-22 (2012).
199. Liao, X. *et al.* Krüppel-like factor 4 regulates macrophage polarization. *J. Clin. Invest.* **121**, 2736-2749 (2011).
200. Lujambio, A. *et al.* Non-Cell-Autonomous Tumor Suppression by p53. *Cell* **153**, 449-460 (2013).
201. Lago, C.U., Sung, H.J., Ma, W., Wang, P.-y. & Hwang, P.M. p53, Aerobic Metabolism, and Cancer. *Antioxid. Redox Signal.* **15**, 1739-1748 (2011).
202. Vogelstein, B., Lane, D. & Levine, A.J. Surfing the p53 network. *Nature* **408**, 307-310 (2000).
203. Tomasini, R. *et al.* TAp73 is required for macrophage-mediated innate immunity and the resolution of inflammatory responses. *Cell Death Differ.* **20**, 293-301 (2013).
204. Williams, L.M. & Ridley, A.J. Lipopolysaccharide Induces Actin Reorganization and Tyrosine Phosphorylation of Pyk2 and Paxillin in Monocytes and Macrophages. *J. Immunol.* **164**, 2028-2036 (2000).
205. Kleveta, G. *et al.* LPS induces phosphorylation of actin-regulatory proteins leading to actin reassembly and macrophage motility. *J. Cell. Biochem.* **113**, 80-92 (2012).
206. Isambert, H. *et al.* Flexibility of actin filaments derived from thermal fluctuations. Effect of bound nucleotide, phalloidin, and muscle regulatory proteins. *J. Biol. Chem.* **270**, 11437-11444 (1995).
207. Volkmann, N. & Hanein, D. Actomyosin: law and order in motility. *Curr. Opin. Cell Biol.* **12**, 26-34 (2000).
208. Hallett, M.A., Dagher, P.C. & Atkinson, S.J. Rho GTPases show differential sensitivity to nucleotide triphosphate depletion in a model of ischemic cell injury. *Am. J. Physiol. Cell Physiol.* **285**, C129-C138 (2003).
209. Atkinson, S.J., Hosford, M.A. & Molitoris, B.A. Mechanism of Actin Polymerization in Cellular ATP Depletion. *J. Biol. Chem.* **279**, 5194-5199 (2004).
210. Bernstein, B.W. & Bamburg, J.R. Actin-ATP Hydrolysis Is a Major Energy Drain for Neurons. *J. Neurosci.* **23**, 1-6 (2003).
211. Gourlay, C.W. & Ayscough, K.R. The actin cytoskeleton: a key regulator of apoptosis and ageing? *Nat. Rev. Mol. Cell Biol.* **6**, 583-589 (2005).
212. van Horssen, R. *et al.* Modulation of Cell Motility by Spatial Repositioning of Enzymatic ATP/ADP Exchange Capacity. *J. Biol. Chem.* **284**, 1620-1627 (2009).
213. Waingeh, V.F. *et al.* Glycolytic Enzyme Interactions with Yeast and Skeletal Muscle F-Actin. *Biophys. J.* **90**, 1371-1384 (2006).
214. Pagliaro, L. & Taylor, D.L. Aldolase exists in both the fluid and solid phases of cytoplasm. *J. Cell Biol.* **107**, 981-991 (1988).
215. Beitner, R. Control of glycolytic enzymes through binding to cell structures and by glucose-1,6-bisphosphate under different conditions. The role of Ca2+ and calmodulin. *Int. J. Biochem.* **25**, 297-305 (1993).
216. Jia, Z. *et al.* Tumor Cell Pseudopodial Protrusions: Localized signaling domains coordinating cytoskeleton remodeling, cell adhesion, glycolysis, RNA translocation, and protein translation. *J. Biol. Chem.* **280**, 30564-

30573 (2005).
217. Nguyen, T.N., Wang, H.-J., Zalzal, S., Nanci, A. & Nabi, I.R. Purification and Characterization of β-Actin-Rich Tumor Cell Pseudopodia: Role of Glycolysis. *Exp. Cell Res.* **258**, 171-183 (2000).
218. Tochio, T., Tanaka, H., Nakata, S. & Hosoya, H. Fructose-1,6-bisphosphate aldolase A is involved in HaCaT cell migration by inducing lamellipodia formation. *J. Dermatol. Sci.* **58**, 123-129 (2010).
219. Casey, J.R., Grinstein, S. & Orlowski, J. Sensors and regulators of intracellular pH. *Nat. Rev. Mol. Cell Biol.* **11**, 50-61 (2010).

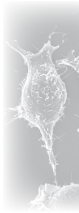

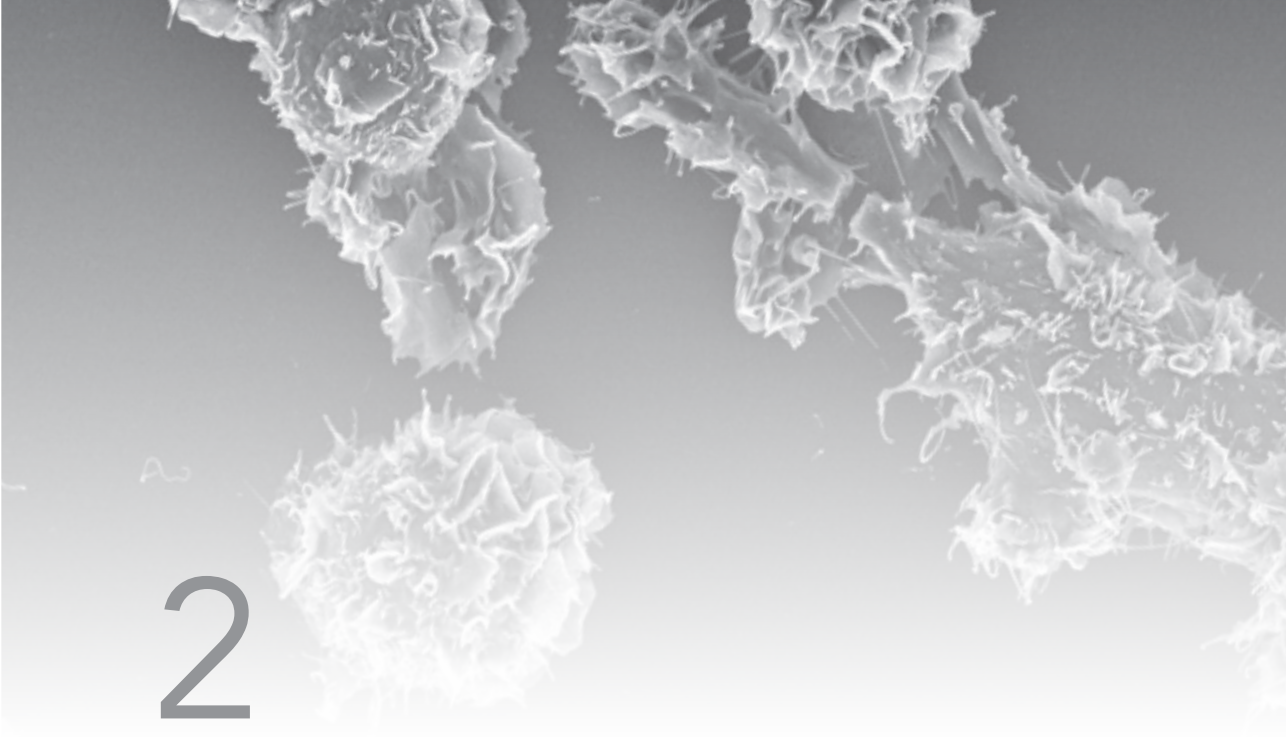

2

A comparative study of RAW 264.7 and *MafB/c-Maf* deficient (Maf-DKO) macrophage proliferation, morphology, phagocytosis, and carbohydrate metabolism *in vitro*

Gerda Venter, Mietske Wijers, Frank T. J. J. Oerlemans, Jack A. M. Fransen, and Bé Wieringa

Department of Cell Biology, Radboud Institute for Molecular Life Sciences, Radboud University Medical Centre, Nijmegen, The Netherlands

Abstract

For *in vitro* studies of macrophage function different macrophage lineages with a cancerous phenotype, of which RAW 264.7 cells are typical representatives, are commonly used. Recently, a new lineage of macrophages of non-tumorigenic origin, Maf-DKO cells, which were isolated from a mouse with a *MafB/c-Maf* deficient hematopoietic system, has become available. To study which cell type resembles primary macrophages most closely we here compared gross features of carbohydrate metabolism, proliferative capacity, and morphofunctional properties of Maf-DKO and RAW 264.7 macrophages.

Although RAW 264.7 cells had a significantly higher proliferation rate, Maf-DKO cells appeared to be morphodynamically more active, since they formed strikingly more surface membrane protrusions and phagocytosed complement opsonized particles more efficiently. Carbohydrate catabolism did, however, not overtly differ between the two cell lines. We conclude that the Maf-DKO cell line shares many characteristics with both primary macrophages and existing macrophage cell lines, and could be an ideal intermediate cell model for extending our knowledge on the intricate relationships between metabolism, form, and function of macrophages.

Introduction

Macrophages are vital players in host defense against pathogens and in maintaining tissue homeostasis. The name "macrophage" is in fact the collective noun for rather heterogeneous populations of highly versatile immune cells that were originally classified under the mononuclear phagocyte system (MPS). Use of this classification system implies that macrophages are derived from monocytes that develop from a common myeloid progenitor cell in the bone marrow [1]. Recent work by several groups, however, has now also provided evidence for self-renewal of macrophages formed from embryonic progenitors independent of hematopoietic stem cells, via proliferation of cell populations that are already prenatally established in various tissues [2-12]. These new findings support older studies that disputed the MPS-model already at the time of its introduction and suggest that two subsets of tissue macrophages can be distinguished: those of bone marrow-dependent and -independent origin [13, 14].

This differential developmental origin, and the fact that macrophages can occur in their own tissue environment at multiple different stages of functional activation, which allows them to adopt a continuum of phenotypes, makes study of macrophages difficult. Therefore, to investigate macrophage function and characteristics, mostly *in vitro* approaches are taken for relatively homogeneous populations of macrophages. Primary murine macrophages can be isolated from the peritoneal cavity, the lungs, or the bone marrow [15], but after isolation, these macrophages, like most mature differentiated cells, are difficult to manipulate and can be maintained in culture for only a few days [16]. These problems can be overcome by the use of immortal clonally-derived macrophage cell lines which are relatively easy to obtain, such as the murine J744.A and RAW 264.7 monocyte/macrophage cell lines and the human THP-1 cell line, all with a cancerous background. The J744.A cell line is a reticulum cell sarcoma, from an ascites tumor that arose in a female BALB/c/NIH mouse during plasmacytoma induction, which has the morphologic, adherent, and phagocytic properties of macrophages [17]. RAW 264.7 cells (most commonly used) are macrophage-like cells derived from an Abelson murine leukemia virus-induced ascites tumor from a male BAB/14 mouse [18, 19]. THP-1 is a leukemic cell line with monocytic properties, cultured from the blood of a boy with acute monocytic leukemia [20].

Although these macrophage lineages share many properties with primary macrophages, one must keep in mind that they have an unusually high proliferative capacity and behave like cells with a cancerous "Warburg" phenotype [21-24]. Therefore, the question arises to what extent does study of the currently available

macrophage lines that have been established for use in cell culture reveal the true characteristics of primary macrophages in tissues?

In order to shed some light on this issue, we have compared the proliferation capacity, morphology, phagocytosis capacity, and metabolism of RAW 264.7 cells with that of continuously dividing macrophages isolated from mice with a *MafB/c-Maf* deficient hematopoietic system [25]. In the presence of M-CSF, these Maf double knock-out (Maf-DKO) monocytic cells can differentiate into macrophages and be expanded in culture without losing their differentiated phenotype. In contrast to RAW 264.7 cells, Maf-DKO cells do not have a cancerous background and do not produce tumors when transplanted back into mice. On the contrary, these transplanted Maf-DKO cells show homing and functional integration into normal macrophage populations of tissues. Maf-DKO cells are positive for specific monocyte/macrophage surface markers and have a global gene expression profile, morphology, and phagocytic capacity highly similar to wild type cells [25]. Therefore, these cells resemble primary macrophages more closely than RAW 264.7 cells, with features intermediate between transformed and normal cells.

Here, we report that RAW 264.7 cells have a markedly increased proliferation rate compared to Maf-DKO cells and that there are significant differences in phagocytosis capacity and (actin cytoskeleton controlled) morphology between the two cell lines. Metabolically, both cell lines are highly glycolytic and, although we detected some differences in the expression level of certain glycolytic enzymes which may be related to their (non-)cancerous background, no major metabolic differences were observed. We, therefore, consider Maf-DKO cells as an ideal alternative cell line to study macrophage metabolism and function.

Materials and Methods

Reagents
All reagents were obtained from Sigma-Aldrich (St. Louis, MO, USA), unless stated otherwise.

Cell culture
RAW 264.7 cells (kind gift from Dr. Hong-Hee Kim, Department of Cell and Developmental Biology, School of Dentistry, Seoul National University, Korea) [26] were maintained in high-glucose DMEM (Gibco, Life Technologies, Paisley, UK) supplemented with 10% heat inactivated FBS (PAA laboratories, Pasching, Austria), 1 mM sodium pyruvate, and 4 mM GlutaMAX (Gibco, Life Technologies, Paisley, UK), at 37°C in a humidified atmosphere with 7.5% CO_2. Maf-DKO cells (kind gift from Dr. Michael H. Sieweke, Centre d'Immunologie de Marseille-Luminy (CIML), Université Aix-Marseille, France) [25] were maintained in the same way except that medium was supplemented with 20% conditioned medium (CM) from macrophage colony stimulating factor (M-CSF)-producing L929-cells [27].

Proliferation assay
Cell proliferation was analyzed by sulforhodamine B (SRB) staining of protein content according to the protocol developed by Skehan et al. [28]. To compare proliferation in the presence and absence of M-CSF, RAW 264.7 and Maf-DKO cells were seeded in three 96-well plates (25,000 cells/well) in 100 µl culture medium with or without 20% L929-cell CM and incubated at 37°C. After 6 (T0), 21 (T15), and 30 (T24) hours the plates were washed twice with cold PBS and fixed with 10% trichloroacetic acid (TCA; J.T.Baker, Deventer, Holland) for 1 hour at 4°C. After fixation, plates were washed five times with water and stored at -20°C until all plates were collected. Cellular protein was stained with 50 µl 0.5% SRB in 1% acetic acid for 20 minutes after which wells were washed four times with 1% acetic acid. Plates were dried at 60°C for 3 hours, protein was dissolved in 150 µl 10 mM Tris-HCl (pH 10.5), and the absorbance of each well was measured at 510nm on a BioRad Benchmark Plus micro plate reader. Values were corrected for background SRB staining by subtracting the average absorbance value of wells that contained medium only, from that of wells with cells. To determine the effect of 2-DG and oligomycin on proliferation, RAW 264.7 and Maf-DKO cells were seeded in three 96 well plates at a density of 7,500 and 25,000 cells/well, respectively. RAW 264.7 cells were incubated for 6 hours and Maf-DKO cells overnight before wells were washed once with medium containing either 10 mM 2-deoxy-D-glucose (2-DG) or 2.5 µM oligomycin and cells

were incubated in the same medium for 24, 48 or 72 hours. Cells were then fixed and stained as described above.

Scanning electron microscopy

RAW 264.7 and Maf-DKO cells were seeded on 12 mm glass coverslips in 24-well plates in medium with or without L929-cell CM and activated with 100 ng/ml LPS or left non-activated. Cells were washed once with PBS and fixed with 2% glutaraldehyde in 0.1 M sodium cacodylate buffer for 1 hour. After washing cells twice with sodium cacodylate buffer, coverslips were stored in the same buffer at 4°C until further fixation with 1% OsO_4 (osmium tetroxide) for 30 minutes. Coverslips were then washed once with water and dehydrated in a graded series of alcohol, critical point dried, and mounted for scanning electron microscopy (JEOL SEM6340F Field Emission Scanning Electron microscope). Images were acquired at 500x as well as a 2000x magnification.

Cellular actin staining

RAW 264.7 and Maf-DKO cells were seeded on 12 mm glass coverslips in 24-well plates in medium with or without L929-cell CM and activated with 100 ng/ml LPS or left non-activated. Cells were washed twice with PBS and fixed in 2% paraformaldehyde in 0.2 M sodium phosphate buffer for 30 minutes. After washing twice with PBS and twice with PBS containing 20 mM glycine (MP Biomedicals, Illkirch Cedex, France; PBS-G) cells were permeabilized with 0.1% saponine/PBS-G for 20 minutes. This was followed by actin staining with Alexa 568-labeled phalloidin (1:600 in 0.1% saponine/PBS-G) for 1 hour. Cells were successively washed four times for 2-4 minutes with 0.1% saponine/PBS-G and once with PBS alone. Coverslips were removed from wells, rinsed once in water, air dried, and embedded in MoWiol on microscope slides. Images were acquired on a Zeiss LSM510 META confocal laser scanning microscope using a 63x objective and processed using Fiji imaging software.

Phagocytosis assay

Phagocytic activity was determined as zymosan ingestion capacity essentially as described by Kuiper et al. [29]. Zymosan particles were dissolved in PBS at 10 mg/ml and left to rehydrate for at least one hour. Next, zymosan was sonicated three times for 5 seconds, spun down, resuspended in carbonate buffer (pH 9.6), sonicated, and incubated with 1 µg/ml fluorescein isothiocyanate (FITC) for 1 hour at room temperature, in the dark. After FITC labeling, zymosan was washed three times with carbonate buffer and incubated in 1 M Tris-HCl, pH 8.0, for 30 minutes. Zymosan was then washed twice with PBS and finally resuspended in PBS. After one more

sonication step, FITC-labeled zymosan was divided in aliquots, frozen in liquid nitrogen, and stored at -20°C.

For phagocytosis assays without M-CSF, 100,000 RAW 264.7 cells were seeded per well in normal culture medium and 200,000 Maf-DKO cells per well in medium with 20% L929-cell CM. For assays with M-CSF, both RAW 264.7 and Maf-DKO cells were seeded in medium containing L929-cell CM at a density of 75,000 and 200,000 cells/well, respectively. Where applicable, cells were pre-incubated in medium containing 2.5 µM oligomycin (0 or 24 hours) or 10 mM 2-DG (3 hours) and activated overnight with 100 ng/ml LPS. FITC-labeled zymosan particles were complement opsonized by incubation in fetal bovine serum for 1 hour at 37°C, washed twice with PBS, and finally resuspended in serum-free medium with or without L929-cell CM and, where applicable, with or without oligomycin and 2-DG. Cells were washed once with serum-free medium and incubated with 1 ml zymosan suspension for 30 minutes at 37°C. The particle-to-cell ratio was approximately 10:1. Particle engulfment was terminated by washing cells twice with PBS and removing extracellular zymosan by treatment with 500 µl 100 U/ml lyticase for 10 minutes at room temperature. Successively, cells were detached with 0.05% trypsin/0.5 mM EDTA (Gibco, Life Technologies, Paisley, UK), resuspended in 1 ml medium with serum, pelleted, and finally resuspended in 200 µl 1% paraformaldehyde in PBS. Samples were analyzed by FACS and phagocytosis efficiency was determined by measuring the fluorescence intensity of the FITC positive population as well as the percentage of cells in that population. The phagocytic index of each sample was calculated as the product of the mean FITC intensity of the positive population times the % of FITC positive cells.

Western blot analysis

Protein expression was analyzed by western blot analysis. After washing cells twice with cold PBS in 6 cm culture dishes, cell lysates were prepared in lysis buffer (50 mM Tris-HCl pH 7.5, 100 mM NaCl, 5 mM $MgCl_2$, and 0.5% NP-40; 4°C) and stored at -20°C until analysis. Lysates containing ± 10 µg protein were mixed with 5x sample buffer (0.25 % Bromophenol Blue, 0.5 M DTT, 50 ml glycerol, 10 %SDS, and 0.25 M Tris-HCl pH 6.8), heated at 95°C for 5 minutes, and loaded onto 10 or 12% SDS-PAGE gels, depending on the size of the protein of interest. After electrophoretic separation, proteins were blotted onto PVDF membranes. Membranes were blocked with 5% (w/v) skimmed milk in PBS-T (HXK1, HXK2, LDH-A, actin) or TBS-T (PKM2) for 1 hour and labeled overnight with a mouse anti-Tubulin (1:5000; DSHB, University of Iowa) and either a goat anti-HXK1 (1:200; Santa Cruz Biotechnology), goat anti-HXK2 (1:200; Santa Cruz Biotechnology), goat anti-LDH-A (1:5000; Cell Signaling

Technology), rabbit anti-PKM2 (1:1000; Cell Signaling Technology), or rabbit anti-actin (1:1000; Cytoskeleton Inc.) antibody at 4°C. After washing the membranes three times for 5 minutes with PBS-T or TBS-T, they were incubated with IRDye secondary antibodies (donkey anti-goat 680, goat anti-rabbit 680, goat anti-rabbit 800, goat anti-mouse 680, and/or goat anti-mouse 800) for one hour at room temperature. This was followed by 4 wash steps of 5 minutes each in PBS-T or TBS-T, a final wash step in PBS, and signal detection on the Odyssey Infrared Imaging System (LI-COR Biosciences, Lincoln, NE, USA). Tubulin served as loading control and reference for calculation of protein expression.

Glucose and Lactate measurements

Glucose consumption measurements were based on the Amplex Red Glucose/Glucose Oxidase assay kit from Molecular probes (Life Technologies, Eugene, Oregon, USA). Glucose, glucose oxidase, and Amplex Red reagent were used from the kit but horseradish peroxidase was obtained from Sigma-Aldrich (St. Louis, MO, USA) and 1x reaction buffer was replaced with 0.05 M Tris-HCl, pH 7.5. Apart from these minor changes, the kit protocol was followed as described by the manufacturer. Lactate production was measured using the same protocol as for glucose consumption but replacing glucose oxidase with lactate oxidase and including a lactate standard series instead of glucose. Cells were seeded in 12 well tissue culture plates in medium containing 20% L929-cell CM and incubated overnight. For glucose measurements, medium containing 5 mM glucose was used while lactate production was measured for cells grown in 25 mM glucose medium. The next day, wells were rinsed with pure DMEM containing no glucose and fresh control medium (containing 10% heat inactivated dialyzed FBS, 1 mM sodium pyruvate, and 4 mM GlutaMAX) or medium containing 2.5 μM oligomycin was added. After 6 hours, medium was collected and supernatants were snap frozen in liquid nitrogen and stored at -20°C until analysis. Cytosolic extracts were prepared in lysis buffer (50 mM Tris-HCl pH 7.5, 100 mM NaCl, 5 mM $MgCl_2$, and 0.5% NP-40; 4°C) and total protein was determined with the Bradford assay. Glucose consumption was calculated by subtracting the amount of glucose in the sample from that in medium without cells. Lactate production was calculated by subtracting the concentration of any lactate in the medium without cells from that of the samples. Glucose and lactate assays were performed in parallel.

LDH-isoenzyme expression

LDH-isoenzymes were separated using the SAS-MX LDH Isoenzyme gel electrophoresis test from Helena Biosciences Europe, according to the manufacturer's specifications. Cell lysates were prepared as for western blot and protein concentration

was determined with the Bradford assay. Per lane, approximately 2.8 µg protein was loaded.

Oxygen consumption measurements

An Oroboros Oxygraph-2k respirometer was used to measure oxygen consumption in RAW 264.7 and Maf-DKO cells according to a standard protocol provided by the manufacturer. RAW 264.7 cells were incubated in medium with 20% L929-cell CM for at least 24 hours prior to assay. The two cell lines were analyzed in parallel in two separate chambers of the respirometer. After air calibration of the medium in the chambers and stabilization of the signal, 1 x 10^6 cells (in 60 µl medium) were injected into the respective chambers. Basal respiration rate was measured at the point where the O_2-flux signal stabilized. Oligomycin (2.5 µM) was added to each chamber and the leak respiration rate was determined after stabilization of the signal. Next, 7 µM carbonyl cyanide-*p*-trifluoromethoxyphenylhydrazone (FCCP, a mitochondrial uncoupler) was added to reach maximal oxygen consumption in the cells. Finally, 30 nM rotenone was added and after stabilization of the system, the residual oxygen consumption could be determined. The data was analyzed using the DatLab software provided with the instrument.

Statistical analysis

Data was analyzed either with the Student's t-test or using a two-way ANOVA and the Bonferroni post-test (GraphPad software, Inc., Version 4). Values are expressed as mean +/-SEM. Values were considered to be significantly different when *p* values were < 0.05.

RAW 264.7 and Maf-DKO proliferation in the presence of M-CSF

MafB/c-Maf deficient (Maf-DKO) monocytes require macrophage colony stimulating factor (M-CSF or CSF-1) for their *in vitro* differentiation into macrophages [25]. For RAW 264.7 cells to achieve this state of differentiation *in vitro*, continuous presence of M-CSF is no prerequisite. *In vivo*, M-CSF is found in the circulation from where it regulates the survival, proliferation, and differentiation of monocytes and macrophages [30] after being secreted by various cells including monocytes, macrophages, fibroblasts, endothelial cells, and malignant cells [31-35].

To better compare the potential coupling between metabolic phenotype and proliferative capacity of RAW 264.7 and Maf-DKO cells in culture we analyzed first the effects of absence or presence of M-CSF (in conditioned medium from L929 cells) on cell proliferation. Under standard medium conditions (DMEM supplemented with FBS, pyruvate and GlutaMax but without M-CSF) RAW 264.7 cells had a high proliferation rate (Figure 1). In the presence of M-CSF, added as 20% CM, RAW 264.7 proliferation was further increased. Maf-DKO cells, on the other hand, failed to divide without M-CSF but even in the presence of M-CSF Maf-DKO cells had a significantly slower growth rate compared to RAW 264.7. The high rate of traverse through cell cycle and the independence of RAW 264.7 proliferation on M-CSF most likely reflect the malignant background of these cells, while the fact that M-CSF is obligatory for Maf-DKO survival and their slow proliferation rate again suggests that these cells have retained features that are typical for primary macrophages.

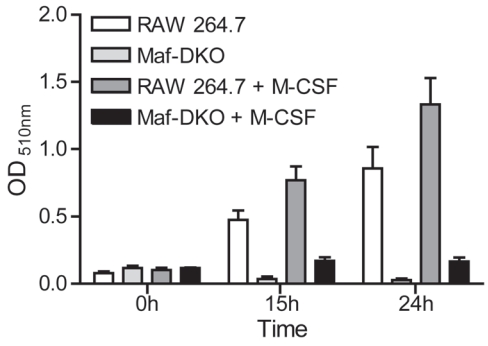

Figure1. The effect of M-CSF on RAW 264.7 and Maf-DKO cells in culture. *The SRB assay for total cell protein mass was used to follow proliferation of RAW 264.7 and Maf-DKO cells in the presence and absence of L929-cell CM (M-CSF). The increase in cell mass is plotted as the change in optical density at 510nm. Data represent means ± SEM of three independent experiments performed in triplicate.*

Morphodynamic properties of RAW 264.7 and Maf-DKO cells

Since M-CSF also induces morphology changes in macrophages [36], we became curious to see how the morphofunctional properties of RAW 264.7 and Maf DKO depend on M-CSF. Firstly, we used scanning electron microscopy to compare the morphology of RAW 264.7 cells that were grown in medium with and without L929-cell CM,

to that of Maf-DKO cells in medium with L929-cell CM. Cells were additionally stimulated overnight with 100 ng/ml LPS before fixation and image acquisition. Strikingly, profound differences were observed in the growth pattern and morphology of RAW 264.7 cells in the presence and absence of M-CSF. Without M-CSF, RAW 264.7 cells grew in a clump-wise fashion and had a rounded shape (Figure 2A,B), while the addition of M-CSF induced the formation of cellular protrusions and caused the cells to arrange themselves more loosely, similar to Maf-DKO cells (Figure 2E,F). Interestingly, Maf-DKO cells displayed a more complex surface morphology compared to RAW 264.7. Maf-DKO cell surfaces were densely decorated with protrusive membrane structures, which we henceforth designate as membrane ruffles throughout this piece (Figure 2I-L). RAW 264.7 cell surfaces were more 'bald', displaying only a few ruffles. LPS induces an inflammatory phenotype in macrophages that is accompanied by morphological change [37, 38]. Under our culture conditions cell spreading was prominently induced by LPS in RAW 264.7 both in the absence and presence of M-CSF (Figure 2C,D,G,H), as well as in Maf-DKO cells (Figure 2K,L).

To us, the relative high abundance of ruffle-like structures on Maf-DKO cells suggests that these cells have a dynamically more active cortical actin cytoskeleton than RAW 264.7 cells that helps them to continuously probe the environment. Possibly, under the conditions used, a high percentage of the "cell-dorsal" surface protrusions represent the membrane folds that are actively involved in the non-selective uptake of molecules, nutrients, and antigens from the medium through a process called macropinocytosis [39]. Our results thus suggest that Maf-DKO cells may be much more active in this uptake than RAW 264.7. Indeed, this interpretation would be consistent with the findings of Aziz et al. [40], who observed that the actin organization of *mafB*-deficient macrophages is altered and that a number of proteins involved in actin polymerization, as well as actin itself, were upregulated compared to control cells, thereby suggesting a role for MafB in the regulation of actin dynamics. Our own findings corroborate this picture, and suggest a differential role for actin in Maf-DKO and RAW 264.7 cells. Firstly, when normalized to tubulin expression, we found that Maf-DKO cells expressed considerably more actin than RAW 264.7 cells (Figure 3A). Secondly, staining with phalloidin revealed that RAW 264.7 and Maf-DKO cells have a noticeably different morphology of the actin cytoskeleton (Figure 3B,C). In RAW 264.7 cells, prominent actin-rich filopodial structures could be distinguished, while Maf-DKO cells displayed a more 'cloudy' actin staining. This 'cloudy' staining could be the result of the dense organization of membrane sheets and ruffles on the surface of Maf-DKO cells, making it difficult to distinguish separate structures. In the presence of LPS, Maf-DKO cells also developed actin rich filopodia, but these structures were still more prominent in RAW 264.7 cells (Figure 3D,E).

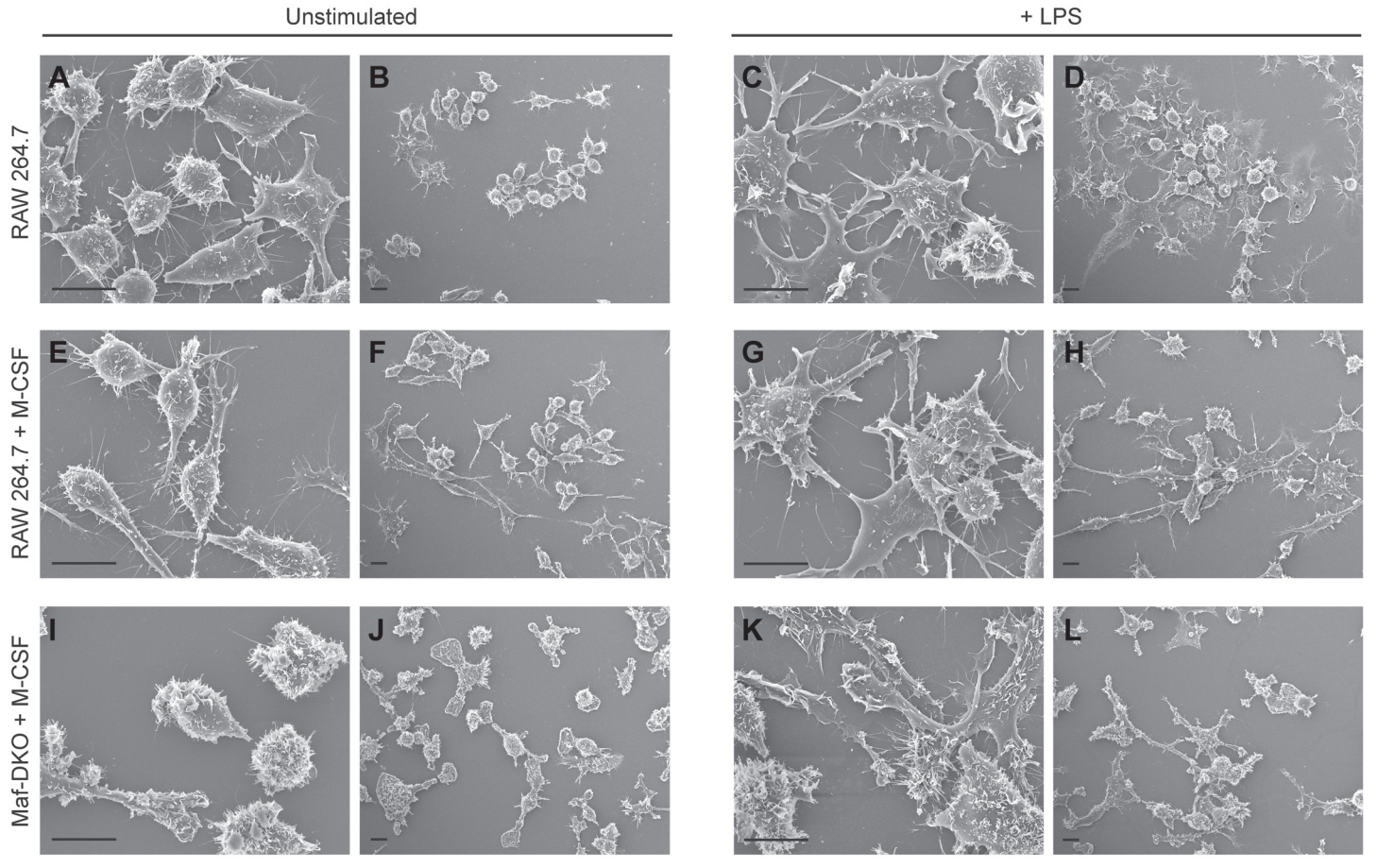

Figure 2. Scanning electron microscope images of RAW 264.7 and Maf-DKO cells, cultured in the presence and absence of M-CSF and LPS. *RAW 264.7 cells in normal culture medium **(A-D)**, RAW 264.7 cells in medium containing 20% L929-cell CM **(E-H)**, Maf-DKO cells in medium containing 20% L929-cell CM **(I-L)**. (Bars = 10 µm)*

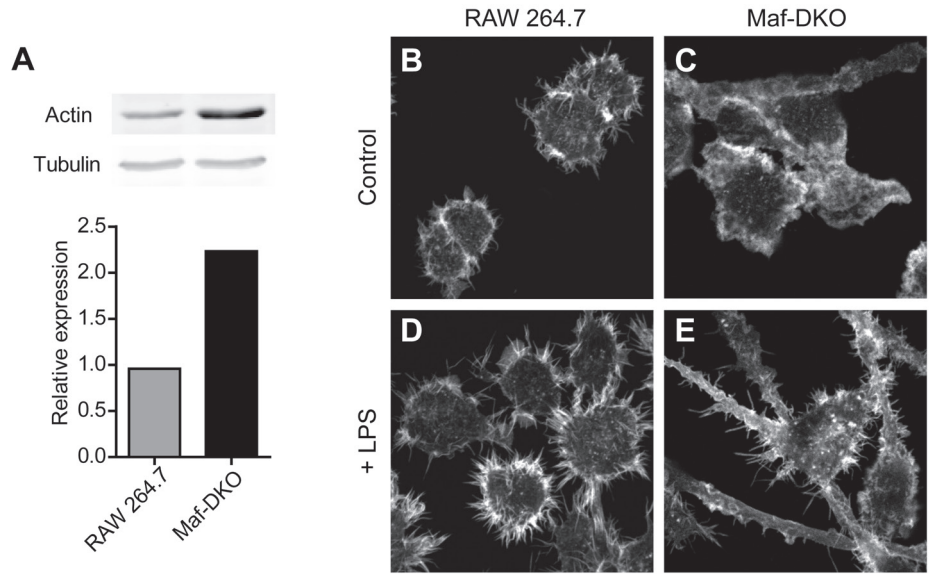

Figure 3. Actin cytoskeletal morphology and actin expression in RAW 264.7 and Maf-DKO cells. *Western blot quantification of actin expression in RAW 264.7 and Maf-DKO cells relative to tubulin* ***(A)****. Data represent ratios of actin and tubulin band intensities of one blot.* ***B-E****, Cells were seeded on glass coverslips and stimulated overnight with LPS (100 ng/ml) or left unstimulated. After fixation, cells were stained with Alexa568-labled phaloidin and imaged on a Zeiss LSM510 META confocal laser scanning microscope.*

To assess in a quantitative way how these actin-related features could differentially affect the morphofunctional characteristics of the two cell lines, we decided to measure phagocytosis efficiency of complement opsonized zymosan (COZ) in the presence and absence of LPS and M-CSF. RAW 264.7 phagocytosis was low in the absence of LPS and M-CSF (-LPS; Figure 4). In the presence of LPS, the ability to engulf COZ was markedly improved, while the addition of M-CSF reduced the RAW 264.7 phagocytosis efficiency. Aziz et al. [25] reported that, compared to primary wild type macrophages, the phagocytic activity of Maf-DKO cells is not altered. We found here that, compared to RAW 264.7 cells, they exhibited a significantly greater phagocytosis efficiency, even in the absence of LPS or M-CSF (Figure 4). Pre-stimulation with LPS did not affect COZ engulfment by Maf-DKO cells, while M-CSF increased the phagocytosis efficiency significantly. The two cell lines, therefore, clearly have a differential dependency on M-CSF for phagocytosis. Most literature studies report on a stimulatory effect of M-CSF on phagocytosis [30, 41-43] in agreement with our observation for the Maf-DKO cells, although an inhibitory effect of M-CSF on phagocytosis of serum opsonized yeast cells in resident peritoneal macrophages is mentioned in one study [36]. Currently it is unclear how M-CSF can have such differential effects on phagocytosis in different macrophage cells. Although truly opposing effects are

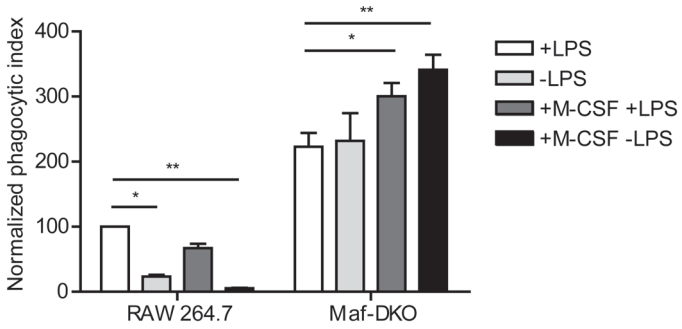

Figure 4. Phagocytosis of COZ in RAW 264.7 and Maf-DKO cells in the presence and absence of M-CSF, LPS, or metabolic inhibitors. *Phagocytic index of RAW 264.7 and Maf-DKO cells was determined with or without LPS (±LPS) and with or without L929-cell CM (± M-CSF). All bars were normalized to the RAW 264.7+LPS bar. Data represent means ± SEM of three independent experiments performed in triplo. (*p < 0.05, **p < 0.01, ***p < 0.001, Two-way ANOVA and Bonferroni posttest)*

difficult to explain, it is possible that activity of the receptor for M-CSF (CSF-1R) or downstream pathways in M-CSF-induced signaling are differentially controlled in macrophages of different origin. Our observation that RAW 264.7 cells required LPS induction to obtain reasonable phagocytosis activity, while Maf-DKO cells were far more efficient in phagocytosis of COZ particles even in the absence of any additional external stimulus strengthen this possibility. Another explanation may be that the difference is not in signaling pathways but that (as we show in Figure 2A,E) Maf-DKO cells are structurally better equipped to capture phagocytic targets than RAW 264.7 cells, because their surface is permanently more abundantly decorated with membrane sheets and ruffles, structures that have been shown to be involved in the capturing of complement opsonized particles [44]. Upon stimulation with LPS, membrane ruffle formation is induced (Figure 2C,D), along with the activation of the complement receptor [45], explaining why phagocytosis is improved with LPS.

Glycolytic and mitochondrial metabolism

For macrophages, alike many other cell types, an inverse reciprocal relationship between proliferation capacity and morphological and functional specialization upon polarization has been demonstrated [46]. Furthermore, proliferative and morpho-functional characteristics are also coupled to specific metabolic adaptations [23, 47]. The increased proliferation rate of tumor cells, like RAW 264.7, is usually accompanied by a shift in metabolism to aerobic glycolysis. Macrophages are, however, perhaps special cells in that even in the untransformed state they appear highly glycolytic [48, 49]. In order to determine and compare the extent to which RAW 264.7 and Maf-DKO cells depend on glycolysis or mitochondrial oxidative phosphorylation (OXPHOS), we assessed proliferation in the presence and absence of the glycolysis inhibitor 2-deoxy-D-glucose (2-DG) and the OXPHOS inhibitor oligomycin. In both

cell lines glucose metabolism via glycolysis appeared to be the primary pathway to fuel proliferation. In the presence of 2-DG, proliferation ceased within 24 hours (Figure 5A,B). In contrast, in the presence of oligomycin, both cell lines continued to proliferate for at least 72 hours, although their growth rate was significantly reduced (Figure 5A,B). These results confirm that RAW 264.7 and Maf-DKO cells – in accordance with their monocyte-macrophage character - are both highly glycolytic but that mitochondrial OXPHOS capacity must be intact, and is used, to attain maximal growth rates.

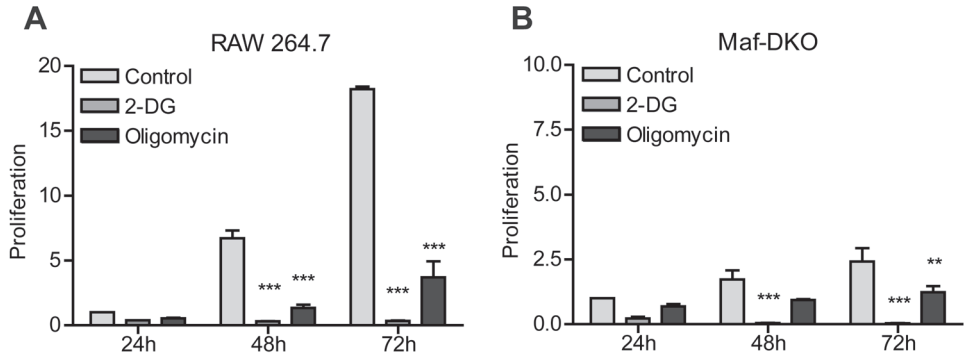

Figure 5. Proliferation of RAW 264.7 and Maf-DKO cells in the presence of glycolysis inhibitor 2-DG and OXPHOS inhibitor oligomycin. *RAW 264.7* ***(A)*** *and Maf-DKO* ***(B)*** *cells were incubated in control medium or medium containing 10mM 2-DG or 2.5 µM oligomycin for 24, 48, or 72 hours, after which protein content was determined. Data represent means ± SEM of three independent experiments performed in triplicate. (**p < 0.01, ***p < 0.001, Two-way ANOVA and Bonferroni posttest)*

To study and compare RAW 264.7 and Maf-DKO metabolism more closely, we next measured glucose consumption and lactate production, compared the expression of certain glycolytic enzymes, and determined mitochondrial respiration. Glucose consumption and lactate production were measured relative to the amount of protein per well. No significant differences were found in the amount of glucose consumed (Figure 6A) and, although Maf-DKO cells tended to produce less lactate (Figure 6B), both cell lines showed a high glycolytic flux to lactate, with RAW 264.7 cells converting 75% and Maf-DKO cells converting 70% of all glucose to lactate (ratio control bars, Figure 6A,B). This percentage is lower than what was reported for quiescent peritoneal macrophages in an earlier study by Rodríguez-Prados et al. [50] where these cells converted 95% of all glucose to lactate. In the same study RAW 264.7 were shown to have a glucose-lactate-conversion of 80%, but to have an increased glycolytic flux rate (i.e. consume and produce more glucose and lactate, respectively). Maf-DKO cells, therefore, seem to have a glycolytic flux and flux rate more comparable to RAW 264.7 cells than to quiescent peritoneal macrophages under the culture conditions that we used in our analyses. In both cell lines glucose

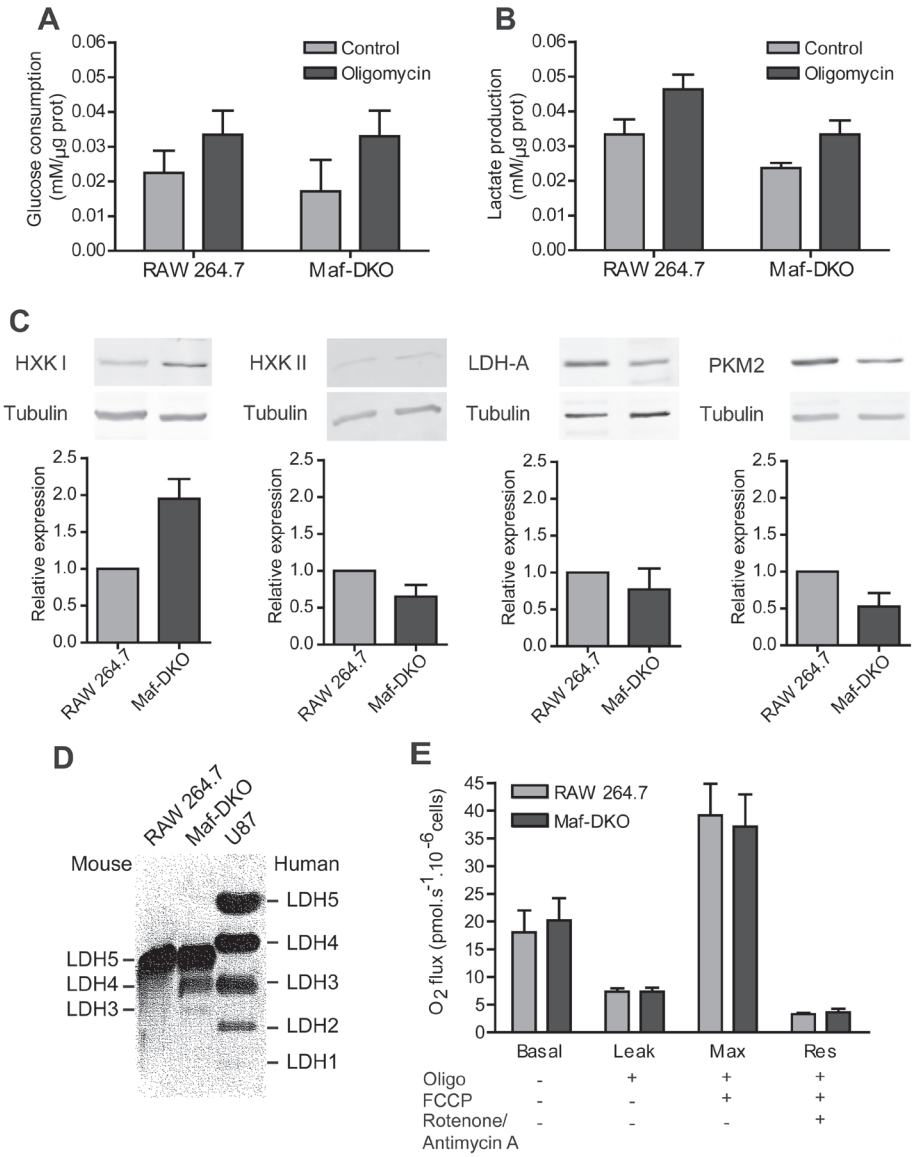

Figure 6. RAW 264.7 and Maf-DKO cells are highly glycolytic. *Glucose consumption **(A)** and lactate production **(B)** in RAW 264.7 and Maf-DKO cells in the presence and absence of the OXPHOS inhibitor oligomycin. **(C)** Expression levels of four metabolic enzymes that were noticeably different between the two cell lines. Protein expression (relative to tubulin) was calculated from the band intensities of three different blots and normalized to the expression in RAW 264.7. **D**, Lactate dehydrogenase isoenzyme expression in RAW 264.7 and Maf-DKO cells. **E**, Mitochondrial respiration measured as the basal oxygen consumption (Basal), the leak respiration (Leak), maximal oxygen consumption (Max), and residual oxygen consumption (Res). Data in (C) represent band intensities of HXK I, HXK II, LDH-A, and PKM2 of one blot, relative to tubulin. Data in A and B represent means ± SEM of three independent experiments performed in triplicate, and in E means ± SEM of four experiments performed with RAW 264.7 and Maf-DKO cells in parallel.*

consumption and lactate production was increased when mitochondrial OXPHOS was inhibited with oligomycin, although the differences were not statistically significant.

Glycolytic enzymes are often differentially regulated in cancer cells [51]. When the expression levels of some glycolytic enzymes were compared on western blot, we did not observe any overt differences. We did, however, notice that the expression levels of hexokinase (HXK) II, lactate dehydrogenase A (LDH-A), and pyruvate kinase M2 (PKM2) tended to be higher in RAW 264.7 cells, while the opposite was true for HXK I (Figure 6C). This profile would correspond with the changes in glycolytic enzyme expression that is normally associated with cancer cells. Hexokinase II is upregulated in cancer cells to maintain an increased rate of glucose consumption and sustain a high glycolytic rate [52-55]. Whether glucose is used for ATP production (via breakdown to pyruvate and conversion to lactic acid) or used for the synthesis of anabolic material is determined by PKM2, a splice isoform of PKM [56]. PKM2 catalyzes the conversion of phosphoenolpyruvate to pyruvate and is the preferred form that is expressed in all types of proliferating cells, including cancer cells. Contrary to first believe, a recent study has demonstrated that increased PKM2 expression is not associated with increased proliferation in these cells. Proliferation appeared rather favored by downregulation/inactivation of total PKM activity [57], creating conditions wherein glycolysis intermediates can be used for nucleotide, amino acid, or fatty acid anabolism rather than the production of ATP. Proliferating cells, therefore, probably prefer the low PKM activity of isoform M2 to further cell growth. The conversion of pyruvate to lactate is catalyzed by LDH. Alike in the human system, in cancer cells of mice the expression of this enzyme is up-regulated and its subunit composition is changed, leading to increased lactate production [58, 59]. Lactate dehydrogenase may exist in five different isoforms (LDH1-5) that differ from one another with regard to the ratio of the A and B subunits in the tetramer. We performed a LDH zymogram analysis to compare the isoenzyme distribution in our macrophage lines. To verify the gel's capacity to separate LDH1-LDH5 isoforms of mouse and human origin, a lysate of the human glioma cell line U87 (which expresses all five isoforms) was run in parallel as a control (according to Eyben et al. [60]). We found that Maf-DKO cells, in contrast to RAW 264.7 cells, express low amounts of LDH-B that enables the production of LDH3 and LDH4. Still, LDH5 is by far most dominantly expressed in both cell types (Figure 6D). The LDH isoenzymes have different Km values for pyruvate and lactate and therefore the speed at which pyruvate and lactate are interconverted may differ. The LDH isoenzyme pattern may, therefore, play an important role during rapid changes in cellular energy metabolism, when the glycolytic rate, and thus the production of pyruvate, is markedly altered [61]. However,

under steady state conditions the physiological significance of a differential LDH isoenzyme pattern is still not well understood.

When pyruvate is not converted to lactate it is transported across the mitochondrial membrane and catabolized via the TCA-cycle and used to produce ATP via OXPHOS. In order to compare the mitochondrial activity of RAW 264.7 and Maf-DKO cells, we measured oxygen consumption in absence and presence of certain OXPHOS inhibitors in order to determine basal O_2-consumption as well as the amount of oxygen that is consumed without producing ATP (leak), the respiration capacity (maximal respiration rate), and the amount of oxygen consumption by systems other than the electron transport chain (residual oxygen consumption), for example NADPH oxidases [62]. Both cell lines exhibited a relatively low O_2-consumption (~20 pmol.s^{-1}.10^{-6} cells compared to ~100 pmol.s^{-1}.10^{-6} cells for mouse embryonic fibroblasts [63]; Figure 6E). Indeed, if only a minor fraction of glucose-derived pyruvate enters the TCA cycle and ultimately serves to fuel OXPHOS, this may explain why treatment with oligomycin did not significantly alter the glycolytic flux (Figure 6A,B). Of note, no differences were detected in basal oxygen consumption between RAW 264.7 and Maf-DKO, neither did the cell lines differ in leak, maximal, or residual O_2-consumption (Figure 6E).

Summarizing conclusions

We have compared gross features of carbohydrate metabolism, proliferative capacity and morphofunctional properties of Maf-DKO and RAW 264.7 macrophages, two macrophage cell lines that have an entirely different origin and history of development. The two cell lines exhibited vastly different proliferation rates, with the RAW 264.7 lineage having a markedly shorter doubling time, consistent with its tumorigenic origin. Maf-DKO cells, on the other hand, were morphodynamically more active, displaying a strikingly more complex cell surface morphology and significantly greater phagocytosis efficiency. Apart from subtle differences in the expression level of some glycolytic enzymes, RAW 264.7 and Maf-DKO cells share many metabolic characteristics, despite the conspicuous differences in the speed at which they traverse through cell cycle. This apparent dichotomy may be best explained by assuming that, although the global rate of glycolysis is similar for both cell lineages, there is differential use for this pathway, either mainly as supply pathway for ATP to deliver fuel for morphodynamic activity in Maf-DKO cells, or for the production of precursors of building blocks (nucleotides, proteins, lipids) for generation of cell biomass, in RAW 264.7 cells. More cell biological study is certainly necessary on the different processes that can be preferentially served by glycolysis in macrophages, to better understand the complex reality of macrophage biology, and specifically the coupling between metabolism, proliferation, and activity in phagocytosis, membrane ruffling and other changes in these highly plastic cell types. Based on our findings we consider Maf-DKO cells, that also exhibit many of the other typical properties of primary wild type macrophages [25], as well suited intermediate models for such studies.

Acknowledgements

We are grateful to Dr. Hong-Hee Kim (Department of Cell and Developmental Biology, School of Dentistry, Seoul National University, Korea) for providing the RAW 264.7 cell line, Dr. Michael H. Sieweke (Centre d'Immunologie de Marseille-Luminy (CIML), Université Aix-Marseille, France) for providing the Maf-DKO cells, and Ganesh Manjeri (Department of Biochemistry, NCMLS, Radboud UMC, Nijmegen, The Netherlands) for help with the oxygen consumption assays.

References

1. van Furth, R. *et al.* The mononuclear phagocyte system: a new classification of macrophages, monocytes, and their precursor cells. *Bull. World Health Organ.* **46**, 845-852 (1972).
2. Davies, L.C. *et al.* A quantifiable proliferative burst of tissue macrophages restores homeostatic macrophage populations after acute inflammation. *Eur. J. Immunol.* **41**, 2155-2164 (2011).
3. Yona, S. *et al.* Fate Mapping Reveals Origins and Dynamics of Monocytes and Tissue Macrophages under Homeostasis. *Immunity* **38**, 79-91 (2013).
4. Hashimoto, D. *et al.* Tissue-Resident Macrophages Self-Maintain Locally throughout Adult Life with Minimal Contribution from Circulating Monocytes. *Immunity* **38**, 792-804 (2013).
5. Jenkins, S.J. *et al.* Local Macrophage Proliferation, Rather than Recruitment from the Blood, Is a Signature of TH2 Inflammation. *Science* **332**, 1284-1288 (2011).
6. Jenkins, S.J. *et al.* IL-4 directly signals tissue-resident macrophages to proliferate beyond homeostatic levels controlled by CSF-1. *J. Exp. Med.* **210**, 2477-2491 (2013).
7. Chorro, L. *et al.* Langerhans cell (LC) proliferation mediates neonatal development, homeostasis, and inflammation-associated expansion of the epidermal LC network. *J. Exp. Med.* **206**, 3089-3100 (2009).
8. Schulz, C. *et al.* A Lineage of Myeloid Cells Independent of Myb and Hematopoietic Stem Cells. *Science* **336**, 86-90 (2012).
9. Murphy, J., Summer, R., Wilson, A.A., Kotton, D.N. & Fine, A. The Prolonged Life-Span of Alveolar Macrophages. *Am. J. Respir. Cell Mol. Biol.* **38**, 380-385 (2008).
10. Ajami, B., Bennett, J.L., Krieger, C., Tetzlaff, W. & Rossi, F.M.V. Local self-renewal can sustain CNS microglia maintenance and function throughout adult life. *Nat. Neurosci.* **10**, 1538-1543 (2007).
11. Kanitakis, J., Petruzzo, P. & Dubernard, J.-M. Turnover of Epidermal Langerhans' Cells. *N. Engl. J. Med.* **351**, 2661-2662 (2004).
12. Sieweke, M.H. & Allen, J.E. Beyond Stem Cells: Self-Renewal of Differentiated Macrophages. *Science* **342** (2013).
13. Volkman, A., Chang, N.C., Strausbauch, P.H. & Morahan, P.S. Differential effects of chronic monocyte depletion on macrophage populations. *Lab. Invest.* **49**, 291-298 (1983).
14. Davies, L.C., Jenkins, S.J., Allen, J.E. & Taylor, P.R. Tissue-resident macrophages. *Nat. Immunol.* **14**, 986-995 (2013).
15. Davies, J. & Gordon, S. Isolation and Culture of Murine Macrophages, in *Basic Cell Culture Protocols*, Vol. 290. (eds. C. Helgason & C. Miller) 91-103 (Humana Press, 2005).
16. Zhang, X., Goncalves, R. & Mosser, D.M. The Isolation and Characterization of Murine Macrophages, in *Current Protocols in Immunology* (John Wiley & Sons, Inc., 2001).
17. Ralph, P., Prichard, J. & Cohn, M. Reticulum Cell Sarcoma: An Effector Cell in Antibody-Dependent Cell-Mediated Immunity. *J. Immunol.* **114**, 898-905 (1975).
18. Raschke, W.C., Baird, S., Ralph, P. & Nakoinz, I. Functional macrophage cell lines transformed by abelson leukemia virus. *Cell* **15**, 261-267 (1978).
19. Raschke, W.C., Ralph, P., Watson, J., Sklar, M. & Coon, H. Oncogenic transformation of murine lymphoid cells by in vitro infection with Abelson leukemia virus. *J. Natl. Cancer Inst.* **54**, 1249-1253 (1975).
20. Tsuchiya, S. *et al.* Establishment and characterization of a human acute monocytic leukemia cell line (THP-1). *Int. J. Cancer* **26**, 171-176 (1980).
21. Hanahan, D. & Weinberg, R.A. The Hallmarks of Cancer. *Cell* **100**, 57-70 (2000).
22. Marusyk, A. & Polyak, K. Cancer Cell Phenotypes, in Fifty Shades of Grey. *Science* **339**, 528-529 (2013).
23. Vander Heiden, M.G., Cantley, L.C. & Thompson, C.B. Understanding the Warburg Effect: The Metabolic Requirements of Cell Proliferation. *Science* **324**, 1029-1033 (2009).
24. Warburg, O. On the Origin of Cancer Cells. *Science* **123**, 309-314 (1956).
25. Aziz, A., Soucie, E., Sarrazin, S. & Sieweke, M.H. MafB/c-Maf Deficiency Enables Self-Renewal of Differentiated Functional Macrophages. *Science* **326**, 867-871 (2009).
26. Chang, E.-J. *et al.* Brain-type creatine kinase has a crucial role in osteoclast-mediated bone resorption. *Nat. Med.* **14**, 966-972 (2008).
27. Stanley, E.R. & Heard, P.M. Factors regulating macrophage production and growth. Purification and some properties of the colony stimulating factor from medium conditioned by mouse L cells. *J. Biol. Chem.* **252**, 4305-4312 (1977).
28. Skehan, P. *et al.* New Colorimetric Cytotoxicity Assay for Anticancer-Drug Screening. *J. Natl. Cancer Inst.* **82**, 1107-1112 (1990).
29. Kuiper, J.W.P. *et al.* Creatine Kinase–Mediated ATP Supply Fuels Actin-Based Events in Phagocytosis. *PLoS Biol.* **6**, e51 (2008).
30. Nemunaitis, J. Macrophage function activating cytokines: potential clinical application. *Crit. Rev. Oncol. He-*

matol. **14**, 153-171 (1993).
31. Takashima, A. *et al.* Colony-stimulating factor-1 secreted by fibroblasts promotes the growth of dendritic cell lines (XS series) derived from murine epidermis. *J. Immunol.* **154**, 5128-5135 (1995).
32. Devaraj, S., Yun, J.-M., Duncan-Staley, C. & Jialal, I. C-reactive protein induces M-CSF release and macrophage proliferation. *J. Leukoc. Biol.* **85**, 262-267 (2009).
33. Gerharz, C.-D., Reinecke, P., Schneider, E.M., Schmitz, M. & Gabbert, H.E. Secretion of GM-CSF and M-CSF by human renal cell carcinomas of different histologic types. *Urology* **58**, 821-827 (2001).
34. Kacinski, B.M. CSF-1 and Its Receptor in Ovarian, Endometrial and Breast Cancer. *Ann. Med.* **27**, 79-85 (1995).
35. Lee, M.T., Kaushansky, K., Ralph, P. & Ladner, M.B. Differential expression of M-CSF, G-CSF, and GM-CSF by human monocytes. *J. Leukoc. Biol.* **47**, 275-282 (1990).
36. Brummer, E. & Stevens, D.A. Effect of macrophage colony-stimulating factor (M-CSF) on macrophage morphology, phagocytosis, and intracellular multiplication of Histoplasma capsulatum. *Int. J. Immunopharmacol.* **16**, 171-176 (1994).
37. Kleveta, G. *et al.* LPS induces phosphorylation of actin-regulatory proteins leading to actin reassembly and macrophage motility. *J. Cell. Biochem.* **113**, 80-92 (2012).
38. Williams, L.M. & Ridley, A.J. Lipopolysaccharide Induces Actin Reorganization and Tyrosine Phosphorylation of Pyk2 and Paxillin in Monocytes and Macrophages. *J. Immunol.* **164**, 2028-2036 (2000).
39. Lim, J.P. & Gleeson, P.A. Macropinocytosis: an endocytic pathway for internalising large gulps. *Immunol. Cell Biol.* **89**, 836-843 (2011).
40. Aziz, A. *et al.* Development of Macrophages with Altered Actin Organization in the Absence of MafB. *Mol. Cell. Biol.* **26**, 6808-6818 (2006).
41. Roilides, E., Lyman, C.A., Sein, T., Petraitiene, R. & Walsh, T.J. Macrophage colony-stimulating factor enhances phagocytosis and oxidative burst of mononuclear phagocytes against Penicillium marneffei conidia1. *FEMS Immunol. Med. Microbiol.* **36**, 19-26 (2003).
42. Smith, A. *et al.* M-CSF increases proliferation and phagocytosis while modulating receptor and transcription factor expression in adult human microglia. *Journal of Neuroinflammation* **10**, 85 (2013).
43. Mitrasinovic, O.M., Vincent, V.A.M., Simsek, D. & Murphy Jr, G.M. Macrophage colony stimulating factor promotes phagocytosis by murine microglia. *Neurosci. Lett.* **344**, 185-188 (2003).
44. Patel, P.C. & Harrison, R.E. Membrane Ruffles Capture C3bi-opsonized Particles in Activated Macrophages. *Mol. Biol. Cell* **19**, 4628-4639 (2008).
45. Caron, E., Self, A.J. & Hall, A. The GTPase Rap1 controls functional activation of macrophage integrin αMβ2 by LPS and other inflammatory mediators. *Curr. Biol.* **10**, 974-978 (2000).
46. Suzu, S. *et al.* M-CSF-mediated macrophage differentiation but not proliferation is correlated with increased and prolonged ERK activation. *J. Cell. Physiol.* **212**, 519-525 (2007).
47. Albina, J.E. & Mastrofrancesco, B. Modulation of glucose metabolism in macrophages by products of nitric oxide synthase. *Am. J. Physiol. Cell Physiol.* **264**, C1594-C1599 (1993).
48. Newsholme, P., Curi, R., Gordon, S. & Newsholme, E.A. Metabolism of glucose, glutamine, long-chain fatty acids and ketone bodies by murine macrophages. *The Biochemical journal* **239**, 5 (1986).
49. Calder, P.C. Fuel utilization by cells of the immune system. *Proc. Nutr. Soc.* **54**, 65-82 (1995).
50. Rodríguez-Prados, J.-C. *et al.* Substrate Fate in Activated Macrophages: A Comparison between Innate, Classic, and Alternative Activation. *J. Immunol.* **185**, 605-614 (2010).
51. Dang, C.V. & Semenza, G.L. Oncogenic alterations of metabolism. *Trends Biochem. Sci.* **24**, 68-72 (1999).
52. Bustamante, E., Morris, H.P. & Pedersen, P.L. Energy metabolism of tumor cells. Requirement for a form of hexokinase with a propensity for mitochondrial binding. *J. Biol. Chem.* **256**, 8699-8704 (1981).
53. Nakashima, R.A., Paggi, M.G., Scott, L.J. & Pedersen, P.L. Purification and Characterization of a Bindable Form of Mitochondrial Bound Hexokinase from the Highly Glycolytic AS-30D Rat Hepatoma Cell Line. *Cancer Res.* **48**, 913-919 (1988).
54. Mathupala, S.P., Heese, C. & Pedersen, P.L. Glucose Catabolism in Cancer Cells: The type II hexokinase promoter contains functionally active response elements for the tumor suppressot p53. *J. Biol. Chem.* **272**, 22776-22780 (1997).
55. Mathupala, S.P., Rempel, A. & Pedersen, P.L. Glucose Catabolism in Cancer Cells: Isolation, sequence, and activity of the promoter for type II hexokinase. *J. Biol. Chem.* **270**, 16918-16925 (1995).
56. Mazurek, S. Pyruvate kinase type M2: A key regulator of the metabolic budget system in tumor cells. *Int. J. Biochem. Cell Biol.* **43**, 969-980 (2011).
57. Israelsen, William J. *et al.* PKM2 Isoform-Specific Deletion Reveals a Differential Requirement for Pyruvate Kinase in Tumor Cells. *Cell* **155**, 397-409 (2013).
58. de Groof, A. *et al.* Increased OXPHOS activity precedes rise in glycolytic rate in H-RasV12/E1A transformed fibroblasts that develop a Warburg phenotype. *Molecular Cancer* **8**, 54 (2009).
59. Goldman, R.D., Kaplan, N.O. & Hall, T.C. Lactic Dehydrogenase in Human Neoplastic Tissues. *Cancer Res.* **24**, 389-399 (1964).

60. Eyben, F., Skude, G., Tropé, C., Wennerberg, J. & Mikulowski, P. Lactate dehydrogenase isoenzyme 1 (LDH-1) in athymic mice with xenografts of a human testicular germ cell tumor. *Molecular and General Genetics MGG* **186**, 427-431 (1982).
61. Quistorff, B. & Grunnet, N. The isoenzyme pattern of LDH does not play a physiological role; except perhaps during fast transitions in energy metabolism. *Aging (Albany NY)* **3**, 457-460 (2011).
62. Brand, M.D. & Nicholls, D.G. Assessing mitochondrial dysfunction in cells. *Biochem. J.* **435**, 297-312 (2011).
63. Valsecchi, F. *et al.* Metabolic consequences of NDUFS4 gene deletion in immortalized mouse embryonic fibroblasts. *Biochim. Biophys. Acta* **1817**, 1925-1936 (2012).

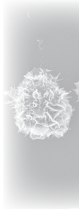

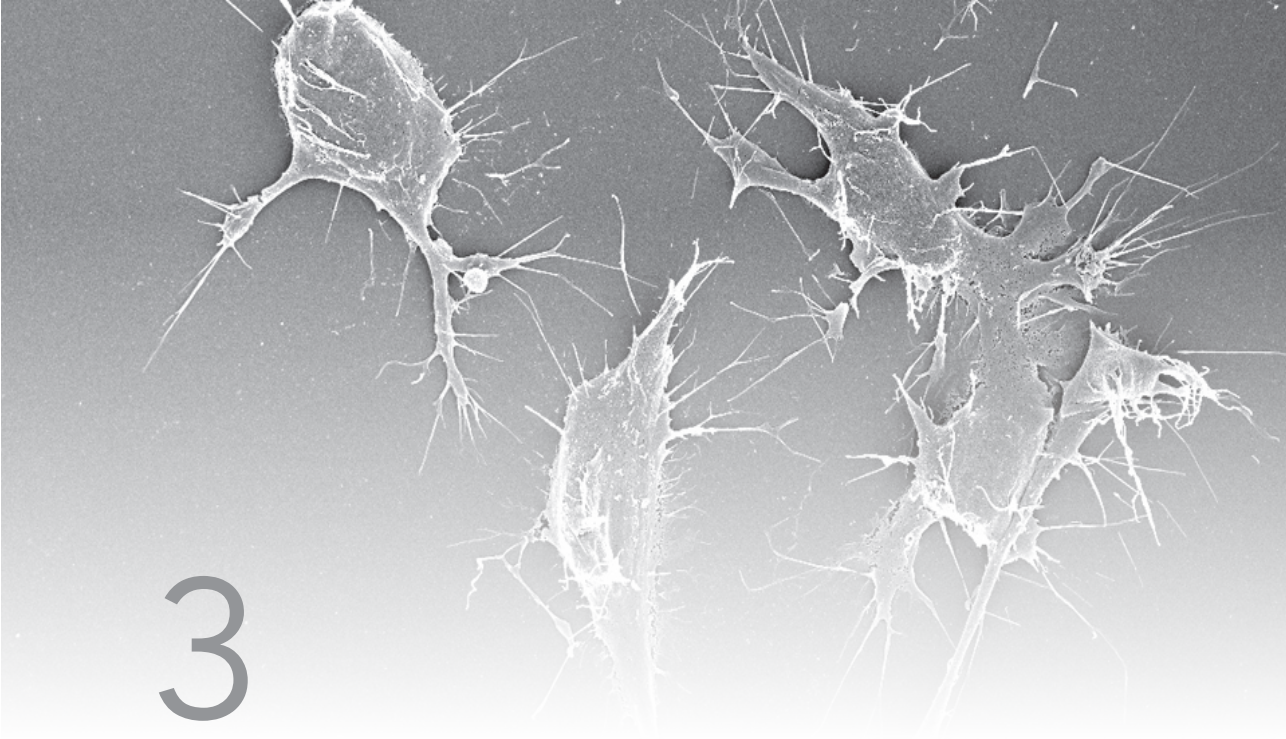

3

Submembraneous recruitment of creatine kinase B supports formation of dynamic actin-based protrusions of macrophages and relies on its C-terminal flexible loop

Gerda Venter[1], Saskia Polling[1], Helma Pluk[1], Hanka Venselaar[2], Mietske Wijers[1], Marieke Willemse[1], Jack A. M. Fransen[1], and Bé Wieringa[1]

[1]Department of Cell Biology and [2]Centre for Molecular and Biomolecular Informatics, Radboud Institute for Molecular Life Sciences, Radboud University Medical Centre, Nijmegen, The Netherlands

(Submitted)

Abstract

Subcellular partitioning of creatine kinase contributes to the formation of patterns in intracellular ATP distribution and the fuelling of cellular processes with a high and sudden energy demand. We have previously shown that brain-type creatine kinase (CK-B) accumulates at the phagocytic cup in macrophages where it is involved in the compartmentalized generation of ATP for actin remodeling. Here, we report that CK-B catalytic activity helps in the formation of protrusive ruffle structures which are actin-dependent and abundant on the surface of both unstimulated and LPS-activated macrophages. Recruitment of CK-B to these structures occurred transiently and inhibition of the enzyme's catalytic activity with cyclocreatine led to a general smoothening of surface morphology as visualized by scanning electron microscopy. Comparison of the dynamics of distribution of YFP-tagged CK-mutants and isoforms by live imaging revealed that amino acid residues in the C-terminal segment (aa positions 323-330) that forms one of the protein's two mobile loops determine its partitioning over inner regions of the cytosol and nearby sites where membrane protrusions occur during induction of phagocytic cup formation. Whereas wt CK-B, muscle-type CK (CK-M), and a catalytically dead CK-B-E232Q mutant with intact loop region were normally recruited from the cytosolic pool, no dynamic transition to the phagocytic cup area was seen for the CK-homologue arginine kinase and a CK-B-D326A mutant protein. Bioinformatics analysis helped us to predict that conformational flexibility of the C-terminal loop, independent from conformational changes induced by substrate binding or catalytic activity, is likely involved in exposing the enzyme for binding at or near the sites of membrane protrusion formation.

Introduction

The creatine kinase-phosphocreatine (CK-PCr) phosphagen system [1] serves to store chemical energy in the form of high-energy phosphoryl groups and to connect subcellular sites of ATP utilization with sites of glycolytic or mitochondrial ATP production without the need for ATP and ADP to diffuse back and forth [2]. To fulfill this energy-transport role, transfer reactions are involved in which the reversible exchange of a high energy phosphoryl group between phosphocreatine and ATP is catalyzed by different creatine kinases (CKs) [3, 4]. In vertebrates, this CK-PCr system is farthest evolved and comprises a set of multimeric enzyme isoforms that are expressed in a tissue- and cell-specific manner and are subcellularly compartmentalized. Four different genes encode the CK subunits that form the different homo- or heteromeric proteins. Functional cytosolic isoforms BB-, BM- and MM-CKs are found as dimeric proteins predominantly in brain and many other tissues, in heart, and in skeletal muscle, respectively. Mitochondrial isoforms UbCKmit (or Mi_a-CK) and ScCKmit (or Mi_b-CK) occur as dimeric and octameric proteins and are ubiquitously expressed, or found only in skeletal muscle cells, respectively [5]. Many ATP-dependent systems, for example, the Na^{2+}/K^{+}-ATPase [6], ATP-gated K^{+} channel [7], Ca^{2+}-ATPase [8] and actin-myosin ATPase for muscle contraction [9-11] rely on this phosphagen-mediated ATP-supply. Lack of CK isoforms *in vivo*, however, is not associated with complete loss of viability and function because of redundancy in the brain, heart and muscle systems for ATP supply and because of structural adaptation and physiological compensation [12].

We ourselves have shown that actin-based cell motility in non-muscle cells like astrocytes, macrophages and osteoclasts is also fuelled by CK-mediated ATP transfer [13, 14]. In astrocytes, brain-type creatine kinase (CK-B) is most prevalent. It transiently accumulates in membrane ruffles and ablation of its activity reduces spreading and migration performance. Also in macrophages, which accumulate PCr at a molar level that is three- to five-fold higher than that of ATP [15], CK-B is the most abundant isoform [3]. Its expression increases upon differentiation of monocytes into macrophages. Upon further differentiation of this monocytic lineage into osteoclasts, expression is even further upregulated [16]. During phagocytosis in peritoneal macrophages, obtained as either resident or thioglycollate-elicited cells, 40-50% of the PCr pool is depleted while global ATP levels remain stable [17]. Moreover, CK-B is activated in macrophages after LPS treatment [18, 19], indicating that reversible CrP to creatine (Cr) conversion may play an essential part in the physiological regulation of macrophage end function. In accordance with prevailing ideas based on these observations, we have identified a role for CK-B in morphodynamics in and around the phagocytic cup during CR3-mediated phagocytosis in macrophages, where the

enzyme was found to accumulate and be involved in local actin recruitment and polymerization/depolymerization dynamics. Depletion or pharmacological and genetic blockade of CK activity specifically affected the early stages of phagocytosis, i.e. actin-dependent adhesion of the particle, as well as steps in the internalization process [14]. This suggests a role for CK-B in the formation and/or functioning of the particle capturing machinery, which comprises filopodia and membrane ruffles for probing the cell's environment and capturing phagocytic targets [20-23]. Apart from having a role in phagocytosis, formation of actin-rich protrusive structures may also be involved in macropinocytosis, another highly active endocytic process in macrophages [24]. CK's significance therein and in various other membrane protrusive events remains to be examined.

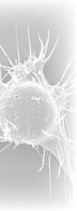

Here, we address the question on how CK-B is recruited to the subcellular sites where actin-dependent membrane protrusions are formed in macrophage cell lines. We report on study of the morphological effects of pharmacological inhibition of CK-B with cyclocreatine and the partitioning behavior of EYFP-tagged wt and mutant homologs. These analyses suggest that the C-terminal flexible loop is crucial for CK-B's recruitment to subcellular regions of the cell where phagocytic cups are formed during ingestion of complement opsonized zymosan (COZ) particles. By analogy, we think that the accumulation of CK-B to spontaneously formed membrane ruffles is controlled similarly.

Material and Methods

Reagents
All reagents were obtained from Sigma (St. Louis, MO, USA), unless stated otherwise.

Cell culture
RAW 264.7 cells (kind gift from Dr. Hong-Hee Kim, Department of Cell and Developmental Biology, School of Dentistry, Seoul National University, Korea) [16] were maintained in high-glucose DMEM (Gibco, Life Technologies, Paisley, UK) supplemented with 10% heat inactivated FBS (PAA laboratories, Pasching, Austria), 1 mM sodium pyruvate, and 4 mM GlutaMAX (Gibco, Life Technologies, Paisley, UK), at 37°C in a humidified atmosphere with 7.5% CO_2. Maf-DKO cells (kind gift from Dr. Michael H. Sieweke, Centre d'Immunologie de Marseille-Luminy (CIML), Université Aix-Marseille, France) [25] were maintained in the same way except that medium was supplemented with 20% conditioned medium from L929-cells containing macrophage colony stimulating factor (M-CSF).

DNA constructs and transfection
The EYFP-CK-B expression vector (pEYFP-CK-B) was constructed as previously described [14]. To generate plasmids EYFP-CK-B-D326A and -E232Q that encode tagged-mutant CK-Bs, we excised EcoRI-XhoI or EcoRI-SalI DNA inserts with the entire CK-ORF from either pSG8-puroCK-B-D326A or pSG8puroCK-B-E232Q (H.Pluk, unpublished) and reintroduced these segments into EcoRI-XhoI or EcoRI-SalI opened pEYFP-C2 (Clontech) vectors, respectively. EGFP-CK-M was subcloned from pCMVsport-EGFP-CK-M [26] into pSG8-puro [27] by EcoRI – XhoI digestion. Arginine kinase (AK) cDNA was amplified by PCR from a pOT2 vector containing DNA from *Drosophila melanogaster* EST clone GH11670 (DGRC, Bloomington, IN) [28]. The 5' PCR primer contained the translation start codon and an EcoRI restriction site (5'-CACGAATTCATGGTTGATGCCGCTGTT-3'), and the 3' PCR primer contained a silent mutation at S^{355} (GCC→GAC) and a BamHI restriction site (5'-GATGGATCCTTACAGACTCTTCTCGAG CTTGATC-3'). The primers were designed using GeneRunner v3.05. The resulting PCR product with AK ORF was cloned into the pEYFP-C2 vector by EcoRI – BamHI digestion. The protein encoding segments of pEYFP-AK and pSG8puro-GFP-CK-M plasmid DNAs were verified by DNA sequencing analysis using as forward primer 5'-CGATCACATGGTCCTGCTGG-3' and reverse primers 5'-GTTTCAGGTTCAGGGGGAGG-3' and 5'-GGACAAACCACAACTAGAATG-3' (Eurogentec), respectively.

Transfection of RAW 264.7 cells was performed with linearized plasmid DNA using Lipofectamine LTX and Plus (Invitrogen, Life Technologies, Paisley, UK). Brief-

ly, opti-MEM (250 µl; Invitrogen, Life Technologies, Paisley, UK) was mixed with 2 µg DNA, 2.5 µl plus reagent and 5 µl LTX, according to the manufacturer's protocol. Prior to use pEYFP, pEYFP-CK-B and pEYFP-AK were linearized with MluI and pSG8puro-GFP-CK-M was linearized with NdeI. To obtain stably transformed cell lines, transfected RAW 264.7 cells were placed under constant drug-selection for two weeks using either puromycin (5 µg/ml) or G418 (500 µg/ml). After this selection, the fraction of fluorescently positive cells in the population was further enriched by FACS sorting.

Western Blot analysis

Protein expression was analyzed by western blot analysis. After washing cells twice with cold PBS in 6 cm culture dishes, cell lysates were prepared in lysis buffer (50 mM Tris-HCl pH 7.5, 100 mM NaCl, 5 mM $MgCl_2$, and 0.5% NP-40; 4°C) and stored at -20°C until analysis. Lysates containing ± 10 µg protein were mixed with 5x sample buffer (0.25 % bromophenolblue, 0.5 M DTT, 50 ml glycerol, 10 %SDS, and 0.25 M Tris-HCl pH 6.8), heated at 95°C for 5 minutes, and loaded onto 12% SDS-PAGE gels. After electrophoretic separation, proteins were blotted onto PVDF membranes. Membranes were blocked with 5% (w/v) skimmed milk in PBS-T for 1 hour and labeled overnight with monoclonal anti-Tubulin (1:5000; DSHB, University of Iowa) and monoclonal anti-CK-B (1:5000; 21E10 [29]) antibodies at 4°C. After washing the membranes three times for 5 minutes with PBS-T, they were incubated with a goat anti-mouse IRDye 800 secondary antibody for one hour at room temperature. This was followed by 4 wash steps of 5 minutes each in PBS-T, a final wash step in PBS, and signal detection on the Odyssey Infrared Imaging System (LI-COR Biosciences, Lincoln, NE, USA). Tubulin served as loading control and reference for calculation of protein expression.

Scanning electron microscopy

For morphological examination, RAW 264.7 (60,000) and Maf-DKO (120,000) cells were seeded on 12 mm glass coverslips in 24-well plates and stimulated overnight with 100 ng/ml LPS or left unstimulated. Prior to fixation, medium was replaced with fresh medium containing 0, 5, 10, or 50 mM cyclocreatine. After 3 hours, cells were washed once with PBS and fixed with 2% glutaraldehyde in 0.1 M sodium cacodylate buffer for 1 hour. After washing cells twice with sodium cacodylate buffer, coverslips were stored in this buffer at 4°C until further fixation with 1% OsO_4 (osmium tetroxide) for 30 minutes. Coverslips were then washed once with water and dehydrated in a graded series of alcohol washes. Finally, coverslips were critical point dried and mounted for scanning electron microscopy on a JEOL SEM6340F Field Emission Scanning Electron microscope.

Immunofluorescence and actin staining

To examine the actin cytoskeletal morphology and assess the presence of CK-B in membrane protrusions, 60,000 RAW 264.7 and/or 120,000 Maf-DKO cells were seeded on glass coverslips in 24 well tissue culture plates and stimulated overnight with 100 ng/ml LPS or left unstimulated. Where applicable, cells were treated with 0, 5, 10, or 50 mM cyclocreatine for three hours, prior to fixation. Cells were fixed in 1% paraformaldehyde (PFA) by adding an equal volume of 2% PFA in 0.2 M phosphate buffer (PB) to cells. Fixative was replaced with fresh 1% PFA/0.2 M PB after 15 minutes, and cells were incubated for an additional 15 minutes. Coverslips were washed twice with PBS and twice with PBS containing 20 mM glycine (MP Biomedicals, Illkirch Cedex, France; PBS-G) before permeabilization with 0.1% saponine/PBS-G for 20 minutes. Cells were then incubated with primary antibody (anti-CK-B (21E10), 1:2000 [29]) in 0.1% saponine/PBS-G for one hour at room temperature. After four wash steps of 2-4 minutes each with 0.1% saponine/PBS-G, cells were incubated with goat anti-mouse Alexa 488-tagged secondary antibody (1:500) and/or Alexa 568-labeled phalloidin (1:600 in 0.1% saponine/PBS-G) for 1 hour. Cells were successively washed four times for 2-4 minutes with 0.1% saponine/PBS-G and once with PBS alone. Coverslips were removed from wells, rinsed once in water, air dried, and imbedded in MoWiol on microscope slides. Images of cells stained for CK-B were acquired on an Olympus FV1000 or a Zeiss LSM510 META confocal laser scanning microscope. Alternatively, z-scans consisting of 20 x 0.5 µm sections and the pinhole adjusted to one airy unit were recorded and merged to one single image (maximal projection) using Fiji imaging software.

Quantification of imaging results

To quantify the number of dorsal surface protrusions, SEM images were used. A region of interest with an area of 20-130 μm^2 was drawn on the cell body of single cells using Fiji imaging software. All protrusive structures (mainly comprising small and large membrane ruffles and not filopodia) within this region were counted and the number of surface protrusions per square micron was calculated. Per condition, 11-35 cells from five different fields were analyzed.

For quantification of filopodia extending laterally from the cell body, lines were drawn to delineate contour segments of cells in areas where no contacts with neighboring cells were seen. The number of filopodia extending from each contour segment was determined. 16-34 line segments, with a total contour length corresponding to the circumference of 10-35 cells, were analyzed per condition.

The percentage of cells with ruffled or actin rich leading edges were determined from SEM and immunofluorescence images, respectively. Per field analyzed, the total number of cells was counted as well as the number of cells that displayed

these structures and the percentage was calculated. Per condition, five SEM fields containing a total of 8-22 cells and 7 fluorescence microscopy fields containing a total of 37-59 cells were analyzed.

Phagocytosis assay

Phagocytic efficiency of complement opsonized zymosan (COZ) was determined as described previously [14]. RAW 264.7 (75,000) and Maf-DKO cells (200,000) were seeded in 12 well tissue culture plates in medium containing 20% L929 conditioned medium and stimulated overnight with 100 ng/ml LPS. Prior to assay, cells were incubated in medium containing 0, 5, 10, or 50 mM cyclocreatine (2-Imino-1-imidazolidineacetic acid) for three hours. FITC-labeled zymosan particles were opsonized by incubation in FBS for 1 hour at 37°C, washed twice with PBS, and finally resuspended in serum-free medium containing 0, 5, 10, or 50 mM cyclocreatine. Cells were washed once with DMEM and incubated with 1 ml COZ suspension for 30 minutes at 37°C. The particle-to-cell ratio was approximately 10:1. Particle engulfment was terminated after washing cells twice with PBS and removing extracellular COZ by treatment with 500 µl 100 U/ml lyticase for 10 minutes at room temperature. Successively, cells were detached with 0.05% trypsin/0.5 mM EDTA (Gibco, Life Technologies, Paisley, UK), resuspended in 1 ml medium with serum, pelleted, and finally resuspended in 200 µl 1% paraformaldehyde in PBS. Samples were analyzed by FACS (BD FACSCalibur) and phagocytosis efficiency was determined by measuring the percentage of FITC positive cells and the fluorescence intensity in these cells. The phagocytic index of each sample was calculated as the product of the mean FITC intensity of the positive population times the % of FITC positive cells.

Live imaging

Unlabeled zymosan was opsonized as described for the phagocytosis assay above. Phagocytosis of COZ was recorded live on a Zeiss LSM510 META confocal laser scanning microscope equipped with a temperature and CO_2 controllable incubation chamber and lens heater. RAW 264.7 cells expressing different fluorescently labeled CK-B constructs or homologues were seeded in WillCo dishes (120,000 cells/dish) and activated either with LPS (100 ng/ml, overnight) or PMA (phorbol 12-myristate 13-acetate; 200 µM, 15 minutes). Before cells were imaged, medium was replaced with phenolred-free DMEM (Gibco, Life Technologies, Paisley, UK) supplemented with 1 mM sodium pyruvate, and 4 mM GlutaMAX. Dishes were mounted on the microscope and cells were allowed to equilibrate (5-10 minutes) before COZ was added. After the addition of COZ, image acquisition was started using a Plan Apochromatic 63x, 1.4 NA oil immersion DIC lens (Carl Zeiss GmbH, Jena, Germany). The

pinhole was adjusted to obtain optical slices of 3 µm and images were taken every 3 seconds.

To determine the increase in fluorescence at the cup, one single frame showing maximal accumulation was selected from each movie by hand by scanning through line plots of al images in the stack using Fiji imaging software. Regions of interest (ROIs) were then drawn around the phagocytic cup and at a region in the cytosol next to the nucleus and the mean fluorescence intensity in these ROIs were measured, also using Fiji imaging software. The increase in fluorescence intensity (fold change) was calculated from the ratio of fluorescence intensities at the cup and in the cytosol.

Bioinformatics analysis

Amino acid sequences of CK-B (mouse; *NCBI: NP_067248*), CK-M (mouse; *NCBI: NP_031736*), and AK (isoform D, *Drosophila melanogaster*; *NCBI: NP_523988*) were compared using CLUSTEL 2.0.8 multiple sequence alignment [30]. Possible post translational modification differences were identified by using prediction software for phosphorylation (NetPhos 2.0 [31]) and sumoylation (SUMOsp2.0 [32]). Possible PKC phosphorylation sites were predicted using MetaPredPS, 2007, University of Minnesota.

In order to study the differences between CK-B, CK-M, and AK in their open and closed conformations we built homology models. To generate the models we used an automatic script in the WHAT IF & YASARA Twinset [33, 34] with standard parameters. The following PDB-files were chosen as templates: CK-B closed form: human brain type CK, *PDB: 3B6R* [35], sequence identity 97%; CK-B open form: bovine retinal CK, *PDB: 1g0w* [36], sequence identity 98%; CK-M closed form: rabbit muscle CK, *PDB: 1u6r* [37], sequence identity 98%; CK-M open form: rabbit muscle CK, *PDB: 2crk* [38], sequence identity 98%; AK closed form: white schrimp AK, *PDB: 4bg4* [39], sequence identity 82%; AK open form: white schrimp AK, *PDB: 4bhl* [39], sequence identity 82%. The models were visualized and studied using the WHAT IF & YASARA Twinset.

Differences in surface accessible residues were assessed by analyzing the CK-B, CK-M, and AK models in ASAview [40]. Residues were considered accessible when the relative accessibility was higher than 0.25.

Statistical analysis

Data was analyzed either using an unpaired t-test or one-way ANOVA and Bonferroni's multiple comparison test (GraphPad software, Inc., Version 4). All values are expressed as mean +/-SEM. Values were considered to be significantly different when p values were < 0.05.

Results and discussion

Cyclocreatine inhibits formation of actin-rich membrane ruffles in macrophages

Stimulation with PMA or LPS induces the activaction and polarization of macrophages with formation of membrane ruffles and the accumulation of Mac-1 ($\alpha_M\beta_2$ integrin/CR3) in these structures [23, 41, 42]. Ruffling behavior enhances phagocytosis of complement opsonized particles and is also involved in mediating reversible cell-substratum interactions during cell spreading and movement. Since CK-B has a role in both the binding and internalization of complement opsonized zymosan (COZ) during phagocytosis [14] and also in facilitating cell mobility [13], we wondered whether inhibition of CK-B would also affect membrane ruffle formation proper. To resolve this issue, knowing that different macrophage populations *in vivo* comprise phenotypically heterogeneous pools of cells [43, 44], we decided to include two distinct types of macrophage lineages, RAW 264.7 and *MafB/c-Maf* deficient (Maf-DKO) cells, in our analysis. RAW 264.7 and *MafB/c-Maf* deficient cells are macrophages of different origin [25, 45] and morphological appearance. To modulate CK activity in these cells we chose for acute pharmacological inhibition with cyclocreatine to avoid the adaptation and compensation that can occur as a long-term effect in the metabolic energy network, upon permanent genetic ablation [12, 26]. Survey with scanning electron microscopy (SEM) revealed, as shown in Figure 1 and 2, that Maf-DKO cells displayed a far more complex surface morphology than RAW 264.7 cells under basal conditions. Whereas the surface of Maf-DKO cells was totally covered by protrusive membrane structures (mainly comprising membrane ruffles of variable size), RAW 264.7 cells displayed only a few such structures (Figure 1A,I and 2A,I). Furthermore, RAW 264.7 cells had multiple long filopodia extending from the cell body, while Maf-DKO cells had less and also shorter filopodia (Figure 1A,K and 2A,K). Upon LPS stimulation the morphology of the two cell lines changed differentially. RAW 264.7 cells underwent a radial spreading while Maf-DKO cells obtained an elongated morphology with two long, thin cellular processes extending from the cell body (Figure 1B and 2B). Strikingly, despite these morphological differences cyclocreatine treatment caused both types of macrophages to display fewer dorsal ruffle structures, resulting in a much smoother appearance (Figure 1A-J and 2A-J). Disappearance of ruffles was already visible upon inhibition with 5 mM cyclocreatine and became even more evident with increasing inhibitor concentrations. Interestingly, the cells preserved their ability to produce lateral filopodia to a large extent (Figure 1K,L and 2K,L), suggesting that CK-B is not directly involved in filopodia formation of macrophages.

To determine whether differential distortion of actin cytoskeletal remodeling could explain the inhibitor effects on surface ruffle formation we analyzed the ap-

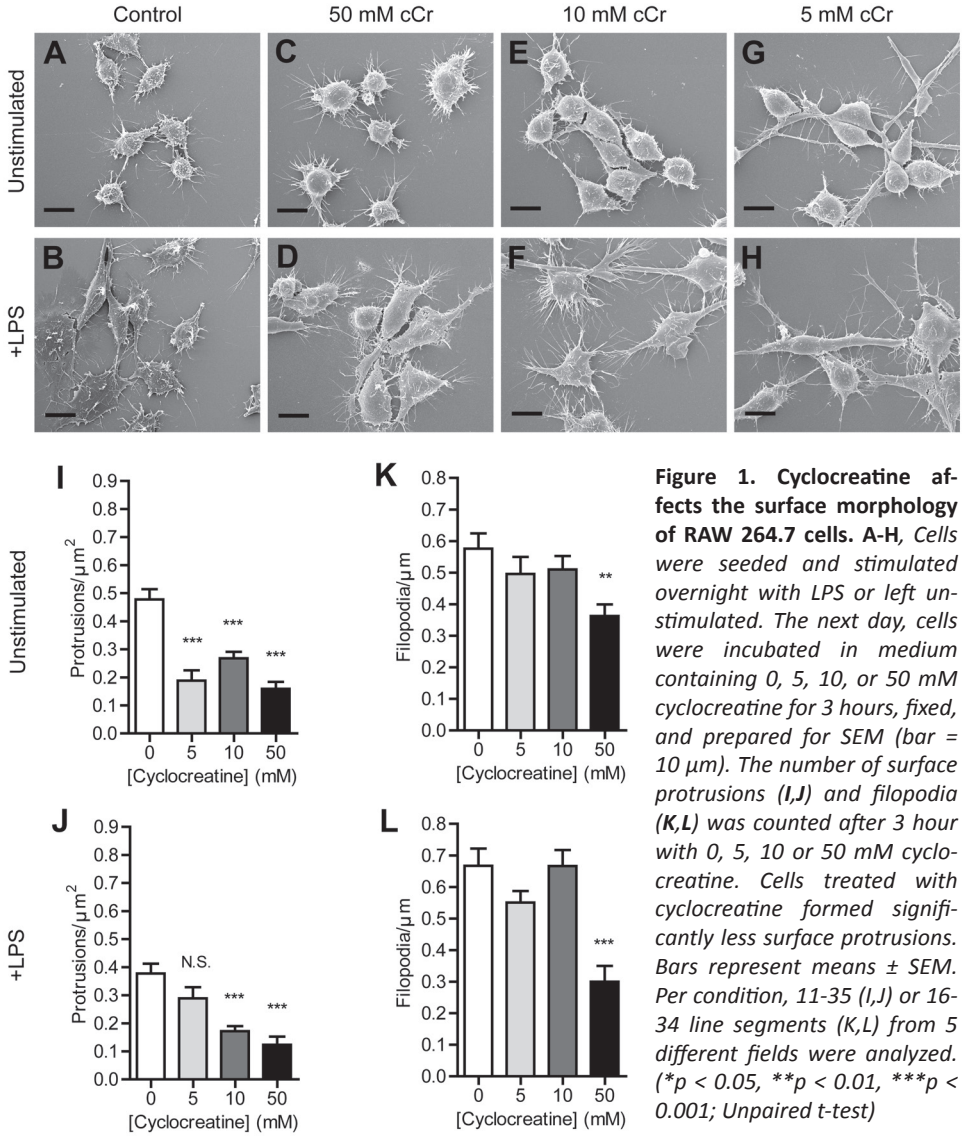

Figure 1. Cyclocreatine affects the surface morphology of RAW 264.7 cells. A-H, *Cells were seeded and stimulated overnight with LPS or left unstimulated. The next day, cells were incubated in medium containing 0, 5, 10, or 50 mM cyclocreatine for 3 hours, fixed, and prepared for SEM (bar = 10 µm). The number of surface protrusions (**I**,**J**) and filopodia (**K**,**L**) was counted after 3 hour with 0, 5, 10 or 50 mM cyclocreatine. Cells treated with cyclocreatine formed significantly less surface protrusions. Bars represent means ± SEM. Per condition, 11-35 (I,J) or 16-34 line segments (K,L) from 5 different fields were analyzed. (*p < 0.05, **p < 0.01, ***p < 0.001; Unpaired t-test)*

pearance of the F-actin structures in Maf-DKO and RAW 264.7 cells in the presence and absence of LPS and different cyclocreatine concentrations. Phalloidin staining revealed that most Maf-DKO cells have a distinct, actin rich leading edge (Figure 3A,B), whereas RAW 264.7 cells lack this polarity (not shown). Comparing the phalloidin images with our SEM results revealed that these actin-rich leading edges were decorated with multiple membrane ruffles (inserts Figure 2A,B). Strikingly, in the presence of 5 mM cyclocreatine the actin staining at these edges became more faint (Figure 3C,D) and with increasing cyclocreatine concentration cells lost

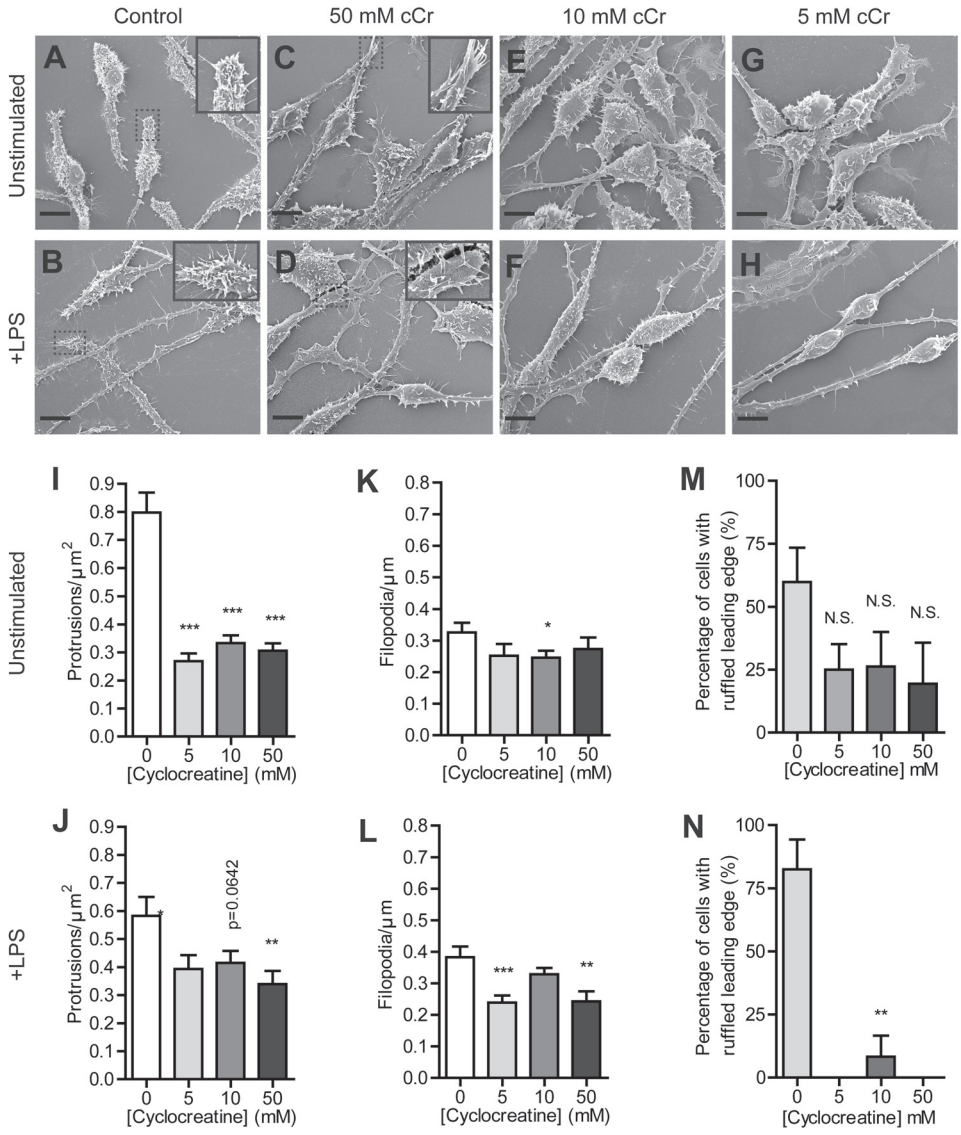

Figure 2. Cyclocreatine affects the surface morphology of Maf-DKO cells. A-H, *Cells were seeded and stimulated overnight with LPS or left unstimulated. The next day, cells were incubated in medium containing 0, 5, 10, or 50 mM cyclocreatine for 3 hours, fixed, and prepared for SEM. Inserts in the right hand upper corner in A, B, C and D are magnifications of the cell tips in the dashed boxes. Note the loss of membrane ruffles on these cell tips in Maf-DKO cells already upon 5 mM cyclocreatine treatment, (bar = 10 µm). The number of surface protrusions (**I**,**J**) and filopodia (**K**,**L**), or the number of ruffled leading edges (**M**,**N**) was counted after 3 hour incubation with 0, 5, 10 or 50 mM cyclocreatine. Bars represent means ± SEM. Per condition, 11-35 (I,J) or 8-22 (M,N) cells, or 16-34 line segments (K,L) from 5 different fields were analyzed. (*p < 0.05, **p < 0.01, ***p < 0.001; Unpaired t-test)*

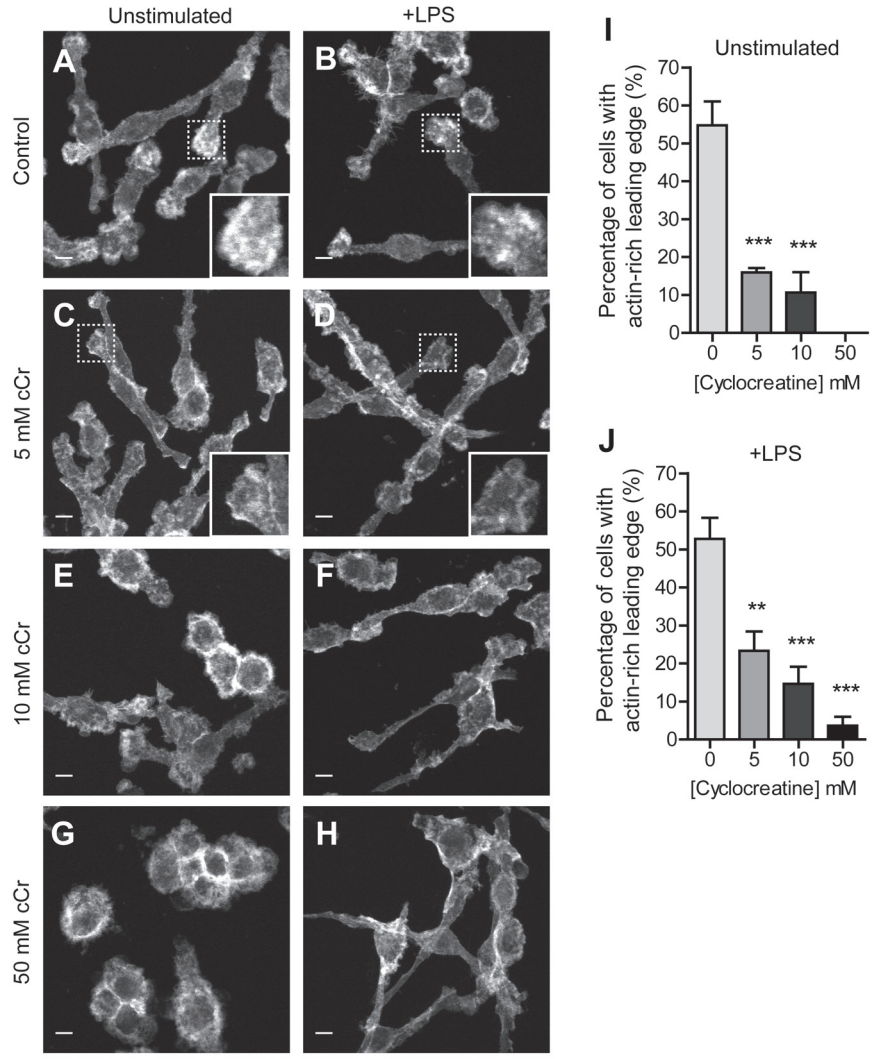

Figure 3. Inhibition of CK-B reduces actin-rich membrane ruffles in macrophages. A-H, *Maf-DKO cells were seeded and stimulated overnight with LPS or left unstimulated. The next day, cells were incubated in medium containing 0, 5, 10, or 50 mM cyclocreatine for 3 hours after which they were fixed in paraformaldehyde and stained with Alexa568-labelled phalloidin. Z-scans were made on a Zeiss LSM510 META confocal laser scanning microscope and merged to one single image (maximal projection) using Fiji imaging software. Inserts in the right hand lower corner in A, B, C and D are magnifications of the cell tips in the dashed boxes. Note the loss of actin staining on these cell tips after 5 mM cyclocreatine treatment and the loss of polarity after 10 and 50 mM cyclocreatine treatment. (Bar = 10 µm).* ***I,J,*** *Quantification of actin-rich leading edges. Cells treated with cyclocreatine formed significantly less actin-rich leading edges in a concentration-dependent manner. (*p < 0.05, **p < 0.01, ***p < 0.001; Unpaired t-test)*

polarity so that no leading edges were recognizable anymore (Figure 3E-H). Correspondingly, our SEM images showed that membrane ruffles were absent from cell tips after inhibition with cyclocreatine (inserts Figure 2C,D). Quantification of the number of ruffled leading edges and the percentage of cells with actin-rich leading edges confirmed that cyclocreatine inhibited the formation of these structures (Figure 2M,N and 3I,J). Together, these observations suggest that CK-B is involved in the formation of some, but perhaps not all, types of actin-dependent membrane protrusions that form the particle capturing or adhesion machinery of macrophages. This apparently differential CK-B dependence could be associated with the stability/turnover rate of the structures. Filopodia serve to attach the cell to the substratum and are therefore less dynamic than membrane ruffles that continuously form and fold back on the cell surface. The more static nature of filopodia may render them less dependent on acute and local CK-B-mediated ATP-supply. In line with this, confocal microscopy also did not reveal specific accumulation of EYFP-CK-B in filopodia of RAW 264.7 cells (unpublished results). Clearly, our analyses permit only tentative conclusions as they are based on the interpretation of still images as a kind of endpoint measurement. In order to distinguish between the local or global role of CK-B and know more about the possible mechanism(s) involved in linking its activity to formation of different types of protrusions, additional experiments, with live recording of the formation or disappearance of these structures under different metabolic conditions, ultimately will be necessary.

COZ phagocytosis is compromised in LPS stimulated RAW 264.7 and Maf-DKO cells after CK-B inhibition with cyclocreatine

Here we decided to concentrate first on the biological significance of ruffling behavior. In order to see whether loss of membrane ruffling activity by blockade of CK-B phosphoryl exchange capacity was indeed also accompanied by a reduction in complement opsonized particle uptake in both cell lines, we monitored the capacity of RAW 264.7 and Maf-DKO cells to phagocytose COZ. Pharmacological inhibition of CK-B with cyclocreatine significantly reduced phagocytosis of COZ in LPS-stimulated RAW 264.7 and Maf-DKO cells (Figure 4). Interestingly, Maf-DKO cells which presented the more complex surface morphology also showed the highest efficiency in phagocytosis. Another conspicuous observation was that an approximately ten times higher concentration of cyclocreatine was needed in these cells to reach the same degree of inhibition as in RAW 264.7 cells. As Western blot analysis revealed no overtly deviant expression level for CK-B in Maf-DKO cells (Figure 5), we cannot explain these quantitative differences by simple correlation to differences in enzyme activity level between the two types of macrophages. Qualitatively, our data support the idea that ruffle activity and phagocytosis efficiency are coupled,

and that CK-B activity mediates the binding and uptake of complement opsonized particles via control over dynamic formation of protrusive membrane structures in macrophages. Indeed, a model in which the surface density of structures is a determining factor in the macrophage's capacity to adhere to and capture foreign particles also explains our earlier observation that CK-B is in control of the initiating steps in phagocytosis [14].

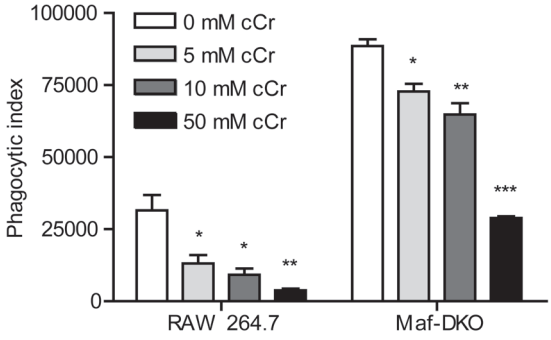

Figure 4. Inhibition of CK-B by cyclocreatine inhibits phagocytosis of COZ in RAW 264.7 and Maf-DKO macrophages. *Cells were seeded and stimulated overnight with LPS. Prior to the assay, cells were treated with 0, 5, 10, or 50 mM cyclocreatine for 3 hours. FITC-labeled COZ was added in serum-free medium and cells were incubated for 30 minutes at 37°C. After washing, cells were detached and fixed for FACS. The phagocytic index was calculated as described in materials and methods. Bars represent means ± SEM of three experiments performed in triplicate. (*p = 0.05, **p = 0.01, ***p = 0.001; Unpaired t-test).*

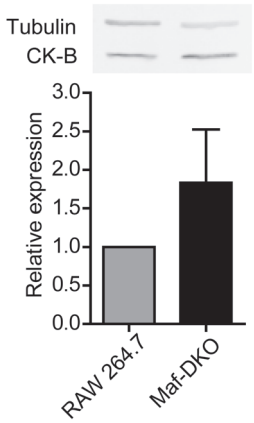

Figure 5. CK-B expression in RAW 264.7 and Maf-DKO cells. *Bars represent the average band intensities ± SD of two blots. Expression was calculated relative to tubulin.*

CK-B localizes to membrane ruffles on macrophage cell tips

Earlier, we have demonstrated that CK-B localizes to membrane ruffles in astrocytes [13] and is actually also present in the phagocytic cup area during particle ingestion in macrophages [14]. Organellar or intracellular compartmentation and local recruitment by association to cellular structures is important for control of CK's phosphoryl exchange capacity [46], and hence the distribution of ATP availability. Here we used im-

munostaining with specific CK-B antibodies because we wished to know whether the association of CK-B with ruffles in macrophages had a permanent or temporal character. Since CK-B localization in the vicinity of sites of membrane ruffle formation could best be visualized in the leading edges of macrophages, and these structures occur relatively abundant on Maf-DKO cells, we included only these cells in our assay. The imaging results in Figure 6 show that CK-B appears to accumulate in some but not all the ruffling tips of Maf-DKO cells, suggesting that recruitment is temporal and that CK-B is not permanently associated with ruffling structures as was also found to be the case in phagocytic cups [14]. Furthermore, although both CK-B and actin localized to these regions, the two proteins did not show complete colocalization in all cells. Also this phenomenon is as observed for phagocytic cups

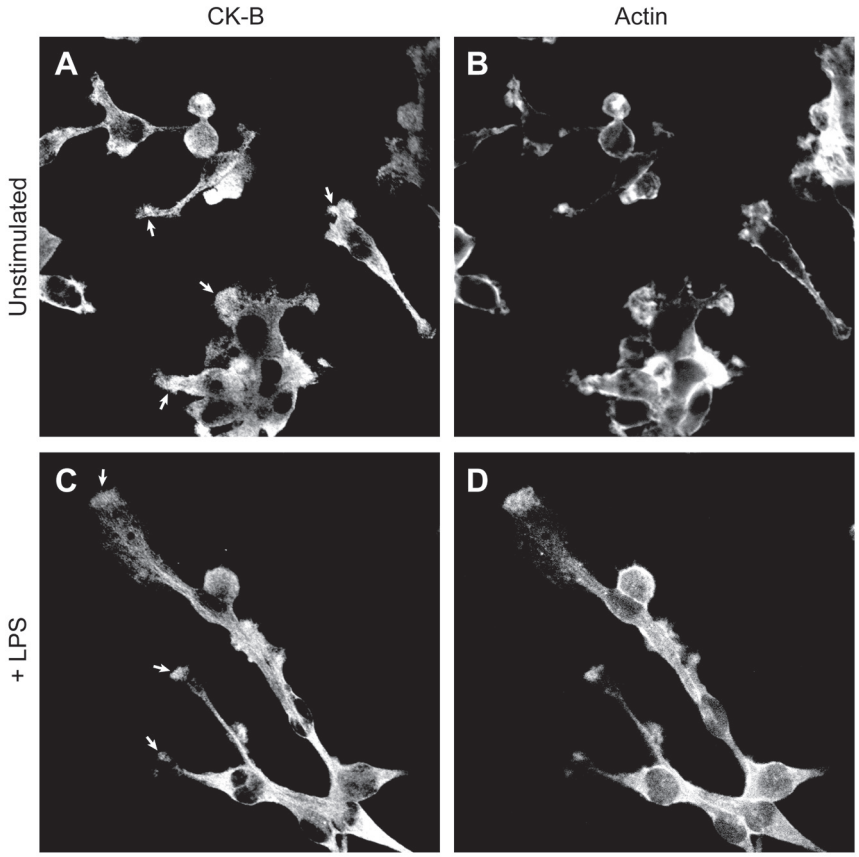

Figure 6. CK-B localizes to membrane ruffles in Maf-DKO macrophages. *Cells were seeded on glass coverslips and stimulated overnight with LPS or left unstimulated. After fixation in paraformaldehyde, cells were stained for CK-B using an antibody against mouse CK-B (**A**,**C**), and actin using Alexa568-labelled phalloidin (**B**, **D**). Images were taken on an Olympus FV1000 confocal laser scanning microscope. Arrows indicate cell tips containing CK-B*

and may be a result of differences in recruitment dynamics between the two proteins [14]. Together, our observations point to a short-term, transient, and local need for CK-B in membrane ruffle-regions wherein the actin cytoskeleton is highly dynamic. Unfortunately, the staining method used on fixed cells only reveals protein presence and did not allow us to correlate actin (de)polymerization activity with CK-B activity within different time windows of ruffle formation.

The C-terminal flexible loop of CK-B is essential for its subcellular localization to dynamic actin-based protrusions

If CK-B recruitment helps to control actin-based morphological processes that steer macrophage function, what could be the principles behind its "mobilization"? In view of the dynamic character of ruffle structures and phagocytic cups, it is not likely that recruitment of CK-B shares commonalities with the mechanism of association of CK-M to the sarcomeric M-band in muscle cells, which involves a permanent binding to myosin via adapter protein MyBPC1 [47]. Although there is a strong overall evolutionary relationship between the M- and B-type CK isoforms, exactly the lysine residues involved in this process are not conserved in CK-B [48, 49]. Also, direct preferential physical association with actin was ruled out by our group through pull-down and FRAP assays, and yeast-2-hybrid studies did not reveal any other possible binding partners [14]. Possibly, since CK-B is prone to undergo post-translational modifications including phosphorylation [50, 51], oxidation [52], methylation [53], and ubiquitination [54], temporal and reversible covalent changes in the CK-B structure itself may direct its non-permanent binding characteristics. Besides, non-covalent binding of substrate may also determine the enzyme's associative properties, as has been shown for CK-M [55].

In order to identify features in CK-B's conformation that determine partitioning behavior of the enzyme, we turned to existing literature and selected different known CK-B mutants for further tests of recruitment behavior. As a first candidate, we chose the non-conservative CK-B-D326A mutant, which exhibits some residual activity [56] but may have abnormal conformational structure [57, 58]. This mutant was studied alongside the catalytically inactive E232Q mutant, in which overall protein structure is conserved but substrate binding is reduced [56, 59]. Comparison of the cellular distribution of these two CK-B-mutants with that of wild type CK-B protein, was performed via confocal microcopy imaging of RAW 264.7 cells expressing EYFP-tagged wt CK-B, EYFP-tagged mutants CK-B-E232Q or CK-B-D326A, or free EYFP. In resting cells EYFP-CK-B-E232Q was present throughout the cytosol but excluded from the nucleus, with a slight perinuclear accumulation very similar to EYFP-CK-B (Figure 7 A,B), while EYFP-CK-B-D326A was dispersed throughout the cytoplasm like free EYFP (Figure 7C,D). Most forms of membrane protrusion formation are sponta-

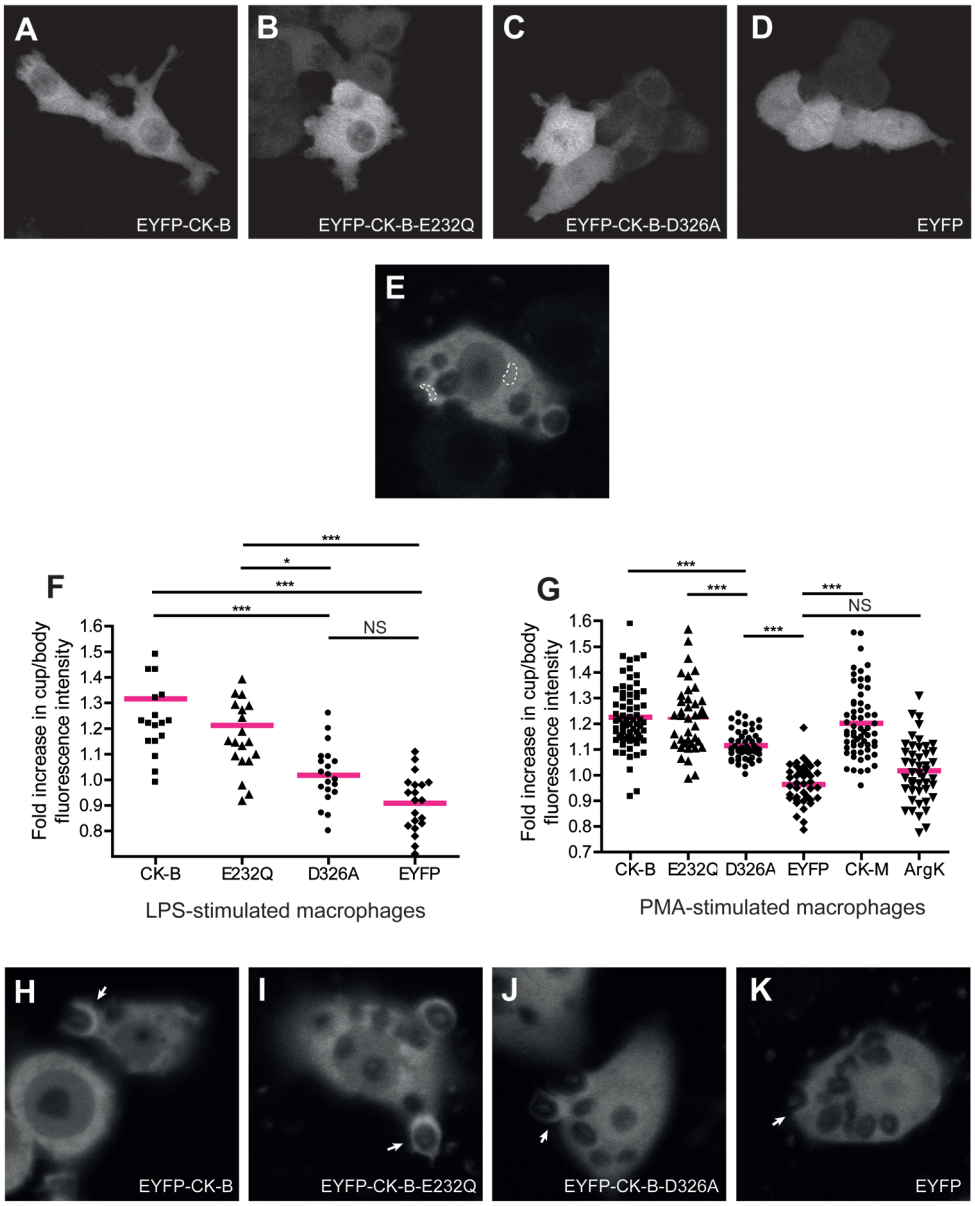

Figure 7. The D326-residue of CK-B is essential for subcellular localization. *RAW 264.7 cells expressing EYFP-CK-B (**A**), EYFP-CK-B-E232Q (**B**), EYFP-CK-B-D326A (**C**), or EYFP (**D**) were seeded on glass coverslips, incubated overnight, and fixed the next day. Images were taken on a Zeiss LSM510 meta confocal laser scanning microscope. Recruitment of the different fluorescently labeled CK-B mutants during phagocytosis of COZ was investigated by live imaging on a Zeiss LSM510 meta confocal laser scanning microscope equipped with a temperature-regulated lens and stage enclosed in a chamber with continuous CO2-supply. Cells were seeded in WillCo dishes and stimulated overnight with LPS. Before imaging, medium was replaced with phenol red- and serum-free medium. COZ was added and phago-*

*cytic uptake events were recorded live. Single frames showing maximal fluorescence intensity at the cup were selected and the mean grey value of a region at the cup and in the cell body was measured (**E**). The cup-to-body-ratio was plotted as the fold increase in fluorescence intensity at the cup (**F**). Recruitment of the different CK-B mutants as well as CK-M and AK was assessed in RAW 264.7 cells stimulated with PMA for 15 minutes (**G**). Movies were analyzed as described in E and F. Symbols in F and G represent single events (1 per cell; 20-45 per cell line) recorded on at least 2 different days in at least 4 separate dishes, and horizontal lines indicate the means of all events. (*p = 0.05, **p = 0.01, ***p = 0.001; one-way ANOVA and Bonferroni's multiple comparison test). **H-K**, Examples of single frames selected for analysis showing recruitment of EYFP-CK-B and EYFP-CK-B-E232Q but minimal or no recruitment of EYFP-CK-B-D326A and EYFP to the phagocytic cup (arrows)*

neous processes, which occur seemingly randomly in space and time and currently cannot be easily manipulated or controlled experimentally. Hence, recruitment of CK-B to such sites of local actin polymerization is difficult to follow by dynamic imaging. To monitor the actual mobilization and translocation dynamics of the different mutant CK-Bs by live-cell microscopy we therefore focused on events in LPS-stimulated RAW 264.7 cells that occur during phagocytic cup formation, where the start and site of protrusion formation is COZ particle-induced and experimentally better controllable [14]. Here, RAW 264.7 cells were selected since the individual membrane protrusions actively involved in particle uptake could be better distinguished than in Maf-DKO cells. For recording of dynamics of EYFP-CK-B variants, the fold increase in fluorescence intensity at the cup was determined by measuring the mean fluorescence intensity in the cup region and in an area in the cell body with comparable thickness (e.g. the perinuclear region; dashed lines Figure 7E). EYFP-CK-B showed a fold increase of 1.32 ± 0.25 which was in agreement with our previous results in PMA-stimulated macrophages [14]. The E232Q mutant was recruited to the same extend (1.21 ± 0.27 fold increase), while the D326A mutant and EYFP did not show any significant localization to the phagocytic cup (1.02 ± 0.11 and 0.91 ± 0.11 fold increase, respectively; Figure 7F and H-K). To ratify our findings, the behavior of these two CK-B mutants was also assessed in macrophages stimulated with PMA. Also here, EYFP-CK-B-E232Q accumulated at the cup to a similar extent as EYFP-CK-B, while the fluorescence intensity at the cup was significantly lower in EYFP-CK-B-D326A cells (Figure 7G). These results suggest that the C-terminal flexible loop, i.e. the segment harboring the D326A mutation, plays a cardinal role in CK-B recruitment during phagocytosis.

To further investigate a potential involvement of this loop in the subcellular localization of CK-B, we additionally assessed the recruitment behavior of two other phosphagen kinases (GFP-CK-M and EYFP-AK) that are related to CK-B but differ from one another with regard to this domain. CK-M exhibits high sequence similarity (76%) to CK-B with both the negatively charged cluster (residues 230-234) which is critical for enzyme activity [59], and the flexible loop region (residues 60-70 and 323-330) that closes over the active site during catalysis, conserved. Since CK-M is

an isoform of CK-B, it catalyzes the same reaction. AK (arginine kinase), on the other hand, is more distantly related (44% sequence identity) and has retained the negatively charged cluster but not the flexible loop region. AK can bind phosphocreatine, but shows no creatine kinase activity [60]. Our live imaging results revealed that GFP-CK-M could be recruited to the phagocytic cup to the same extent as EYFP-CK-B, but that EYFP-AK did not accumulate at the cup (Figure 7G). Interestingly, GFP-CK-M exhibited the same cellular distribution as EYFP-CK-B and –E232Q, while EYFP-AK remained again dispersed throughout the cytoplasm (not shown). The finding that CK-M and CK-B displayed similar "cup recruitment" behavior is particularly interesting, because Hornemann et al. [49] have shown that CK-B and CK-M have a different tendency for association to the M-band in muscle fibers. As already mentioned above, findings regarding this differential behavior by them and others [47] can be explained by the fact that CK-B lacks the essential lysine residues that enable association of CK-M via the adapter protein MyBPC1. Conversely, to explain our own findings by analogous reasoning we would like to suggest that the residues that are involved in the CK recruitment to the phagocytic cup must be conserved between CK-B and CK-M. Therefore, we tend to believe that the Asp^{326} residue in the conformational mobile loop region spanned by amino acid residues 323-333, which is involved in the substrate-induced conformational change of the enzyme, also (co) determines the subcellular distribution of CK-B. In contrast, substrate binding and catalytic activity, which are both determined by the negatively charged cluster [59] and expected to be compromised in the E232Q mutant, do not seem to control localization of the enzyme.

CK-B's C-terminal flexible loop contains multiple surface accessible residues that may be involved in enzyme recruitment

In an attempt to independently pinpoint residues in the CK molecule that may have a crucial role in determining enzyme conformation and/or recruitment behavior, we performed a bio-informatics comparison between the three natural phosphagen kinases studied above. When amino acid sequences were compared (Figure 8A), the likelihood of possible posttranslational modification differed for several residues between CK-B, CK-M, and AK. Amongst a number of lysine residues that could be modified, only Lys^{381} was predicted to be sumoylated in both CK-B and CK-M but not in AK. CK contains multiple threonine residues in the active site that are autophosphorylated, thereby modifying the enzyme kinetics [61]. However, these residues were not predicted to be differently phosphorylated in CK and AK by our bioinformatics analysis. Of the different phosphorylation sites that were predicted, we specifically found three possible PKC phosphorylation sites (Ser^{129}, Thr^{133}, and Ser^{136}) in CK-M and CK-B that were either not predicted or not conserved in AK.

Phosphorylation of these residues by PKC has been shown to regulate the activity of CK-B [50, 51]. The LPS and PMA used to activate the cells for CR3-mediated phagocytosis in our phagocytosis experiments are both potent activators of PKC [62, 63]. However, whether phosphorylation of these residues by PKC is involved in determining the localization of the enzyme remains to be proven. The same applies for predicted differences in other phosphorylation, methylation, or sumoylation sites. Mutational studies of the residues involved may provide new insights. Simple changes in the charge distribution may determine binding specificity, as has been shown for CK-M [49]. Concomitantly, such changes may also affect subcellular localization, as has been suggested by Yeung et al. [64] for proteins functioning at the cell membrane. Yet another possibility is that protein localization is determined by a combination of factors or post translational modifications that influence the overall structure of the enzyme.

Since amino acid residues that could play a role in the recruitment of CK would be expected to be accessible for interaction with accessory or modifying proteins, we constructed 3D models of the open and closed states of CK-B, CK-M, and AK and assessed the surface availability of amino acid residues in all six models using ASAview online software [40]. Although the differences that were found between CK and AK were spread across the whole molecule (not shown) and not localized to one specific region, we made one observation of interest. In CK, the hydrophobic Ala^{328} and Val^{330} are respectively replaced by a hydrophilic Glu^{317} and Glu^{319} in AK (Figure 8B). These amino acids are situated within the C-terminal flexible loop (containing CK Asp^{326} or AK Glu^{314}) which extends into the solvent in the open conformation and closes over the active site upon substrate binding (Figure 8C). Val^{330} and Ala^{328} are both surface accessible in the open and in the closed conformation of CK (Figure 8D). Together with these two residues, Cantwell et al. [56] identified two other amino acids within eight residues of the CK Asp^{326} or AK Glu^{314} that had different side-chain properties between the two enzymes, namely the non-polar Gly^{323} and Val^{325} in CK which is replaced by charged Arg^{312} and His^{315} in AK. Our surface accessibility assessment revealed that Gly^{323} is also accessible in both the open and closed conformation, with a relative accessibility >0.5 (Figure 8D). The second residue (Val^{325}) is only accessible (>0.5) in the open conformation. This valine residue forms a hydrophobic specificity pocket that accommodates the methyl group distinctive of Cr [57, 65, 66], explaining why it isn't accessible in the closed state anymore. The Asp^{326} residue itself was also found to have a relative surface accessibility in both the open and the closed conformation, but since it is predicted to interact with His^{66} in the N-terminal flexible loop upon closure, it is not expected to associate simultaneously with binding partners to facilitate recruitment.

How important is maintenance of enzyme transition state, i.e. closure of the mo-

A

```
CK-B mouse      MPFSNSHNTQKLRFPAEDEFPDLSSHNNHMAKVLTPELYAELRAKCT-PS  49
CK-M mouse      MPFGNTHNKFKLNYKPQEEYPDLSKHNNHMAKVLTPDLYNKLRDKET-PS  49
AK dmel         MVDAAVLAKLEEGYA---KLA-ASDSKSLLKKYLTKEVFDNLKNKVTPTF  46

CK-B mouse      GFTLDDAIQKGVDNPGHPYIMTVGAVAGDEESYDVFKDLFDPIIEERHGG  99
CK-M mouse      GFTLDDVIQKGVDNPGHPFIMTVGCVAGDEESYTVFKDLFDPIIQDRHGG  99
AK dmel         KSTLLDVIQSGLENHDS----GVGIYAPDAEAYTVFADLFDPIIEDYHGG  92

CK-B mouse      YQPSDEHK-TDLNPDNLQGGDDLDPNYVLSSRVRTGRSIRGFCLPPHCSR 148
CK-M mouse      YKPTDKHK-TDLNHENLKGGDDLDPNYVLSSRVRTGRSIKGYTLPPHCSR 148
AK dmel         FKKTDKHPASNFGDVSTFGNVDPTNEYVISTRVRCGRSMQGYPFNPCLTE 142

CK-B mouse      GERRAIEKLAVEALSSLDGDLSGRYYALKSMTEAEQQQLIDDHFLFDKPV 198
CK-M mouse      GERRAVEKLSVEALNSLTGEFKGKYYPLKSMTEQEQQQLIDDHFLFDKPV 198
AK dmel         AQYKEMESKVSSTLSGLEGELKGKFYPLTGMEKAVQQQLIDDHFLFKE-G 191

CK-B mouse      SPLLLASGMARDWPDARGIWHNDNKTFLVWINEEDHLRVISMQKGGNMKE 248
CK-M mouse      SPLLLASGMARDWPDARGIWHNDNKSFLVWVNEEDHLRVISMEKGGNMKE 248
AK dmel         DRFLQAANAGRFWPSGRGIYHNDAKTFLVWCNEEDHLRIISMQQGGDLGQ 241

CK-B mouse      VFTRFCTGLTQIETLFKSKNYEFMWNPHLGYILTCPSNLGTGLRAGVHIK 298
CK-M mouse      VFRRFCVGLQKIEEIFKKAGHPFMWNEHLGYVLTCPSNLGTGLRGGVHVK 298
AK dmel         IYKRLVTAVNEIEKRVP-----FSHDDRLGFLTFCPTNLGTTIRASVHIK 286

CK-B mouse      LPHLG-KHEKFSEVLKRLRLQKRGTGGVDTAAVGGVFDVSNADRLGFSEV 347
CK-M mouse      LANLS-KHPKFEEILTRLRLQKRGTGGVDTAAVGAVFDISNADRLGSSEV 347
AK dmel         VPKLASNKAKLEEVAAKYNLQVRGTRGEHTEAEGGVYDISNKRRMGLTEF 336

CK-B mouse      ELVQMVVDGVKLLIEMEQRLEQGQAIDDLMPAQK 381
CK-M mouse      EQVQLVVDGVKLMVEMEKKLEKGQSIDDMIPAQK 381
AK dmel         EAVKEMYDGITELIKLEKSL-------------- 356
```

C

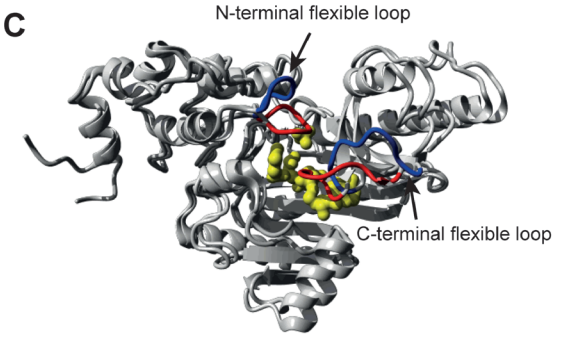

D

```
Open    CK-B mouse      315 LRLQKRGTGGVDTAAVGGVFDVSN 338
        CK-M mouse      315 LRLQKRGTGGVDTAAVGAVFDISN 338
        AK dmel         304 YNLQVRGTRGEHTEAEGGVYDISN 327

Closed  CK-B mouse      315 LRLQKRGTGGVDTAAVGGVFDVSN 338
        CK-M mouse      315 LRLQKRGTGGVDTAAVGAVFDISN 338
        AK dmel         304 YNLQVRGTRGEHTEAEGGVYDISN 327
```

B

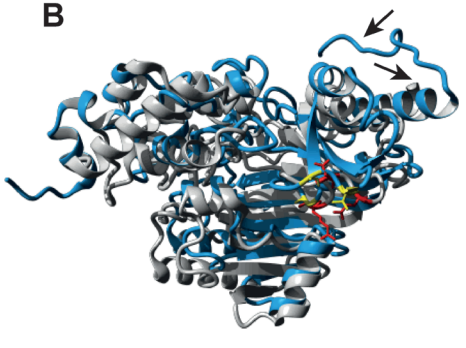

E

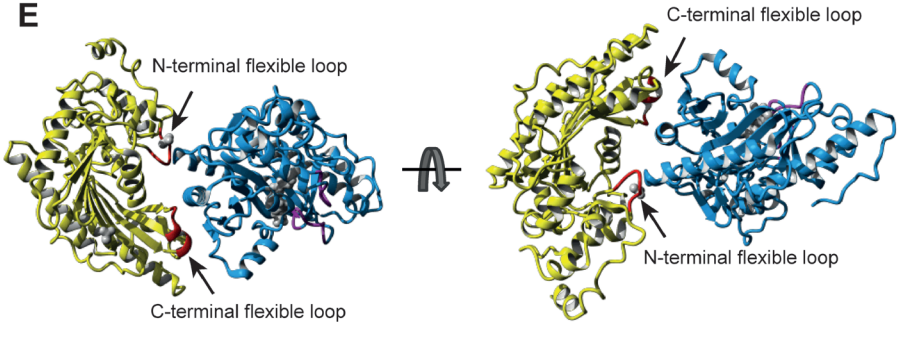

Figure 8. Sequence and structural comparison of CK and AK. A, *The amino acid sequences of mouse CK-B and CK-M, and Drosophila melanogaster AK were compared. The highly conserved negative cluster is shaded grey and the C-terminal flexible loop region is in pink. Indicated in green are residues in AK that differ from the same position in CK-B and CK-M. Residues that were predicted to be differently post translationally modified are also indicated: lysine residues (methylation, ubiquitination, or sumoylation) are shaded blue, phosphorylation sites are shaded purple, and PKC phosphorylation sites are shaded yellow.* **B**, *CK-B and AK structures were compared by superimposing the two molecules in the closed conformation. The ribbon presentation of AK is depicted in grey and CK-B in blue. Note the difference between surface accessible residues within the C-terminal flexible loops: Arg312, Glu317 and Glu319 (colored in red) in AK are replaced by Gly323, Ala328 and Val330 (colored in yellow) in CK-B.* **C**, *A model was constructed depicting CK-B in the open and the closed conformation. The two flexible loops are colored blue in the open conformation and red in the closed conformation. The ATP- Mg2+ and creatine substrates are colored yellow.* **D**, *The surface accessibility of CK and AK residues was assessed. Residues in the C-terminal flexible loop region that had a relative accessibility of > 0.5 are shaded dark blue and those with a relative accessibility of > 0.25 and < 0.5 are shaded light blue.* **E**, *The ribbon representation of the crystal structure of dimeric human CK-B (PDB: 3B6R 35) is presented. Individual subunits are shown in yellow and blue. The left panel shows a bottom view of the dimer, while the right panel shows a top view. The N- and C-terminal flexible loops are colored red and magenta in the yellow (ligand-free) and blue (TSAC) subunit, respectively.*

bile loops comprising residues 60-70 and 323-333 over the nucleotide and creatine binding sites, for maintenance of associative properties and regional recruitment of CK-B? On the basis of the emerging conformational models and the finding that phagocytic cup accumulation was not impaired for the E232Q mutant (although it is generally accepted that this mutant is unable to bind substrate!), we consider it unlikely that changes in transition state structure, as such, determine CK-B's ability for recruitment and association with other proteins. We may therefore better concentrate on the study of the role of individual residues rather than on the general conformational properties of the flexible loop structure. As explained above, among the loop residues that flank the Asp^{326} position, have high surface accessibility in both the open and the closed state, and show no engagement in interactions with other residues in the protein, the role of Gly^{323}, Ala^{328}, and Val^{330} is perhaps most intriguing as these are the residues that are not found in other phosphagen kinases like AK (which itself is not recruited!). For the hydrophilic Asp^{326} residue itself, we predict that its substitution for a hydrophobic Ala in the D326A mutant may have modified the conformation of the entire small loop segment, thereby changing the accessibility of adjacent residues and reducing interaction possibilities with binding partners.

Finally, analysis of amino acid positions in the C-terminal flexible loop of the ligand-free subunit in the human dimeric CK-B and a structural comparison with AK (see Figures 8B, E), revealed the possibility that residues in one loop could be occupied for binding between identical enzyme subunits, while residues in the loop of the other subunit remain available for other types of associations. We must thus even leave open the possibility that homodimer formation is an important interme-

diary step in the partitioning dynamics of the enzyme in macrophages. Differences between the amino acid sequences of flexible loops in members of the phosphagen kinase family could thereby explain differences in partitioning behavior, such as those between dimeric CK-B of mammals and monomeric AK of other species that we report here.

Concluding remarks: Combined, our experimental findings and bioinformatics predictions support a role for CK-B's conformational mobile C-terminal loop in the spatio-temporal recruitment of enzyme activity to sites where dynamic, actin-dependent, membrane protrusions form in macrophages. Mobilization of CK-B activity appears to support membrane ruffling activity, and therewith macrophage immune functions. For better understanding of the coupling between CK-B's structure, intracellular enzyme compartmentalization dynamics, and the biological significance thereof, we now need first an assessment of the consequences of conservative vs. non-conservative substitutions for any of the relevant amino acid positions in the flexible C-terminal loop. This requires experiments that are clearly outside the scope of this study and should be reserved for follow-up studies.

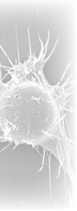

Acknowledgements

We thank Dr. Hong-Hee Kim (Department of Cell and Developmental Biology, School of Dentistry, Seoul National University, Korea) for providing the RAW 264.7 cell line, Dr. Michael H. Sieweke (Centre d'Immunologie de Marseille-Luminy (CIML), Université Aix-Marseille, France) for providing the Maf-DKO cells. This work was financed by the Radboud University Medical Centre.

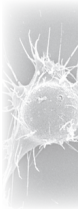

References

1. Ellington, W.R. Evolution and physiological roles of phosphagen systems. *Annu. Rev. Physiol.* **63**, 289-325 (2001).
2. Wallimann, T., Tokarska-Schlattner, M. & Schlattner, U. The creatine kinase system and pleiotropic effects of creatine. *Amino Acids* **40**, 1271-1296 (2011).
3. Wallimann, T. & Hemmer, W. Creatine kinase in non-muscle tissues and cells. (1994).
4. Dzeja, P.P. & Terzic, A. Phosphotransfer networks and cellular energetics. *J. Exp. Biol.* **206**, 2039-2047 (2003).
5. Wallimann, T., Wyss, M., Brdiczka, D., Nicolay, K. & Eppenberger, H.M. Intracellular compartmentation, structure and function of creatine kinase isoenzymes in tissues with high and fluctuating energy demands: the 'phosphocreatine circuit' for cellular energy homeostasis. *Biochem. J.* **281**, 21-40 (1992).
6. Guerrero, M.L. *et al.* Metabolic support of Na^+ pump in apically permeabilized A6 kidney cell epithelia: role of creatine kinase. *Am. J. Physiol.* **272**, C697-706 (1997).
7. Dzeja, P.P. & Terzic, A. Phosphotransfer reactions in the regulation of ATP-sensitive K^+ channels. *FASEB J.* **12**, 523-529 (1998).
8. Steeghs, K. *et al.* Altered Ca^{2+} Responses in Muscles with Combined Mitochondrial and Cytosolic Creatine Kinase Deficiencies. *Cell* **89**, 93-103 (1997).
9. van Deursen, J. *et al.* Skeletal muscles of mice deficient in muscle creatine kinase lack burst activity. *Cell* **74**, 621-631 (1993).
10. Wallimann, T., Schlösser, T. & Eppenberger, H.M. Function of M-line-bound creatine kinase as intramyofibrillar ATP regenerator at the receiving end of the phosphorylcreatine shuttle in muscle. *J. Biol. Chem.* **259**, 5238-5246 (1984).
11. Ventura-Clapier, R., Mekhfi, H. & Vassort, G. Role of creatine kinase in force development in chemically skinned rat cardiac muscle. *J. Gen. Physiol.* **89**, 815-837 (1987).
12. Dzeja, P.P. *et al.* Rearrangement of energetic and substrate utilization networks compensate for chronic myocardial creatine kinase deficiency. *J. Physiol.* **589**, 5193-5211 (2011).
13. Kuiper, J.W.P. *et al.* Local ATP Generation by Brain-Type Creatine Kinase (CK-B) Facilitates Cell Motility. *PLoS ONE* **4**, e5030 (2009).
14. Kuiper, J.W.P. *et al.* Creatine Kinase–Mediated ATP Supply Fuels Actin-Based Events in Phagocytosis. *PLoS Biol.* **6**, e51 (2008).
15. Loike, J.D., Kozler, V.F. & Silverstein, S.C. Creatine kinase expression and creatine phosphate accumulation are developmentally regulated during differentiation of mouse and human monocytes. *J. Exp. Med.* **159**, 746-757 (1984).
16. Chang, E.-J. *et al.* Brain-type creatine kinase has a crucial role in osteoclast-mediated bone resorption. *Nat. Med.* **14**, 966-972 (2008).
17. Loike, J.D., Kozler, V.F. & Silverstein, S.C. Increased ATP and creatine phosphate turnover in phagocytosing mouse peritoneal macrophages. *J. Biol. Chem.* **254**, 9558-9564. (1979).
18. Weintz, G. *et al.* The phosphoproteome of toll-like receptor-activated macrophages. *Mol Syst Biol* **6** (2010).
19. Nau, G.J. *et al.* Human macrophage activation programs induced by bacterial pathogens. *Proc. Natl. Acad. Sci. U. S. A.* **99**, 1503-1508 (2002).
20. Flannagan, R.S., Harrison, R.E., Yip, C.M., Jaqaman, K. & Grinstein, S. Dynamic macrophage "probing" is required for the efficient capture of phagocytic targets. *J. Cell Biol.* **191**, 1205-1218 (2010).
21. Vonna, L., Wiedemann, A., Aepfelbacher, M. & Sackmann, E. Micromechanics of filopodia mediated capture of pathogens by macrophages. *Eur. Biophys. J.* **36**, 145-151 (2007).
22. Kress, H. *et al.* Filopodia act as phagocytic tentacles and pull with discrete steps and a load-dependent velocity. *Proc. Natl. Acad. Sci. U. S. A.* **104**, 11633-11638 (2007).
23. Patel, P.C. & Harrison, R.E. Membrane Ruffles Capture C3bi-opsonized Particles in Activated Macrophages. *Mol. Biol. Cell* **19**, 4628-4639 (2008).
24. Lim, J.P. & Gleeson, P.A. Macropinocytosis: an endocytic pathway for internalising large gulps. *Immunol. Cell Biol.* **89**, 836-843 (2011).
25. Aziz, A., Soucie, E., Sarrazin, S. & Sieweke, M.H. MafB/c-Maf Deficiency Enables Self-Renewal of Differentiated Functional Macrophages. *Science* **326**, 867-871 (2009).
26. De Groof, A.J.C. in Department of Celbiology, Vol. PhD thesis (Radboud University, Nijmegen; 2002).
27. de Bruin, W., Oerlemans, F. & Wieringa, B. Adenylate kinase I does not affect cellular growth characteristics under normal and metabolic stress conditions. *Exp. Cell Res.* **297**, 97-107 (2004).
28. Rubin, G.M. *et al.* A Drosophila Complementary DNA Resource. *Science* **287**, 2222-2224 (2000).

29. Sistermans, E. *et al.* Tissue- and cell-specific distribution of creatine kinase B: A new and highly specific monoclonal antibody for use in immunohistochemistry. *Cell Tissue Res.* **280**, 435-446 (1995).
30. Larkin, M.A. *et al.* Clustal W and Clustal X version 2.0. *Bioinformatics* **23**, 2947-2948 (2007).
31. Blom, N., Gammeltoft, S. & Brunak, S. Sequence and structure-based prediction of eukaryotic protein phosphorylation sites. *J. Mol. Biol.* **294**, 1351-1362 (1999).
32. Xue, Y., Zhou, F., Fu, C., Xu, Y. & Yao, X. SUMOsp: a web server for sumoylation site prediction. *Nucleic Acids Res* **34**, W254-W257 (2006).
33. Krieger, E., Koraimann, G. & Vriend, G. Increasing the precision of comparative models with YASARA NOVA--a self-parameterizing force field. *Proteins* **47**, 393-402 (2002).
34. Vriend, G. WHAT IF: A molecular modeling and drug design program. *J. Mol. Graph.* **8**, 52-56 (1990).
35. Bong, S.M. *et al.* Structural studies of human brain-type creatine kinase complexed with the ADP–Mg^{2+}–NO^{3-}–creatine transition-state analogue complex. *FEBS Lett.* **582**, 3959-3965 (2008).
36. Tisi, D., Bax, B. & Loew, A. The three-dimensional structure of cytosolic bovine retinal creatine kinase. *Acta Crystallogr. Sect. D. Biol. Crystallogr.* **57**, 187-193 (2001).
37. Ohren, J.F., Kundracik, M.L., Borders, C.L., Edmiston, P. & Viola, R.E. Structural asymmetry and intersubunit communication in muscle creatine kinase. *Acta Crystallogr. Sect. D. Biol. Crystallogr.* **63**, 381-389 (2007).
38. Mohana Rao, J.K., Bujacz, G. & Wlodawer, A. Crystal structure of rabbit muscle creatine kinase. *FEBS Lett.* **439**, 133-137 (1998).
39. Lopez-Zavala, A.A. *et al.* Crystal structure of shrimp arginine kinase in binary complex with arginine-a molecular view of the phosphagen precursor binding to the enzyme. *J. Bioenerg. Biomembr.* **45**, 511-518 (2013).
40. Ahmad, S., Gromiha, M., Fawareh, H. & Sarai, A. ASAView: Database and tool for solvent accessibility representation in proteins. *BMC Bioinformatics* **5**, 51 (2004).
41. Bianco, C., Griffin, F.M. & Silverstein, S.C. Studies of the macrophage complement receptor. Alteration of receptor function upon macrophage activation. *J. Exp. Med.* **141**, 1278-1290 (1975).
42. Wright, S.D. & Meyer, B.C. Phorbol esters cause sequential activation and deactivation of complement receptors on polymorphonuclear leukocytes. *J. Immunol.* **136**, 1759-1764 (1986).
43. Mosser, D.M. & Edwards, J.P. Exploring the full spectrum of macrophage activation. *Nat. Rev. Immunol.* **8**, 958 (2008).
44. Sica, A. & Mantovani, A. Macrophage plasticity and polarization: in vivo veritas. *J. Clin. Invest.* **122**, 787-795 (2012).
45. Raschke, W.C., Baird, S., Ralph, P. & Nakoinz, I. Functional macrophage cell lines transformed by abelson leukemia virus. *Cell* **15**, 261-267 (1978).
46. Wallimann, T. & Eppenberger, H.M. The subcellular compartmentation of creatine kinase isozymes as a precondition for a proposed phosphoryl-creatine circuit. *Prog. Clin. Biol. Res.* **344**, 877-889 (1990).
47. Chen, Z. *et al.* Slow skeletal muscle myosin-binding protein-C (MyBPC1) mediates recruitment of muscle-type creatine kinase (CK) to myosin. *Biochem. J.* **436**, 437-445 (2011).
48. Hornemann, T. *et al.* Muscle-type creatine kinase interacts with central domains of the M-band proteins myomesin and M-protein. *J. Mol. Biol.* **332**, 877-887 (2003).
49. Hornemann, T., Stolz, M. & Wallimann, T. Isoenzyme-Specific Interaction of Muscle-Type Creatine Kinase with the Sarcomeric M-Line Is Mediated by Nh2-Terminal Lysine Charge-Clamps. *J. Cell Biol.* **149**, 1225-1234 (2000).
50. Chida, K. *et al.* Purification and identification of creatine phosphokinase B as a substrate of protein kinase C in mouse skin in vivo. *Biochem. Biophys. Res. Commun.* **173**, 351-357 (1990).
51. Chida, K., Tsunenaga, M., Kasahara, K., Kohno, Y. & Kuroki, T. Regulation of creatine phosphokinase B activity by protein kinase C. *Biochem. Biophys. Res. Commun.* **173**, 346-350 (1990).
52. Aksenov, M., Aksenova, M., Butterfield, D.A. & Markesbery, W.R. Oxidative modification of creatine kinase BB in Alzheimer's disease brain. *J. Neurochem.* **74**, 2520-2527 (2000).
53. Iwabata, H., Yoshida, M. & Komatsu, Y. Proteomic analysis of organ-specific post-translational lysine-acetylation and -methylation in mice by use of anti-acetyllysine and -methyllysine mouse monoclonal antibodies. *Proteomics* **5**, 4653-4664 (2005).
54. Zhao, T.J., Yan, Y.B., Liu, Y. & Zhou, H.M. The generation of the oxidized form of creatine kinase is a negative regulation on muscle creatine kinase. *J. Biol. Chem.* **282**, 12022-12029 (2007).
55. Zurmanova, J. *et al.* Creatine kinase binds more firmly to the M-band of rabbit skeletal muscle myofibrils in the presence of its substrates. *Mol. Cell. Biochem.* **305**, 55-61 (2007).
56. Cantwell, J.S. *et al.* Mutagenesis of Two Acidic Active Site Residues in Human Muscle Creatine Kinase: Implications for the Catalytic Mechanism. *Biochemistry (Mosc).* **40**, 3056-3061 (2001).
57. Lahiri, S.D. *et al.* The 2.1 Å Structure of Torpedo californica Creatine Kinase Complexed with the ADP-Mg^{2+}–NO^{3-}–Creatine Transition-State Analogue Complex. *Biochemistry (Mosc).* **41**, 13861-13867 (2002).

58. Forstner, M., Kriechbaum, M., Laggner, P. & Wallimann, T. Structural Changes of Creatine Kinase upon Substrate Binding. *Biophys. J.* **75**, 1016-1023 (1998).
59. Eder, M., Stolz, M., Wallimann, T. & Schlattner, U. A Conserved Negatively Charged Cluster in the Active Site of Creatine Kinase Is Critical for Enzymatic Activity. *J. Biol. Chem.* **275**, 27094-27099 (2000).
60. Azzi, A., Clark, S.A., Ellington, W.R. & Chapman, M.S. The role of phosphagen specificity loops in arginine kinase. *Protein Sci.* **13**, 575-585 (2004).
61. Stolz, M., Hornemann, T., Schlattner, U. & Wallimann, T. Mutation of conserved active-site threonine residues in creatine kinase affects autophosphorylation and enzyme kinetics. *Biochem. J.* **363**, 785-792 (2002).
62. Loegering, D.J. & Lennartz, M.R. Protein Kinase C and Toll-Like Receptor Signaling. *Enzyme Res* **2011**, 7 (2011).
63. Wu-Zhang, A.X. & Newton, A.C. Protein kinase C pharmacology: refining the toolbox. *Biochem. J.* **452**, 195-209 (2013).
64. Yeung, T. *et al.* Membrane Phosphatidylserine Regulates Surface Charge and Protein Localization. *Science* **319**, 210-213 (2008).
65. Jourden, M.J. *et al.* Changing the substrate specificity of creatine kinase from creatine to glycocyamine: Evidence for a highly evolved active site. *Biochim. Biophys. Acta* **1774**, 1519-1527 (2007).
66. Novak, W.R.P., Wang, P.-F., McLeish, M.J., Kenyon, G.L. & Babbitt, P.C. Isoleucine 69 and Valine 325 Form a Specificity Pocket in Human Muscle Creatine Kinase. *Biochemistry (Mosc).* **43**, 13766-13774 (2004).

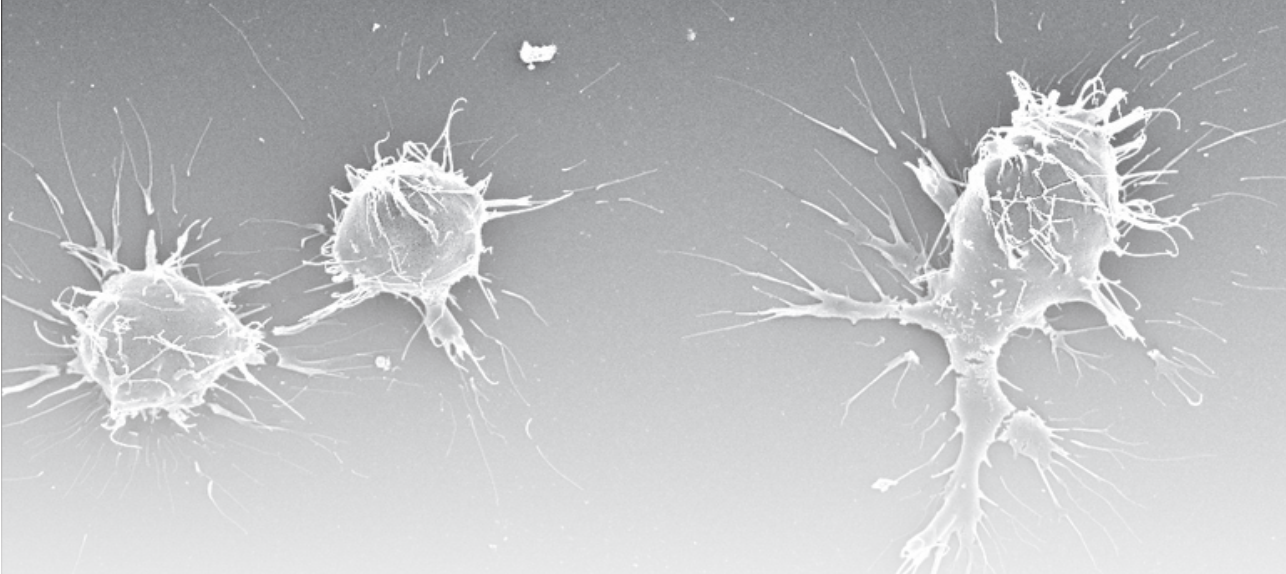

4

Glucose controls morphodynamics of LPS-stimulated macrophages

Gerda Venter, Frank T. J. J. Oerlemans, Mietske Wijers, Marieke Willemse, Jack A. M. Fransen, and Bé Wieringa

Department of Cell Biology, Radboud Institute for Molecular Life Sciences, Radboud University Medical Centre, Nijmegen, The Netherlands

PLoS ONE 9(5): e96786 (2014)

Abstract

Macrophages constantly undergo morphological changes when quiescently surveying the tissue milieu for signs of microbial infection or damage, or after activation when they are phagocytosing cellular debris or foreign material. These morphofunctional alterations require active actin cytoskeleton remodeling and metabolic adaptation.

Here we analyzed RAW 264.7 and Maf-DKO macrophages as models to study whether there is a specific association between aspects of carbohydrate metabolism and actin-based processes in LPS-stimulated macrophages. We demonstrate that the capacity to undergo LPS-induced cell shape changes and to phagocytose complement-opsonized zymosan (COZ) particles does not depend on oxidative phosphorylation activity but is fueled by glycolysis. Different macrophage activities like spreading, formation of cell protrusions, as well as phagocytosis of COZ, were thereby strongly reliant on the presence of low levels of extracellular glucose. Since global ATP production was not affected by rewiring of glucose catabolism and inhibition of glycolysis by 2-deoxy-D-glucose and glucose deprivation had differential effects, our observations suggest a non-metabolic role for glucose in actin cytoskeletal remodeling in macrophages, e.g. via posttranslational modification of receptors or signaling molecules, or other effects on the machinery that drives actin cytoskeletal changes. Our findings impute a decisive role for the nutrient state of the tissue microenvironment in macrophage morphodynamics.

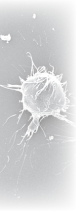

Introduction

Macrophages are present in all tissues where they provide a first line of defense against pathogens and help to maintain steady-state tissue homeostasis by eliminating foreign matter and apoptotic cells via phagocytosis [1, 2]. To exert these functions they migrate and constantly survey their immediate environment for signs of tissue damage or presence of invading organisms [1]. During surveillance, danger signals are detected through Toll-like receptors (TLRs), intracellular pattern recognition receptors (PRRs) and interleukin(IL)-receptors [2]. When macrophages encounter stimuli like inflammatory cytokines (IFN-g, TNF, or IL-4), foreign material (e.g. lipopolysaccharide; LPS), or immunoglobulin G (IgG) immune complexes, tissue-resident macrophages become activated to undergo a phenotypic change towards a classically activated M1 or alternatively activated (suppressive) M2 polarization state [1, 3, 4], which is accompanied by metabolic adaptation. Because M1 and M2 phenotypes represent extremes in a continuum of phenotypes that macrophages can adopt, we still have no clear picture of the (possibly reciprocal) relationship between their metabolic profile and activation state. The prevailing idea is that, in the resting state, macrophages utilize glucose at a high rate and convert 95% of it to lactate [5]. Upon polarization towards a M1 phenotype (e.g. after stimulation with LPS) glucose import via GLUT, as well as the glycolytic flux, is even further upregulated [5-7]. M2 macrophages, on the other hand, do not undergo such extensive metabolic change but have a metabolic profile comparable to that of unstimulated cells, with higher TCA-cycle and oxidative activity [5, 8]. Recently, Haschemi et al. [7] have shown that carbohydrate kinase-like protein (CARKL) orchestrates macrophage activation through metabolic control. CARKL overexpression drove cells towards an oxidative state and sensitized macrophages towards a M2 polarization state, while CARKL-loss promoted a rerouting of glucose from aerobic to anaerobic metabolism and induced a mild M1 phenotype. Conversely, Tannahill et al. [9] have demonstrated that LPS stimulation of macrophages causes an increase in the intracellular TCA-cycle intermediate succinate, which stabilizes M1-associated HIF-1α and thereby regulates the expression of the pro-inflammatory cytokine IL-1β.

Besides overall metabolic versatility, macrophages also exhibit a wide range of morphodynamic activities, needed to exert their tasks in tissue surveillance and host defense. To control these activities before and after polarization, macrophages continuously form actin-rich membrane protrusions and extend filopodia from their cell surface [10, 11]. Changes in the organization of the actin cytoskeleton thereby enable the cell to dynamically adapt its morphology to suit its particular function and differentiation state. For example, LPS induces polymerization of cytoskeletal actin filaments, cell spreading, and the formation of filopodia, lamellipodia, and

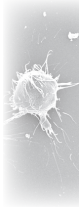

membrane ruffles in monocytes and macrophages [12, 13]. Likewise, IL-4, which is released during tissue injury, causes the rearrangement of actin-rich podosomes to form rosettes in M2 macrophages, enabling degradation of - and migration through - dense extracellular matrices [14].

The rearrangements of cytoskeletal actin filaments that steer this behavior comprise multiple steps, including the nucleation and elongation of new filaments from ATP-bound G-actin monomers, the addition of these monomers to the barbed ends of existing filaments, the hydrolysis of actin-bound ATP within the growing filament, and the dissociation of ADP-G-actin at the pointed end [15-18]. ADP on liberated G-actin is substituted with ATP, producing new ATP-G-actin monomers for incorporation. The ensemble of activities in this complex process is regulated by more than a hundred actin-associated proteins (ABPs), several of which are influenced by the availability of ATP. Metabolism, specifically the binding and hydrolysis of ATP and ATP-ADP exchange, thereby not only dictates the behavior of the actin filaments themselves [19-21], but also controls the activity of regulatory factors like the Arp2/3 protein complex [22, 23], or upstream signaling such as the ROCK/Rho-GTPase pathway [24]. The idea that actin remodeling is a major cellular energy drain is corroborated by the observation that actin filaments are stabilized under conditions of global ATP-depletion in order to prevent ATP-hydrolysis within the filament and, thereby, ATP-consumption [25, 26].

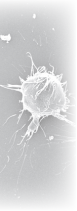

Besides ATP availability [27, 28], intracellular pH and $NAD(P)^+$/NAD(P)H ratio are other key metabolic parameters that influence actin network dynamics and cell motility [29], either by modifying actin itself [30-32] or by regulating the activity of proteins such as the actin depolymerizing factor cofilin, mical, and the actin severing protein gelsolin [33-35]. In most mammalian cells, production of ATP, NAD^+/NADH, and H^+ is dominated by carbohydrate catabolism via glycolysis and mitochondrial TCA cycle/oxidative phosphorylation (OXPHOS) pathways. Importantly, various glycolytic pathway enzymes that handle these metabolites/cofactors appear compartmentalized and are found associated with the actin cytoskeleton and with actin dependent cellular structures, such as pseudopodia, membrane ruffles, and lamellipodia [36-39]. Indeed, this coupling helps to explain the dependency of cell motility on glycolysis [40, 41]. Also phagocytosis by macrophages depends on glycolysis [42-44], but not much work has been done to study this association in detail. Seeing their vital role in host defense and maintenance of tissue homeostasis and their surprising versatility in adaptation of functioning in many different tissue environments, we wondered whether there is a link between the activation of glucose metabolism and the extent of morphodynamic change that macrophages undergo. To apprehend the coupling between actin cytoskeletal remodeling and metabolic state we here investigated the ability of LPS-stimulated (M1) RAW 264.7 and Maf-DKO macrophages to maintain

functional activity under conditions where they were forced to shift between a (anaerobic) glycolytic or oxidative metabolism. RAW 264.7 and Maf-DKO cell lines were chosen because they are *in vitro* manipulable models that have retained marked plasticity to stimulus-directed polarized activation, but lack the phenotypic heterogeneity that is characteristic for primary macrophages [45, 46]. We report on a stringent dependency of morphodynamics of LPS-stimulated macrophages upon sufficient glucose supply.

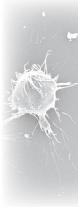

Materials and Methods

Reagents
All reagents were obtained from Sigma-Aldrich (St. Louis, MO, USA), unless stated otherwise.

Cell culture
RAW 264.7 cells (kind gift from Dr. Hong-Hee Kim, Department of Cell and Developmental Biology, School of Dentistry, Seoul National University, Korea) [47] were maintained in high-glucose DMEM (Gibco, Life Technologies, Paisley, UK) supplemented with 10% heat inactivated FBS (PAA laboratories, Pasching, Austria), 1 mM sodium pyruvate, and 4 mMGlutaMAX (Gibco, Life Technologies, Paisley, UK), at 37°C in a humidified atmosphere with 7.5% CO_2. Maf-DKO cells (kind gift from Dr. Michael H. Sieweke, Centre d'Immunologie de Marseille-Luminy (CIML), Université Aix-Marseille, France) [46] were maintained in the same way except that medium was supplemented with 20% conditioned medium from L929-cells containing macrophage colony stimulating factor (M-CSF).

DNA constructs and transfection
Plasmid pEYFP-N1-ΔATG-Lifeact was constructed as follows: Lifeact [48] cDNA, containing human codon sequences flanked by a 5' BglII and 3' EcoRI restriction site, was commercially synthesized and ligated in a pUC57 plasmid by GenScript USA Inc. A forward primer (5'-CT CAG ATC TCC ACC *ATG* GGC GTG GCC GAC C-3') was designed to introduce a BglII site and a Kozak sequence in front of the Lifeact start codon. Use of this primer together with the M13 universal reverse primer enabled amplification of the Lifeact encoding insert from pUC57 by PCR. PCR products were digested with BglII and EcoRI and ligated into pEYFP-N1-ΔATG plasmid DNA (pEYFP-N1 from Clontech with ATG on position 679 mutated to GCG).

For transfection, RAW 264.7 cells were seeded in 6 well plates at 300,000 cells/well and incubated overnight. Plasmid pEYFP-N1-ΔATG-Lifeact DNA (12 µg; linearized with *AseI*) was diluted in 1 ml serum-free DMEM and incubated for 20 minutes at 37°C with 24 µl Targefect-RAW transfection reagent (Targeting Systems, El Cajon, CA, USA). Transfection complexes (250 µl) were added to wells containing 2 ml fresh culture medium and incubated for 4 hours at 37°C after which medium was refreshed. A stable cell pool was established by culturing cells for two weeks in medium containing 500 µg/ml G418, followed by limited dilution cloning.

Media for metabolic manipulation
For cell culture under glucose free conditions, glucose-free DMEM (Gibco, Life Tech-

nologies, Paisley, UK) was supplemented with 10 mM galactose. As control, medium supplemented with 25 mM glucose was used. Low glucose medium was prepared by supplementing glucose free DMEM with 1 mM glucose and 10 mM galactose (gluc/gal). Media were further supplemented with 10% heat inactivated dialyzed FBS, 1 mM sodium pyruvate, and 4 mM GlutaMAX. For inhibition of glycolysis, high (25 mM) glucose DMEM containing 10 mM 2-deoxy-D-glucose (2-DG), 10% heat inactivated FBS, 1 mM sodium pyruvate, and 4 mMGlutaMAX was used. Inhibition of OXPHOS was achieved by adding 2.5 µM oligomycin to normal culture medium (containing 25 mM glucose). For live imaging, phenol red-free media were prepared using DMEM Base powder from Sigma-Aldrich to which sodium bicarbonate, GlutaMAX, sodium pyruvate, glucose and/or galactose, 2-DG, or oligomycin were added.

Proliferation assay

For cell proliferation analysis, the protocol developed by Skehan et al. [49] was used. RAW 264.7 cells were seeded in four 96-well plates (30,000 cells/well) in 100 µl culture medium and incubated for eight hours. At T0, plates were washed once and the medium in plates T6, T15, and T24 was replaced with either control, galactose, gluc/gal, 2-DG, or oligomycin medium containing 100 ng/ml LPS, while plate T0 was fixed for sulforhodamine B (SRB) staining of protein content. After 0, 6, 15, and 24 hours, cells were washed twice with cold PBS and fixed with 10% trichloroacetic acid (TCA; J.T.Baker, Deventer, Holland) for 1 hour at 4°C. After fixation, plates were washed five times with water and stored at -20°C until all plates were collected. Cellular protein was stained with 50 µl 0.5% SRB in 1% acetic acid for 20 minutes after which wells were washed four times with 1% acetic acid. Plates were dried at 60°C for 3 hours, protein was dissolved in 150 µl 10 mM Tris-HCl (pH 10.5), and the absorbance of each well was measured at 510nm on a BioRad Benchmark Plus micro plate reader. Values were corrected for background SRB staining by subtracting the average absorbance value of wells that contained medium only, from that of wells with cells.

Apoptosis assay

Apoptosis of RAW 264.7 cells was measured using a biosensor (pSIVA) developed by Kim et al. [50] (generous gift from Dr. Ralf Langen, University of Southern California). Briefly, cells (20,000/well) were seeded in a BD Falcon 96-well imaging plate and incubated overnight. On the day of assay, wells were washed once and medium was replaced with phenol red-free control, galactose, 2-DG, or oligomycin medium containing 8 ng/µl pSIVA or non-labeled control. The plate was immediately imaged for 24 hours, continuously, on a BD Pathway high-content spinning disc confocal microscope equipped with a temperature and CO_2 controllable incubation cham-

ber, using a 20x objective and 2x2 montage capture. Three wells were imaged per condition and the amount of apoptosis was determined by analyzing the increase in GFP-signal. For each well the threshold of the whole GFP-image series was adjusted and the total pixel area/frame was determined using Fiji imaging software [51] and plotted against time.

ATP assay

Intracellular ATP was determined using the CellTiter-Glo cell viability assay kit from Promega.

500,000 cells (RAW 264.7) were seeded per well of a 6-well plate and incubated in control medium, galactose medium or 1mM glucose medium for 4 and 14 hours, 2-DG medium for 1 and 3 hours, or oligomycin-containing medium for 0.5 or 24 hours prior to assay. Cells were washed twice with ice cold PBS and then scraped in 350 µl ice cold 0.6 M perchloric acid (PCA). PCA extracts were centrifuged for 3 minutes at 4000 rpm and 4°C to pellet all cellular protein. Supernatants were neutralized with 140-155 µl 2 M KOH/0.2 M KH_2PO_4, pH 7.5 and diluted 1:10 in water. Per well, 100 µl diluted PCA extract was added to 100 µl CellTiter-Glo reagent and the luminescence intensity per well was measured on a LUMIstar OPTIMA microplate luminometer. The ATP concentration was determined using an ATP standard series. For determination of total cellular protein, pellets were dissolved in 250 µl 1 M NaOH and heated for 30 minutes at 95°C. Protein concentration was then measured in 1:50 diluted NaOH extracts.

Glucose and lactate assays

Glucose consumption measurements were based on the Amplex Red Glucose/Glucose Oxidase assay kit from Molecular probes (Life Technologies, Eugene, Oregon, USA). Glucose, glucose oxidase, and Amplex Red reagent were used from the kit but horseradish peroxidase was obtained from Sigma-Aldrich and 1x reaction buffer was replaced with 0.05 M Tris-HCl, pH 7.5. Otherwise, the kit protocol was followed as described by the manufacturer. Lactate production was measured using the same protocol as for glucose consumption but replacing glucose oxidase with lactate oxidase and including a lactate standard series instead of glucose. RAW 264.7 cells were seeded in 12 well tissue culture plates and incubated for 6 or 24 hours in either 1 ml control or 1 ml 2.5 µM oligomycin medium. For glucose measurements, medium containing 5 mM glucose was used while lactate production was measured for cells grown in 25 mM glucose medium. For measurement of glucose consumption or lactate production during the last 6 hours of the 24 hour incubation period, medium was refreshed after 18 hours in one of the 24 hour plates. Prior to addition of incubation media, wells were always rinsed with pure DMEM containing no glu-

cose. Medium was collected at the end of the 6 or 24 hour incubation period and supernatants were snap frozen in liquid nitrogen and stored at -20°C until analysis. Cytosolic extracts were prepared in lysis buffer (50mMTris-HCl pH 7.5, 100 mM NaCl, 5 mM $MgCl_2$, and 0.5% NP-40; 4°C) and total protein was determined with the Bradford assay. Glucose consumption was calculated by subtracting the amount of glucose in the sample from that in medium without cells. Lactate production was calculated by subtracting the concentration of any lactate in the medium without cells from that of the samples. Glucose and lactate assays were performed in parallel.

Oxygen consumption measurements

Mitochondrial respiration was assessed by measuring oxygen consumption on an Oroboros Oxygraph-2k respirometer according to a standard protocol provided by the manufacturer. RAW 264.7 and Maf-DKO cells were analyzed in parallel in two separate chambers of the respirometer. After air calibration of medium in the chambers and stabilization of the signal, 1 x 10^6 cells (in 60 µl medium) were injected into the respective chambers. Basal respiration rate was measured at the point where the O_2-flux signal stabilized. Oligomycin (2.5 µM) was added to each chamber and the leak respiration rate was determined after stabilization of the signal. Next, 7 µM carbonyl cyanide-*p*-trifluoromethoxyphenylhydrazone (FCCP, a mitochondrial uncoupler) was added to reach maximal oxygen consumption in the cells. Finally, 30 nM rotenone was added and after stabilization of the system, the residual oxygen consumption could be determined. The data were analyzed using the DatLab software provided with the instrument.

Cellular actin staining

RAW 264.7 cells on coverslips were pre-incubated in control or 2-DG medium (3 hours), gluc/gal medium (4 and 24 hours), galactose medium (4 and 24 hours), or oligomycin-containing medium (0.5 and 24 hours) and stimulated with 100 ng/ml LPS overnight or left unstimulated. Medium was removed and cells were immediately fixed in 2% paraformaldehyde in 0.2 M sodium phosphate buffer for 30 minutes. Coverslips were washed twice with PBS and twice with PBS containing 20 mM glycine (MP Biomedicals, Illkirch Cedex, France; PBS-G) before permeabilization with 0.1% saponine/PBS-G for 20 minutes. This was followed by actin staining with Alexa 568-labeled phalloidin (1:600 in 0.1% saponine/PBS-G) for 1 hour. Cells were successively washed four times for 2-4 minutes with 0.1% saponine/PBS-G and once with PBS alone. Coverslips were removed from wells, rinsed once in water, air dried, and imbedded in MoWiol on microscope slides. Z-scans consisting of 25 x 0.5 µm sections and the pinhole adjusted to one airy unit were recorded on a Zeiss

LSM510 META confocal laser scanning microscope and merged to one single image using Fiji imaging software. Coverslips were prepared in duplo and per condition twelve different fields were analyzed.

Scanning electron microscopy

Cells were seeded on 12 mm glass coverslips in 24-well plates and pre-incubated in control or galactose medium (4 hours), 2-DG medium (3 hours), oligomycin medium (0.5and 24 hours), or gluc/gal medium (4 hours). In addition, cells were stimulated with 100 ng/ml LPS or left unstimulated. Cells were washed once with PBS and fixed with 2% glutarealdehyde in 0.1 M sodium cacodylate buffer for 1 hour. After washing cells twice with sodium cacodylate buffer, coverslips were stored in this buffer at 4°C until further fixation with 1% OsO_4 (osmium tetroxide) for 30 minutes. Coverslips were then washed once with water and dehydrated in a graded series of alcohol washes. Finally, coverslips were critical point dried and mounted for scanning electron microscopy on a JEOL SEM6340F Field Emission Scanning Electron microscope. Coverslips were prepared in duplo and per condition 8-10 different fields were analyzed.

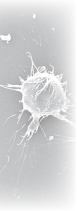

Quantification of filopodia and cell circumference

For quantification of filopodia, fluorescence microscopy or SEM images of fixed cells were analyzed. Lines were drawn to delineate contour segments of cells in areas where no contacts with neighboring cells were seen. The length and number of filopodia extending from each contour segment were determined. For phalloidin stained cells, 30-40 different line segments with a total contour length corresponding to the circumference of 20-50 cells, were included per condition. From the SEM images 20-26 line segments, with a total contour length corresponding to the circumference of 10-17 cells, were analyzed per condition.

To compare circumferences of whole cells, contour lengths of circular lines around individual cells were measured. Per condition, 20-50 cells were analyzed from both the fluorescence and electron microscopy image collection.

Spreading assay

RAW 264.7 cells expressing Lifeact-EYFP were stimulated with 100 ng/ml LPS overnight and simultaneously pre-incubated in control or galactose, 2-DG, oligomycin, or gluc/gal medium for 0, 3, 15, or 24 hours before they were harvested by treatment with 1 mM EDTA/PBS (10 min at 37°C). After washing, the cells were suspended in medium with 1% bovine serum albumin. A recovery period of 20 minutes at 37°C was allowed before cells were seeded in a fibronectin coated (50 µg/ml for 2h at 37°C) BD Falcon 96-well imaging plate at 4,000 cells/well in the presence of

100 ng/ml LPS. Cell spreading was monitored for three hours by recording the increase in EYFP-pixel area per cell (20 cells/well) on a BD Pathway high-content spinning disc confocal microscope, using a 20x objective and 3x3 montage capture. In order to combine the data from three independent experiments (performed in duplicate), the time axes had to be synchronized. To achieve this, a Boltzmann simulation curve was produced for each data set between time points 0 and 200 in steps of 2 minutes using OriginLab data analysis and graphing software (OriginPro 6.1). Data sets were then combined and analyzed for statistical significance by applying a repeated measures analysis using PASW statistics 18 SPSS software. Three time frames (consisting of 30 data points each) of each curve were compared with the corresponding three time frames of the control curve.

Phagocytosis assay

Phagocytic activity was determined as zymosan ingestion capacity essentially as described by Kuiper et al. [27]. Zymosan particles were dissolved in PBS at 10 mg/ml and left to rehydrate for at least one hour. Next, zymosan was sonicated three times for 5 seconds, spun down, resuspended in sodium carbonate buffer (pH 9.6), sonicated, and incubated with 1 µg/ml fluorescein isothiocyanate (FITC) for 1 hour at room temperature, in the dark. After FITC labeling, zymosan was washed three times with sodium carbonate buffer and incubated in 1 M Tris HCl, pH 8.0, for 30 minutes. Zymosan was then washed twice with PBS and finally resuspended in PBS. After one more sonication step, FITC-labeled zymosan was divided in aliquots, frozen in liquid nitrogen, and stored at -20°C.

Phagocytosis assays were performed in 12-well plates in which cells were seeded the day before. The number of cells seeded was adjusted for some conditions, due to the inhibitory effect on proliferation. To compensate for reduced proliferation rate, 150,000 and 200,000 RAW 264.7 cells were seeded per well for 14h and 24h galactose treatment, respectively. For all other conditions 100,000 RAW 264.7 cells were seeded per well. For assays with Maf-DKO cells, 200,000 cells were seeded per well. Prior to assay, cells were pre-incubated in control or galactose medium (0, 4, and 14 hours), 2-DG medium (0, 1, and 3 hours), oligomycin medium (0, 0.5, 3, 15, and 24 hours), or gluc/gal medium (0, 4, and 14 hours), and activated overnight with 100 ng/ml LPS. For assays with Maf-DKO cells in galactose medium, L929-cell conditioned medium was omitted to ensure that no glucose was present in the medium. FITC-labeled zymosan particles were opsonized by incubation in fetal bovine serum for 1 hour at 37°C, washed twice with PBS, and finally resuspended in serum-free control, galactose-, 2-DG-, oligomycin-, or gluc/gal-medium. Cells were washed once with glucose-free DMEM and incubated with 1 ml zymosan suspension for 30 minutes at 37°C. The particle-to-cell ratio was approximately 10:1. Particle engulf-

ment was terminated after washing cells twice with PBS and removing extracellular zymosan by treatment with 500 µl 100 U/ml lyticase for 10 minutes at room temperature. Successively, cells were detached with 0.05% trypsin/0.5 mM EDTA (Gibco, Life Technologies, Paisley, UK), resuspended in 1 ml medium with serum, pelleted, and finally resuspended in 200 µl 1% paraformaldehyde in PBS. Samples were analyzed by FACS (BD FACS Calibur) and phagocytosis activity was determined by measuring the percentage of FITC positive cells and the fluorescence intensity in these cells. The phagocytic index of each sample was then calculated as the product of the mean FITC intensity of the positive population times the % of FITC positive cells.

For the glucose rescue assay, 100,000 Maf-DKO and 60,000 RAW 264.7 cells were seeded per well in 24 well plates in medium containing 20% L929 cell conditioned medium and stimulated with 100ng/ml LPS overnight. Cells were washed with glucose-free DMEM and incubated with FITC-COZ in galactose medium for 30 minutes at 37°C. Then, 1mM glucose or glucose-free DMEM was added and the cells were incubated for another 30 minutes. Thereafter, cells were detached and prepared for FACS.

Adhesion and Internalization assay

Internalization efficiency was determined essentially as described by Sahlin et al. [52]. RAW 264.7 cells and zymosan particles were prepared as for the phagocytosis assay. Pre-incubation in different media without or with inhibitors was as follows: galactose 0 hours; 2-DG, 1 hour; oligomycin, 0 and 24 hours; and gluc/gal, 0 hours. After 30 minute incubation with serum opsonized zymosan at 37°C, plates were transferred to ice and wells were washed twice with ice cold PBS. Cells were then scraped in 1 ml cold medium, divided in two equal portions, transferred to microcentrifuge tubes, and spun down. Cells in one portion were resuspended in 0.05 % trypan blue in potassium dihydrogen citrate/saline, pH4.4 to quench all extracellular FITC-COZ, and cells in the other portion were taken up in the same buffer but without trypan blue. Samples were analyzed by FACS.

Statistical analysis

Data were analyzed either with the Student's t-test, one-sample t-test for relative values, or using a two-way ANOVA and the Bonferroni post-test (GraphPad software, Inc., Version 4). All values are expressed as mean +/-SEM. Values were considered to be significantly different when p values were < 0.05.

Results

The effect of glycolysis and OXPHOS inhibition on RAW 264.7 cell proliferation and viability

Tissue-resident macrophages, dependent on the niche that is occupied within the body, may become exposed to dramatically different nutrient conditions, including variation in oxygen and carbohydrate supply. Their functional plasticity relies thereby largely on the capacity to adapt and switch between carbohydrate metabolism via glycolysis or mitochondrial TCA cycle and OXPHOS reactions. For study of different aspects of this coupling we chose to focus on the well-established macrophage model, RAW 264.7 [45], and used another macrophage model, Maf-DKO cells [46], for comparison of the key findings. In order to find a range of conditions wherein the metabolic state of RAW 264.7 macrophages can be manipulated without compromising cell proliferation and viability, we monitored cells for a period of at least 24 hours in the presence of the complex V OXPHOS inhibitor oligomycin, the competitive glycolysis inhibitor 2-deoxy-D-glucose (2-DG), or in the absence of glucose. Cell proliferation was determined as the increase in total protein mass both in the absence and presence of LPS. Since the effect of metabolic inhibitors on cell proliferation appeared independent of this stimulation, we chose to present only results obtained in the presence of LPS (Figure 1A-C). Cell viability was monitored using the the pSIVA apoptosis biosensor with switchable fluorescence states (Figure 1D). When pSIVA binds to annexin V that is exposed on the surface of early apoptotic cells its fluorescence can be detected at an emission wavelength between 500 and 550 nm. In the absence of apoptotic cells, pSIVA remains unbound and is non-fluorescent and non-detectable, therefore, an increase in the pSIVA fluorescence signal (plotted as pSIVA pixel area on the y-axis in Figure 1D) correlates with an increase in the amount of apoptotic cells.

Incubation with 2.5 µM oligomycin caused a 60-70% inhibition of OXPHOS activity (measured as the decrease in O_2-consumption, Figure S1) and a marked reduction in proliferation rate (Figure 1A) without inducing excessive apoptosis (Figure 1D). Inhibition of glycolysis with 10 mM 2-DG induced apoptosis at an early time point (i.e. after 3-4 hours) in a relatively small % of cells in the population and, under this condition, proliferation ceased (Figure 1B and 1D). Upon substitution of glucose with 10 mM galactose (glucose deprivation) apoptotic cells began to appear after about 10 hours (Figure 1D), in a pool of cells with already significantly reduced proliferation capacity (Figure 1C). These results imply that the proliferation of RAW 264.7 cells is dependent on both glycolysis and mitochondrial activity, but that viability is better preserved by glycolysis alone than by mitochondrial TCA/OXPHOS activity alone.

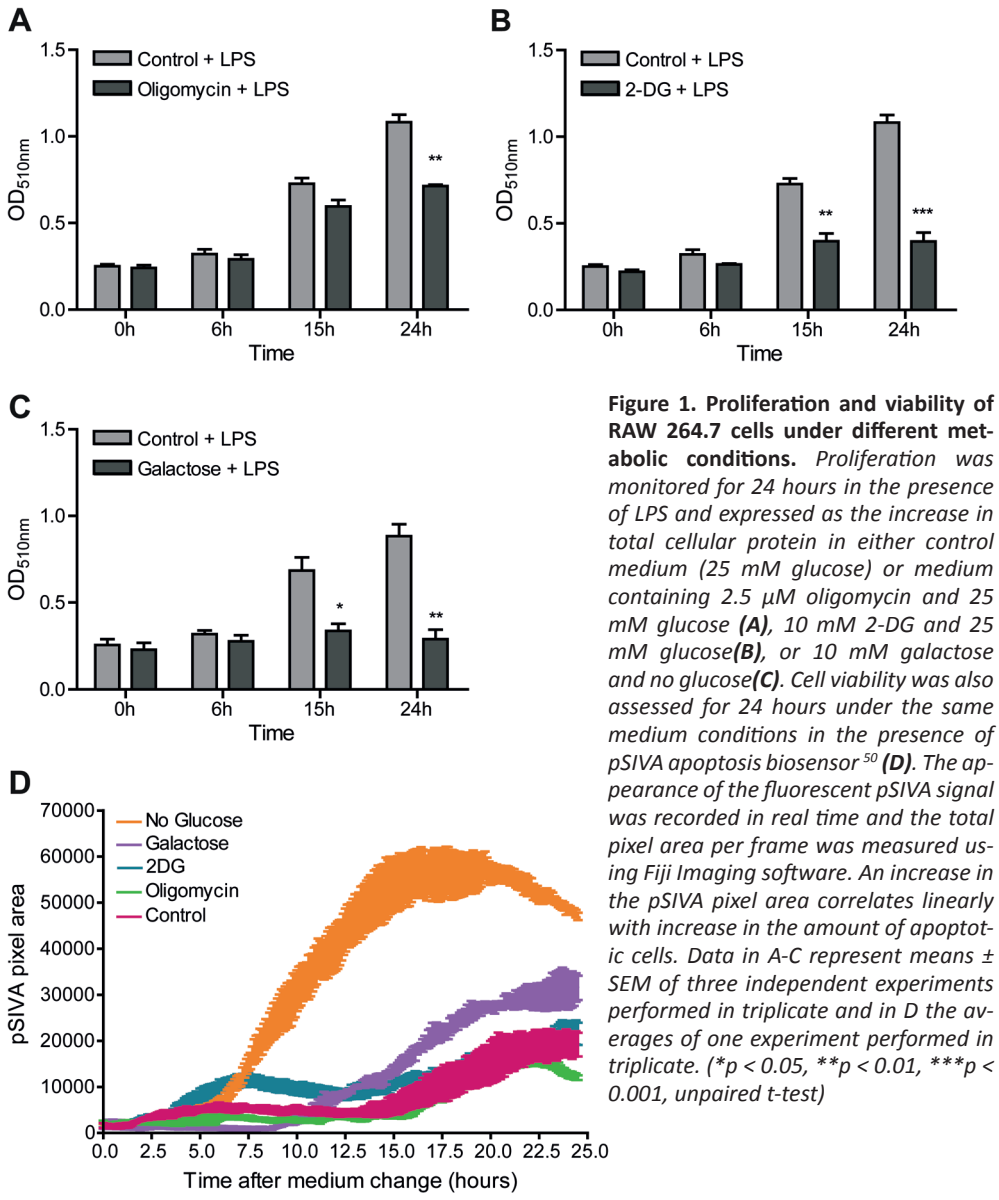

Figure 1. Proliferation and viability of RAW 264.7 cells under different metabolic conditions. *Proliferation was monitored for 24 hours in the presence of LPS and expressed as the increase in total cellular protein in either control medium (25 mM glucose) or medium containing 2.5 µM oligomycin and 25 mM glucose* ***(A)****, 10 mM 2-DG and 25 mM glucose****(B)****, or 10 mM galactose and no glucose****(C)****. Cell viability was also assessed for 24 hours under the same medium conditions in the presence of pSIVA apoptosis biosensor* [50] ***(D)****. The appearance of the fluorescent pSIVA signal was recorded in real time and the total pixel area per frame was measured using Fiji Imaging software. An increase in the pSIVA pixel area correlates linearly with increase in the amount of apoptotic cells. Data in A-C represent means ± SEM of three independent experiments performed in triplicate and in D the averages of one experiment performed in triplicate. (*p < 0.05, **p < 0.01, ***p < 0.001, unpaired t-test)*

ATP metabolism during metabolic inhibition of RAW 264.7 cells

Since macrophages produce cellular ATP mainly via glycolysis [53, 54], inhibition of this pathway or limitation of its starting substrate glucose may have a significant impact on cellular energy homeostasis if there is no adequate compensation by mitochondrial ATP production. To study whether macrophages are versatile enough to accommodate changes in ATP supply pathways, we first followed [ATP] in RAW 264.7

cells during early stages and modes of inhibition, under conditions where cells were still fully viable (1 hour oligomycin and 2-DG, 4 hours galactose). Comparison was drawn to [ATP] found at later stages of inhibition when either apoptosis was initiated (3 hours 2-DG and 14 hours galactose) or proliferation was significantly reduced (24 hours oligomycin). Compared to control cells, short term oligomycin treatment (1h) did not affect ATP level (Figure 2A). Upon prolonged incubation in presence of oligomycin (24h) we even did not observe the 50% drop in ATP level that occurred in RAW 264.7 cells, presumably as a result of medium depletion. We currently ex-

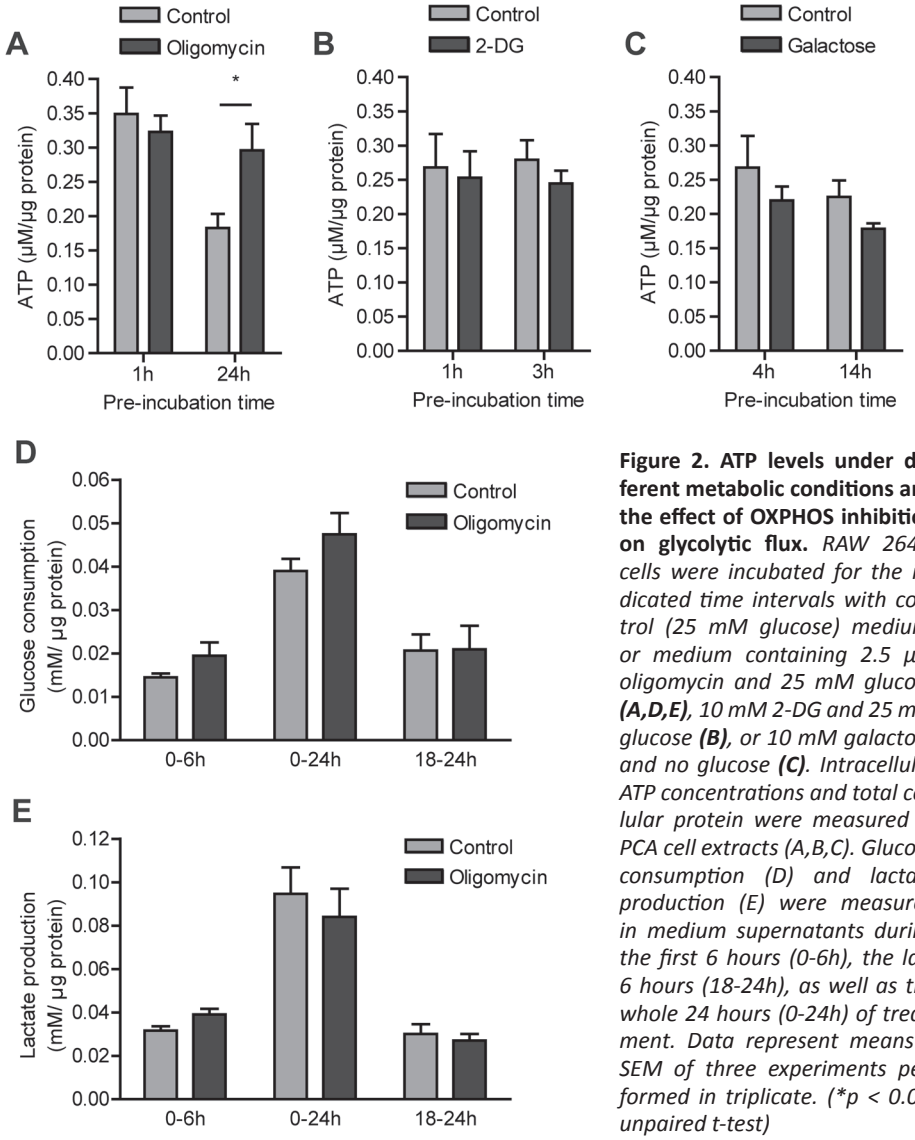

Figure 2. ATP levels under different metabolic conditions and the effect of OXPHOS inhibition on glycolytic flux. *RAW 264.7 cells were incubated for the indicated time intervals with control (25 mM glucose) medium, or medium containing 2.5 µM oligomycin and 25 mM glucose **(A,D,E)**, 10 mM 2-DG and 25 mM glucose **(B)**, or 10 mM galactose and no glucose **(C)**. Intracellular ATP concentrations and total cellular protein were measured in PCA cell extracts (A,B,C). Glucose consumption (D) and lactate production (E) were measured in medium supernatants during the first 6 hours (0-6h), the last 6 hours (18-24h), as well as the whole 24 hours (0-24h) of treatment. Data represent means ± SEM of three experiments performed in triplicate. (*p < 0.05, unpaired t-test)*

plain this observation by assuming that continuous presence of oligomycin forces rewiring of (mitochondrial) metabolism and that this protects against this depletion. More study is needed to obtain the evidence to support this explanation. In the presence of 2-DG, cells managed to maintain ATP levels beyond the 3 hours before apoptosis was induced (Figure 2B). Also in the presence of galactose, i.e. under conditions of glucose deprivation, no marked decrease in cellular ATP was observed until 14 hours, compared to control cells (Figure 2C).

Under conditions where carbohydrate catabolism had to be rewired, i.e. under oligomycin treatment, we observed a trend towards higher glucose consumption by treated compared to control cells, although the difference was not statistically significant (Figure 2D). Oligomycin treatment did not, however, increase the flux of glucose to lactate (Figure 2E). Normally, already about 95% of all glucose consumed is converted into lactate and only a very small fraction of pyruvate is imported into the mitochondria in macrophages [5]. This explains why inhibition of OXPHOS cannot cause a significant increase in the turnover of pyruvate to lactate and why no significant increase in lactate production was observed.

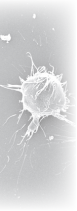

Deviant actin cytoskeleton and cell surface morphology of M1 macrophages in the absence of glucose

Polarization of macrophages towards a M1 phenotype with LPS is accompanied by an increase in glucose uptake and an accelerated conversion to lactate, while the rate of OXPHOS is reduced [5, 6]. Concomitantly, LPS induces extensive remodeling of the actin cytoskeleton of macrophages. *In vivo*, the collective changes in cell morphology and the formation of specific membrane structures, like filopodia and membrane ruffles on the surface of macrophages [12, 13] form the morphodynamic adjustments that help macrophages in adhering to the tissue matrix and in probing and capturing phagocytic targets. In order to determine whether the metabolic changes in LPS-stimulated macrophages have any true morphofunctional significance, we metabolically challenged RAW 264.7 cells, using conditions under which cells remained fully viable. First, we assessed the surface morphology and appear-

Figure 3. Actin cytoskeletal structural changes induced by inhibition of glycolysis or mitochondrial OXPHOS. *RAW 264.7 cells were seeded on glass coverslips, incubated in control medium or medium containing 2.5 μM oligomycin and 25 mM glucose* ***(A-F)****, 10 mM 2-DG and 25 mM glucose* ***(G-J)****, 10 mM galactose and no glucose* ***(M-P)****, or 1 mM glucose and 10 mM galactose* ***(Q-T)*** *for the indicated time periods and stimulated overnight with LPS or left unstimulated. After fixation in 2% PFA, cellular actin was stained with phalloidin-Alexa568 and cells were imaged on a Zeiss LSM510 meta confocal laser scanning microscope. The number of filopodia extending radially from the cell surface (expressed as # filopodia per* **μM** *contour length; see M&M) was determined for control cells and cells treated for 24 hours with oligomycin, in the presence and absence of LPS (K). The average cell circumference was determined for cells in control medium or medium containing 10 mM galactose, or 1 mM glucose and 10 mM galactose (L). (*p < 0.05, **p < 0.01, ***p < 0.001, unpaired t-test)*

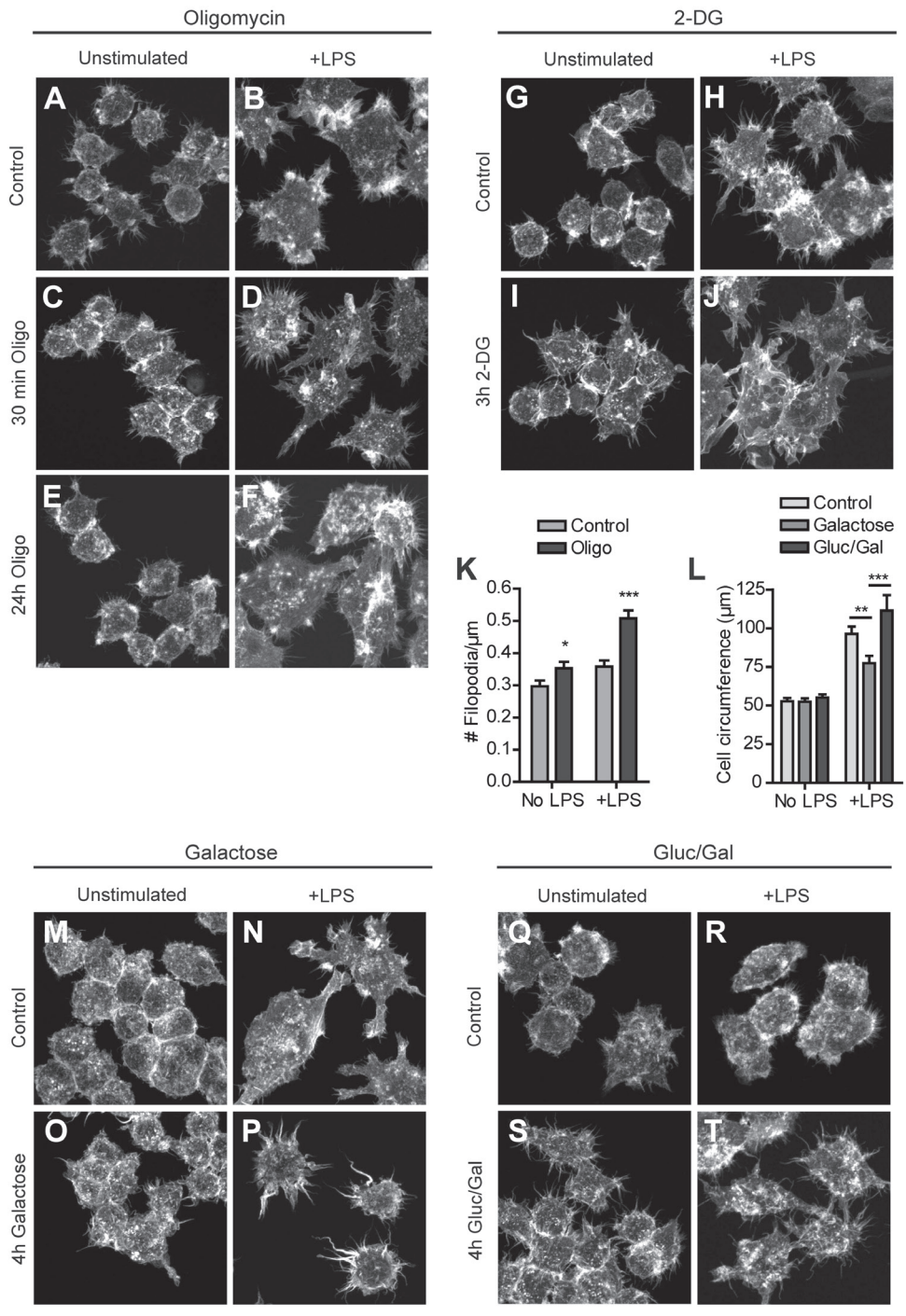
Oligomycin
2-DG
Unstimulated
+LPS
Control
30 min Oligo
24h Oligo
3h 2-DG
A
B
C
D
E
F
G
H
I
J
K
L
Control
Oligo
Filopodia/µm
No LPS
+LPS
Galactose
Gluc/Gal
Cell circumference (µm)
M
N
O
P
Q
R
S
T
4h Galactose
4h Gluc/Gal

ance of actin-based membrane protrusions, by scanning electron microscopy (SEM) and fluorescence microscopy of (phalloidin-stained) RAW 264.7 cells before and after LPS-stimulation. Oligomycin treated cells preserved the ability to spread upon LPS-stimulation and appeared to have more filopodia than control cells (Figure 3A-F and Figure 4A-F). These thorn-like protrusions became clearly visible after 6 hours (not shown) and were observed on both LPS stimulated and unstimulated cells. Quantification of the number of filopodia extending radially from the cell body after 24 hours, confirmed that oligomycin induced filopodia formation in RAW 264.7 cells (Figure 3K and 4K) although the extent of oligomycin effects (on cells with and without LPS) as determined by fluorescence and SEM microscopy varied. Partly this variation may be due to differential effects of the fixation-staining, and also to the semi-quantitative nature of protrusion recognition and scoring in the image analyses, for the light- and electron microscopy assays. Importantly, removing glucose from the culture medium markedly affected cell morphology. Although the actin cytoskeletal morphology of unstimulated galactose treated cells did not deviate much from control cells after 4 hours, LPS stimulated galactose treated cells had markedly different actin cytoskeletal morphology (Figure 3L-P). Instead of expanding their surface area and forming distinct protrusions, galactose cells stayed rounded and had a smaller cell circumference than control cells (Figure 3L; see also SEM results Figure 4L-P). When galactose-containing medium was supplemented with 1 mM glucose, the LPS-induced modifications of the cytoskeleton and surface morphology were similar to those seen in control cells (Figure 3L,Q-T and Figure 4L,Q-T). In contrast, inhibition of glycolysis with 2-DG did not alter the actin cytoskeleton or the cell morphology in either LPS- or unstimulated cells (Figure 3G-J and Figure 4G-J). In combination, our observations suggest that the presence or uptake of glucose, but not necessarily its use in metabolic breakdown, is involved in LPS-induced morphodynamic transitions in RAW 264.7 macrophages.

LPS-induced macrophage spreading depends on constant glucose supply

Next, to further investigate the role of glucose in LPS-induced protrusive actin dynamics and obtain a more quantitative measure of the effect of the different meta-

Figure 4. Effect of glucose deprivation and glycolysis or OXPHOS inhibition on morphology of RAW 264.7 cells. *Cells were seeded on glass coverslips, incubated in control medium or medium containing 2.5 µM oligomycin and 25 mM glucose **(A-F)**, 10 mM 2-DG and 25 mM glucose **(G-J)**, 10 mM galactose and no glucose **(M-P)**, or 1 mM glucose and 10 mM galactosel **(Q-T)** for the indicated time periods and stimulated overnight with LPS or left unstimulated. Coverslips were fixed and subjected to scanning electron microscopy. The number of filopodia extending radially from the cell surface was determined for control cells and cells treated for 24 hours with oligomycin, in the presence and absence of LPS (K). The average cell circumference was determined for cells in control medium or medium containing 10 mM galactose, or 1 mM glucose and 10 mM galactose (L). (***p < 0.001, unpaired t-test). (Bar = 10 µm)*

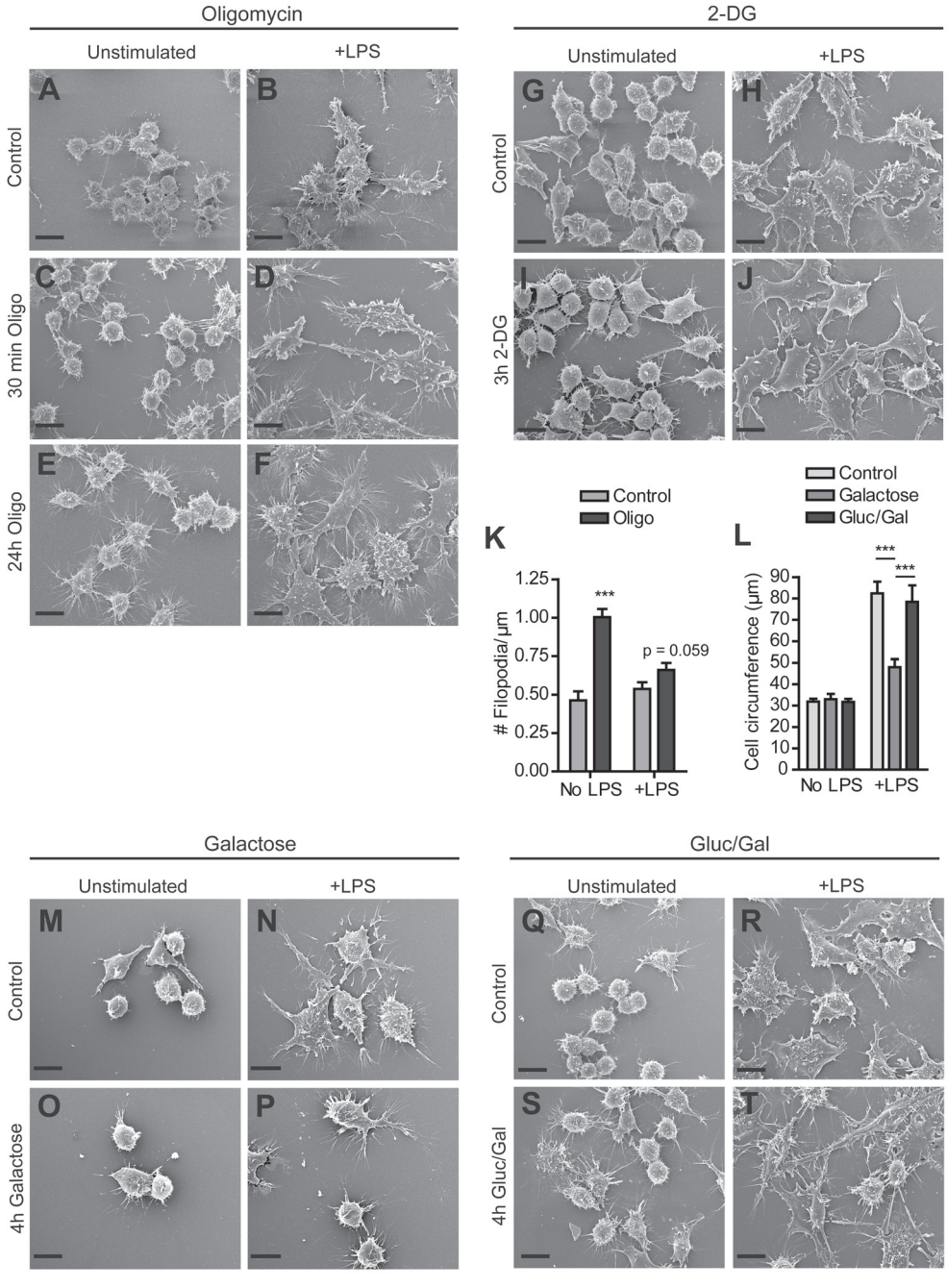
Oligomycin
Unstimulated
+LPS
Control
30 min Oligo
24h Oligo
A
B
C
D
E
F
2-DG
Unstimulated
+LPS
Control
3h 2-DG
G
H
I
J
K
Control
Oligo
Filopodia/µm
1.25
1.00
0.75
0.50
0.25
0.00
***
p = 0.059
No LPS
+LPS
L
Control
Galactose
Gluc/Gal
Cell circumference (µm)
90
80
70
60
50
40
30
20
10
0
***
***
No LPS
+LPS
Galactose
Unstimulated
+LPS
Control
4h Galactose
M
N
O
P
Gluc/Gal
Unstimulated
+LPS
Control
4h Gluc/Gal
Q
R
S
T

bolic conditions on global macrophage morphodynamics, we analyzed the spreading ability of RAW 264.7 cells on fibronectin-coated glass. During cell spreading, the increase in cell size is determined by global reorganization of the cellular actin cytoskeleton [55]. Inhibition of OXPHOS with oligomycin had no significant effect (Figure 5A), whereas 2-DG treatment caused slight retardation of spreading (Figure 5B). In contrast, removal of glucose from the medium and replacement with galactose dramatically inhibited surface expansion. Even without pre-incubation (0h), cells spread less efficient in the absence of glucose. With pre-incubation in glucose-free medium, spreading was further inhibited and already significantly impaired after 3 hours of pre-treatment (Figure 5C). Typically, in the presence of 1 mM glucose cells largely retained the ability to expand their surface area (Figure 5D). Altogether, our findings are in keeping with the morphological observations and indicate that the availability of glucose is indispensable for LPS-induced spreading of macrophages.

Phagocytosis of complement-opsonized zymosan by LPS-stimulated macrophages is fueled by glycolysis and requires the presence of extracellular glucose

We finally examined whether metabolic conditions (with differential nutrient supply or inhibitor conditions as above) also affect phagocytosis, the main actin-dependent function of macrophages [27]. Formation of the phagocytic cup is driven by local polymerization of actin filaments, associated with membrane alterations and regionally confined topological alterations at the cell surface. Unlike cell spreading, particle uptake via phagocytosis, therefore, is localized and determined by mechanistic events that occur within the small area of contact between cell and particle. Acute inhibition (0h pre-incubation) of OXPHOS initially led to a reduction in internalization efficiency as well as the overall phagocytic index of RAW 264.7 cells (Figure 6A,B), however, after three hours, phagocytosis efficiency was restored and with longer oligomycin treatment (24h) phagocytic index and the particle internalization capacity was even higher than in control cells. In the presence of ample glucose (25 mM), competitive inhibition of glycolysis by 2-DG only inhibited phagocytosis significantly after pre-incubation (Figure 6C). 2-DG did not have an acute effect, but after 1 hour of 2-DG pre-incubation phagocytosis was markedly down (p = 0.055). This effect became even more pronounced with prolonged (3h) pre-treatment, a period wherein cell viability was still not affected (Figure 1D). The efficiency of particle internalization was, however, not compromised (Figure 6D) by addition of 2-DG. Phagocytosis in the presence of oligomycin and 2-DG was also assessed in a second macrophage cell line (Maf-DKO cells). In these cells, oligomycin treatment had no effect at all, while 2-DG inhibited Maf-DKO phagocytosis to the same extend as in RAW 264.7 cells (Figure S2A,B).

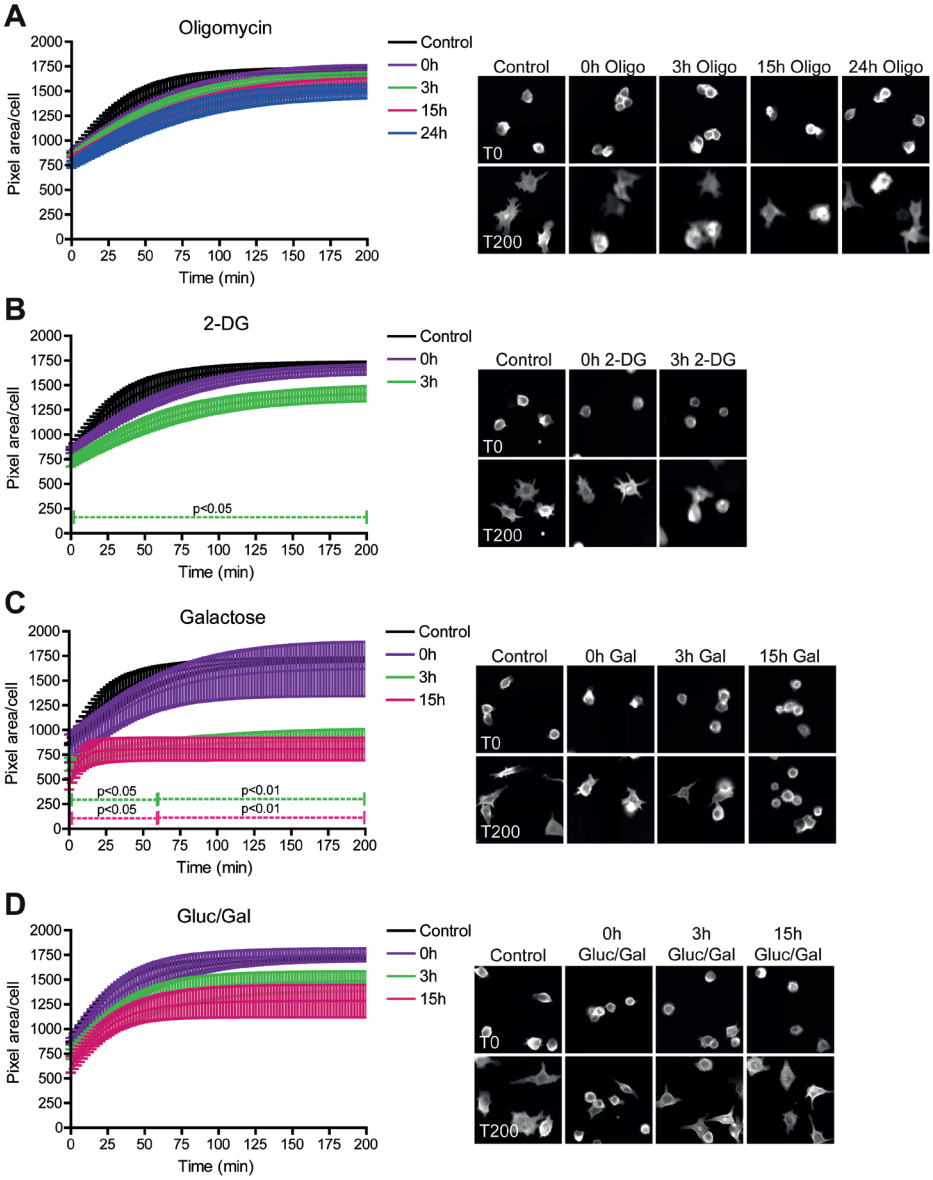

Figure 5. LPS-stimulated spreading of RAW 264.7 macrophages is compromised by glucose deprivation. *RAW 264.7 macrophages expressing Lifeact-EYFP were pre-incubated in control medium or medium containing 2.5 µM oligomycin and 25 mM glucose (**A**), 10 mM 2-DG and 25 mM glucose (**B**), 10 mM galactose and no glucose (**C**), or 1 mM glucose and 10 mM galactosel (**D**) medium for the indicated time periods. To assess spreading efficiency, cells were detached with EDTA, re-suspended, seeded in 96 well plates and allowed to adhere. Cell spreading of EYFP-positive cells was recorded over time using a BD Pathway high content microscope. The average pixel area per cell was determined at 10 minute intervals. Lines and bars represent means ± SEM of three independent experiments performed in triplicate. For every condition, representative images of cells at 0 and 200 minutes are presented in the panel on the right*

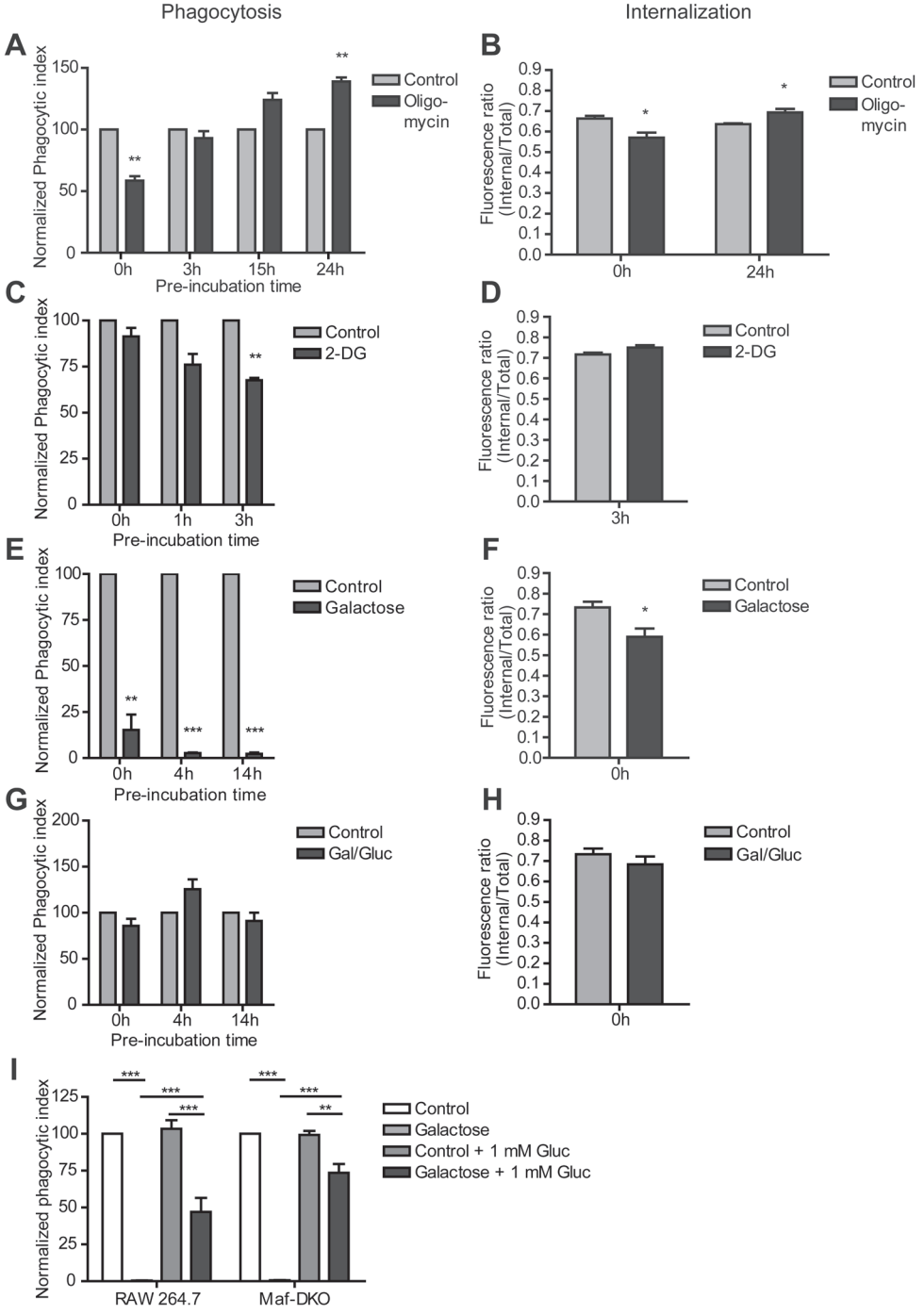
Phagocytosis
Internalization
A
Normalized Phagocytic index
Control
Oligo-mycin
Pre-incubation time
0h
3h
15h
24h
B
Fluorescence ratio (Internal/Total)
C
Control
2-DG
1h
3h
D
E
Galactose
4h
14h
F
G
Gal/Gluc
H
I
Normalized phagocytic index
Control + 1 mM Gluc
Galactose + 1 mM Gluc
RAW 264.7
Maf-DKO

Figure 6. Macrophages require glucose for phagocytosis of COZ. *RAW 264.7 cells were incubated for the indicated times with control medium, or medium containing 2.5 µM oligomycin and 25 mM glucose **(A,B)**, 10 mM 2-DG and 25 mM glucose **(C,D)**, 10 mM galactose and no glucose **(E,F)**, or 10 mM galactose and 1 mM glucose **(G,H)** and stimulated o/n with 100 ng/ml LPS. The phagocytic index (A,C,E,G) was determined by incubating cells in the respective media with FITC-labeled complement opsonized zymosan (COZ) particles for 30 min, analyzed by FACS and calculated as described in materials and methods. The internalization efficiency (B,D,F&H) was determined by quenching extracellular FITC-COZ of one sample fraction with 0.05 % trypan blue in potassium dihydrogen citrate/saline, pH 4.4. Unquenched fractions were used to determine the total fluorescence per cell (internalized and external particles), while quenched fractions were used to measure only the internal fluorescence per cell. The effect of reintroducing glucose (+ 1 mM Gluc) in the medium after 30 minutes of phagocytosis in glucose-free medium was assessed in both RAW 264.7 and Maf-DKO cells **(I)**. Values in A,C,E,G&I represent normalized means ±SEM of three or four independent experiments performed in triplicate (*p<0.05, **p<0.01, ***p < 0.001; one-sample t-test (A-H) or two-way ANOVA and Bonferroni posttest (I)). Values in B,D,F&H represent means ±SEM of three experiments performed in triplicate. (*p<0.05; unpaired t-test)*

Upon total glucose deprivation (by substitution with galactose), the phagocytic index in both RAW 264.7 and Maf-DKO cells dropped immediately below 20% (Figure 6E and Figure S2C). An even bigger drop was seen in RAW 264.7 cells after 4 and 14 hours (Figure 6E). It is important to note that at 0 and 4 hours the cells were still fully viable. Thus, we conclude that the reduction in phagocytic activity must be solely the result of insufficiency in glucose availability and not be a secondary effect of functional incapacitation. The low phagocytic index in the absence of glucose was accompanied by a reduction in particle internalization efficiency (Figure 6F) as well as a reduction in the binding capacity of the cells since the percentage of FITC-COZ positive cells was also reduced by more than 50% (results not shown). These results suggest that glucose availability is essential for both particle binding and internalization. Interestingly, and in keeping with this conclusion, supplementation of galactose medium with 1 mM glucose enabled the cells to maintain full phagocytosis capacity (Figure 6G,H).

Finally, we wanted to determine whether the inhibitory effect of acute glucose deprivation on phagocytosis could be directly rescued by reintroducing glucose. RAW 264.7 and Maf-DKO cells were incubated with FITC-COZ in galactose medium for 30 minutes after which 1 mM of glucose was added and cells were incubated for another 30 minutes. RAW 264.7 phagocytosis capacity was restored to 45% while Maf-DKO cells regained 75% of their phagocytosis capacity (Figure 6I). Taken together, our findings imply that glycolysis is critical for phagocytosis of COZ while OXPHOS activity is dispensable. Moreover, our results suggest that macrophages require the presence of glucose in order to successfully bind and internalize COZ particles.

Discussion

Increased morphodynamic activity, facilitated by rearrangement of the actin cytoskeleton, is a cellular response characteristic to LPS-stimulated macrophages. This dynamic actin remodeling is essential to macrophage function and considered to be an energy draining process. In endothelial cells, actin-ATP hydrolysis accounts for almost a fifth (18%) of total ATP consumption [56] and in platelets and neurons it is estimated to be more than 50% [26, 57]. Cellular energy metabolism and actin-based cell dynamics are, therefore, tightly coupled processes. Against this backdrop LPS also induces a shift in macrophage redox metabolism, accompanied by increased fluxes through glycolysis as well the pentose phosphate pathway for NADPH production [5, 7]. Here we asked the question whether these temporal associations also involve a functional regulatory coupling between metabolic and morphodynamic changes in LPS stimulated macrophages.

Our results show that the contribution of mitochondrial OXPHOS to cellular energy production is significantly smaller than that of glycolysis and that mitochondrial OXPHOS activity is not essential for fueling of morphodynamic processes in macrophages. We found that oxygen consumption in resting RAW 264.7 and Maf-DKO cells is two to four times lower than, for example, in mouse embryonic fibroblasts (Figure S1 and Valsecchi et al. [58]). More direct support for the dispensability of mitochondrial metabolism comes from the observation that, even under conditions where we enforced an almost complete dependency on glycolysis by treatment with oligomycin, the ability of RAW 264.7 macrophages to undergo LPS-induced actin cytoskeleton remodeling remained intact. Although phagocytosis capacity in RAW 264.7 cells was initially inhibited upon acute oligomycin treatment, this was restored within three hours and did not occur in Maf-DKO cells at all. Our observations are consistent with an earlier study by Kvarstein [59], wherein it was shown that OXPHOS inhibition with oligomycin and antimycin only had an effect on phagocytosis when used in combination with 2-DG. Another study by Cifarelli et al. [43] showed minor inhibition of phagocytosis with sodium azide and 2-4-dinitrophenol only after 3 hours. Our findings additionally showed that OXPHOS has also a negligible role in other aspects of macrophage morphodynamics.

In contrast, glucose metabolism through glycolysis (the dominating metabolic route of LPS-stimulated macrophages) was clearly indispensable. Perturbation of this pathway was achieved either by using the glycolytic inhibitor 2-DG, or by replacing glucose with galactose in the culture medium, thereby forcing the cells to synthesize and use mitochondrial ATP instead of ATP obtained from glycolysis [60, 61]. Although 2-DG treatment did not affect the LPS-induced morphology of RAW 264.7 cells, it caused a minor inhibition of the spreading ability of these cells. Additionally,

inhibition of glycolysis with 2-DG also led to a significant reduction in phagocytosis capacity. This has been reported before for leukocytes in general and peritoneal macrophages [42, 59, 62]. Here, we extend these observations and additionally show that phagocytosis of complement opsonized zymosan by both RAW 264.7 and Maf-DKO cells depends on the presence of glucose in the cultivation medium during the time of uptake. We know only of two other papers that have reported on direct effects of glucose deprivation. In these studies, phagocytosis of unopsonized *P. aeruginosa* by human and murine peritoneal and alveolar macrophages was shown to depend on the presence of glucose in the culture medium [63, 64]. However, the glucose dependency did not apply to phagocytosis of *P. aeruginosa* opsonized with polyclonal rabbit serum, latex particles, unopsonized zymosan, or RBCs opsonized with IgG or IgM and complement. Although we only examined COZ phagocytosis and used only two macrophage cell lines here, our findings suggest that glucose availability may be important for a wider range of actin-dependent processes and monocyte cell types. One rarely discussed process in this context is macropinocytosis activity, which also requires a dynamic actin cytoskeleton. Macropinocytosis activity of macrophages is AMPK-mediated and induced by low glucose conditions [65]. In turn, macropinocytosis may contribute to nutrient uptake capacity, although glucose import probably occurs mainly through GLUT in LPS-stimulated macrophages [6]. Here we would like to speculate that the differences in membrane ruffling (not shown) and recovery of phagocytic activity upon reintroduction of glucose (75% vs. 45%) that we observed between Maf-DKO and RAW 264.7 cells may have to do with the extend of macropinocytosis activity - and metabolic regulation thereof - in these cell lines. It is of note here that phagocytosis and macropinocytosis are mechanistically related processes, and - especially in the initiation phase - also share many morphological features. Alteration of the actin organization, due to loss of MafB, may also explain the differences between the two types of macrophages studied here [66].

Why is presence of glucose so important for formation of actin rich protrusions and spreading and other functional activities of LPS-stimulated macrophages? One possible answer is that there is a direct link to local ATP-production, even though global ATP levels were not affected under the conditions applied. Commonly, when glycolytic ATP-production is disturbed, cells adapt to the use of other substrates such as fatty acids and amino acids (especially glutamine) for ATP production. It has been shown that thioglycollate elicited mouse peritoneal macrophages (which are partially M2-polarized) utilize fatty acids to fuel phagocytosis, especially when glucose is limiting. However, in LPS-stimulated macrophages, the mitochondrial route for ATP-production from fatty acid oxidation is overtly downregulated [8]. This suggests that LPS-stimulated macrophages do not have many alternative sources

for fast supply of ATP. Moreover, the intracellular distribution of ATP may play a role. We and others have shown that adenylate kinase or creatine kinase catalyzed phosphotransfer reactions may help in the local ATP supply that is needed for remodeling of the cortical areas of cells during phagocytosis and migration [27, 28, 67, 68]. Since it is generally accepted that actin-rich membrane structures such as filopodia, lamellipodia, ruffles, and maybe also the phagocytic cup, are too thin to contain mitochondria, glucose and its breakdown via glycolysis may be the only source for local ATP production in these structures in LPS-stimulated macrophages. In other cell types, glycolytic enzymes such as aldolase and GAPDH have been shown to be compartmentalized in cortical actin structures, such as pseudopodia, invadopodia, and lamellipodia, and to associate with the actin cytoskeleton [37, 39, 40, 69, 70]. Although very little is known about the proteome of the early forming phagocytic cup, proteomic studies of the phagosome have also identified a role for GAPDH in phagocytosis [71]. A role for glucose catabolism via glycolysis in local - not global - ATP homeostasis may thus explain our findings. A second metabolic role for glucose could be the supply of intermediates in reactions that supply fatty acids and phospholipids for direct local incorporation into the cell membrane [72]. This process is important for maintaining membrane fluidity and for supply of membrane components during formation of protrusions or maturation of the phagocytic cup and movement of the phagosome, respectively. In addition, LPS-stimulated macrophages secrete inflammatory compounds such as IL-1, IL-6, and TNFα. High glycolytic activity may be essential for the synthesis and post-translational modifications of these compounds, as has been shown for quiescent fibroblasts which maintain high glycolytic activity for the synthesis of extracellular matrix proteins [73].

Striking, although considered a gentler way of modulating cell metabolism, since glucose is still available, 2-DG treatment induced cell death earlier than glucose deprivation in our unstimulated cells, although it had a less severe effect on LPS-induced morphodynamics. This raises the possibility that, apart from providing fuel and anabolic material, glucose could affect cellular morphodynamics through another (non-metabolic) mechanism. Indeed, several studies have revealed a direct role for glucose metabolism in posttranslational modification of proteins and signaling to the actin cytoskeleton. Although not known for complement receptor 3, other macrophage receptors that are involved in phagocytosis and adhesion to the extracellular matrix, like CD36, FcγRIII, and CR5a, contain sites for N-linked glycosylation [74-76]. 2-DG has been shown to interfere with (i.e. poison) N-linked glycosylation in tumor cells, a process that could be reversed by exogenous addition of mannose [77]. It may, therefore, be possible that 2-DG interfered with normal macrophage receptor expression and function. Michl et al. [42] suggested that 2-DG interferes with reactions that link Fcγ- and C3-receptors with the

intracellular contractile apparatus, based on the observation that cellular ATP levels were not disturbed after 2-DG treatment and that the inhibitory effect of 2-DG on phagocytosis was reversed upon addition of mannose or high glucose concentrations. Furthermore, in studies on glucose-induced insulin secretion in pancreatic islet cells and other insulin-secreting cells, such as INS-1, HIT, and MIN6 cells, glucose metabolism has been implicated in the activation of the small GTPase Cdc42, an upstream regulator of actin remodeling. Nevins and Thurmond [78] showed in MIN6 β-cells, that glucose stimulation promotes actin cytoskeletal remodeling by causing alterations in the cycling of Cdc42 between its active GTP-bound and inactive GDP-bound form. Transient activation involves the carboxylmethylation of Cdc42, and occurs rapidly (within 15-30 sec) [79], while deactivation of Cdc42 involves glycosylation of this small RhoGTPase and correlates with transient depolymerization of cortical actin [78]. This suggests that glucose regulates the cortical actin network through modulation of Cdc42 cycling. Transient activation of Cdc42 leads to activation of PAK1 and then Rac1 (another small GTPase involved in actin cytoskeletal remodeling) within 15 minutes after glucose exposure [80]. Finally, Uenishi et al. [81] have recently shown that glucose activates N-WASP via Cdc42 and induces its translocation to the cell membrane of insulin-secreting clonal pancreatic β-cells (MIN6-K8 β-cells). Moreover, glucose stimulation caused LIMK1-mediated phosphorylation and deactivation of cofilin via Cdc42 and PAK1. The timing of these effects may explain why acute removal of glucose from the culture medium had a markedly inhibitory effect on phagocytosis and also why reintroduction of glucose instantaneously restored phagocytosis capacity in our study. Interestingly, LPS signaling to the cytoskeleton also involves the Cdc42-PAK1-Rac1-LIMK1-pathway [82]. LPS stimulation additionally increases glucose uptake and metabolism via PI3K/Akt which are signaling molecules upstream of Cdc42 and Rac1 [83-86]. Therefore, by incorporating glucose as signaling molecule, the metabolic changes that are induced by LPS may serve to reinforce the functional changes that macrophage must undergo in order to fulfill their function in host defense and tissue homeostasis.

In summary, our results further establish a pivotal role for glucose and its breakdown via glycolysis in the control of morphodynamic activity in LPS-stimulated macrophages. Based on findings in other cell systems, we consider it likely that for exerting this role, the multitalented properties of glucose as metabolic precursor and molecule for use in post-translational modification of cytoskeletal (associated) structural proteins, receptors or signaling proteins are being used. More in depth investigation is required to further unravel these glucose-related events that control the activities of macrophages.

Acknowledgements

We are grateful to Dr. Hong-Hee Kim (Department of Cell and Developmental Biology, School of Dentistry, Seoul National University, Korea) for providing the RAW 264.7 cell line, Dr.Ralf Langen (University of Southern California) for supplying the pSIVA apoptosis biosensor, Dr. Michael H. Sieweke (Centre d'Immunologie de Marseille-Luminy (CIML), Université Aix-Marseille, France) for providing the Maf-DKO cells, Ganesh Manjeri (Department of Biochemistry, NCMLS, Radboud UMC, Nijmegen, The Netherlands) for help with the oxygen consumption assays, and Cindy Dieteren and Ineke van der Zee (Department of Cell Biology, NCMLS, Radboud UMC, Nijmegen, The Netherlands) for statistical advice with regard to the spreading assays.

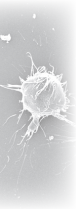

Supplementary material

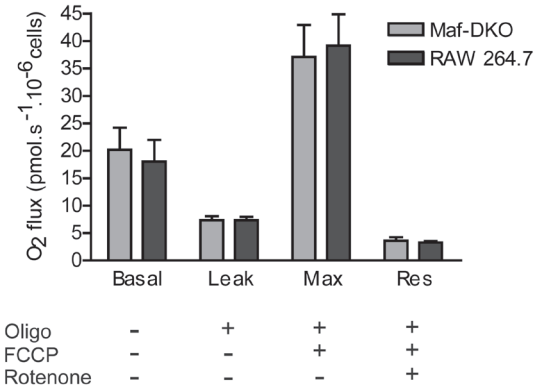

Figure S1. Oxygen consumption in RAW 264.7 and Maf-DKO macrophages. *Oxygen consumption was measured in suspensions of 1 x 10^6 cells on an Oroboros Oxygraph-2k respirometer. RAW 264.7 and Maf-DKO cells were analyzed in parallel on the same day. The basal oxygen consumption was measured where after oligomycin, FCCP, and rotenone was added successively in order to determine the leak respiration, maximal respiration (Max), and residual oxygen consumption (Res). Columns represent means ± SEM of four experiments*

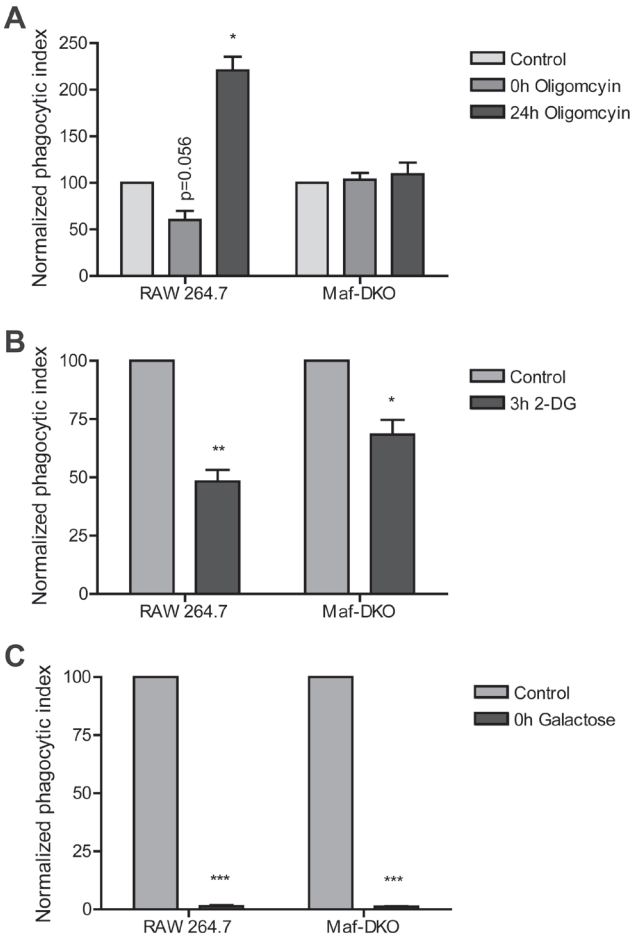

Figure S2. Macrophages require glucose for phagocytosis of COZ. *RAW 264.7 and Maf-DKO cells were incubated for the indicated times in control medium, or medium containing 2.5 µM oligomycin and 25 mM glucose **(A)**, 10 mM 2-DG and 25 mM glucose **(B)**, or 10 mM galactose and no glucose **(C)** and stimulated o/n with 100 ng/ml LPS. Phagocytosis efficiency was determined by incubating cells in the respective media with FITC-labeled complement opsonized zymosan (COZ) particles for 30 min and analyzing samples by FACS. Values represent normalized means ±SEM of three independent experiments performed in triplicate. (*p < 0.05, **p < 0.01, ***p < 0.001; one-sample t-test)*

References

1. Murray, P.J. & Wynn, T.A. Protective and pathogenic functions of macrophage subsets. *Nat. Rev. Immunol.* **11**, 14 (2011).
2. Mosser, D.M. & Edwards, J.P. Exploring the full spectrum of macrophage activation. *Nat. Rev. Immunol.* **8**, 958 (2008).
3. Mills, C.D., Kincaid, K., Alt, J.M., Heilman, M.J. & Hill, A.M. M-1/M-2 Macrophages and the Th1/Th2 Paradigm. *J. Immunol.* **164**, 6166-6173 (2000).
4. Mantovani, A., Sica, A. & Locati, M. Macrophage Polarization Comes of Age. *Immunity* **23**, 344-346 (2005).
5. Rodríguez-Prados, J.-C. *et al.* Substrate Fate in Activated Macrophages: A Comparison between Innate, Classic, and Alternative Activation. *J. Immunol.* **185**, 605-614 (2010).
6. Fukuzumi, M., Shinomiya, H., Shimizu, Y., Ohishi, K. & Utsumi, S. Endotoxin-induced enhancement of glucose influx into murine peritoneal macrophages via GLUT1. *Infect. Immun.* **64**, 108-112 (1996).
7. Haschemi, A. *et al.* The Sedoheptulose Kinase CARKL Directs Macrophage Polarization through Control of Glucose Metabolism. *Cell Metab.* **15**, 813-826 (2012).
8. Vats, D. *et al.* Oxidative metabolism and PGC-1β attenuate macrophage-mediated inflammation. *Cell Metab.* **4**, 13-24 (2006).
9. Tannahill, G.M. *et al.* Succinate is an inflammatory signal that induces IL-1b through HIF-1a. *Nature* **496**, 238-242 (2013).
10. Kress, H. *et al.* Filopodia act as phagocytic tentacles and pull with discrete steps and a load-dependent velocity. *Proc. Natl. Acad. Sci. U. S. A.* **104**, 11633-11638 (2007).
11. Vonna, L., Wiedemann, A., Aepfelbacher, M. & Sackmann, E. Micromechanics of filopodia mediated capture of pathogens by macrophages. *Eur. Biophys. J.* **36**, 145-151 (2007).
12. Williams, L.M. & Ridley, A.J. Lipopolysaccharide Induces Actin Reorganization and Tyrosine Phosphorylation of Pyk2 and Paxillin in Monocytes and Macrophages. *J. Immunol.* **164**, 2028-2036 (2000).
13. Kleveta, G. *et al.* LPS induces phosphorylation of actin-regulatory proteins leading to actin reassembly and macrophage motility. *J. Cell. Biochem.* **113**, 80-92 (2012).
14. Cougoule, C. *et al.* Blood leukocytes and macrophages of various phenotypes have distinct abilities to form podosomes and to migrate in 3D environments. *Eur. J. Cell Biol.* **91**, 938-949 (2012).
15. Pollard, T.D. & Cooper, J.A. Actin, a Central Player in Cell Shape and Movement. *Science* **326**, 1208-1212 (2009).
16. Dos Remedios, C.G. *et al.* Actin Binding Proteins: Regulation of Cytoskeletal Microfilaments. *Physiol. Rev.* **83**, 433-473 (2003).
17. Carlier, M.F. Actin: protein structure and filament dynamics. *J. Biol. Chem.* **266**, 1-4 (1991).
18. Carlier, M.-F. & Pantaloni, D. Control of Actin Assembly Dynamics in Cell Motility. *J. Biol. Chem.* **282**, 23005-23009 (2007).
19. Isambert, H. *et al.* Flexibility of actin filaments derived from thermal fluctuations. Effect of bound nucleotide, phalloidin, and muscle regulatory proteins. *J. Biol. Chem.* **270**, 11437-11444 (1995).
20. Pfaendtner, J., Branduardi, D., Parrinello, M., Pollard, T.D. & Voth, G.A. Nucleotide-dependent conformational states of actin. *Proc. Natl. Acad. Sci. U. S. A.* **106**, 12723-12728 (2009).
21. Romero, S. *et al.* How ATP Hydrolysis Controls Filament Assembly from Profilin-Actin: Implication for formin processivity. *J. Biol. Chem.* **282**, 8435-8445 (2007).
22. Ingerman, E., Hsiao, J.Y. & Mullins, R.D. Arp2/3 complex ATP hydrolysis promotes lamellipodial actin network disassembly but is dispensable for assembly. *J. Cell Biol.* **200**, 619-633 (2013).
23. Pollard, T.D. Regulation of Actin Filament Assembly by Arp2/3 Complex and Formins. *Annu. Rev. Biophys. Biomol. Struct.* **36**, 451-477 (2007).
24. Hallett, M.A., Dagher, P.C. & Atkinson, S.J. Rho GTPases show differential sensitivity to nucleotide triphosphate depletion in a model of ischemic cell injury. *Am. J. Physiol. Cell Physiol.* **285**, C129-C138 (2003).
25. Atkinson, S.J., Hosford, M.A. & Molitoris, B.A. Mechanism of Actin Polymerization in Cellular ATP Depletion. *J. Biol. Chem.* **279**, 5194-5199 (2004).
26. Bernstein, B.W. & Bamburg, J.R. Actin-ATP Hydrolysis Is a Major Energy Drain for Neurons. *J. Neurosci.* **23**, 1-6 (2003).
27. Kuiper, J.W.P. *et al.* Creatine Kinase–Mediated ATP Supply Fuels Actin-Based Events in Phagocytosis. *PLoS Biol.* **6**, e51 (2008).
28. van Horssen, R. *et al.* Modulation of Cell Motility by Spatial Repositioning of Enzymatic ATP/ADP Exchange Capacity. *J. Biol. Chem.* **284**, 1620-1627 (2009).
29. van Horssen, R. *et al.* Intracellular NAD(H) levels control motility and invasion of glioma cells. *Cell. Mol. Life Sci.*, 1-16 (2013).
30. Crevenna, A.H. *et al.* Electrostatics control actin filament nucleation and elongation kinetics. *J. Biol. Chem.*

288, 12102-12113 (2013).
31. Dalle-Donne, I., Rossi, R., Milzani, A., Di Simplicio, P. & Colombo, R. The actin cytoskeleton response to oxidants: from small heat shock protein phosphorylation to changes in the redox state of actin itself. *Free Radic. Biol. Med.* **31**, 1624-1632 (2001).
32. Hung, R.-J., Pak, C.W. & Terman, J.R. Direct Redox Regulation of F-Actin Assembly and Disassembly by Mical. *Science* **334**, 1710-1713 (2011).
33. Frantz, C. *et al.* Cofilin is a pH sensor for actin free barbed end formation: role of phosphoinositide binding. *J. Cell Biol.* **183**, 865-879 (2008).
34. Garg, R., Peddada, N., Sagar, A., Nihalani, D. & Ashish, F.N.U. Visual insight into how low pH alone can induce actin severing ability in gelsolin under calcium free conditions. *J Bio Chem* (2011).
35. Kim, J.-S., Huang, T.Y. & Bokoch, G.M. Reactive Oxygen Species Regulate a Slingshot-Cofilin Activation Pathway. *Mol. Biol. Cell* **20**, 2650-2660 (2009).
36. Nguyen, T.N., Wang, H.-J., Zalzal, S., Nanci, A. & Nabi, I.R. Purification and Characterization of β-Actin-Rich Tumor Cell Pseudopodia: Role of Glycolysis. *Exp. Cell Res.* **258**, 171-183 (2000).
37. Pagliaro, L. & Taylor, D.L. Aldolase exists in both the fluid and solid phases of cytoplasm. *J. Cell Biol.* **107**, 981-991 (1988).
38. Pagliaro, L. & Taylor, D.L. 2-Deoxyglucose and cytochalasin D modulate aldolase mobility in living 3T3 cells. *The Journal of Cell Biology* **118**, 859-863 (1992).
39. Jia, Z. *et al.* Tumor Cell Pseudopodial Protrusions: Localized signaling domains coordinating cytoskeleton remodeling, cell adhesion, glycolysis, RNA translocation, and protein translation. *J. Biol. Chem.* **280**, 30564-30573 (2005).
40. Tochio, T., Tanaka, H., Nakata, S. & Hosoya, H. Fructose-1,6-bisphosphate aldolase A is involved in HaCaT cell migration by inducing lamellipodia formation. *J. Dermatol. Sci.* **58**, 123-129 (2010).
41. De Bock, K. *et al.* Role of PFKFB3-Driven Glycolysis in Vessel Sprouting. *Cell* **154**, 651-663 (2013).
42. Michl, J., Ohlbaum, D.J. & Silverstein, S.C. 2-Deoxyglucose selectively inhibits Fc and complement receptor-mediated phagocytosis in mouse peritoneal macrophages. I. Description of the inhibitory effect. *J. Exp. Med.* **144**, 1465-1483 (1976).
43. Cifarelli, A., Pepe, G., Paradisi, F. & Piccolo, D. The influence of some metabolic inhibitors on phagocytic activity of mouse macrophages in vitro. *Res. Exp. Med. (Berl).* **174**, 197-204 (1979).
44. Paradisi, F., D'Onofrio, C., Pepe, G., Cifarelli, A. & Piccolo, D. Phagocytosis and cellular metabolism. *Ric. Clin. Lab.* **9**, 47-60 (1979).
45. Raschke, W.C., Baird, S., Ralph, P. & Nakoinz, I. Functional macrophage cell lines transformed by abelson leukemia virus. *Cell* **15**, 261-267 (1978).
46. Aziz, A., Soucie, E., Sarrazin, S. & Sieweke, M.H. MafB/c-Maf Deficiency Enables Self-Renewal of Differentiated Functional Macrophages. *Science* **326**, 867-871 (2009).
47. Chang, E.-J. *et al.* Brain-type creatine kinase has a crucial role in osteoclast-mediated bone resorption. *Nat. Med.* **14**, 966-972 (2008).
48. Riedl, J. *et al.* Lifeact: a versatile marker to visualize F-actin. *Nat. Methods* **5**, 605-607 (2008).
49. Skehan, P. *et al.* New Colorimetric Cytotoxicity Assay for Anticancer-Drug Screening. *J. Natl. Cancer Inst.* **82**, 1107-1112 (1990).
50. Kim, Y.E., Chen, J., Chan, J.R. & Langen, R. Engineering a polarity-sensitive biosensor for time-lapse imaging of apoptotic processes and degeneration. *Nat. Methods* **7**, 67-73 (2010).
51. Schindelin, J. *et al.* Fiji: an open-source platform for biological-image analysis. *Nat. Methods* **9**, 676-682 (2012).
52. Sahlin, S., Hed, J. & Runfquist, I. Differentiation between attached and ingested immune complexes by a fluorescence quenching cytofluorometric assay. *J. Immunol. Methods* **60**, 115-124 (1983).
53. Newsholme, P. Why Is l-Glutamine Metabolism Important to Cells of the Immune System in Health, Postinjury, Surgery or Infection? *J. Nutr.* **131**, 2515S-2522S (2001).
54. Newsholme, P., Gordon, S. & Newsholme, E.A. Rates of utilization and fates of glucose, glutamine, pyruvate, fatty acids and ketone bodies by mouse macrophages. *Biochem. J.* **242**, 631-636 (1987).
55. Xiong, Y. *et al.* Mechanisms Controlling Cell Size and Shape during Isotropic Cell Spreading. *Biophys. J.* **98**, 2136-2146 (2010).
56. Culic, O., Gruwel, M.L. & Schrader, J. Energy turnover of vascular endothelial cells. *Am. J. Physiol.* **273**, C205-C213 (1997).
57. Daniel, J.L., Molish, I.R., Robkin, L. & Holmsen, H. Nucleotide exchange between cytosolic ATP and F-actin-bound ADP may be a major energy-utilizing process in unstimulated platelets. *Eur. J. Biochem.* **156**, 677-683 (1986).
58. Valsecchi, F. *et al.* Metabolic consequences of NDUFS4 gene deletion in immortalized mouse embryonic fibroblasts. *Biochim. Biophys. Acta* **1817**, 1925-1936 (2012).
59. Kvarstein, B. The Effect of Temperature, Metabolic Inhibitors, and EDTA on Phagocytosis of Polystyrene Latex

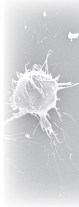

Particles by Human Leucocytes. *Scand. J. Clin. Lab. Invest.* **24**, 271-277 (1969).
60. Marroquin, L.D., Hynes, J., Dykens, J.A., Jamieson, J.D. & Will, Y. Circumventing the Crabtree Effect: Replacing Media Glucose with Galactose Increases Susceptibility of HepG2 Cells to Mitochondrial Toxicants. *Toxicol. Sci.* **97**, 539-547 (2007).
61. Aguer, C. *et al.* Galactose Enhances Oxidative Metabolism and Reveals Mitochondrial Dysfunction in Human Primary Muscle Cells. *PLoS ONE* **6**, e28536 (2011).
62. Mazur, M. & Williamson Macrophage deformability and phagocytosis. *J. Cell Biol.* **75**, 185-199 (1977).
63. Speert, D.P. & Gordon, S. Phagocytosis of unopsonized Pseudomonas aeruginosa by murine macrophages is a two-step process requiring glucose. *J. Clin. Invest.* **90**, 1085-1092 (1992).
64. Wong, S.Y.C., Guerdoud, L.M., Cantin, A. & Speert, D.P. Glucose Stimulates Phagocytosis of Unopsonized Pseudomonas aeruginosa by Cultivated Human Alveolar Macrophages. *Infect. Immun.* **67**, 16-21 (1999).
65. Guest, C., Chakour, K. & Freund, G. Macropinocytosis is decreased in diabetic mouse macrophages and is regulated by AMPK. *BMC Immunol.* **9**, 42 (2008).
66. Aziz, A. *et al.* Development of Macrophages with Altered Actin Organization in the Absence of MafB. *Mol. Cell. Biol.* **26**, 6808-6818 (2006).
67. Loike, J.D., Kozler, V.F. & Silverstein, S.C. Increased ATP and creatine phosphate turnover in phagocytosing mouse peritoneal macrophages. *J. Biol. Chem.* **254**, 9558-9564. (1979).
68. Kuiper, J.W.P. *et al.* Local ATP Generation by Brain-Type Creatine Kinase (CK-B) Facilitates Cell Motility. *PLoS ONE* **4**, e5030 (2009).
69. Waingeh, V.F. *et al.* Glycolytic Enzyme Interactions with Yeast and Skeletal Muscle F-Actin. *Biophys. J.* **90**, 1371-1384 (2006).
70. Attanasio, F. *et al.* Novel invadopodia components revealed by differential proteomic analysis. *Eur. J. Cell Biol.* **90**, 115-127 (2011).
71. Garin, J. *et al.* The Phagosome Proteome: Insight into Phagosome Functions. *J. Cell Biol.* **152**, 165-180 (2001).
72. Ecker, J. *et al.* Induction of fatty acid synthesis is a key requirement for phagocytic differentiation of human monocytes. *Proc. Natl. Acad. Sci. U. S. A.* **107**, 7817-7822 (2010).
73. Lemons, J.M.S. *et al.* Quiescent Fibroblasts Exhibit High Metabolic Activity. *PLoS Biol.* **8**, e1000514 (2010).
74. Drescher, B., Witte, T. & Schmidt, R.E. Glycosylation of FcγRIII in N163 as mechanism of regulating receptor affinity. *Immunology* **110**, 335-340 (2003).
75. Hoosdally, S.J., Andress, E.J., Wooding, C., Martin, C.A. & Linton, K.J. The Human Scavenger Receptor CD36: Glycosylation status and its role in trafficking and function. *J. Biol. Chem.* **284**, 16277-16288 (2009).
76. Pease, J.E. & Barker, M.D. N-linked glycosylation of the C5a receptor. *Biochem. Mol. Biol. Int.* **31**, 19-26 (1993).
77. Kurtoglu, M. *et al.* Under normoxia, 2-deoxy-d-glucose elicits cell death in select tumor types not by inhibition of glycolysis but by interfering with N-linked glycosylation. *Mol. Cancer Ther.* **6**, 3049-3058 (2007).
78. Nevins, A.K. & Thurmond, D.C. Glucose regulates the cortical actin network through modulation of Cdc42 cycling to stimulate insulin secretion. *Am. J. Physiol. Cell Physiol.* **285**, C698-C710 (2003).
79. Kowluru, A. *et al.* Glucose- and GTP-dependent stimulation of the carboxyl methylation of CDC42 in rodent and human pancreatic islets and pure beta cells. Evidence for an essential role of GTP-binding proteins in nutrient-induced insulin secretion. *J. Clin. Invest.* **98**, 540-555 (1996).
80. Wang, Z., Oh, E. & Thurmond, D.C. Glucose-stimulated Cdc42 Signaling Is Essential for the Second Phase of Insulin Secretion. *J. Biol. Chem.* **282**, 9536-9546 (2007).
81. Uenishi, E. *et al.* Actin Dynamics Regulated by the Balance of Neuronal Wiskott-Aldrich Syndrome Protein (N-WASP) and Cofilin Activities Determines the Biphasic Response of Glucose-induced Insulin Secretion. *J. Biol. Chem.* **288**, 25851-25864 (2013).
82. Kong, L. & Ge, B.-X. MyD88-independent activation of a novel actin-Cdc42/Rac pathway is required for Toll-like receptor-stimulated phagocytosis. *Cell Res.* **18**, 745-755 (2008).
83. Riley, J.K., Carayannopoulos, M.O., Wyman, A.H., Chi, M. & Moley, K.H. Phosphatidylinositol 3-Kinase Activity Is Critical for Glucose Metabolism and Embryo Survival in Murine Blastocysts. *J. Biol. Chem.* **281**, 6010-6019 (2006).
84. Gottlob, K. *et al.* Inhibition of early apoptotic events by Akt/PKB is dependent on the first committed step of glycolysis and mitochondrial hexokinase. *Genes Dev.* **15**, 1406-1418 (2001).
85. Hill, M.M. *et al.* A Role for Protein Kinase Bβ/Akt2 in Insulin-Stimulated GLUT4 Translocation in Adipocytes. *Mol. Cell. Biol.* **19**, 7771-7781 (1999).
86. Schultze, S.M., Hemmings, B.A., Niessen, M. & Tschopp, O. PI3K/AKT, MAPK and AMPK signalling: protein kinases in glucose homeostasis. *Expert Rev. Mol. Med.* **14**, null-null (2012).

5

NAMPT-mediated salvage synthesis of NAD^+ controls morphofunctional changes of macrophages

Gerda Venter, Frank T. J. J. Oerlemans, Marieke Willemse, Mietske Wijers, Jack A. M. Fransen, and Bé Wieringa

Department of Cell Biology, Radboud Institute for Molecular Life Sciences, Radboud University Medical Centre, Nijmegen, The Netherlands

PLoS ONE 9(5): e97378 (2014)

Abstract

Functional morphodynamic behavior of differentiated macrophages is strongly controlled by actin cytoskeleton rearrangements, a process in which also metabolic cofactors ATP and NAD(H) (i.e. NAD^+ and NADH) and NADP(H) (i.e. $NADP^+$ and NADPH) play an essential role. Whereas the link to intracellular ATP availability has been studied extensively, much less is known about the relationship between actin cytoskeleton dynamics and intracellular redox state and NAD^+-supply. Here, we focus on the role of nicotinamide phosphoribosyltransferase (NAMPT), found in extracellular form as a cytokine and growth factor, and in intracellular form as one of the key enzymes for the production of NAD^+ in macrophages**.** Inhibition of NAD^+ salvage synthesis by the NAMPT-specific drug FK866 caused a decrease in cytosolic NAD^+ levels in RAW 264.7 and Maf-DKO macrophages and led to significant downregulation of the glycolytic flux without directly affecting cell viability, proliferation, ATP production capacity or mitochondrial respiratory activity. Concomitant with these differential metabolic changes, the capacity for phagocytic ingestion of particles and also substrate adhesion of macrophages were altered. Depletion of cytoplasmic NAD^+ induced cell-morphological changes and impaired early adhesion in phagocytosis of zymosan particles as well as spreading performance. Restoration of NAD^+ levels by NAD^+, NMN, or $NADP^+$ supplementation reversed the inhibitory effects of FK866. We conclude that direct coupling to local, actin-based, cytoskeletal dynamics is an important aspect of NAD^+'s cytosolic role in the regulation of morphofunctional characteristics of macrophages.

Introduction

Important elements of neutrophil and monocyte/macrophage function in innate immunity like cell adhesion, locomotion, phagocytosis and regulation of cell shape are determined by their ability to regulate actin cytoskeleton reorganization [1]. Multiple regulatory principles, established via differentiation programming, play a role in this coupling. After extravasation, monocytes migrate into target tissue areas and differentiate into macrophages. In response to environmental cues, macrophages become polarized, giving rise to different macrophage subtypes. Although other nomenclature has been suggested [2], phenotypically polarized macrophages are broadly classified as classically activated M1 and alternatively activated M2 macrophages [3,4]. *In vitro*, differentiation toward an inflammatory M1 subtype can be induced by lipopolysaccharide (LPS) stimulation, while IL-4 and IL-13 promote the alternative activation of macrophages towards a suppressive M2 subtype. In keeping with their differential roles in either the initial immune response or the resolution phase of inflammation and tissue healing, the typical morphodynamic activities, including adhesion to the extracellular matrix, or the capturing, adhesion and internalization of cells, debris, or foreign particles via phagocytosis, differ between the M1- and M2-polarized macrophages. Recent work has demonstrated that also the mode of migration, amoeboid or mesenchymal, in 2D and 3D environments differs [5]. However, as pointed out by Cougoule and co-workers [5] it is important to realize that distinction between macrophage shape and motility behavior is often based on *in vitro* studies and that *in vivo*, macrophages may occur in a continuum of phenotypes, with less explicit differences between differentiation-induction effects on morphofunctional properties. Diversity in macrophage phenotype is thus to a large extent the result of variable cues from the tissue microenvironment [6].

One of the most variable environmental cues is nutrient availability which may be dramatically reduced in diseased tissue due to local disruption of the normal blood flow. Macrophages have been shown to sense changes in nutrient availability via sirtuin-1 (SirT1)[7] and modulate the inflammatory response accordingly. Here, we study with a M1 macrophage model whether the metabolic state also has control over one archetypal process in this response, the dynamic remodeling of the actin cytoskeleton that follows induction with bacterial products (like LPS) and the stimulation of phagocytosis by foreign particles [8,9]. Multiple actin-associated proteins have a role in the spatiotemporal aspects of this remodeling. For proper regulation of actin polymerization and the activity of accessory proteins the cell requires sufficient ATP [10-12], supplied via either glycolysis or mitochondrial oxidative phosphorylation (OXPHOS) in a locally demand-controlled manner [13,14]. That tight regulation of fuel supply is also important for macrophage function is illustrated by

the observation that glucose influx through GLUT1 is enhanced when macrophages are exposed to LPS [15], or that glucose consumption via glycolysis is increased when macrophages are incubated with zymosan [16]. Unfortunately, not much more is known about the relative contributions of cytoplasmic and mitochondrial energy-redox reactions to specific morpho-physiological functioning of these cells, although macrophage activities are thought to be generally more dependent on glycolytic metabolism than on oxidative pathways [17-19]. In order to produce ATP in sufficient quantities and sustain a high flux through glycolysis, glycolytic cells such as macrophages [20] need to maintain a delicate NAD^+/NADH balance and threshold concentration of NAD(H) (i.e. oxidized and reduced form) in the cytoplasm. In order to achieve this, NAD^+ can be synthesized *de novo* from tryptophan, although most of the cellular NAD^+ in mammalian cells comes from salvage pathways using the NAD^+ precursors nicotinamide (NAM), nicotinic acid (NA), or nicotinamide riboside (NR) as starting substrates [21]. The first reaction in the conversion of NAM to NAD^+ is catalyzed by nicotinamide phosphoribosyltransferase (NAMPT) and is the rate limiting step in the pathway, yielding nicotinamide mononucleotide (NMN) as intermediate product.

NAMPT, also known as pre-B cell colony-enhancing factor (PBEF) or visfatin, is one of the more than hundred gene products that undergo conspicuous upregulation upon functional differentiation of macrophages [22, 23]. Apart from having an intracellular enzymatic function in NAD^+ salvage synthesis, NAMPT is also secreted into the extracellular environment [24-26]. Extracellular NAMPT (eNAMPT) appears not to exhibit enzymatic activity but functions as a cytokine by inducing pro-inflammatory responses in macrophages and neutrophils, a role that is unaffected by treatment with the specific inhibitor FK866 (also known as APO866) [27-29]. In contrast, inhibition of intracellular NAMPT (iNAMPT) by FK866 decreases intracellular NAD^+ and LPS-stimulated TNF levels in THP-1 cells and primary mouse and human monocytes as well as IL-1β and IL-6 levels in mouse monocytes [30-32]. These observations suggest that a global link exists between NAD^+ salvage metabolism and the inflammatory response of M1 macrophages. However, whether there is coupling to specific aspects of macrophage functioning or a role of NAD^+/NADH compartmentalization over mitochondrial and cytosolic pools therein, has not yet been determined.

We have recently, by genetic and pharmacological modulation of NAMPT-dependent NAD^+ salvage synthesis, provided evidence for a controlling role of NAD(H) (predominantly cytosolic NAD(H)) in the motile behavior of malignant glioma cells [33]. Here we extend this work by extrapolation of these findings to the metabolic control over cellular functions in macrophages. We report on a specific link between cytoplasmic NAD^+ homeostasis and aspects of adhesion, spreading and

phagocytosis in LPS-stimulated cells from the RAW 264.7 lineage and in continuously proliferating MafB/c-Maf deficient (Maf-DKO) macrophages [34]. Pharmacological inhibition of NAMPT was used as a tool to selectively and differentially modulate intracellular NAD^+ concentration.

Materials and methods

Reagents
FK866 was obtained from Enzo Life Sciences (Antwerpen, Belgium). All other reagents were obtained from Sigma-Aldrich (St. Louis, MO, USA), unless stated otherwise.

Cell culture
RAW 264.7 cells (gift from Dr. Hong-Hee Kim, Department of Cell and Developmental Biology, School of Dentistry, Seoul National University, Korea) [35] were maintained in high-glucose DMEM (Gibco, Life Technologies, Paisley, UK) supplemented with 10% heat inactivated FBS (PAA laboratories, Pasching, Austria), 1 mM sodium pyruvate, and 4 mM GlutaMAX (Gibco, Life Technologies, Paisley, UK), at 37°C in a humidified atmosphere with 7.5% CO_2. Maf-DKO cells (gift from Dr. Michael H. Sieweke, Centre d'Immunologie de Marseille-Luminy (CIML), Université Aix-Marseille, France) [34] were maintained in the same way except that medium was supplemented with 20% conditioned medium from L929-cells containing macrophage colony stimulating factor (M-CSF).

DNA constructs and transfection
pEYFP-N1-ΔATG-Lifeact was constructed as follows: Lifeact [36] cDNA, containing human codon sequences flanked by a 5' BglII and 3' EcoRI restriction site, was synthesized by GenScript Corporation and provided in a pUC57 plasmid. The Lifeact-fragment did not contain a Kozak sequence, therefore, a forward primer (5'-CT CAG ATC TCC ACC *ATG* GGC GTG GCC GAC C-3') was designed to induce a BglII site and a Kozak sequence in front of the Lifeact start codon and used together with the M13 universal reverse primer to amplify Lifeact from pUC57 by PCR. PCR products were digested with BglII and EcoRI and ligated into pEYFP-N1-ΔATG plasmid DNA (pEYFP-N1 from Clontech with ATG on position 679 mutated to GCG). For transfection, cells were seeded in 6 well plates at 300,000 cells/well and incubated overnight. DNA (12 µg; linearized with *AseI*) was diluted in 1 ml serum-free DMEM and incubated for 20 minutes at 37°C with 24 µl Targefect-RAW transfection reagent (Targeting Systems, El Cajon, CA, USA). Transfection complexes (250 µl) were added to wells containing 2 ml fresh culture medium and incubated for 4 hours at 37°C after which medium was refreshed. A stable cell population was established by culturing cells for two weeks in medium containing 500 µg/ml G418 and cloning by limited dilution.

NAMPT and NAPRT expression
NAMPT and NAPRT expression was analyzed by western blot analysis. Whole cell ly-

sates were prepared using 5x SDS-sample buffer (10% (w/v) SDS, 25% β-mercaptoethanol, 50% glycerol, 0.05% w/v bromophenolblue, and 312.5 mM Tris-Cl, pH 6.8) and stored at -20°C until analysis. Before lysates were loaded onto 12% SDS-PAGE gels, they were heated at 95°C for 5 minutes. After electrophoretic separation, proteins were blotted onto PVDF membranes. Membranes were blocked with 5% skimmed milk in PBS-T (NAMPT) or TBS-T (NAPRT) for 1 hour and labeled overnight with mouse anti-tubulin (1:5000; DSHB, University of Iowa) and either rabbit anti-NAMPT (1:2500; Bethyl Laboratories, Montgomery, TX,USA) or anti-NAPRT (1:1000; Sigma-Aldrich, St. Louis, MO, USA) antibodies at 4°C. After washing the membranes three times for 5 minutes with PBS-T or TBS-T, they were incubated with IRDye secondary antibodies (goat anti-rabbit 800 and goat anti-mouse 680) for one hour at room temperature. This was followed by 4 wash steps of 5 minutes each in PBS-T or TBS-T, a final wash step in PBS, and signal detection on the Odyssey Infrared Imaging System (LI-COR Biosciences, Lincoln, NE, USA). Cell lysate from mouse embryonic fibroblasts (MEFs) was used as positive control for detection of NAPRT.

NAD(H)/NADP(H) measurements

Intracellular NAD(H)/NADP(H) was measured according to the protocol published by Wosikowski et al. [37]. Cells (2.0×10^6) were seeded in 25 cm^2 tissue culture flasks and incubated in either control medium or medium with 10 nM FK866 for 3, 6, 15, or 24 hours prior to sample collection. Cells were detached mechanically by scraping in fresh culture medium and counted. Suspensions of 2.0×10^6 cells were spun down and cell pellets were resuspended in 2 ml 0.9% NaCl (Merck, Darmstadt, Germany), split in two and kept on ice. Both fractions were spun down and NaCl was removed. One fraction was used to measure NADH and NADPH levels, and the other fraction was used to measure NAD^+ and $NADP^+$ levels. For NAD(P)H measurement, cell pellets were resuspended in 200 µl 0.02 M NaOH (Merck, Darmstadt, Germany) containing 0.5 mM L-cysteine (Merck, Darmstadt, Germany) and incubated at 60°C for 10 minutes. The alkaline lysates were then neutralized with 60 µl 0.5 M Gly-Gly buffer, pH 7.6, and kept on ice. For $NAD(P)^+$ measurement, cells were lysed in 200 µl ice cold 0.5 M perchloric acid (PCA; Fluka) and incubated at 4°C for 15 minutes. The acidic lysates were neutralized by initially adding 80 µl 2 M KOH/0.2 M KH_2PO_4, pH 7.5, and adjusting the pH by further addition of 1-5 µl buffer until reaching neutral pH. Extracts were centrifuged at 13,000 rpm at 4°C for 3 minutes. Supernatants were snap frozen in liquid nitrogen and stored at -20°C until analysis. $NAD(P)^+$/NAD(P)H was measured spectrophotometrically in an enzymatic cycling assay. The NAD^+/NADH content of 10 µl sample was measured in 140 µl reaction mix containing 1.8 mM 3-(4,5-dimethylthiazol-2-yl)-2,5-diphenyl-tetrazolium bromide, 70 µM 1-methoxy-5-methyl-phenzzinium methyl sulfate, 64 mM nicotinamide, 0.32 M ethanol,

64 mM Gl-Gly buffer (pH 7.4), 20 mM succinate (SAFC supply solutions), and 20U alcohol dehydrogenase. The $NADP^+$/NADPH content of 10 µl sample was measured in 140 µl reaction mix containing 1.8 mM 3-(4,5-dimethylthiazol-2-yl)-2,5-diphenyl-tetrazolium bromide, 70 µM 1-methoxy-5-methyl-phenzzinium methyl sulfate, 5 mM glucose-6-phosphate, 50 mM Tris-HCl (pH 8.0; Invitrogen), 20 mM succinate, and 0.45 units glucose-6-phosphate dehydrogenase. After addition of reaction mixes, plates were incubated at 37°C for 30-60 minutes and absorbance measured at 510nm on a BioRad Benchmark Plus micro plate reader. NAD(H) and NADP(H) concentrations were calculated from an NAD^+ and $NADP^+$ standard curve, respectively. Absorbance values were corrected for blank absorbance (without NAD^+ or $NADP^+$) before concentrations were determined. All samples were corrected for the dilution factor.

NAD(P)H autofluorescence measurements

Cellular autofluorescence was determined as a measure of mitochondrial NAD(P)H-level. Cells were seeded in glass-bottom WillCo dishes and incubated with or without 5 nM FK866 for 24 hours. Using the 340 nm filter block, cells were exited for 500 ms and autofluorescence was recorded of at least 10 different fields using the Olympus IX-71 wide field fluorescence microscope (Olympus Mitico) equipped with an EM-CCD camera (Hamamatsu ImagEM). Per field analyzed, the background fluorescence as well as the fluorescence of each cell in the field was measured by determining the average grey value of two regions of interest in the background of the image and of two regions of interest in the cell body. Per cell, the autofluorescence was determined by subtracting the average background fluorescence from the average fluorescence inside the cell. Per condition, 80-110 cells were analyzed.

Glucose and lactate assays

Glucose consumption measurements were based on the Amplex Red Glucose/Glucose Oxidase assay kit from Molecular probes (Life Technologies, Eugene, Oregon, USA). Glucose, glucose oxidase, and Amplex Red reagent were used from the kit but horseradish peroxidase was obtained from Sigma-Aldrich (St. Louis, MO, USA) and 1x reaction buffer was replaced with 0.05 M Tris-HCl, pH 7.5. Apart from these minor changes, the kit protocol was followed as described by the manufacturer. Lactate production was measured using the same protocol as for glucose consumption but replacing glucose oxidase with lactate oxidase and including a lactate standard series instead of glucose. Cells were seeded in 12 well tissue culture plates and incubated for 24 hours in either 1 ml control or 1 ml 5 nM FK866 medium. For glucose measurements, medium containing 5 mM glucose was used while lactate production was measured for cells grown in 25 mM glucose medium. After 18 hours, me-

dium was refreshed in some wells for measurement of glucose consumption or lactate production during the last 6 hours of incubation. Prior to addition of incubation media, wells were always rinsed with pure DMEM containing no glucose. Medium was collected at the end of the 24 hour incubation period and supernatants were snap frozen in liquid nitrogen and stored at -20°C until analysis. Cytosolic extracts were prepared in lysis 100 buffer (50 mM Tris-HCl pH 7.5, 100 mM NaCl, 5 mM $MgCl_2$, and 0.5% NP-40; 4°C) and total protein was determined with the Bradford assay. Glucose consumption was calculated by subtracting the amount of glucose in the sample from that in medium without cells. Lactate production was calculated by subtracting the concentration of any lactate in the medium without cells from that of the samples. Glucose and lactate assays were performed in parallel.

ATP assay

Intracellular ATP was determined using the CellTiter-Glo cell viability assay kit from Promega. A total of 500,000 cells were seeded per well of a 6-well plate and treated with 5 nM FK866 for 1, 3, or 24 hours prior to assay. Cells were washed twice with ice cold PBS and then scraped in 350 µl ice cold 0.6 M perchloric acid (PCA; Fluka). PCA extracts were centrifuged for 3 minutes at 4000 rpm and 4°C to pellet all cellular protein. Supernatants were neutralized with 140-155 µl 2 M KOH/0.2 M KH_2PO_4, pH 7.5 and diluted 1:10 in water. Per well, 100 µl diluted PCA extract was added to 100 µl CellTiter-Glo reagent and the ATP concentration was determined using an ATP standard series. For determination of total cellular protein, pellets were dissolved in 250 µl 1 M NaOH and heated for 30 minutes at 95°C. Protein concentration was then measured in 1:50 diluted NaOH extracts.

Oxygen consumption measurements

Mitochondrial respiration was assessed by measuring oxygen consumption on an Oroboros Oxygraph-2k respirometer according to a standard protocol provided by the manufacturer. Control and 24 hour FK866 treated cells were analyzed in parallel in two separate chambers of the respirometer. After air calibration of control or FK866 medium in the chambers and stabilization of the signal, 1 x 10^6 cells (in 60 µl medium) were injected into the respective chambers. Basal respiration rate was measured at the point where the O_2-flux signal stabilized. Oligomycin (2.5 µM) was added to each chamber and the leak respiration rate was determined after stabilization of the signal. Next, 7 µM carbonyl cyanide-*p*-trifluoromethoxyphenylhydrazone (FCCP, a mitochondrial uncoupler) was added to reach maximal oxygen consumption in the cells. Finally, 30 nM rotenone was added and after stabilization of the system, the residual oxygen consumption could be determined. The data was analyzed using the DatLab software provided with the instrument.

Proliferation assay

For cell proliferation measurement, the protocol developed by Skehan et al. [38] was used. Cells were seeded in four 96-well plates (20,000 cells/well) in 100 µl culture medium and incubated overnight. At T0, the medium of plates T6, T15, and T24 were replaced with medium containing 0, 1, 5, or 10 nM FK866 and plate T0 was fixed for sulforhodamine B (SRB) staining of protein content. After 0, 6, 15, and 24 hours of FK866 treatment, cells were washed twice with cold PBS and fixed in 10% trichloroacetic acid (TCA; J.T.Baker, Deventer, Holland) for 1 hour at 4°C. After fixation, plates were washed five times with water and stored at -20°C until all plates were collected. Cellular protein was stained with 50 µl 0.5% SRB in 1% acetic acid for 20 minutes after which wells were washed four times with 1% acetic acid. Plates were dried at 60°C for 3 hours, protein was dissolved in 150 µl 10 mM Tris-HCl (pH 10.5), and the absorbance of each well was measured at 510nm on a BioRad Benchmark Plus micro plate reader. Values were corrected for background SRB staining by subtracting the average absorbance value of wells that contained medium only, from that of wells with cells.

In order to monitor proliferation up to 72 hours, cells were seeded at a lower density (7,500/well) to avoid any confluency in the cell monolayer and incubated in medium with 10 nM FK866 for 24, 48, and 72 hours. Plates were fixed and stained as described above.

Apoptosis assay

Apoptosis of cells was measured using a biosensor (pSIVA) developed by Kim et al. [39]. Briefly, cells (20,000/well) were seeded in a BD Falcon 96-well imaging plate and incubated overnight. On the day of assay, cells were washed once with control or FK866 containing medium before adding 100 µl of fresh control or FK866 medium containing 8 ng/µl pSIVA or non-labeled control (generous gift from Dr.Ralf Langen, University of Southern California). The plate was immediately imaged for 24 hours, continuously, on a BD Pathway high-content spinning disc confocal microscope, using a 20x objective and 2x2 montage capture. Three wells were imaged per condition and the amount of apoptosis was determined by analyzing the increase in GFP-signal. For each well the threshold of the whole GFP-image series was adjusted and the total pixel area/frame was determined using Fiji imaging software and plotted against time.

Spreading assay

RAW 264.7 cells expressing Lifeact-EYFP were pre-incubated in control or 5 nM FK866 medium for 0, 3, 15, or 24 hours before they were harvested by treatment with 1 mM EDTA/PBS (10 min at 37°C). After washing, the cells were suspended

in medium with 1% BSA. A recovery period of 20 minutes at 37°C was allowed before cells were seeded in a fibronectin coated (50 µg/ml for 2h at 37°C) BD Falcon 96-well imaging plate at 4000 cells/well. Cell spreading was monitored for three hours by recording the increase in EYFP-pixel area per cell (20 cells/well) on a BD Pathway high-content spinning disc confocal microscope, using a 20x objective and 3x3 montage capture. In order to combine the data from three independent experiments (performed in duplicate), the time axes had to be synchronized. To achieve this, a Boltzmann simulation curve was produced for each data set between time points 0 and 200 in steps of 2 minutes using OriginLab data analysis and graphing software (OriginPro 6.1). Data sets were then combined and analysed for statistical significance by applying a repeated measures analysis using PASW statistics 18 SPSS software. Three time frames (consisting of 30 data points each) of each FK866 curve were compared with the corresponding three time frames of the control curve.

Scanning electron microscopy
Cells were seeded on 12 mm glass coverslips in 24-well plates and treated with 10 nM FK866 for 3, 6, 15, or 24 hours. In addition, cells were activated with 100 ng/ml LPS or left non-activated. Cells were washed once with PBS and fixed with 2% glutarealdehyde in 0.1 M sodium cacodylate buffer for 1 hour. After washing cells twice with cacodylate buffer, coverslips were stored in the same buffer at 4°C until further fixation with 1% OsO_4 (osmium tetroxide) for 30 minutes. Coverslips were then washed once with water and dehydrated in a graded series of alcohol washes. Finally, coverslips were critical point dried and mounted for scanning electron microscopy (JEOL SEM6340F Field Emission Scanning Electron microscope).

Cellular actin staining
Cells on coverslips were incubated in control or FK866 medium for 24 hours and stimulated with 100 ng/ml LPS overnight or left unstimulated. Cells were washed twice with PBS and fixed in 2% paraformaldehyde in 0.2 M sodium phosphate buffer for 30 minutes. Coverslips were washed twice with PBS and twice with PBS containing 20 mM glycine (MP Biomedicals, Illkirch Cedex, France; PBS-G) before permeabilization with 0.1% saponine/PBS-G for 20 minutes. This was followed by actin staining with Alexa 568-labeled phalloidin (1:600 in 0.1% saponine/PBS-G) for 1 hour. Cells were successively washed four times for 2-4 minutes with 0.1% saponine/PBS-G and once with PBS alone. Coverslips were removed from wells, rinsed once in water, air dried, and embedded in MoWiol on microscope slides. Z-scans consisting of 25 x 0.5 µm sections with the pinhole adjusted to 1 airy unit were recorded on a Zeiss LSM510 META confocal laser scanning microscope and merged to one single image using Fiji imaging software.

Phagocytosis assay

Phagocytic activity was determined as zymosan ingestion capacity essentially as described by Kuiper et al. [13]. Zymosan particles were dissolved in PBS at 10 mg/ml and left to rehydrate for at least one hour. Next, zymosan was sonicated three times for 5 seconds, spun down, resuspended in carbonate buffer (pH 9.6), sonicated, and incubated with 1 µg/ml fluorescein isothiocyanate (FITC) for 1 hour at room temperature, in the dark. After FITC labeling, zymosan was washed three times with carbonate buffer and incubated in 1 M Tris-HCl, pH 8.0, for 30 minutes. Zymosan was then washed twice with PBS and finally resuspended in PBS. After one more sonication step, FITC-labeled zymosan was divided in aliquots, frozen in liquid nitrogen, and stored at -20°C.

Phagocytosis assays were performed in 12-well plates in which 100,000 cells were seeded per well the day before. Cells were incubated in control or FK866 containing medium for 3, 15, or 24 hours prior to assay and activated overnight with 100 ng/ml LPS. FITC-labeled zymosan particles were complement opsonized by incubation in FBS for 1 hour at 37°C, washed twice with PBS, and finally resuspended in serum-free control or FK866 medium. Cells were washed once with serum-free medium and incubated with 1 ml zymosan suspension for 30 minutes at 37°C. The particle-to-cell ratio was approximately 10:1. Particle engulfment was terminated by washing cells twice with PBS and removing extracellular zymosan by treatment with 500 µl 100 U/ml lyticase for 10 minutes at room temperature. Successively, cells were detached with 0.05% trypsin/0.5 mM EDTA (Gibco, Life Technologies, Paisley, UK), resuspended in 1 ml medium with serum, pelleted, and finally resuspended in 200 µl 1% paraformaldehyde in PBS. Samples were analyzed by FACS and phagocytosis efficiency was determined by measuring the fluorescence intensity of the FITC positive population as well as the percentage of cells in that population. The phagocytic index of each sample was calculated as the product of the mean FITC intensity of the positive population times the % of FITC positive cells.

To determine the effect of nucleotide supplementation on the phagocytosis efficiency of control and FK866-treated cells, RAW 264.7 cells were incubated for 24 hours with 100 µM NAD^+, 100 µM NMN or 50 µM $NADP^+$ alone or in combination with 5 nM FK866 and phagocytosis efficiency was determined as described above.

Adhesion and Internalization assay

Internalization efficiency was determined essentially as described by Sahlin et al. [40]. Cells and zymosan particles were prepared as for the phagocytosis assay. After 30 minute incubation with serum opsonized zymosan at 37°C, plates were transferred to ice and wells were washed twice with ice cold PBS. Cells were then scraped in 1 ml cold medium, divided in two fractions, transferred to microcentrifuge tubes, and

spun down. One fraction of each sample was resuspended in 0.05 % trypan blue in 13 mM potassium dihydrogen citrate/saline, pH4.4, to quench the fluorescence of all extracellular particles, and the other fraction in the same buffer but without trypan blue. Samples were analyzed by FACS.

Statistical analysis

Data was analyzed either with the Student's t-test or one-sample t-test for normalized values. All values are expressed as mean +/-SEM. Values were considered to be significantly different when p values were < 0.05.

Results

FK866 inhibits cellular NAD⁺ synthesis

NAMPT mRNA levels in leukocytes are significantly higher than average levels in various mammalian tissues as determined by quantitative real time PCR [24]. However, within the lineage differences exist between leukocyte subtypes in that monocytes and granulocytes express higher NAMPT mRNA and protein levels than lymphocytes. To test if possible variations in mode or capacity of NAD^+ synthesis could also exist among different macrophage lines, we first determined the relative expression levels of NAMPT and NAPRT, essential enzymes for NAD^+ synthesis from nicotinamide or nicotinic acid, respectively, in RAW 264.7 macrophages and in *MafB/c-Maf* deficient (Maf-DKO) macrophages [34]. Despite differences in cell origin [34, 41, 42] and proliferative doubling between these macrophage subtypes (Supplementary Figure S1A), only NAMPT appeared to be expressed at comparable and detectable level (Figure 1A) in both, suggesting that their capacity for NAD^+ synthesis is similar and primarily determined by the NAMPT reaction step only. Therefore, we considered modulation of NAD^+ levels by inhibition of NAMPT activity with FK866 a suitable strategy for our further studies into metabolic-morphodynamic relationships in macrophages.

Since NAD^+ can be converted into other pyridine nucleotides, we compared not only cellular NAD^+ levels but also determined NADH, $NADP^+$, and NADPH levels in the presence and absence of FK866. Strikingly, although most mammalian cells contain at least 5-10 fold more total NAD(H) than NADP(H) [33, 43-45], RAW264.7 macrophages and Maf-DKO macrophages appeared relatively rich in NADP(H). In RAW 264.7 cells NAD(H) and NADP(H) levels were about equal (Figure 1B,C,E,F) and in Maf-DKO cells NADP(H) levels were at least one third of that of NAD(H) (Figure 1H,I,K,L). Prolonged FK866 treatment affected NAD(H) and NADP(H) differentially, in a time dependent manner. Within 3 hours, total NAD^+ levels in RAW 254.7 cells were already reduced by approximately 60% ($p < 0.05$; Figure 1B) while NADH, $NADP^+$ and NADPH levels remained within the range of the control (Figure 1C,E,F). After 6 hours of FK866 treatment the levels of NAD^+, NADH, and NADPH were significantly decreased. While NAD^+ and NADH fell back to levels that were barely detectable, the cellular NADPH concentration remained at 30- 40% and did not decline further with prolonged treatment. FK866-mediated NAD(H)-depletion occurred slower in Maf-DKO cells. After 3 hours NAD^+ levels were not significantly affected and although there was a marked reduction, NAD^+ was still not fully depleted after 6 hours (Figure 1H). A slower proliferation rate of Maf-DKO cells (Supplementary Figure S1A), and/or effects of other metabolic differences, may explain the delayed effect of FK866 inhibition in these cells. Nevertheless, upon near complete

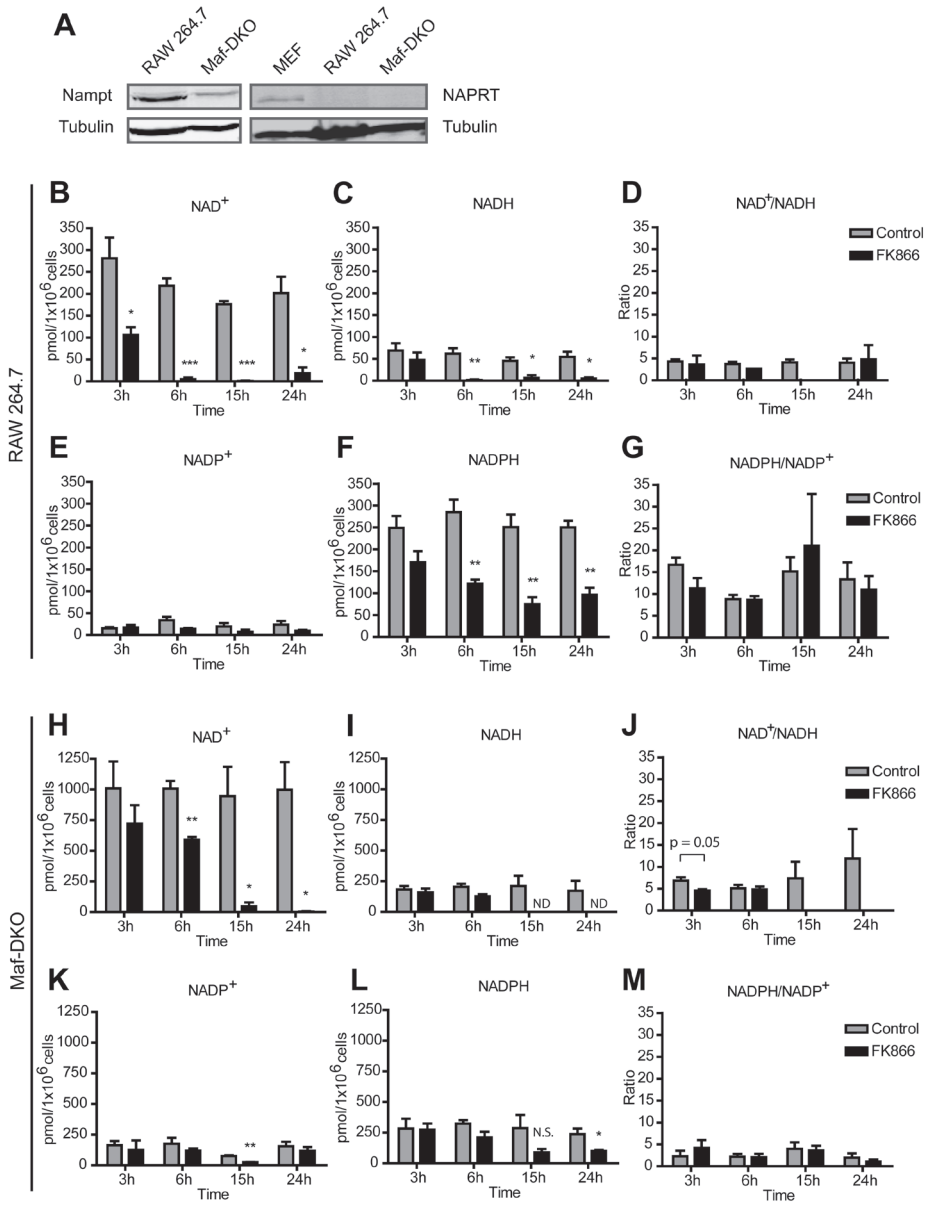

Figure 1. FK866 treatment causes a time dependent decrease in cellular NAD⁺/NADH and NADP⁺/NADPH content. ***A****, Western blot analysis of NAMPT and NAPRT expression in RAW 264.7 and Maf-DKO macrophages.Lysate from mouse embryonic fibroblasts (MEF) was used as positive control for NAPRT expression. Note that relative high amounts of lysate were used (intense tubulin control signal) for detection of NAPRT.* ***B,C,E,F****, Pyridine nucleotide levels in RAW 264.7 cells incubated for the indicated time periods with or without 10 nM FK866.* ***H,I,K,L****, Pyridine nucleotide levels in Maf-DKO cells incubated for the indicated time periods with or without 5 nM FK866. D,G,J,M, NAD⁺/NADH and NADPH/NADP⁺ ratios were calculated from the data in A&B, E&F, H&I, and K&L. Data in B-M represent means of three experiments performed in triplicate. ND, not detected. (N.S., not significant, *p < 0.05, **p < 0.01, ***p < 0.001, unpaired t-test)*

depletion of cellular NAD(H), after 6 hours for RAW 264.7 and 15 hours for Maf-DKO cells, also NADP(H) levels were profoundly affected. A significant number of cellular reactions depend on the NAD^+/NADH or $NADP^+$/NADPH redox potential, rather than on the absolute concentration of the oxidized and reduced forms of these pyridine nucleotides. We noticed that the NADPH/$NADP^+$ ratio fluctuated somewhat (within a two-fold ratio change; Figure 1G,M) during the monitoring period, both with and without the FK866 inhibitor, while this seemed less apparent for the NAD^+/NADH ratio (Figure 1D,J). However, at some time points (15h and 24h) in incubations with inhibitor the NAD^+ and NADH levels became simply too low to accurately calculate a ratio. Whether the fluctuations observed are an experimental artifact or a feature that is associated with oscillations in cellular redox state, as has been described for yeast cells [46], remains to be determined.

FK866 inhibition of NAMPT reduces glycolytic flux but not intracellular ATP

Since the NAD(P)(H) profiles of the two macrophage cell lines were highly similar and FK866 affected the NAD(P)(H) levels to the same extent, we chose to continue our study with main focus on the RAW 264.7 cell line and made comparisons with the Maf-DKO cell line where appropriate. In order to determine the metabolic effect of NAD^+-depletion we assessed glycolytic activity and ATP production. Other studies already demonstrated that macrophages depend strongly on glycolysis for cellular ATP production [20, 47]. Instead of complete oxidation via the mitochondrial route through the TCA cycle and oxidative phosphorylation (OXPHOS), 80% of the glucose molecules that are imported, are ultimately converted into lactate [19]. For the RAW 264.7 lineage we confirmed this picture and found that ~75% of all glucose used is converted into lactate, yielding approximately 1.5 moles of lactate per mole glucose (ratio of control bars, Figure 2A,B). In glycolysis, NAD^+ is converted into NADH by glyceraldehyde-3-phosphate-dehydrogenase (GAPDH), producing 1,3-biphosphoglycerate from glyceraldehyde-3-phosphate. In concert therewith, the end reaction of glycolysis (pyruvate-to-lactic acid conversion by lactate dehydrogenase; LDH), helps to restore the cytoplasmic NAD^+/NADH balance. Therefore, in view of the crucial role of NAD^+ availability in maintenance of glycolytic flux, and on the basis of our data shown in Figure 1B, we expected a strong effect of FK866 on glycolytic activity. Metabolic comparison between RAW 264.7 cells cultured in presence and absence of FK866 confirmed this prediction, showing a reduction of 65% and 50% in the amount of glucose consumed and lactate produced, respectively (Figure 2A,B). Simultaneously, the efficacy of lactate formation increased to 1.8 moles of lactate produced per mole of glucose consumed.

In spite of the significant changes in glycolytic activity, we did not observe a significant effect on cellular ATP production capacity. Intracellular [ATP] measured

at time points 3, 15, and 24h after FK866 addition remained in range of the control (around 0.3 µM/µg protein after 3 hours and 0.2 µM/µg protein after 15 and 24 hours; Figure 2C), whereas NAD^+ levels were already significantly reduced at these time points (Figure 1B). The 30-40% drop in ATP level that occurred in RAW 264.7 cells after 15 and 24 hours was observed repeatedly and can be best explained as a direct result of medium depletion.

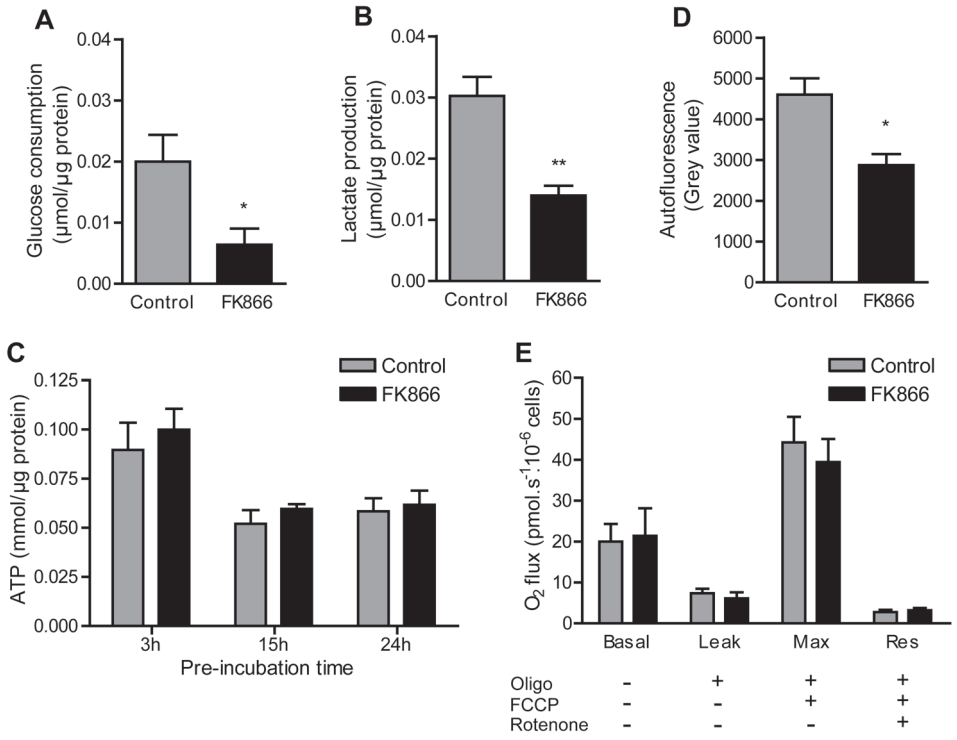

Figure 2. The effect of FK866 on RAW 264.7 metabolism. ***A,B****, Glucose consumption and lactate production in the presence and absence of FK866. Cells were incubated in control or FK866 medium for a total of 24 hours. Glucose and lactate was measured in medium supernatants collected over the last 6 hours (18-24h) of incubation. C, Intracellular ATP levels of RAW 264.7 macrophages treated with 5 nM FK866 for 3, 15, or 24 hours. D, Mitochondrial NAD(P)H-level. Cellular autofluorescence was measured after 24 hour incubation in control medium or medium with 5 nM FK866. E, After 24 hour pre-incubation with or without FK866, oxygen consumption was measured in suspensions of 1 x 10^6 cells in either FK866 or control medium. Control and FK866 treated cells were analyzed in parallel on the same day. The basal oxygen consumption was measured where after oligomycin, FCCP, and rotenone was added successively in order to determine the leak respiration, maximal respiration (Max), and residual oxygen consumption (Res). Data in A-C represent means ± SEM of three experiments performed in triplicate, in D means ± SEM of three experiments, and in E means ± SEM of five experiments. (*p < 0.05, **p < 0.01; unpaired t-test)*

Inhibition of NAMPT-mediated NAD^+ synthesis does not affect mitochondrial respiration

A large fraction of the cell's content of reduced pyridine nucleotides is compartmentalized in the mitochondria. Cellular NAD(P)H autofluorescence is therefore considered a reliable measure for assessing the mitochondrial NAD(P)H status [48]. We utilized this parameter to determine whether FK866 mediated inhibition of NAMPT affected mitochondrial NAD(P)(H) pools of RAW 264.7 cells. Although the autofluorescence intensity of 24 hour FK866-treated cells was reduced by 38% (Figure 2D), it did not mirror the dramatic (60-90%) reduction observed in total cellular NAD(P)H after 24 hours (Figure 1C,F). One possible explanation for this apparent discrepancy may be that FK866 hardly affects mitochondrial NAD(P)(H) levels (see also Pittelli et al. [49]). However, controversy exists around the source of mitochondrial $NAD(P)^+$ [50, 51], as the level of this pool appears still to be linked - directly or indirectly - to the level of cytosolic $NAD(P)^+$. Therefore, by reducing cytosolic NAD^+, NAMPT inhibition may ultimately affect the mitochondrial pool, but with differential kinetics.

Another explanation for the roughly one-third shift in autofluorescence signal would be that adaptation in mitochondrial OXPHOS occurs, to compensate for the loss in glycolytic ATP-production. Thereby a situation would be created wherein an increased fraction of total mitochondrial NAD(H) would appear in the (invisible) oxidized form (NAD^+). In order to obtain a better view on the consequences for mitochondrial respiration capacity, we therefore measured basal oxygen consumption in RAW 264.7 cells pre-treated with 5 nM FK866 for 24 hours and also determined the leak respiration, maximal respiration, and residual oxygen consumption in the presence and absence of FK866. The leak respiration gives an indication of the amount of oxygen that is consumed without producing ATP. The maximal respiration rate is a measure for the respiration capacity, while the residual oxygen consumption after addition of rotenone is a measure for oxygen consumption by systems other than the electron transport chain, for example NADPH oxidases. Figure 2E shows the respiratory values obtained after sequential addition of mitochondrial inhibitors oligomycin, carbonyl cyanide-*p*-trifluoromethoxyphenylhydrazone (FCCP), and rotenone, after measurement of the basal respiration rate. Importantly, we found that FK866 did not affect any of these parameters and therefore left mitochondrial metabolism virtually untouched. We believe, therefore, that the decrease in autofluorescence must represent a reduction in total cellular NAD(P)H, caused by the global FK866-mediated depletion of cytosolic NAD^+.

Inhibition of NAD^+ salvage synthesis does not affect cell proliferation or viability

Next, we investigated the effects of blockade in NAD^+ salvage synthesis on cell viability and proliferation capacity. Figure 3A shows the increase in total protein

mass as a consequence of growth in RAW 264.7 cell populations, cultivated in absence or presence of different concentrations of FK866. Within the entire 24 hour period of incubation, FK866 at concentrations up to 10 nM had no - or only a very minor - effect on the rate of proliferation of RAW 264.7 macrophages. Due to their slower growth rate, proliferation of Maf-DKO cells was monitored for 72 hours and also found not to be affected at these concentrations up to 48 hours (Figure 3B). Furthermore, use of a polarity-sensitive annexin-based apoptosis biosensor (pSIVA)

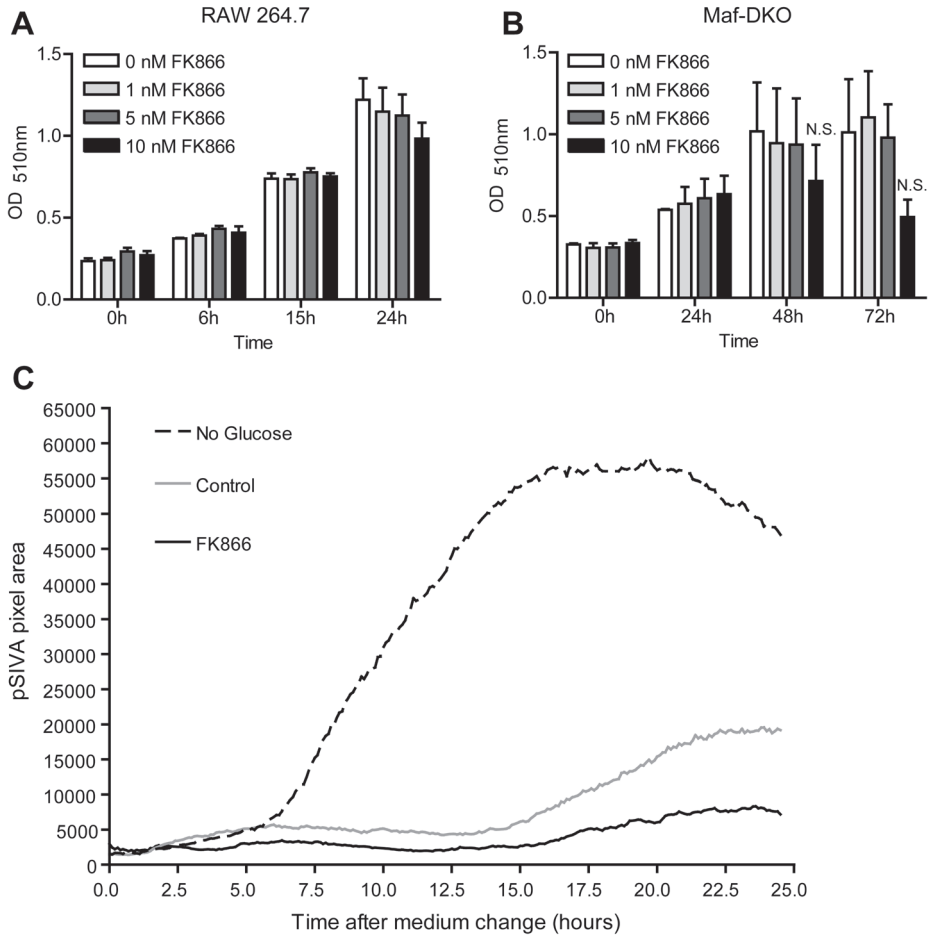

Figure 3. Inhibition of NAD⁺ salvage synthesis with FK866 does not affect proliferation or viability of macrophages. ***A,B****, RAW 264.7 and Maf-KDO proliferation in the presence of different concentrations of FK866, monitored by measuring the increase in protein mass at different intervals over a 24 or 72 hour period. Data represent means of three independent experiments performed in triplicate.* ***C****, RAW 264.7 cell viability in the presence of 10 nM FK866. The appearance of the fluorescent apoptosis-specific pSIVA signal was recorded over time and the total pSIVA pixel area was determined per frame using Fiji Imaging software and plotted against time. Lines represent averages from one experiment performed in triplicate. (N.S., not significant; unpaired t-test)*

with switchable fluorescence states [39] also did not reveal an increase in the frequency of RAW 264.7 apoptosis within the 24 hours of FK866 treatment (Figure 3C). In contrast, upon cultivation in glucose-free medium, used as a control-condition for apoptosis induction, pSIVA signal strength increased strongly, indicating that RAW 264.7 cells underwent massive apoptosis within 10 hours. Together, these observations indicate that cell viability and cell growth are not compromised within the test period and under the conditions used for inhibition of NAD^+ salvage synthesis with FK866.

LPS-stimulated spreading and formation of actin-rich membrane protrusions are inhibited in FK866 treated macrophages

The immune activity of macrophages requires the dynamic remodeling of their cortical actin cytoskeleton, active transport of membrane components, and a diverse set of receptor-ligand binding reactions at the cell surface. Together, these are processes with a large cellular energy demand [10, 11, 13]. Remodeling of the cytoskeleton and engagement in adhesion to particles, or binding to other cells or the ECM are also under control of other aspects of metabolism, including calcium and redox homeostasis [52-56]. In order to disclose possible involvement of NAD^+ in the morpho-functional behavior of macrophages we first analyzed whether NAMPT inhibition affected cell surface morphology. Scanning electron microscopy (SEM) images of resting RAW 264.7 cells after different FK866 incubation periods revealed no differences compared to control cells (not shown). Next, we analyzed the adhesive ability of cells with normal or impaired NAD^+ salvage capacity after LPS-stimulation. Interestingly, the ability to undergo spreading and the formation of LPS-induced cellular protrusions appeared affected by NAMPT inhibition. Cells treated with FK866 failed to spread upon LPS stimulation already after 15 hours (Figure 4A,B) but the effect was most prominent after 24 hours (Figure 4C,D). In order to quantify the effect of FK866 on cell spreading, we followed the adhesion and spreading of RAW 264.7 cells expressing Lifeact-EYFP in real time. The cells were stimulated with LPS overnight and pre-incubated with 5 nM FK866 for 0, 3, 15 and 24 hours after which they were seeded in 96 well plates and allowed to adhere. FK866 clearly inhibited the spreading ability of the cells in a time dependent manner (Figure 4E). Three hour pre-incubation with FK866 only had a minor affect, while spreading was significantly impaired after 15 and 24 hours of NAMPT inhibition. A notable observation was that 24 hour FK866-treated cells already covered a smaller cellular pixel area at T0. This may indicate that NAMPT inhibition affected the pliability of the cells, causing them to maintain a rounded shape after reaching the well bottom instead of undergoing ventral flattening. Alternatively, it may indicate that the formation of cellular adhesion structures has been disturbed. Using TIRF microscopy we attempted

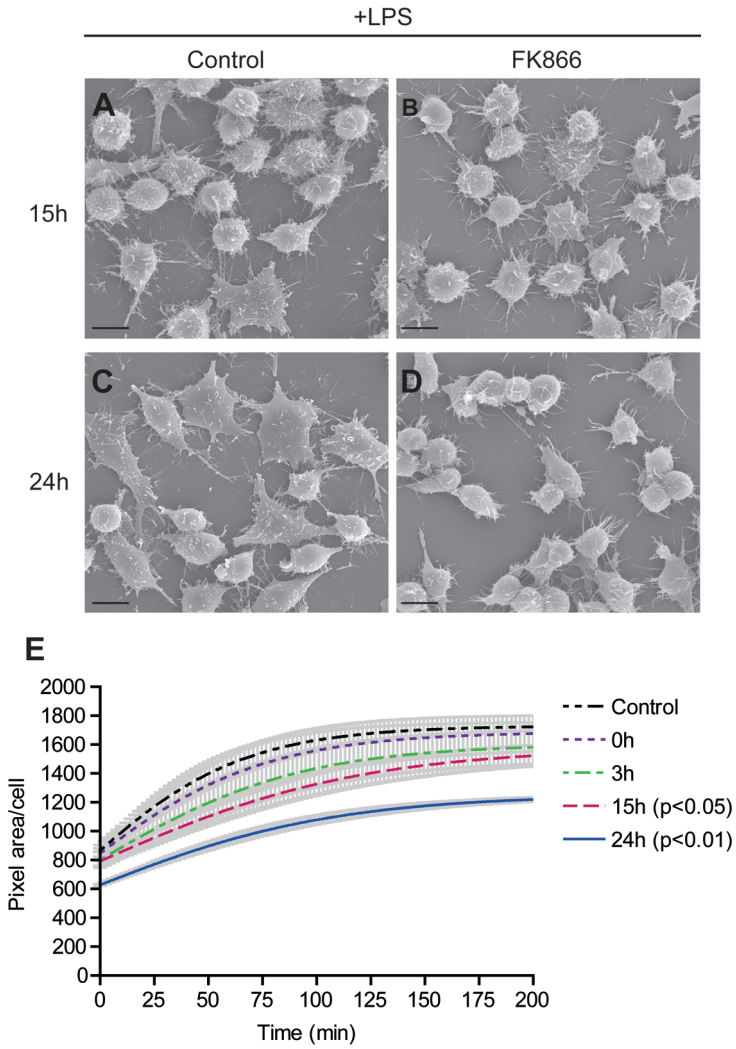

Figure 4. LPS-stimulated spreading is inhibited during NAMPT inhibition in RAW 264.7 macrophages. ***A-D****, RAW 264.7 cells were treated with 10 nM FK866 for 15 or 24 hours and simultaneously stimulated overnight with LPS. A representative image of each condition is shown, (Bar = 10 µm).* ***E****, To quantify spreading efficiency, RAW 264.7 macrophages expressing lifeact-EYFP were pre-treated with 5 nM FK866 for the indicated time periods, detached, resuspended, seeded in 96 well plates and allowed to adhere. Adherence and spreading of EYFP-positive cells were recorded over time. The average pixel area per cell was determined at every 10 minute interval. Lines represent means ± SEM (grey bars) of three experiments performed in duplicate*

to detect differences in the formation of actin-based adhesion structures between control and FK866-treated cells but, unfortunately, our results were inconclusive.

To know otherwise whether the organization of the actin cytoskeleton of the cells was affected by FK866, cells were again stimulated overnight with LPS and treated with FK866 for 3, 6, 15, and 24 hours. After this treatment they were fixed and stained with Alexa568-labelled phalloidin. No difference was observed in the actin cytoskeleton after 3 and 6 hours of FK866 treatment (not shown). However, after 15 hours and especially after 24 hours, the formation of actin-rich membrane structures was disrupted in FK866 treated cells. Control cells developed multiple cellular protrusions upon LPS stimulation with a dense and straight appearance, while this was less well visible or even absent in the FK866 treated cells (Figure 5A-D).

Phalloidin staining of Maf-DKO cells revealed that the cells themselves as well as their actin-rich surface structures have a strikingly different morphology compared to RAW 264.7 cells (Supplementary Figure S2A,E). Nevertheless, upon LPS-stimulation, Maf-DKO control cells also developed sharp membrane protrusions which were, of note, also inhibited in the presence of FK866 (Supplementary Figure S2A-H). Blocking of NAD^+ salvage synthesis therefore clearly affects LPS-induced macrophage morphology, spreading ability, and the formation of actin-rich membrane protrusions.

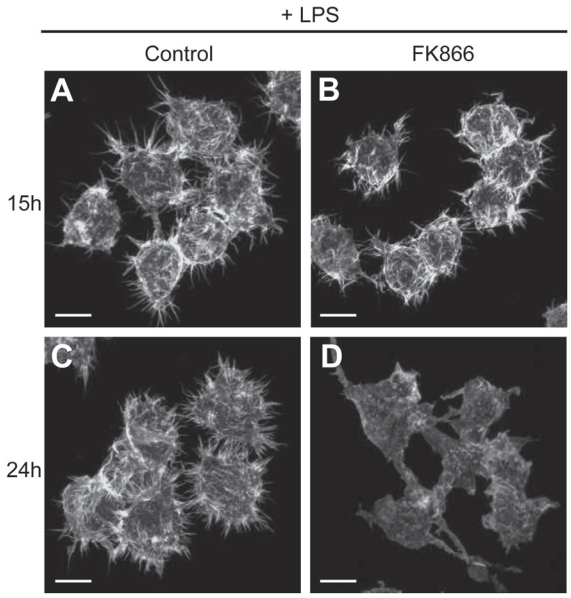

Figure 5. Actin reorganization is altered during NAMPT inhibition in RAW 264.7 macrophages. *Actin organization was assessed in wild type cells seeded on glass coverslips, treated with FK866 for 15 or 24 hours, and simultaneously stimulated overnight with 100 ng/ml LPS. After fixation in 2% PFA, cellular actin was stained with phalloidin-Alexa568 and cells were imaged on a Zeiss LSM510 META confocal laser scanning microscope. (Bar = 10 µm)*

Phagocytosis of serum opsonized zymosan is hampered when NAD^+ salvage synthesis is inhibited

Finally, we assessed NAD^+'s role in phagocytosis, the most typical immune function of macrophages which requires special morphodynamic activity. The mechanism of phagocytosis shares many similarities with that of adhesive spreading of cells [57]. Intracellular uptake of FITC-labeled, complement (serum) opsonized zymosan (COZ particles) by RAW 264.7 macrophages was impaired after 15 and 24 hour FK866 treatment (Figure 6A-C). Both the percentage of cells that engaged in phagocytosis (Figure 6A) and the mean fluorescence intensity of active cells (Figure 6B) were significantly reduced at these two time points. Of note, at 3 hours of incubation with FK866 we observed no effect, although the NAD^+ level was already significantly lowered (Figure 1B). In Maf- DKO cells, phagocytosis of COZ was assessed after 24 hour FK866 incubation and also found to be significantly inhibited (Supplementary Figure

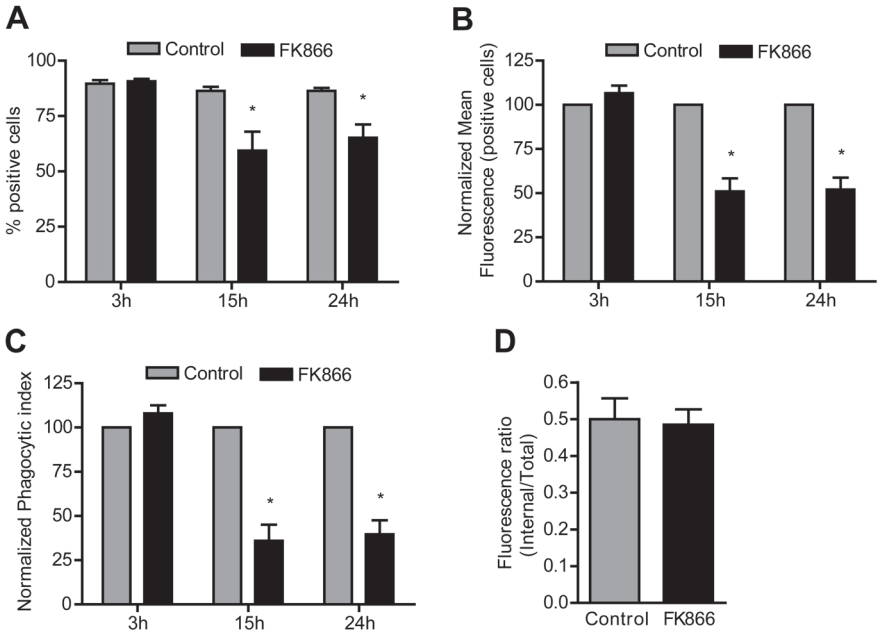

Figure 6. Phagocytosis efficiency is reduced when NAD⁺ salvage synthesis is inhibited. *Cells were pretreated with 10 nM FK866 for the indicated times and activated with LPS before they were incubated with FITC-labeled complement opsonized zymosan (COZ) particles for 30 min and analyzed by FACS. For each sample the percentage of FITC positive cells* ***(A)*** *and mean fluorescence of FITC positive cells* ***(B)*** *were measured. The phagocytic index* ***(C)*** *was calculated as the product of these two parameters. The internalization efficiency* ***(D)*** *was determined by quenching the extracellular FITC-COZ of one sample fraction with 0.05 % trypan blue in potassium dihydrogen citrate/saline, pH4.4. Unquenched fractions were used to determine the total fluorescence per cell (internalized and external particles), while quenched fractions were used to measure only the internal fluorescence per cell. Data represent means ± SEM of three assays performed in triplicate. Values were normalized to controls in b and c. (*p < 0.05; paired t-test)*

S3), indicating that both these cell lines rely on NAMPT-mediated NAD⁺ synthesis for efficient phagocytosis. In addition, supplying cells with extracellular NAD⁺, NMN, or NADP⁺ stimulated phagocytosis of COZ and prevented this inhibitory effect of FK866 (Figure 7). Although it is not exactly clear how NAD⁺ and NADP⁺ are taken up by the cell, this result further supports our idea that NAD⁺ is a principal compound in the control of phagocytosis efficiency and confirms that FK866 exerts its effect on morphofunctional activity via a reduction in concentration of this pyridine nucleotide.

As the number of actively phagocytosing cells and the number of COZ particles engulfed per cell (Figure 6A and B, respectively) do not provide information about the internalization efficiency, i.e. the fraction of bound COZ particles that is actually engulfed, we decided to perform also an internalization efficiency assay. Since the inhibitory effects of 15 and 24 hour NAMPT inhibition were comparable, we treated cells with FK866 for the entire period of 24 hours. After incubation with COZ, the

extracellular particles were not removed by lyticase, but samples were split and the fraction of internalized particles determined from the signal ratio between trypan blue quenched (internal) and total unquenched fluorescence (see Materials and Methods for details). Figure 6D shows that the ability to internalize particles was not compromised in the presence of FK866. The association with the phagocytic target is a crucial early step in phagocytosis and is mediated by multiple actin-rich membrane structures (filopodia, pseudopodia, and membrane ruffles) that are displayed on the cell surface [58-60]. Macrophages use these protrusive structures to probe the environment and capture targets for phagocytosis. When combined, the findings listed in Figures 4 and 5, together with the observation that fewer cells engaged in phagocytosis (Figure 6A) and their internalization ability was not affected (Figure 6D), suggest that macrophages treated with FK866 may have lost the ability to capture COZ efficiently, perhaps by loss of the ability to form proper membrane protrusions and adherence structures. Once contact between cell and particle is established, [NAD^+] variation apparently has no effect on successful internalization.

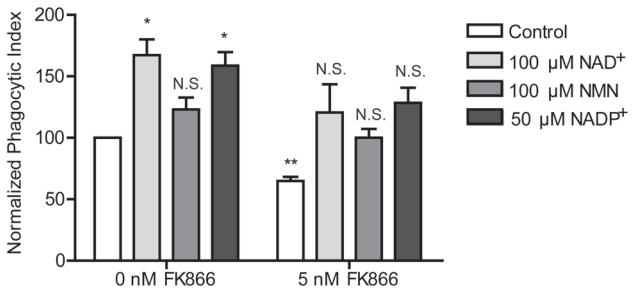

Figure 7. NAD^+, NMN, and $NADP^+$ supplementation stimulate phagocytosis and give reversal of FK866 effects. *Cells were incubated for 24 hours with 100 µM NAD^+, 100 µM NMN or 50 µM $NADP^+$ in the presence or absence of 5 nM FK866 and activated overnight with LPS before they were incubated with FITC-labeled complement opsonized zymosan (COZ) particles for 30 min and analyzed by FACS. Values were normalized to the 0 nM FK866 control. Data represent normalized means ± SEM of four (0 nM FK866) or three (5 nM FK866) experiments performed in duplicate. (N.S., not significant, *p < 0.05, **p < 0.01; paired t-test)*

Discussion

Macrophage function involves efficient migration into tissues, adhesion to the extracellular matrix, probing or sampling of their extracellular environment via filopodia, and - most importantly - phagocytosis of the pathogens and foreign particles they encounter. These processes rely on proper regulation of polymerization and depolymerization, branching and debranching of the actin cytoskeleton and on adequate cellular ATP supply, but the precise metabolic requirements and mechanisms involved are not yet fully understood. The NAD^+ biosynthetic enzyme NAMPT has been implicated in linking NAD^+ metabolism and the inflammatory cytokine response of monocytes and macrophages and to play a regulatory role in cancer cell motility [30-33]. Here we have investigated the importance of NAMPT dependent NAD^+ synthesis for the actin driven processes of adhesion and spreading and phagocytosis in macrophages. As a novel finding we report that these morphofunctional activities depended heavily on NAD^+ availability, even under metabolic conditions whereby cell growth and viability and intracellular ATP levels appeared not (yet!) affected. How these metabolic and morphodynamic activities are mechanistically controlled remains to be further investigated, but possibilities are discussed further below and graphically summarized in Figure 8.

Although the biosynthetic pathways involved in the synthesis of NAD(H) and NADP(H) are generally quite well conserved in mammalian cells, their synthetic capacity and also the intracellular levels of NAD(H) and NADP(H) may differ dramatically between cell types [21, 61]. NAD^+ can be produced via *de novo* synthesis from tryptophan or via three salvage pathways. It also serves as precursor for the other three pyridine nucleotides, NADH, $NADP^+$, and NADPH. Its reduced form, NADH, is produced in reactions catalyzed by dehydrogenases (mainly by LDH and in the TCA cycle) while $NADP^+$ is synthesized through the phosphorylation of NAD^+ by NAD kinase (NADK). $NADP^+$ is subsequently and very quickly reduced, so that cellular NADP(H) occurs mostly as NADPH [62]. In contrast, cellular NAD(H) occurs mainly in the oxidized form, i.e. NAD^+. Our measurements shown in Figure 1 confirm that this general picture also holds for RAW 264.7 and Maf-DKO macrophages. However, one striking observation was that RAW 264.7 cells contain remarkably high levels of NADP(H) and appear to maintain these levels during FK866 treatment. FK866 inhibition caused a marked reduction in NAD^+ level already after 3 hours of treatment, while NADP(H) levels were not significantly affected. At later time points, NAD^+ and NADH were totally depleted while 40% of the cellular NADPH still remained. That cellular NAD(H) is more sensitive to NAMPT inhibition by FK866 was also observed for the Maf-DKO cell line and for U251 glioma cells and activated T cells in previous studies [33, 63]. Although the mitochondrial NAD(P)(H)-pool was not

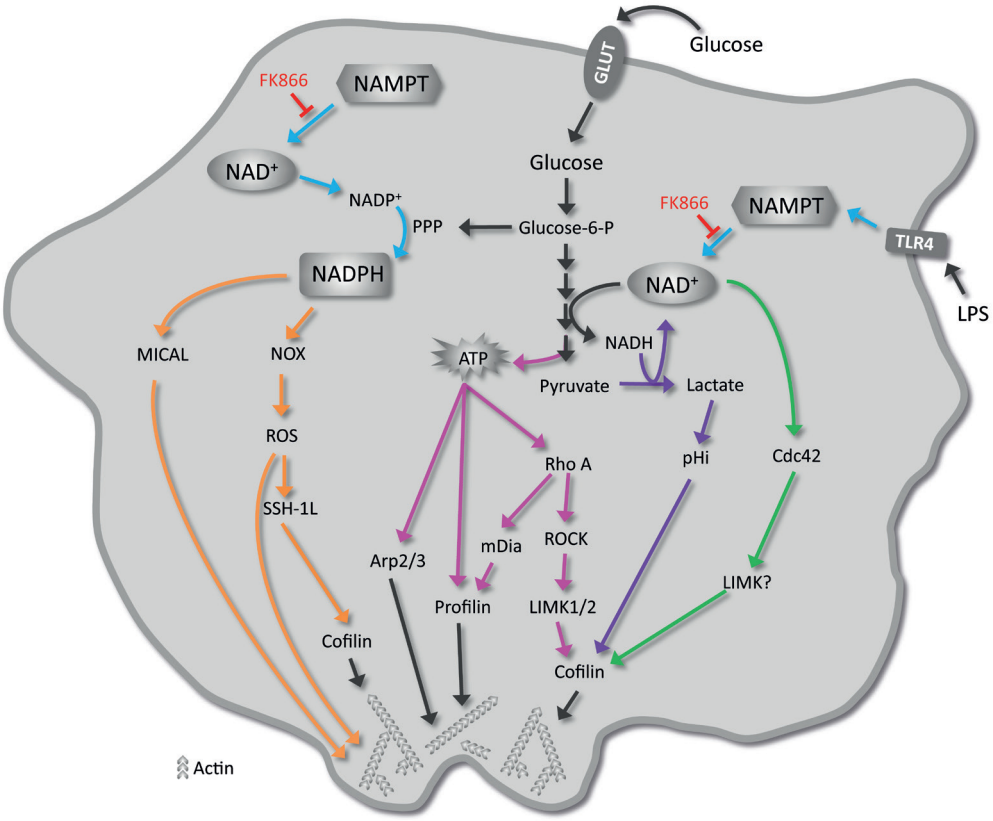

Figure 8. NAMPT-mediated salvage synthesis of NAD⁺ controls morphofunctional changes of macrophages: Synthesis of literature evidence. *NAD⁺ is required to sustain high glycolytic activity in macrophages. Metabolism of glucose yields cellular ATP which is loaded onto G-actin monomers by profilin before incorporation into an actin filament, or used to activate the Arp2/3 complex. ATP also binds to Rho GTPase Rho A, which in turn also stimulates actin polymerization (pink arrows). LPS stimulation induces the expression of the NAD⁺ synthesizing enzyme NAMPT (turquoise arrows). NAMPT-mediated NAD⁺ synthesis may regulate actin dynamics by activating Cdc42 (green arrows) or by influencing cellular metabolism and, thereby, intracellular pH and cofilin activity (purple arrows). Alternatively, NAMPT may control redox regulation of the actin cytoskeleton via mical or NADPH oxidase by regulating NADPH levels (orange arrows). GLUT, glucose transporter; NOX, NADPH oxidase; PPP, pentose phosphate pathway; ROS, reactive oxygen species; SSH-1L, slingshot-1L; TLR4, toll-like receptor 4*

left completely untouched, it was clearly less sensitive to NAMPT inhibition. More importantly, FK866-mediated

NAMPT inhibition did not noticeably affect mitochondrial respiration. Multiple divergent explanations are possible for these combined observations. Firstly, mitochondria may not be solely dependent on NAMPT activity to build up a pool of NAD⁺. Some studies show that these organelles do not even contain NAMPT themselves, although this is an issue of some controversy [49,64]. According to Nikiforov

et al. [50], NMNAT3 is the only enzyme of NAD^+ synthesis in mitochondria of human cells. This enzyme uses NMN, formed by cleavage of cytosolic NAD^+, as substrate for intramitochondrial synthesis of NAD^+. However, a more recent study by Felici et al. [51] contradicts these assertions showing that cytosolic NAD^+ maintains the mitochondrial NAD^+ pool and that neither NMNAT3v1 nor its splice variant FKSG76 is detectable in human cells. Moreover, upon of transfection of NMNAT3v1, FKSG76 was the isoform found to be localized to the mitochondria but to be involved in NAD^+ splicing rather than synthesis. What remains, is that the mitochondrial NAD(P)(H) pool in our macrophage model cells reacts differently, but appears not to be completely separated from the cytosolic pool. Therefore, the reduction in mitochondrial autofluorescence signal (Figure 2D) can be best explained as an effect of a drop in cytosolic NAD^+.

The global NAD^+ depletion after 24 hours resulted in a reduced glycolytic rate but the cells nevertheless managed to maintain cellular ATP production. How this is accomplished is currently not completely clear to us. Recently Tan et al. [65], showed that FK866 treatment of cancer cells led to an attenuation of glycolysis at the GAPDH reaction resulting in a carbon overflow into the pentose phosphate pathway, a reduced carbon flow into the TCA cycle, and eventually a reduction in cellular ATP. They also showed that the inhibitory effect on the TCA cycle was less when glutamine was not limiting in the culture medium. Since our cells were cultured in the presence of glutamine and glycolysis was clearly inhibited, glutamine consumption may have been upregulated in the presence of FK866. Upon glutaminolysis, glutamine is converted into pyruvate and, finally, lactate via the formation of TCA-cycle intermediates α-ketoglutarate, succinate, fumarate, and malate, yielding NADH and $FADH_2$ for ATP production via OXPHOS. This could also explain the minor increase in lactate formation from 1.5 to 1.8 moles of lactate per mole of glucose consumed (ratio of bars, Figure 2A,B). We did not observe any increase in basal mitochondrial OXPHOS activity (Figure 2E), however, indicating that ATP production was not significantly upregulated via this route. Thus, any increase in glutaminolysis probably only matched the reduced carbon flow from glycolysis into the TCA cycle but did not contribute to ATP homeostasis.

Can we thus rule out limited availability of ATP, due to lack of NAD^+, as the cause of morphofunctional change in FK866 treated macrophages? Earlier we showed that microcompartmentation of ATP-supply plays a role in the control of cell migratory activity of cells [66]. It remains therefore possible that FK866-mediated NAD^+ reduction is associated with a local change in ATP supply capacity, which may be not sufficient to meet the highly variable and transient demand for cytoskeletal remodeling and phagocytosis. Under these conditions global cellular ATP concentrations may not be overtly affected. Interestingly, after 3 hours of NAMPT inhibition still no inhibitory

effect was observed on either phagocytosis, spreading, or LPS induced morphology change, while global NAD^+ was already significantly reduced. In addition, the accumulated glucose consumption and lactate production over the entire 24 hour incubation period was not significantly different for control and FK866 treated cells (results not shown). The decrease in glycolytic flux only became substantial towards the end of the 24 hour treatment (Figure 2A,B). Thus, if metabolic coupling of NAD^+ concentration to local or global ATP supply is not the primary mechanism that accounts for FK866 effects on macrophage morphodynamics, what other mechanisms could be involved?

Apart from limiting the ATP supply, NAD^+-depletion may have other metabolic consequences that could (directly or indirectly) interfere with actin dependent morphodynamics. For example, the production of lactate in the last step of glycolysis, together with release of protons from the conversion of NADH to NAD^+, influences global intracellular pH (pHi). Locally, the lactate molecules, when transported out of the cell by the monocarboxylate transporter (MCT1) together with the H^+ [67, 68], form a pH gradient across the membrane, which is thought to induce cytoskeletal rearrangement via actin-binding proteins gelsolin, cofilin, and talin [69]. By inhibiting the glycolytic flux to lactate, NAD^+-depletion may thus exert direct effects on global and local pH homeostasis. In line with this, we have recently shown that both the pHi and the pericellular pH (pHe) of FK866 treated and NAMPT knockdown U251 cells were elevated compared to control cells and that the addition of lactic acid to culture media restored the inhibitory effect of FK866 on U251-shNAMPT cell migration [33]. Whether [NAD^+] changes also cause shifts in lactate dehydrogenase (LDH) activity in macrophages, and thereby affect the remodeling of the acto-myosin cytoskeleton in the micro-environment of phagocytic cup formation remains a topic for further study.

Upon stimulation with LPS, macrophages undergo dynamic morphological changes and reorganization of their actin cytoskeleton [8, 9]. LPS forms a complex with LPS binding protein (LBP) present in serum, binds to CD14, and finally to the TLR4/MD-2 complex on the macrophage cell membrane [70, 71]. LPS signaling via TLR4 induces Src family kinase mediated phosphorylation of Pyk2 and paxillin [8, 9, 72] as well as phosphorylation of the PI3K/AKT pathway [73]. These are molecules acting upstream of the small GTPases Rho, Rac and Cdc42 which regulate stress fiber, lamellipodia and membrane ruffle, and filopodia formation, respectively [74-76]. As a consequence, LPS stimulation induces cell spreading and the formation of protrusive membrane structures. In addition, LPS is responsible for the activation of the complement receptor (CR3) that is involved in the recognition of serum opsonized particles via Rap1 and RhoA [77, 78]. Together, this enhances the phagocytic capacity of macrophages. We observed here that NAD^+-depletion upon NAMPT

inhibition markedly reduced the phagocytic capacity of RAW 264.7 and Maf-DKO cells, even though they were still able to internalize particles once these were bound. Recently, NAMPT was shown to regulate directionally persistent migration of vascular smooth muscle cells (SMCs), mediated by Cdc42 activation [79]. Although Cdc42 has been implicated in IgG-mediated and not CR3-mediated phagocytosis [80], it is also involved in filopodia formation, the assembly of multimolecular focal complexes [76], and in integrin-mediated adhesion and spreading [81] by regulating actin network reorganization via LIMK2-mediated phosphorylation/inactivation of cofilin [82]. This, in combination with the knowledge that phagocytosis is an area-restricted form of cell adhesion and spreading [57], suggests that our findings can also be explained by direct NAMPT activity effects on the Cdc42-mediated probing, particle capturing, and adhesion activity of macrophages.

Finally, yet another determinant of proper actin cytoskeletal remodeling is cellular redox state [53, 54], in which NAD^+/NADH and $NADP^+$/NADPH play an important role. In macrophages, cellular NADPH may influence redox regulation of actin remodeling in several ways. Professional phagocytes express NADPH oxidases (NOX) which use NADPH to transfer an electron to molecular oxygen during the respiratory burst. This gives rise to superoxide which can further be converted into hydrogen peroxide (H_2O_2) and other reactive oxygen species (ROS), both intra- and extracellularly. Extracellularly and in the phagosomal lumen, these ROS serve a microbicidal function, thereby offering protection against pathogens. Intracellularly, the ROS is involved in redox signaling, mediating the production of cytokines via NFκβ-dependent mechanisms [83] but also regulating the activity of cofilin [84] which increases the recycling of actin monomers at the pointed end of actin filaments. At the same time, NADPH is also responsible for the regeneration of antioxidant molecules such as glutathione (GSH) and thioredoxin (Trx), thereby offering protection against oxidative stress, which may affect the redox state of actin itself [85]). NADPH may also regulate the balance between ROS-mediated activation/deactivation of signaling molecules (GTPases) that control the actin cytoskeleton [54]. Furthermore, NADPH is required for the disassembly of actin filaments by MICAL redox enzymes [86] which have been shown to regulate actin dynamics in many cell types [87-90], including macrophages [91]. Our findings suggest that NADP(H) may even be a principal pyridine nucleotide in coupling NAD^+-metabolism to actin-based morphodynamics, based on the following arguments: i) RAW 264.7 cells have a relatively high level of cellular NADPH, ii) NADP(H) levels were relatively spared during the initial phases of FK866 inhibition and - in association - morpho-functional changes became only apparent at later time points when cellular NADPH reached critical levels, i.e. after 6, 15, or 24 hours of NAMPT inhibition, and finally, iii) supplementation with $NADP^+$ quite effectively rescued phagocytosis in FK866 treated cells (Figure 7).

Studies during the last decade have identified FK866 as a promising drug against many different cancers. Currently, this compound is being tested in phase two clinical trials [92-94]. Tumor cells are more sensitive to inhibition of NAD^+ synthesis than normal cells since they are metabolically highly glycolytic and, therefore, FK866 is an effective inhibitor of tumor cell growth. Earlier we have shown in glioma cells [33], and here now also in macrophages, that morphodynamic behavior (motility, phagocytosis, spreading) is significantly inhibited at moderately effective FK866 concentrations, during treatment periods wherein proliferation and viability were not yet affected. When extrapolating these findings to the *in vivo* situation, we expect that the magnitude of effects of FK866 will be dependent on a tumor-cell's nutrient state and its capacity for NAD^+ synthesis via different metabolic pathways (i.e. via *de novo* or salvage pathways, via NAPRT or NAMPT). Treatment with FK866 may thus have broad consequences, particularly also for normal glycolytic cells in tumors such as macrophages. For example, our findings thus leave open the possibility that FK866 could affect the morphodynamics of tumor associated macrophages (TAMs), which have a promoting role in tumor cell migration [95], tumor cell proliferation and angiogenesis [96]. From a treatment perspective, this could help to further enhance FK866's anti-cancer effect. On the other hand, FK866 treatment could have adverse effects and lead to an overall repression of macrophage migratory and phagocytic function, with less clearance of apoptotic cells and debris from dying tumors. These effects – even in a more broader sense – are also a point of concern for use of FK866 as anti-inflammatory drug for the treatment of autoimmune diseases such as rheumatoid arthritis, inflammatory bowel disease, or Crohn's disease. Further study in patients and animal models *in vivo* is, therefore, necessary to fully understand all possible consequences of FK866 treatment regimes.

In summary, we report here that FK866 mediated inhibition of NAMPT causes NAD^+-depletion and down regulation of glycolysis in macrophage model cells. Inhibition of NAD^+ salvage synthesis did not affect cell viability, proliferative capacity, or ATP levels but significantly impaired morphofunctional changes involved in phagocytosis and spreading. Future research should elucidate how NAD^+ production and these processes are exactly linked.

Acknowledgements

We are grateful to Dr. Hong-Hee Kim (Department of Cell and Developmental Biology, School of Dentistry, Seoul National University, Korea) for providing the RAW 264.7 cell line, Dr.Ralf Langen (University of Southern California) for supplying the pSIVA apoptosis biosensor, Dr. Michael H. Sieweke (Centre d'Immunologie de Marseille-Luminy (CIML), Université Aix-Marseille, France) for providing the Maf-DKO cells, and Ganesh Manjeri (Department of Biochemistry, NCMLS, Radboud UMC, Nijmegen, The Netherlands) for help with the oxygen consumption assays.

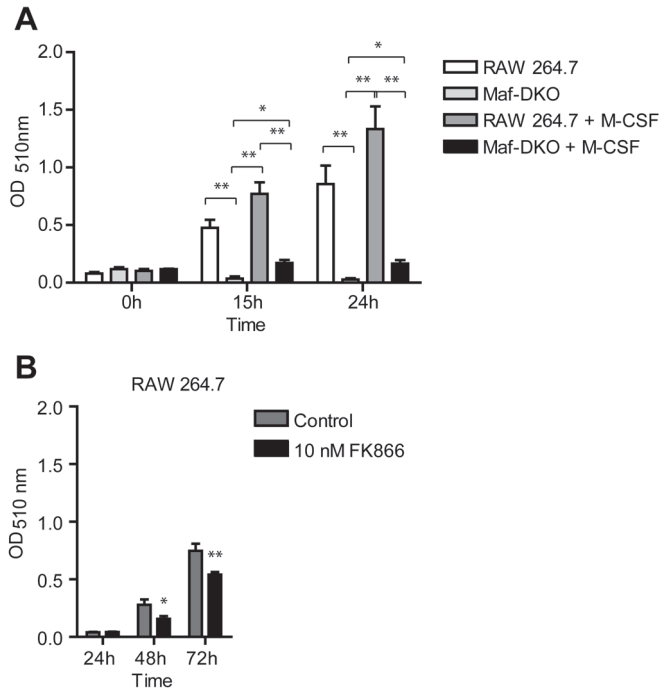

Figure S1. RAW 264.7 and Maf-DKO proliferation. ***A****, Proliferation of RAW 264.7 and Maf-DKO cells in the presence and absence of L929 cell conditioned medium (M-CSF).* ***B****, RAW 264.7 proliferation in the presence of FK866 over a period for 72 hours. Proliferation was monitored by measuring the increase in protein mass at the indicated time periods. Data represent means of three independent experiments performed in triplicate. (*p < 0.05, **p < 0.01; unpaired t-test)*

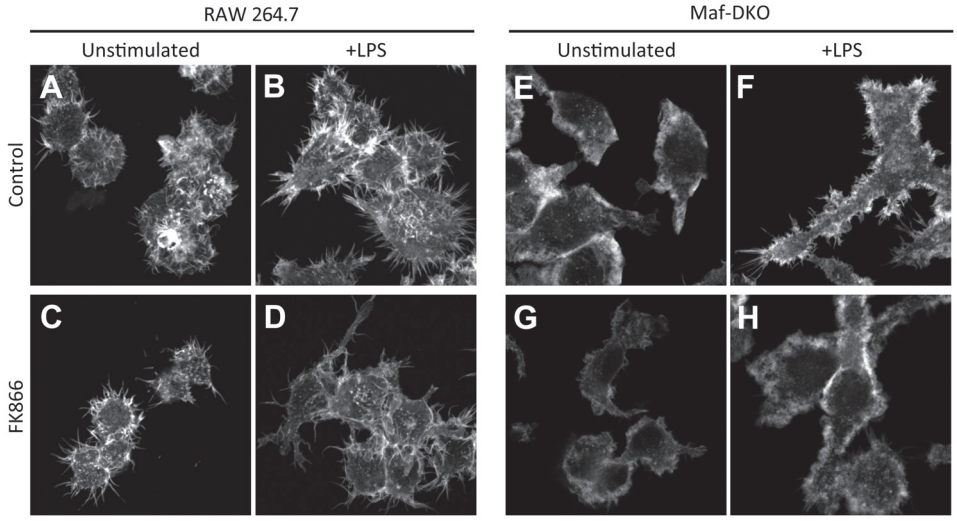

Figure S2. RAW 264.7 and Maf-DKO morphology and actin structures are affected during NAD⁺-depletion. *RAW 264.7* ***(A-D)*** *and Maf-DKO* ***(E-H)*** *macrophages were seeded on glass coverslips in RAW264.7 (without M-CSF) and Maf-DKO (with M-CSF) medium, respectively. Cells were incubated for 24h in control 5 nM FK866 medium and stimulated o/n with 100 ng/ml LPS or left unstimulated. Cells were fixed in 2% PFA, stained with phalloidin-Alexa568, and imaged on a Zeiss LSM510 META confocal laser scanning microscope*

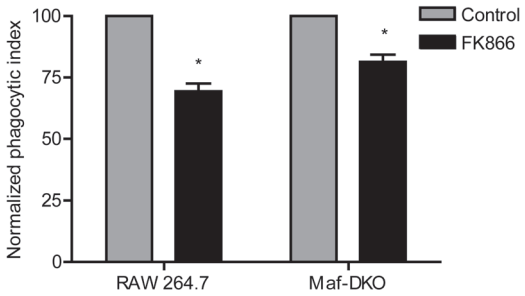

Figure S3. FK866-mediated NAD⁺-depletion reduces RAW 264.7 and Maf-DKO phagocytosis efficiency. *Cells were seeded in medium containing 20% conditioned medium from L929-cell cultures (+M-CSF) and incubated for 24 hours in the presence or absence of 5 nM FK866. Cells were additionally stimulated overnight with 100 ng/ml LPS. After 30 minutes incubation with FITC-labelled complement opsonized zymosan (COZ) particles, cells were harvested, fixed, and analyzed by FACS. The percentage of FITC positive cells were measured as well as the mean fluorescence of this population. The product of these two parameters were used to calculated the phagocytic index. Data represent normlaized means ± SEM of three experiments performed in duplicate. (*p < 0.05; paired t-test)*

References

1. Vicente-Manzanares, M. & Sanchez-Madrid, F. Role of the cytoskeleton during leukocyte responses. *Nat. Rev. Immunol.* **4**, 110-122 (2004).
2. Mosser, D.M. & Edwards, J.P. Exploring the full spectrum of macrophage activation. *Nat. Rev. Immunol.* **8**, 958 (2008).
3. Mills, C.D., Kincaid, K., Alt, J.M., Heilman, M.J. & Hill, A.M. M-1/M-2 Macrophages and the Th1/Th2 Paradigm. *J. Immunol.* **164**, 6166-6173 (2000).
4. Sica, A. & Mantovani, A. Macrophage plasticity and polarization: in vivo veritas. *J. Clin. Invest.* **122**, 787-795 (2012).
5. Cougoule, C. *et al.* Blood leukocytes and macrophages of various phenotypes have distinct abilities to form podosomes and to migrate in 3D environments. *Eur. J. Cell Biol.* **91**, 938-949 (2012).
6. Stout, R.D. & Suttles, J. Functional plasticity of macrophages: reversible adaptation to changing microenvironments. *J. Leukoc. Biol.* **76**, 509-513 (2004).
7. Kotas, M.E., Gorecki, M.C. & Gillum, M.P. Sirtuin-1 is a nutrient-dependent modulator of inflammation. *Adipocyte* **2**, 36-35 (2013).
8. Williams, L.M. & Ridley, A.J. Lipopolysaccharide Induces Actin Reorganization and Tyrosine Phosphorylation of Pyk2 and Paxillin in Monocytes and Macrophages. *J. Immunol.* **164**, 2028-2036 (2000).
9. Kleveta, G. *et al.* LPS induces phosphorylation of actin-regulatory proteins leading to actin reassembly and macrophage motility. *J. Cell. Biochem.* **113**, 80-92 (2012).
10. Atkinson, S.J., Hosford, M.A. & Molitoris, B.A. Mechanism of Actin Polymerization in Cellular ATP Depletion. *J. Biol. Chem.* **279**, 5194-5199 (2004).
11. Huang, T.Y., Minamide, L.S., Bamburg, J.R. & Bokoch, G.M. Chronophin Mediates an ATP-Sensing Mechanism for Cofilin Dephosphorylation and Neuronal Cofilin-Actin Rod Formation. *Dev. Cell* **15**, 691-703 (2008).
12. Ingerman, E., Hsiao, J.Y. & Mullins, R.D. Arp2/3 complex ATP hydrolysis promotes lamellipodial actin network disassembly but is dispensable for assembly. *J. Cell Biol.* **200**, 619-633 (2013).
13. Kuiper, J.W.P. *et al.* Creatine Kinase–Mediated ATP Supply Fuels Actin-Based Events in Phagocytosis. *PLoS Biol.* **6**, e51 (2008).
14. Kuiper, J.W.P. *et al.* Local ATP Generation by Brain-Type Creatine Kinase (CK-B) Facilitates Cell Motility. *PLoS ONE* **4**, e5030 (2009).
15. Fukuzumi, M., Shinomiya, H., Shimizu, Y., Ohishi, K. & Utsumi, S. Endotoxin-induced enhancement of glucose influx into murine peritoneal macrophages via GLUT1. *Infect. Immun.* **64**, 108-112 (1996).
16. Albina, J.E. & Mastrofrancesco, B. Modulation of glucose metabolism in macrophages by products of nitric oxide synthase. *Am. J. Physiol. Cell Physiol.* **264**, C1594-C1599 (1993).
17. Cifarelli, A., Pepe, G., Paradisi, F. & Piccolo, D. The influence of some metabolic inhibitors on phagocytic activity of mouse macrophages in vitro. *Res. Exp. Med. (Berl).* **174**, 197-204 (1979).
18. Paradisi, F., D'Onofrio, C., Pepe, G., Cifarelli, A. & Piccolo, D. Phagocytosis and cellular metabolism. *Ric. Clin. Lab.* **9**, 47-60 (1979).
19. Rodríguez-Prados, J.-C. *et al.* Substrate Fate in Activated Macrophages: A Comparison between Innate, Classic, and Alternative Activation. *J. Immunol.* **185**, 605-614 (2010).
20. Newsholme, P., Curi, R., Gordon, S. & Newsholme, E.A. Metabolism of glucose, glutamine, long-chain fatty acids and ketone bodies by murine macrophages. *Biochem. J.* **239**, 121-125 (1986).
21. Houtkooper, R.H., Canto, C., Wanders, R.J. & Auwerx, J. The Secret Life of NAD+: An Old Metabolite Controlling New Metabolic Signaling Pathways. *Endocr. Rev.* **31**, 194-223 (2010).
22. Nau, G.J. *et al.* Human macrophage activation programs induced by bacterial pathogens. *Proc. Natl. Acad. Sci. U. S. A.* **99**, 1503-1508 (2002).
23. Iqbal, J. & Zaidi, M. TNF regulates cellular NAD+ metabolism in primary macrophages. *Biochem. Biophys. Res. Commun.* **342**, 1312-1318 (2006).
24. Friebe, D. *et al.* Leucocytes are a major source of circulating nicotinamide phosphoribosyltransferase (NAMPT)/pre-B cell colony (PBEF)/visfatin linking obesity and inflammation in humans. *Diabetologia* **54**, 1200-1211 (2011).
25. Jia, S.H. *et al.* Pre–B cell colony–enhancing factor inhibits neutrophil apoptosis in experimental inflammation and clinical sepsis. *J. Clin. Invest.* **113**, 1318-1327 (2004).
26. Samal, B. *et al.* Cloning and characterization of the cDNA encoding a novel human pre-B-cell colony-enhancing factor. *Mol. Cell. Biol.* **14**, 1431-1437 (1994).
27. Li, Y. *et al.* Extracellular Nampt Promotes Macrophage Survival via a Nonenzymatic Interleukin-6/STAT3 Signaling Mechanism. *J. Biol. Chem.* **283**, 34833-34843 (2008).
28. Malam, Z. *et al.* Pre-B Cell Colony-Enhancing Factor (PBEF/Nampt/Visfatin) Primes Neutrophils for Augmented Respiratory Burst Activity through Partial Assembly of the NADPH Oxidase. *J. Immunol.* **186**, 6474-6484

(2011).
29. Hara, N., Yamada, K., Shibata, T., Osago, H. & Tsuchiya, M. Nicotinamide Phosphoribosyltransferase/Visfatin Does Not Catalyze Nicotinamide Mononucleotide Formation in Blood Plasma. *PLoS ONE* **6**, e22781 (2011).
30. Busso, N. *et al.* Pharmacological Inhibition of Nicotinamide Phosphoribosyltransferase/Visfatin Enzymatic Activity Identifies a New Inflammatory Pathway Linked to NAD. *PLoS ONE* **3**, e2267 (2008).
31. Van Gool, F. *et al.* Intracellular NAD levels regulate tumor necrosis factor protein synthesis in a sirtuin-dependent manner. *Nat. Med.* **15**, 206-210 (2009).
32. Schilling, E. *et al.* Inhibition of nicotinamide phosphoribosyltransferase modifies LPS-induced inflammatory responses of human monocytes. *Innate Immun.* **0**, 1-13 (2011).
33. van Horssen, R. *et al.* Intracellular NAD(H) levels control motility and invasion of glioma cells. *Cell. Mol. Life Sci.*, 1-16 (2013).
34. Aziz, A., Soucie, E., Sarrazin, S. & Sieweke, M.H. MafB/c-Maf Deficiency Enables Self-Renewal of Differentiated Functional Macrophages. *Science* **326**, 867-871 (2009).
35. Chang, E.-J. *et al.* Brain-type creatine kinase has a crucial role in osteoclast-mediated bone resorption. *Nat. Med.* **14**, 966-972 (2008).
36. Riedl, J. *et al.* Lifeact: a versatile marker to visualize F-actin. *Nat. Methods* **5**, 605-607 (2008).
37. Wosikowski, K. *et al.* WK175, a Novel Antitumor Agent, Decreases the Intracellular Nicotinamide Adenine Dinucleotide Concentration and Induces the Apoptotic Cascade in Human Leukemia Cells. *Cancer Res.* **62**, 1057-1062 (2002).
38. Skehan, P. *et al.* New Colorimetric Cytotoxicity Assay for Anticancer-Drug Screening. *J. Natl. Cancer Inst.* **82**, 1107-1112 (1990).
39. Kim, Y.E., Chen, J., Chan, J.R. & Langen, R. Engineering a polarity-sensitive biosensor for time-lapse imaging of apoptotic processes and degeneration. *Nat. Methods* **7**, 67-73 (2010).
40. Sahlin, S., Hed, J. & Runfquist, I. Differentiation between attached and ingested immune complexes by a fluorescence quenching cytofluorometric assay. *J. Immunol. Methods* **60**, 115-124 (1983).
41. Raschke, W.C., Baird, S., Ralph, P. & Nakoinz, I. Functional macrophage cell lines transformed by abelson leukemia virus. *Cell* **15**, 261-267 (1978).
42. Raschke, W.C., Ralph, P., Watson, J., Sklar, M. & Coon, H. Oncogenic transformation of murine lymphoid cells by in vitro infection with Abelson leukemia virus. *J. Natl. Cancer Inst.* **54**, 1249-1253 (1975).
43. Reiss, P.D., Zuurendonk, P.F. & Veech, R.L. Measurement of tissue purine, pyrimidine, and other nucleotides by radial compression high-performance liquid chromatography. *Anal. Biochem.* **140**, 162-171 (1984).
44. Pollak, N., Dölle, C. & Ziegler, M. The power to reduce: pyridine nucleotides – small molecules with a multitude of functions. *Biochem. J.* **402**, 205-218 (2007).
45. Klaidman, L.K., Leung, A.C. & Adams, J.D. High-Performance Liquid Chromatography Analysis of Oxidized and Reduced Pyridine Dinucleotides in Specific Brain Regions. *Anal. Biochem.* **228**, 312-317 (1995).
46. Tu, B.P. *et al.* Cyclic changes in metabolic state during the life of a yeast cell. *Proc. Natl. Acad. Sci. U. S. A.* **104**, 16886-16891 (2007).
47. Calder, P.C. Fuel utilization by cells of the immune system. *Proc. Nutr. Soc.* **54**, 65-82 (1995).
48. Heikal, A.A. Intracellular coenzymes as natural biomarkers for metabolic activities and mitochondrial anomalies. *Biomark. Med.* **4**, 241-263 (2010).
49. Pittelli, M. *et al.* Inhibition of Nicotinamide Phosphoribosyltransferase. *J. Biol. Chem.* **285**, 34106-34114 (2010).
50. Nikiforov, A., Dölle, C., Niere, M. & Ziegler, M. Pathways and Subcellular Compartmentation of NAD Biosynthesis in Human Cells: From entry of extracellular precursors to mitochondrial NAD generation. *J. Biol. Chem.* **286**, 21767-21778 (2011).
51. Felici, R., Lapucci, A., Ramazzotti, M. & Chiarugi, A. Insight into Molecular and Functional Properties of NMNAT3 Reveals New Hints of NAD Homeostasis within Human Mitochondria. *PLoS ONE* **8**, e76938 (2013).
52. Chiarugi, P. *et al.* Reactive oxygen species as essential mediators of cell adhesion: the oxidative inhibition of a FAK tyrosine phosphatase is required for cell adhesion. *J. Cell Biol.* **161**, 933-944 (2003).
53. Hurd, T.R., DeGennaro, M. & Lehmann, R. Redox regulation of cell migration and adhesion. *Trends Cell Biol.* **22**, 107-115 (2012).
54. Nimnual, A.S., Taylor, L.J. & Bar-Sagi, D. Redox-dependent downregulation of Rho by Rac. *Nat. Cell Biol.* **5**, 236-241 (2003).
55. Tharmalingam, S. *et al.* Calcium-sensing Receptor Modulates Cell Adhesion and Migration via Integrins. *J. Biol. Chem.* **286**, 40922-40933 (2011).
56. Janmey, P.A. Phosphoinositides and Calcium as Regulators of Cellular Actin Assembly and Disassembly. *Annu. Rev. Physiol.* **56**, 169-191 (1994).
57. Cougoule, C., Wiedemann, A., Lim, J. & Caron, E. Phagocytosis, an alternative model system for the study of cell adhesion. *Semin. Cell Dev. Biol.* **15**, 679-689 (2004).
58. Kress, H. *et al.* Filopodia act as phagocytic tentacles and pull with discrete steps and a load-dependent veloc-

ity. *Proc. Natl. Acad. Sci. U. S. A.* **104**, 11633-11638 (2007).
59. Patel, P.C. & Harrison, R.E. Membrane Ruffles Capture C3bi-opsonized Particles in Activated Macrophages. *Mol. Biol. Cell* **19**, 4628-4639 (2008).
60. Flannagan, R.S., Harrison, R.E., Yip, C.M., Jaqaman, K. & Grinstein, S. Dynamic macrophage "probing" is required for the efficient capture of phagocytic targets. *J. Cell Biol.* **191**, 1205-1218 (2010).
61. Braidy, N. *et al.* Age Related Changes in NAD+ Metabolism Oxidative Stress and Sirt1 Activity in Wistar Rats. *PLoS ONE* **6**, e19194 (2011).
62. Pollak, N., Niere, M. & Ziegler, M. NAD Kinase Levels Control the NADPH Concentration in Human Cells. *J. Biol. Chem.* **282**, 33562-33571 (2007).
63. Bruzzone, S. *et al.* Catastrophic NAD^+ Depletion in Activated T Lymphocytes through Nampt Inhibition Reduces Demyelination and Disability in EAE. *PLoS ONE* **4**, e7897 (2009).
64. Yang, H. *et al.* Nutrient-Sensitive Mitochondrial NAD+ Levels Dictate Cell Survival. *Cell* **130**, 1095-1107 (2007).
65. Tan, B. *et al.* Pharmacological Inhibition of Nicotinamide Phosphoribosyltransferase (NAMPT), an Enzyme Essential for NAD+ Biosynthesis, in Human Cancer Cells: Metabolic basis and potential clinical implications. *J. Biol. Chem.* **288**, 3500-3511 (2013).
66. van Horssen, R. *et al.* Modulation of Cell Motility by Spatial Repositioning of Enzymatic ATP/ADP Exchange Capacity. *J. Biol. Chem.* **284**, 1620-1627 (2009).
67. Poole, R.C. & Halestrap, A.P. Transport of lactate and other monocarboxylates across mammalian plasma membranes. *Am. J. Physiol. Cell Physiol.* **264**, C761-C782 (1993).
68. Hahn, E.L., Halestrap, A.P. & Gamelli, R.L. Expression of the lactate transporter MCT1 in macrophages. *Shock* **13**, 253-260 (2000).
69. Stock, C. & Schwab, A. Protons make tumor cells move like clockwork. *Pfluegers Arch./Eur. J. Physiol.* **458**, 981-992-992 (2009).
70. Beutler, B. Tlr4: central component of the sole mammalian LPS sensor. *Curr. Opin. Immunol.* **12**, 20-26 (2000).
71. Guha, M. & Mackman, N. LPS induction of gene expression in human monocytes. *Cell. Signal.* **13**, 85-94 (2001).
72. Hazeki, K. *et al.* Toll-like receptor-mediated tyrosine phosphorylation of paxillin via MyD88-dependent and -independent pathways. *Eur. J. Immunol.* **33**, 740-747 (2003).
73. Weintz, G. *et al.* The phosphoproteome of toll-like receptor-activated macrophages. *Mol. Syst. Biol.* **6**, 371 (2010).
74. Ridley, A.J. & Hall, A. The small GTP-binding protein rho regulates the assembly of focal adhesions and actin stress fibers in response to growth factors. *Cell* **70**, 389-399 (1992).
75. Ridley, A.J., Paterson, H.F., Johnston, C.L., Diekmann, D. & Hall, A. The small GTP-binding protein rac regulates growth factor-induced membrane ruffling. *Cell* **70**, 401-410 (1992).
76. Nobes, C.D. & Hall, A. Rho, Rac, and Cdc42 GTPases regulate the assembly of multimolecular focal complexes associated with actin stress fibers, lamellipodia, and filopodia. *Cell* **81**, 53-62 (1995).
77. Caron, E., Self, A.J. & Hall, A. The GTPase Rap1 controls functional activation of macrophage integrin αMβ2 by LPS and other inflammatory mediators. *Curr. Biol.* **10**, 974-978 (2000).
78. Kim, J.-G. *et al.* Ras-related GTPases Rap1 and RhoA Collectively Induce the Phagocytosis of Serum-opsonized Zymosan Particles in Macrophages. *J. Biol. Chem.* **287**, 5145-5155 (2012).
79. Yin, H. *et al.* Intrinsic directionality of migrating vascular smooth muscle cells is regulated by NAD^+ biosynthesis. *J. Cell Sci.* **125**, 5770-5780 (2012).
80. Caron, E. & Hall, A. Identification of Two Distinct Mechanisms of Phagocytosis Controlled by Different Rho GTPases. *Science* **282**, 1717-1721 (1998).
81. Price, L.S., Leng, J., Schwartz, M.A. & Bokoch, G.M. Activation of Rac and Cdc42 by Integrins Mediates Cell Spreading. *Mol. Biol. Cell* **9**, 1863-1871 (1998).
82. Sumi, T., Matsumoto, K., Takai, Y. & Nakamura, T. Cofilin Phosphorylation and Actin Cytoskeletal Dynamics Regulated by Rho- and Cdc42-Activated Lim-Kinase 2. *J. Cell Biol.* **147**, 1519-1532 (1999).
83. Forman, H.J. & Torres, M. Reactive Oxygen Species and Cell Signaling: Respiratory Burst in Macrophage Signaling. *Am. J. Respir. Crit. Care Med.* **166**, S4-8 (2002).
84. Kim, J.-S., Huang, T.Y. & Bokoch, G.M. Reactive Oxygen Species Regulate a Slingshot-Cofilin Activation Pathway. *Mol. Biol. Cell* **20**, 2650-2660 (2009).
85. Dalle-Donne, I., Rossi, R., Milzani, A., Di Simplicio, P. & Colombo, R. The actin cytoskeleton response to oxidants: from small heat shock protein phosphorylation to changes in the redox state of actin itself. *Free Radic. Biol. Med.* **31**, 1624-1632 (2001).
86. Hung, R.-J., Pak, C.W. & Terman, J.R. Direct Redox Regulation of F-Actin Assembly and Disassembly by Mical. *Science* **334**, 1710-1713 (2011).
87. Hung, R.J. *et al.* Mical links semaphorins to F-actin disassembly. *Nature* **463**, 823-827 (2010).
88. Beuchle, D., Schwarz, H., Langegger, M., Koch, I. & Aberle, H. Drosophila MICAL regulates myofilament organization and synaptic structure. *Mech. Dev.* **124**, 390-406 (2007).

89. Giridharan, S.S., Rohn, J.L., Naslavsky, N. & Caplan, S. Differential regulation of actin microfilaments by human MICAL proteins. *J. Cell Sci.* **125**, 614-624 (2012).
90. Morinaka, A. *et al.* Thioredoxin mediates oxidation-dependent phosphorylation of CRMP2 and growth cone collapse. *Sci. Signal.* **4**, ra26 (2011).
91. Lee, Byung C. *et al.* MsrB1 and MICALs Regulate Actin Assembly and Macrophage Function via Reversible Stereoselective Methionine Oxidation. *Mol. Cell* **51**, 397-404 (2013).
92. Hasmann, M. & Schemainda, I. FK866, a Highly Specific Noncompetitive Inhibitor of Nicotinamide Phosphoribosyltransferase, Represents a Novel Mechanism for Induction of Tumor Cell Apoptosis. *Cancer Res.* **63**, 7436-7442 (2003).
93. Holen, K., Saltz, L., Hollywood, E., Burk, K. & Hanauske, A.-R. The pharmacokinetics, toxicities, and biologic effects of FK866, a nicotinamide adenine dinucleotide biosynthesis inhibitor. *Invest. New Drugs* **26**, 45-51 (2008).
94. Olesen, U.H., Thougaard, A.V., Jensen, P.B. & Sehested, M. A Preclinical Study on the Rescue of Normal Tissue by Nicotinic Acid in High-Dose Treatment with APO866, a Specific Nicotinamide Phosphoribosyltransferase Inhibitor. *Mol. Cancer Ther.* **9**, 1609-1617 (2010).
95. Guiet, R. *et al.* The Process of Macrophage Migration Promotes Matrix Metalloproteinase-Independent Invasion by Tumor Cells. *J. Immunol.* **187**, 3806-3814 (2011).
96. Solinas, G., Germano, G., Mantovani, A. & Allavena, P. Tumor-associated macrophages (TAM) as major players of the cancer-related inflammation. *J. Leukoc. Biol.* **86**, 1065-1073 (2009).

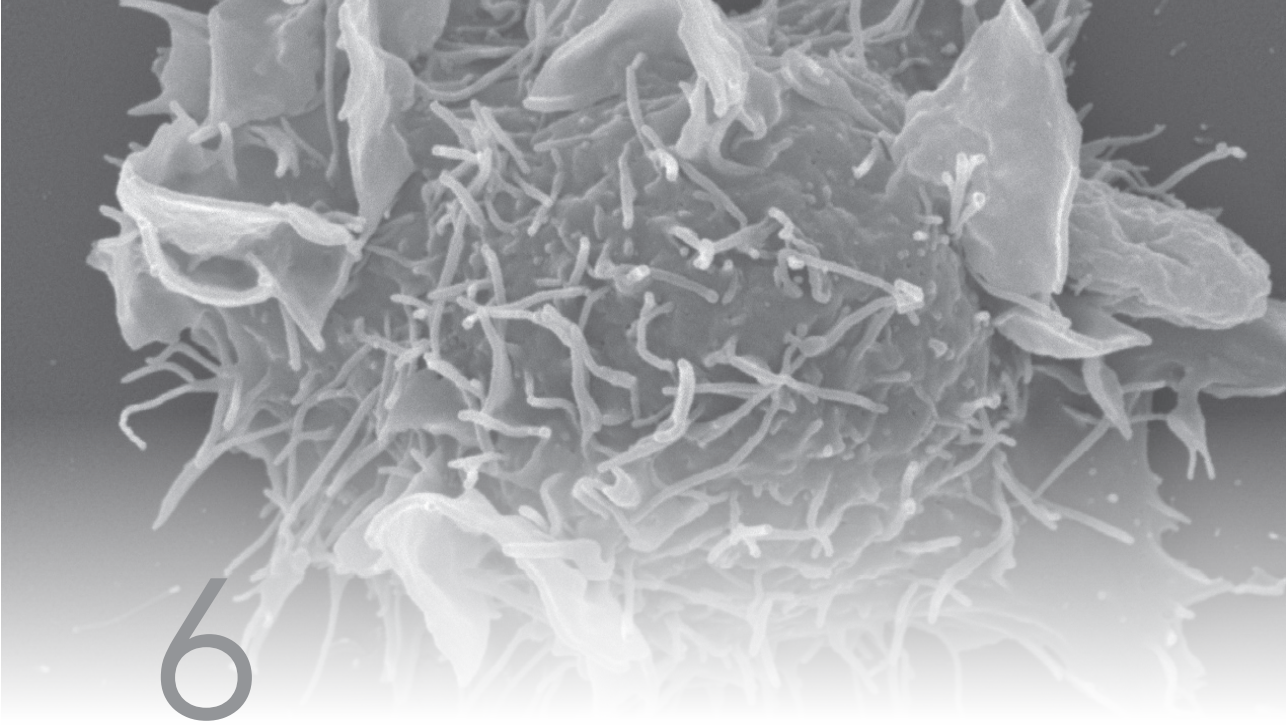

6

General Discussion

General Discussion

Morphodynamics is the collective term for all cellular processes that alter cell morphology through remodeling of the cytoskeletal network of the cell. Instability of microtubules by association and dissociation of tubulin subunits from the protofilaments and reorganization of actin filaments by polymerization and depolymerization of actin subunits are the basic phenomena that regulate this cytoskeletal dynamics. Strong coupling exists between morphodynamics and cell energy metabolism, as the primary determinant of whether microtubules grow or shrink is the rate of GTP hydrolysis [1, 2], and F-actin dynamics is strictly coupled to ATP hydrolysis and phosphate (P_i) release [3-5]. All the different aspects of morphodynamic behavior and coupling thereof to metabolism are much too complex for universal coverage in one holistic study. The research described in this thesis was therefore uniquely focused on the relationship between carbohydrate-energy metabolism and actin-based processes that play a physiological role in one particular cell type, macrophages.

Macrophages are highly morphodynamic cells. In the resting state, they are continuously probing the extracellular environment via the formation of actin-dependent membrane protrusions for the presence of pathogens or signs of injury [6]. When they perceive signals from their tissue environment they become activated and take on a M1 or M2 - or intermediate - polarization state, depending on the type of stimulus [7]. Macrophage polarization is accompanied by morphodynamic changes that are characteristic of the polarization state that is assumed. Lipopolysaccharide (LPS-) stimulation drives macrophages towards an inflammatory (M1) phenotype which is typified by increased pathogen phagocytosis, filopodia and membrane ruffle formation, and radial spreading, while podosome turnover and migration activity is reduced [8-11]. IL-4/IL-13-mediated activation towards an anti-inflammatory (M2) phenotype, on the other hand, is characterized by cellular elongation, formation of podosome rosettes, increased migration in dense matrices, but reduced pathogen phagocytosis [9, 12, 13]. Interestingly, macrophage metabolism is also differentially regulated upon polarization [14]. M1 macrophage metabolism is driven to a reductive mode with increased fluxes through glycolysis and the pentose phosphate pathway (PPP), while M2 macrophages enter an oxidative mode signified by an upregulation of the TCA-cycle and increased fatty acid oxidation [15, 16]. In order to obtain a better understanding of the possible relationship between these two aspects, we have investigated and compared the morphodynamic capacity of two macrophage cell lines under conditions where different aspects of energy metabolism were challenged. Experiments were performed mainly in the RAW 264.7 macrophage cell line but all key findings were confirmed in Maf-DKO cells, a recently established

macrophage cell line that shares characteristics with both RAW 264.7 and primary cells.

The main finding described in this thesis is that glucose is involved at different levels of control over macrophage morphodynamics via pathways that converge in regulation of actin remodeling (Figure 1). Based on a literature survey of possible regulatory mechanisms I speculate on a central mechanistic role for cofilin in this actin dynamics.

Glycolysis is the main fuel in macrophages

Most mammalian cells use mainly mitochondrial oxidative phosphorylation for ATP production. Since complete oxidation of glucose via this pathway delivers 30 moles of ATP per mole of glucose consumed, it is far more efficient than glycolysis alone, which produces only a net of 2 moles of ATP per mole of glucose [17]. Proliferating cells and cancer cells, however, have a reduced aerobic (mitochondrial) metabolism and markedly increased glycolytic rate which favors the production of anabolic material [18]. Macrophages seem to be exceptional in this regard. Although more and more evidence is mounting for self-renewal of macrophages *in vivo*, their proliferation rate does not compare with that of, for example, tumor cells. Still, macrophages have high glycolytic activity and significantly low OXPHOS activity (Newsholme *et al*. [19] and chapter 2). Moreover, upon functional activation towards a M1 or inflammatory phenotype, glucose consumption is further upregulated, while proliferation rate is slowed down (Rodríguez-Prados et al. [15] and chapter 4). This means that the high glycolytic rate in macrophages must have another purpose.

A very recent study by Freemerman et al. [20] has unveiled a role for glucose metabolism in reactive oxygen species (ROS-) mediated regulation of macrophage polarization state. The results described in chapters 2 and 4 of this thesis assign a further role for glucose metabolism in controlling the morphofunctional activities of macrophages. Maf-DKO cells exhibited a markedly slower proliferation rate but had more actin based surface membrane structures and a higher phagocytosis capacity compared to RAW 264.7 cells, while consuming the same amount of glucose. Furthermore, the formation of (LPS-induced) membrane protrusions, spreading, and phagocytosis by both cell lines was inhibited when glycolysis was disturbed.

OXPHOS activity, on the other hand, does not seem to be essential for these processes, since the ability of the cells to form membrane protrusions, expand their surface area, and internalize complement opsonized zymosan (COZ) particles was not compromised in the presence of the complex V inhibitor oligomycin (chapter 4). Interestingly, in both fast growing RAW 264.7 and the slower multiplying Maf-DKO cells low OXPHOS activity was essential to attain maximal proliferation rates (chapter 2). Translated to the *in vivo* situation this may suggest that, even though

cell viability and functionality are not affected, self-renewal of macrophages would be compromised under hypoxic conditions, thereby affecting macrophage numbers in the affected tissues. Thus, in macrophages, both glycolysis and mitochondrial OXPHOS contribute to cellular ATP production to sustain cell viability, but glycolysis fuels energy consuming morphofunctional activities, such as phagocytosis.

Transfer of glycolysis-derived ATP to subcellular compartments

Seemingly, our findings and findings of many others thus point to a model in which ATP derived from glycolysis and mitochondrial OXPHOS is used as distinct "energy currency", i.e. as fuel with differential value for the promotion of cell-wellbeing and growth, and cell-labor. How can we explain this model? Currently, the best explanation is that subcellular compartmentation of energy supply systems is involved. During phagocytosis and the formation of different forms of membrane protrusions (parts of the phagocytic cup, filopodia, lamellopodia, ruffles) there is a need for local actin-driven remodeling of the cell membrane. This remodeling is fuelled by ATP production, which is generated on the spot, at the site of where activity is needed. This can be achieved by local presence of glycolytic ATP-production machinery, as was shown to be the case for fast axonal transport in neurons [21]. Like in axonal segments of neuronal cells, mitochondria may be completely excluded from thin membrane protrusions, such as ruffles and the phagocytic cup, due to the dimension of these structures, thereby leaving the local production of ATP up to the glycolytic pathway. Another way by which energy could be locally generated is by the transfer of ATP from the site of synthesis (via glycolysis or mitochondrial OXPHOS) to the area of membrane protrusion via the creatine kinase/phosphocreatine energy circuit [22]. One cytosolic isoform of creatine kinase, the brain type creatine kinase CK-B, is the main isoform expressed in macrophages. This enzyme accumulates in the phagocytic cup as well as in membrane ruffles (Kuiper *et al.* [22, 23] and chapter 3) where it regulates actin dynamics. Up to now, nothing was known about the mechanism of CK-B recruitment to subcellular sites of actin cytoskeletal remodeling. In chapter 3, we provide evidence that the C-terminal flexible loop of the CK-molecule containing Asp^{326} is involved in its subcellular displacement. This loop has been associated with a conformational change that occurs upon substrate binding to exclude solvent from the active site [24, 25]. We speculate that changes in the loop region may also influence the overall conformation or possibility for subunit interaction in the CK-B dimer, or alter the availability of surface accessible residues. Thereby these changes could influence the association of the enzyme with specific binding partners and promote alteration of its subcellular localization.

The ATP supplied by CK-B may not only be essential for the polymerization and treadmilling of actin filaments but also be used for actin-myosin contraction, and

functioning of actin binding proteins, like the Arp2/3 complex, as well as small GTP-ases [26-30] (Figure 1, pink arrows). Interestingly, however, not all actin driven processes appear equally dependent on CK-B. For example, FcγR-mediated phagocytosis, filipodia formation, as well as LPS-stimulated cell spreading of macrophages seem less sensitive to inhibition of CK-B (chapter 3 and Kuiper *et al.* [22]). It is of note here that these latter processes are mainly regulated by the GTPases Cdc42 and Rac1 [33-35], while CR3-mediated phagocytosis and membrane ruffling require Rho A activity [36-38]. Furthermore, it may be relevant that Rho A is the GTPase most sensitive to ATP depletion [29]. Cdc42 activity appears not to be affected by low ATP levels, while Rac1 (which has also been implicated in membrane ruffle formation [39]) is mildly sensitive. Rho A regulates actin dynamics by activating ROCK which can then either deactivate the actin severing protein cofilin through LIMK1/2 [40, 41] (Figure 1, pink arrows), or stimulate the actin filament crosslinking activity of myosin II by deactivation of MLC phosphatase [42]. In addition, Rho A activates mDia which is involved in actin remodeling in CR3-mediated phagocytosis [43]. CK-B-mediated ATP supply may, therefore, be particularly involved in actin-based processes that depend on Rho A signaling, and it would be interesting to determine whether Rho A (or its upstream signaling molecules) are involved in recruitment of CK-B to subcellular sites of actin polymerization and whether the C-terminal flexible loop is facilitating (possible) interaction. Also, there may be a relationship between the role of CK mediated ATP supply and the turnover dynamics of different surface protrusions and the acto-myosin based structures therein. Further study is thus necessary to discriminate between a transient and permanent role of CK-B in these locales.

Glucose signaling to the actin cytoskeleton

Apart from having a general or local catabolic role, as the principal source for energy, in all living cells, glucose also has an anabolic role, as precursor for amino acids, fatty acids, and phospholipids. Furthermore, glucose can also be involved in the posttranslational modification of proteins. In chapter 4, we provided evidence suggesting that glucose may have a non-metabolic role in regulating actin dynamics in macrophages, as has been described for insulin secreting cells [44] (Figure 1). Glucose stimulation can cause carboxymethylation and *O*-linked glycosylation of Cdc42, leading to its activation and deactivation, respectively [45, 46]. Thus, glucose modulates Cdc42 cycling between its active and inactive forms. Activated Cdc42 interacts and activates N-WASP which then translocates to membrane where it is involved in nucleation of actin polymerization via the Arp2/3 complex [47]. In addition, Cdc42 is a potent activator of PAK1 and Rac1 that in turn activates LIMK1, leading to phosphorylation and inactivation of cofilin [47-49]. Interestingly, this pathway (Cdc42-PAK1-Rac1-LIMK1) is also activated by LPS, along with upstream PI3K/Akt [50, 51

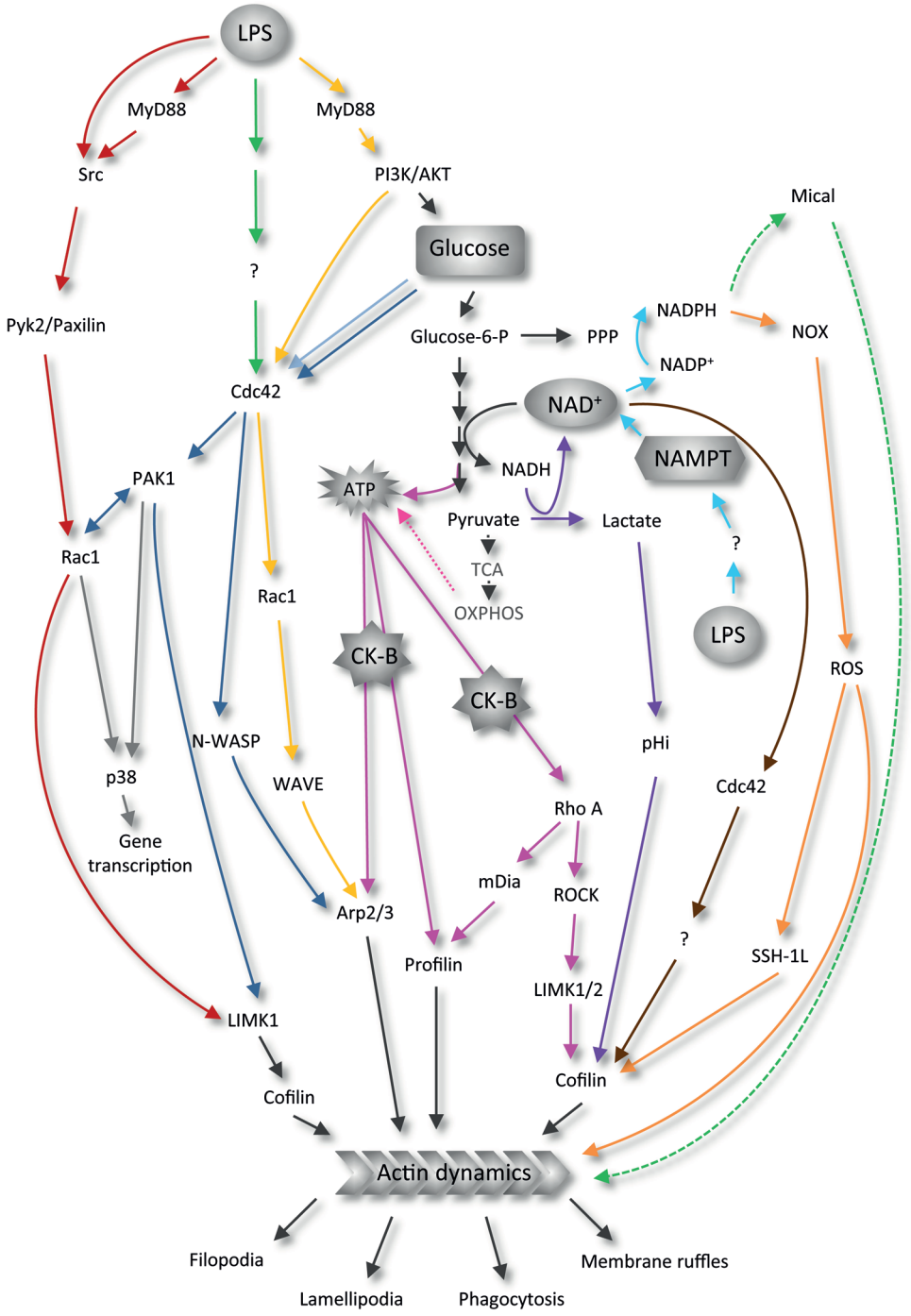
LPS
MyD88
MyD88
Src
PI3K/AKT
Mical
?
Glucose
Pyk2/Paxilin
Glucose-6-P
PPP
NADPH
NOX
NADP+
Cdc42
NAD+
NAMPT
PAK1
ATP
NADH
Pyruvate
Lactate
?
Rac1
TCA
Rac1
OXPHOS
LPS
CK-B
ROS
CK-B
N-WASP
pHi
p38
WAVE
Cdc42
Rho A
Gene
transcription
mDia
ROCK
Arp2/3
?
SSH-1L
Profilin
LIMK1/2
LIMK1
Cofilin
Cofilin
Actin dynamics
Filopodia
Membrane ruffles
Lamellipodia
Phagocytosis

Figure 1. Metabolic regulation of morphodynamics in macrophages. *LPS complexes with LPS binding protein and CD14. This complex binds to and activates TLR4, leading to recruitment of MyD88 [31, 32]. TLR4-signaling leads to phosphorylation of the PI3K/ATK pathway (yellow arrows) and induces phosphorylation of Pyk2 and its substrate paxilin in a Src-family-dependent mechanism through both MyD88-dependent and -independent pathways (red arrows). This leads to the activation of the Rho GTPases Cdc42 and Rac1, although LPS-induced activation of Cdc42 and Rac1 can occur independently of MyD88 (green arrows). The activity of Cdc42 may also be directly controlled via carboxymethylation or glycosylation by glucose (blue arrows). Activation of Rac1 and Cdc42 leads to the activation/deactivation of actin binding proteins Arp2/3 and cofilin. Metabolism of glucose yields cellular ATP which is transported to subcellular sites of actin polymerization via CK-B (pink arrows). The ATP is loaded unto G-actin monomers by profilin before incorporation into an actin filament, or used to activate the Arp2/3 complex or the Rho GTPase Rho A which in turn also stimulate actin polymerization. LPS stimulation induces the expression of the NAD^+ synthesizing enzyme NAMPT (turquoise arrows). NAD^+ can directly activate Cdc42 to affect actin dynamics (brown arrows) or exert a regulatory role by influencing cellular metabolism and thereby intracellular pH (purple arrows). NADPH derived mainly from the pentose phosphate pathway (PPP) may serve as electron donor in reactions catalyzed by NOX or Mical to regulate actin assembly and disassembly in a redox-dependent mechanism (orange and green dashed arrows, respectively).*

(Figure 1, green, yellow, and blue arrows). Moreover, LPS signaling stimulates glucose uptake and metabolism which is known to be mediated by the PI3K/Akt pathway [52-55]. Glucose consumption and LPS-induced morphodynamics may, therefore, be coupled processes in macrophages. However, LPS-signaling may also induce morphodynamics via pathways that do not involve glucose. Activation of TLR4-signaling by LPS leads to recruitment of MyD88 and phosphorylation of the PI3K/ATK pathway which in turn activates Cdc42 and Rac1 [56, 57] (Figure 1, yellow arrows). LPS can also induce phosphorylation of Pyk2 and its substrate paxilin in a Src-family-dependent mechanism through both MyD88-dependent and -independent pathways [11, 58] (Figure 1, red arrows). Whether LPS-induced inactivation of cofilin utilizes glucose as upstream signaling molecule in macrophages or whether LPS- and glucose-induced pathways are activated in parallel remains to be determined. Further study is therefore needed of, for example, the effect of O-linked glycosylation inhibition by *N*-Acetylglucosamine-thiazoline (NAG-thiazoline) or GlcNAcstatin [59] on LPS-induced morphodynamic processes and activation or inactivation of downstream signaling molecules such as Rac1, Cdc42, and cofilin.

Glucose-dependent redox and pH regulation of morphodynamics

Another way in which glucose can exert regulatory effects on actin remodeling is by stimulating NADPH oxidase (NOX)-mediated ROS production. NOX is a multicomponent enzyme complex that catalyzes the transfer of electrons from NADPH (reduced nicotinamide adenine dinucleotide phosphate) to molecular oxygen, thereby producing superoxide and other ROS. Cellular NADPH is mainly produced via the reduction of $NADP^+$ by G6PDH in the PPP, although a very recent report identified folate-dependent NADPH production as a second major source [60].

Interestingly, the flux through the PPP as well as the expression of NOX-1 is increased in macrophages upon LPS-stimulation [61, 62]. NOX-mediated ROS production may not only alter macrophage polarization state [20] but also directly influence actin filament properties and function [63] or regulate actin filament depolymerization and severing through the activation of slingshot-1L (SSH-1L) that in turn dephosphorylates, and activates, cofilin [64] (Figure 1, orange arrows). NADPH is also involved in the oxidation of actin by Mical, a redox enzyme that oxidizes methionine residues in actin, leading to its disassembly [65, 66] (Figure 1, dashed green arrows). In macrophages, re-assembly of actin filaments has been shown to be dependent on the reduction of the Mical-oxidized methionine residues by MsrB1 and essential for LPS-induced actin cytoskeletal remodeling [67].

Cellular $NADP^+$ is generated through NAD^+ kinase-mediated phosphorylation of NAD^+ (nicotinamide adenine dinucleotide), a key metabolite/co-factor in cellular glucose metabolism and regulator of cellular redox state. The enzyme responsible for salvage synthesis of NAD^+ from nicotinamide, NAMPT (nicotinamide phosphoribosyltransferase), is upregulated in macrophages stimulated with LPS [68] (Figure 1, turquoise arrows). Inhibition of NAMPT reduced the levels of cellular NAD(H) as well as NADP(H) in macrophages (chapter 5). This reduction in NAD(P)(H) resulted in irregularities in the actin-based morphology of RAW 264.7 and Maf-DKO cells, reduced spreading ability, as well as a drop in phagocytic capacity of COZ. At this point it is perhaps interesting to note that the global level of NADP(H) in macrophages in comparison to the level of NAD(H) is much higher in macrophages than in most other cell types, where [NAD(H)] is usually in > 10 fold molecular excess over [NADP(H)]. Whether this points to a more elaborate role for $NADP^+$/NADPH than just being a redox-cofactor in lipid biosynthesis and protectant against ROS damage is not known, but it is tempting to hypothesize that its presence reinforces the role of NAD^+, via a collective or individual effect on macrophage morphodynamics. Thus, the mechanism driving this regulation may involve NADPH-mediated ROS-signaling to the actin cytoskeleton as described above, but entirely different modes of coupling NAD^+-linked metabolism to macrophage morphodynamics may also exist. One possibility could be intracellular pH (pHi; Figure 1, purple arrows). The conversion of glycolysis-derived pyruvate into lactate involves, and is regulated by, the conversion of NADH into NAD^+ by lactate dehydrogenase. The lactate is transported across the cell membrane via MCT1 [69, 70], thereby creating a pH gradient across the membrane. A local rise in pHi increases the severing activity of cofilin [71], resulting in rearrangement of the cortical actin cytoskeleton [72]. Although NAD^+ is closely involved in cellular ATP-production, its role in controlling macrophage morphodynamics seems to be independent of this, since global ATP levels were not affected when we inhibited NAMPT-mediated NAD^+ synthesis in RAW264.7 and

Maf-DKO cells with FK866. A last possible principle that I would like to mention is that NAD^+ could regulate actin dynamics by activating upstream signaling molecules such as Cdc42 [73]. Although the exact sequence of events has not been elucidated, this again could result in the regulation of cofilin activity (Figure 1, brown arrows).

A central role for cofilin in metabolic regulation of morphodynamics

Taken together, many of the pathways of glucose regulation of cellular actin dynamics culminate in the activation or deactivation of cofilin (Figure 1). Cofilin activity is regulated by three mechanisms: phosphorylation on Ser3, complex formation with phosphatidylinositol 4,5-biphosphate ($PtdIns(4,5)P_2$), and complex formation with cortactin [74]. Cellular glucose and redox metabolism influences all three mechanisms. Phosphorylation (inactivation) and dephosphorylation (activation) are regulated by LIMK and SSH, respectively, and as described above the activity of both these enzymes is influenced by glucose metabolism. Dephosphorylated cofilin localizes to membrane protrusions where it interacts with $PtdIns(4,5)P_2$ or cortactin to form an inhibitory complex. In both instances, a local rise in the pHi (which may be greatly influenced by glycolytic lactate production and export) releases dephosphorylated cofilin from the complex, resulting in increased actin filament severing. The barbed-ends of filaments that are released in this way can be used to nucleate actin polymerization and support Arp2/3-complex-mediated branching of the actin network. Cofilin also mediates depolymerisation of actin filaments further away from the plasma membrane, thereby promoting actin filament turnover. LIMK-mediated phosphorylation of cofilin bound to ADP-G-actin releases it from actin, making cofilin available for another activation cycle, and ADP-G-actin for nucleotide exchange and incorporation at a new barbed-end. Cofilin, therefore, catalyzes actin polymerization and depolymerization through its severing activity. Whether cofilin-mediated severing results in net filament assembly or disassembly, is determined by the relative concentration of active cofilin and ATP-G-actin, and the availability of other actin modulating proteins [74].

In macrophages, a direct role for LIMK-mediated phosphorylation of cofilin in phagocytosis has been described [75, 76] and in neutrophils cofilin has been shown to translocate to and control membrane ruffle formation [77]. Also in other cell types cofilin localizes to protrusive membrane structures and regulate motility [78-81]. This, along with the findings described in this thesis and discussed above, suggest that cofilin may indeed be the point of convergence between cellular morphodynamics and metabolism. I therefore strongly suggest to make this protein a focal point for further study in a follow-up of my Ph.D. project.

Clinical relevance

Macrophages are involved in many aspects of health and disease. Health problems in which they play an important role are related to communicable (infectious) diseases as well as non-communicable diseases (autoimmune disease, diabetes, cardiovascular disease, and cancer). Therefore, understanding the link between metabolism and function opens up new possibilities for macrophages as therapeutic targets. By augmenting or inhibiting their activities metabolically, disease outcome could be altered. For example, in rheumatoid arthritis (RA) an imbalance exists between inflammatory and anti-inflammatory macrophages in the synovium [82]. Treatment of RA (and other auto-immune diseases) currently mostly involve drugs that deplete macrophages from the synovium (or other inflamed areas) [82, 83], or immune-suppressors that inhibit the entire immune system. Considering the close relationship between metabolism and macrophage phenotype, an alternative approach could be to metabolically inhibit or eliminate highly glycolytic inflammatory macrophages so that the balance between pro- and anti-inflammatory macrophages can be re-established and disease symptoms can be limited. Although the secretion of pro-inflammatory cytokines by macrophages has been implicated as a major process in the pathogenesis and -physiology of autoimmune diseases, the actin cytoskeleton may also play a role herein. Autoantibodies against cofilin, Rho-GDIβ protein (regulator of Rho-family GTPases), and actin-like proteins have been detected in patients that suffer from various autoimmune diseases [84, 85]. However, the significance thereof is still unclear. In RA, dynamic remodeling of the cortical actin cytoskeleton plays a direct role in joint erosion. The inflamed joints are populated by osteoclasts (multinucleated bone resorbing cells derived from macrophages) with increased resorbing activity [86-88]. Bone resorption by osteoclasts entails the formation of a so-called “sealing zone” that consists of multiple actin-rich podosomes through which the cell attaches to the bone, and acidification of the extracellular microenvironment underneath the osteoclast. If the glucose dependency of actin-based protrusive structures of LPS-stimulated macrophages can be extrapolated to the formation and function of podosomes in osteoclasts, metabolic intervention could offer another approach to reduce joint erosion in RA.

Tumor associated macrophages (TAMs) form another subset of target cells for applying metabolic therapies. Although TAMs initially exhibit anti-tumor properties, they obtain an immune-suppressive (M2) phenotype when the tumor is established and promote tumor progression and metastasis as well as angiogenesis [7, 89]. In addition to secreting cytokines and proteases that promote tumor growth and metastasis, macrophage migration promotes tumor cell invasiveness by remodeling the extracellular matrix (ECM) [90]. Therefore, metabolic inhibition of macrophage

morphodynamics may also be relevant in treating cancer patients. The use of FK866 as cancer therapeutic is currently being investigated in phase two clinical trials and has been shown to effectively reduce cancer cell growth and migration [91-93]. In order to protect normal tissues from NAD^+-depletion, FK866 treatment has been combined with nicotinic acid (NA; Vitamin B3) supplementation. The expression of the enzyme involved in converting NA into NAD^+ (nicotinic acid phosphoribosyltransferase; NAPRT) is often lower in tumor cells compared to normal cells. Therefore, NA supplementation selectively rescues NAD^+-synthesis and, thus, survival of normal cells. Macrophages show a strikingly similar metabolic profile to tumor cells. In addition, these cells do not appear to express NAPRT (chapter 5). This renders also macrophages very sensitive to FK866 inhibition of NAD^+ synthesis. As shown in chapter 5 and also in studies by others [94-96], macrophage function is thereby significantly inhibited by FK866, even though viability and proliferation are unaffected. Treating tumors with FK866 may, therefore, have dual action: inhibiting the tumor itself but also the macrophages that promote their growth and migration. However, macrophages remain essential agents in the clearance of pathogens and apoptotic cells to maintain tissue homeostasis. Therefore, when considering macrophages as therapeutic targets for the treatment of diseases like cancer and RA, the method of administration and dosage of metabolic inhibitors applied would have to be carefully selected to ensure that the composition of the macrophage population in the affected tissue returns to, and is maintained at, a state comparable to that of healthy tissue and that susceptibility to infection is kept at a minimum.

References

1. Lodish H, Berk A & Zipursky SL, e.a. in Molecular Cell Biology, Edn. 4th (W. H. Freeman, New York; 2000).
2. Hyman, A.A., Salser, S., Drechsel, D.N., Unwin, N. & Mitchison, T.J. Role of GTP hydrolysis in microtubule dynamics: information from a slowly hydrolyzable analogue, GMPCPP. *Mol. Biol. Cell* **3**, 1155-1167 (1992).
3. Atkinson, S.J., Hosford, M.A. & Molitoris, B.A. Mechanism of Actin Polymerization in Cellular ATP Depletion. *J. Biol. Chem.* **279**, 5194-5199 (2004).
4. Bernstein, B.W. & Bamburg, J.R. Actin-ATP Hydrolysis Is a Major Energy Drain for Neurons. *J. Neurosci.* **23**, 1-6 (2003).
5. van Horssen, R. *et al.* Modulation of Cell Motility by Spatial Repositioning of Enzymatic ATP/ADP Exchange Capacity. *J. Biol. Chem.* **284**, 1620-1627 (2009).
6. Flannagan, R.S., Harrison, R.E., Yip, C.M., Jaqaman, K. & Grinstein, S. Dynamic macrophage "probing" is required for the efficient capture of phagocytic targets. *J. Cell Biol.* **191**, 1205-1218 (2010).
7. Murray, P.J. & Wynn, T.A. Protective and pathogenic functions of macrophage subsets. *Nat. Rev. Immunol.* **11**, 14 (2011).
8. Bianco, C., Götze, O. & Cohn, Z.A. Regulation of macrophage migration by products of the complement system. *Proc. Natl. Acad. Sci. U. S. A.* **76**, 888-891 (1979).
9. Cougoule, C. *et al.* Blood leukocytes and macrophages of various phenotypes have distinct abilities to form podosomes and to migrate in 3D environments. *Eur. J. Cell Biol.* **91**, 938-949 (2012).
10. Williams, L.M. & Ridley, A.J. Lipopolysaccharide Induces Actin Reorganization and Tyrosine Phosphorylation of Pyk2 and Paxillin in Monocytes and Macrophages. *J. Immunol.* **164**, 2028-2036 (2000).
11. Kleveta, G. *et al.* LPS induces phosphorylation of actin-regulatory proteins leading to actin reassembly and macrophage motility. *J. Cell. Biochem.* **113**, 80-92 (2012).
12. McWhorter, F.Y., Wang, T., Nguyen, P., Chung, T. & Liu, W.F. Modulation of macrophage phenotype by cell shape. *Proc. Natl. Acad. Sci. U. S. A.* **110**, 17253-17258 (2013).
13. Varin, A., Mukhopadhyay, S., Herbein, G. & Gordon, S. Alternative activation of macrophages by IL-4 impairs phagocytosis of pathogens but potentiates microbial-induced signalling and cytokine secretion. *Blood* **115**, 353-362 (2010).
14. O'Neill, L.A. & Hardie, D.G. Metabolism of inflammation limited by AMPK and pseudo-starvation. *Nature* **493**, 346-355 (2013).
15. Rodríguez-Prados, J.-C. *et al.* Substrate Fate in Activated Macrophages: A Comparison between Innate, Classic, and Alternative Activation. *J. Immunol.* **185**, 605-614 (2010).
16. Vats, D. *et al.* Oxidative metabolism and PGC-1β attenuate macrophage-mediated inflammation. *Cell Metab.* **4**, 13-24 (2006).
17. Berg, J., Tymoczko, J. & Stryer, L. in Biochemistry, Edn. 5th (W H Freeman, New York; 2002).
18. Vander Heiden, M.G., Cantley, L.C. & Thompson, C.B. Understanding the Warburg Effect: The Metabolic Requirements of Cell Proliferation. *Science* **324**, 1029-1033 (2009).
19. Newsholme, P., Curi, R., Gordon, S. & Newsholme, E.A. Metabolism of glucose, glutamine, long-chain fatty acids and ketone bodies by murine macrophages. *The Biochemical journal* **239**, 5 (1986).
20. Freemerman, A.J. *et al.* Metabolic Reprogramming of Macrophages: Glucose transporter 1 (GLUT1)-mediated glucose metabolism drives a proinflammatory phenotype. *J. Biol. Chem.* **289**, 7884-7896 (2014).
21. Zala, D. *et al.* Vesicular Glycolysis Provides On-Board Energy for Fast Axonal Transport. *Cell* **152**, 479-491 (2013).
22. Kuiper, J.W.P. *et al.* Creatine Kinase–Mediated ATP Supply Fuels Actin-Based Events in Phagocytosis. *PLoS Biol.* **6**, e51 (2008).
23. Kuiper, J.W.P. *et al.* Local ATP Generation by Brain-Type Creatine Kinase (CK-B) Facilitates Cell Motility. *PLoS ONE* **4**, e5030 (2009).
24. Forstner, M., Kriechbaum, M., Laggner, P. & Wallimann, T. Structural Changes of Creatine Kinase upon Substrate Binding. *Biophys. J.* **75**, 1016-1023 (1998).
25. Lahiri, S.D. *et al.* The 2.1 Å Structure of Torpedo californica Creatine Kinase Complexed with the ADP-Mg^{2+}–NO^{3-}–Creatine Transition-State Analogue Complex. *Biochemistry (Mosc).* **41**, 13861-13867 (2002).
26. Ingerman, E., Hsiao, J.Y. & Mullins, R.D. Arp2/3 complex ATP hydrolysis promotes lamellipodial actin network disassembly but is dispensable for assembly. *J. Cell Biol.* **200**, 619-633 (2013).
27. Volkmann, N. & Hanein, D. Actomyosin: law and order in motility. *Curr. Opin. Cell Biol.* **12**, 26-34 (2000).
28. Carlier, M.-F. & Pantaloni, D. Control of Actin Assembly Dynamics in Cell Motility. *J. Biol. Chem.* **282**, 23005-23009 (2007).
29. Hallett, M.A., Dagher, P.C. & Atkinson, S.J. Rho GTPases show differential sensitivity to nucleotide triphosphate depletion in a model of ischemic cell injury. *Am. J. Physiol. Cell Physiol.* **285**, C129-C138 (2003).
30. Pollard, T.D. Regulation of Actin Filament Assembly by Arp2/3 Complex and Formins. *Annu. Rev. Biophys.*

Biomol. Struct. **36**, 451-477 (2007).
31. Guha, M. & Mackman, N. LPS induction of gene expression in human monocytes. *Cell. Signal.* **13**, 85-94 (2001).
32. Beutler, B. Tlr4: central component of the sole mammalian LPS sensor. *Curr. Opin. Immunol.* **12**, 20-26 (2000).
33. Hoppe, A.D. & Swanson, J.A. Cdc42, Rac1, and Rac2 Display Distinct Patterns of Activation during Phagocytosis. *Mol. Biol. Cell* **15**, 3509-3519 (2004).
34. Allen, W.E., Jones, G.E., Pollard, J.W. & Ridley, A.J. Rho, Rac and Cdc42 regulate actin organization and cell adhesion in macrophages. *J. Cell Sci.* **110**, 707-720 (1997).
35. Nobes, C.D. & Hall, A. Rho, Rac, and Cdc42 GTPases regulate the assembly of multimolecular focal complexes associated with actin stress fibers, lamellipodia, and filopodia. *Cell* **81**, 53-62 (1995).
36. Kurokawa, K. & Matsuda, M. Localized RhoA Activation as a Requirement for the Induction of Membrane Ruffling. *Mol. Biol. Cell* **16**, 4294-4303 (2005).
37. Caron, E. & Hall, A. Identification of Two Distinct Mechanisms of Phagocytosis Controlled by Different Rho GTPases. *Science* **282**, 1717-1721 (1998).
38. Kim, J.-G. *et al.* Ras-related GTPases, Rap1 and RhoA collectively induce the phagocytosis of serum-opsonized zymosan particles in macrophages. *J Biol Chem* (2011).
39. Ridley, A.J., Paterson, H.F., Johnston, C.L., Diekmann, D. & Hall, A. The small GTP-binding protein rac regulates growth factor-induced membrane ruffling. *Cell* **70**, 401-410 (1992).
40. Ohashi, K. *et al.* LIM Kinase Has a Dual Role in Regulating Lamellipodium Extension by Decelerating the Rate of Actin Retrograde Flow and the Rate of Actin Polymerization. *J. Biol. Chem.* **286**, 36340-36351 (2011).
41. Sumi, T., Matsumoto, K., Takai, Y. & Nakamura, T. Cofilin Phosphorylation and Actin Cytoskeletal Dynamics Regulated by Rho- and Cdc42-Activated Lim-Kinase 2. *J. Cell Biol.* **147**, 1519-1532 (1999).
42. Riento, K. & Ridley, A.J. Rocks: multifunctional kinases in cell behaviour. *Nat. Rev. Mol. Cell Biol.* **4**, 446-456 (2003).
43. Colucci-Guyon, E. *et al.* A Role for Mammalian Diaphanous-Related Formins in Complement Receptor (CR3)-Mediated Phagocytosis in Macrophages. *Curr. Biol.* **15**, 2007-2012 (2005).
44. Kowluru, A. Small G Proteins in Islet β-Cell Function. *Endocr. Rev.* **31**, 52-78 (2010).
45. Kowluru, A. *et al.* Glucose- and GTP-dependent stimulation of the carboxyl methylation of CDC42 in rodent and human pancreatic islets and pure beta cells. Evidence for an essential role of GTP-binding proteins in nutrient-induced insulin secretion. *J. Clin. Invest.* **98**, 540-555 (1996).
46. Nevins, A.K. & Thurmond, D.C. Glucose regulates the cortical actin network through modulation of Cdc42 cycling to stimulate insulin secretion. *Am. J. Physiol. Cell Physiol.* **285**, C698-C710 (2003).
47. Uenishi, E. *et al.* Actin Dynamics Regulated by the Balance of Neuronal Wiskott-Aldrich Syndrome Protein (N-WASP) and Cofilin Activities Determines the Biphasic Response of Glucose-induced Insulin Secretion. *J. Biol. Chem.* **288**, 25851-25864 (2013).
48. Wang, Z., Oh, E. & Thurmond, D.C. Glucose-stimulated Cdc42 Signaling Is Essential for the Second Phase of Insulin Secretion. *J. Biol. Chem.* **282**, 9536-9546 (2007).
49. Edwards, D.C., Sanders, L.C., Bokoch, G.M. & Gill, G.N. Activation of LIM-kinase by Pak1 couples Rac/Cdc42 GTPase signalling to actin cytoskeletal dynamics. *Nat. Cell Biol.* **1**, 253-259 (1999).
50. Weintz, G. *et al.* The phosphoproteome of toll-like receptor-activated macrophages. *Mol. Syst. Biol.* **6**, 371 (2010).
51. Kong, L. & Ge, B.-X. MyD88-independent activation of a novel actin-Cdc42/Rac pathway is required for Toll-like receptor-stimulated phagocytosis. *Cell Res.* **18**, 745-755 (2008).
52. Gottlob, K. *et al.* Inhibition of early apoptotic events by Akt/PKB is dependent on the first committed step of glycolysis and mitochondrial hexokinase. *Genes Dev.* **15**, 1406-1418 (2001).
53. Hill, M.M. *et al.* A Role for Protein Kinase Bβ/Akt2 in Insulin-Stimulated GLUT4 Translocation in Adipocytes. *Mol. Cell. Biol.* **19**, 7771-7781 (1999).
54. Riley, J.K., Carayannopoulos, M.O., Wyman, A.H., Chi, M. & Moley, K.H. Phosphatidylinositol 3-Kinase Activity Is Critical for Glucose Metabolism and Embryo Survival in Murine Blastocysts. *J. Biol. Chem.* **281**, 6010-6019 (2006).
55. Schultze, S.M., Hemmings, B.A., Niessen, M. & Tschopp, O. PI3K/AKT, MAPK and AMPK signalling: protein kinases in glucose homeostasis. *Expert Rev. Mol. Med.* **14**, null-null (2012).
56. Bosse, T. *et al.* Cdc42 and Phosphoinositide 3-Kinase Drive Rac-Mediated Actin Polymerization Downstream of c-Met in Distinct and Common Pathways. *Mol. Cell. Biol.* **27**, 6615-6628 (2007).
57. Shin, O.S. *et al.* Downstream Signals for MyD88-Mediated Phagocytosis of Borrelia burgdorferi Can Be Initiated by TRIF and Are Dependent on PI3K. *J. Immunol.* **183**, 491-498 (2009).
58. Hazeki, K. *et al.* Toll-like receptor-mediated tyrosine phosphorylation of paxillin via MyD88-dependent and -independent pathways. *Eur. J. Immunol.* **33**, 740-747 (2003).
59. Esko, J. & Bertozzi, C. in Essentials of Glycobiology, Edn. 2nd. (ed. C.R. Varki A, Esko JD) (Cold Spring Harbor (NY): Cold Spring Harbor Laboratory Press, New York; 2009).

60. Fan, J. *et al.* Quantitative flux analysis reveals folate-dependent NADPH production. *Nature* (2014).
61. Maitra, U., Singh, N., Gan, L., Ringwood, L. & Li, L. IRAK-1 Contributes to Lipopolysaccharide-induced Reactive Oxygen Species Generation in Macrophages by Inducing NOX-1 Transcription and Rac1 Activation and Suppressing the Expression of Antioxidative Enzymes. *J. Biol. Chem.* **284**, 35403-35411 (2009).
62. Haschemi, A. *et al.* The Sedoheptulose Kinase CARKL Directs Macrophage Polarization through Control of Glucose Metabolism. *Cell Metab.* **15**, 813-826 (2012).
63. Dalle-Donne, I., Rossi, R., Milzani, A., Di Simplicio, P. & Colombo, R. The actin cytoskeleton response to oxidants: from small heat shock protein phosphorylation to changes in the redox state of actin itself. *Free Radic. Biol. Med.* **31**, 1624-1632 (2001).
64. Kim, J.-S., Huang, T.Y. & Bokoch, G.M. Reactive Oxygen Species Regulate a Slingshot-Cofilin Activation Pathway. *Mol. Biol. Cell* **20**, 2650-2660 (2009).
65. Hung, R.J. *et al.* Mical links semaphorins to F-actin disassembly. *Nature* **463**, 823-827 (2010).
66. Hung, R.-J., Pak, C.W. & Terman, J.R. Direct Redox Regulation of F-Actin Assembly and Disassembly by Mical. *Science* **334**, 1710-1713 (2011).
67. Lee, Byung C. *et al.* MsrB1 and MICALs Regulate Actin Assembly and Macrophage Function via Reversible Stereoselective Methionine Oxidation. *Mol. Cell* **51**, 397-404 (2013).
68. Nau, G.J. *et al.* Human macrophage activation programs induced by bacterial pathogens. *Proc. Natl. Acad. Sci. U. S. A.* **99**, 1503-1508 (2002).
69. Poole, R.C. & Halestrap, A.P. Transport of lactate and other monocarboxylates across mammalian plasma membranes. *Am. J. Physiol. Cell Physiol.* **264**, C761-C782 (1993).
70. Halestrap, A.P. & Price, N.T. The proton-linked monocarboxylate transporter (MCT) family: structure, function and regulation. *Biochem. J.* **343**, 281-299 (1999).
71. Yonezawa, N., Nishida, E. & Sakai, H. pH control of actin polymerization by cofilin. *J. Biol. Chem.* **260**, 14410-14412 (1985).
72. Stock, C. & Schwab, A. Protons make tumor cells move like clockwork. *Pfluegers Arch./Eur. J. Physiol.* **458**, 981-992-992 (2009).
73. Yin, H. *et al.* Intrinsic directionality of migrating vascular smooth muscle cells is regulated by NAD^+ biosynthesis. *J. Cell Sci.* **125**, 5770-5780 (2012).
74. Bravo-Cordero, J.J., Magalhaes, M.A., Eddy, R.J., Hodgson, L. & Condeelis, J. Functions of cofilin in cell locomotion and invasion. *Nat. Rev. Mol. Cell Biol.* **14**, 405-415 (2013).
75. Matsui, S. *et al.* U73122 inhibits the dephosphorylation and translocation of cofilin in activated macrophage-like U937 cells. *Cell. Signal.* **13**, 17-22 (2001).
76. Matsui, S. *et al.* LIM Kinase 1 Modulates Opsonized Zymosan-triggered Activation of Macrophage-like U937 Cells: Possible involvement of phosphorylation of cofilin and reorganization of actin cytoskeleton. *J. Biol. Chem.* **277**, 544-549 (2002).
77. Heyworth, P.G., Robinson, J.M., Ding, J., Ellis, B.A. & Badwey, J.A. Cofilin undergoes rapid dephosphorylation in stimulated neutrophils and translocates to ruffled membranes enriched in products of the NADPH oxidase complex. Evidence for a novel cycle of phosphorylation and dephosphorylation. *Histochem. Cell Biol.* **108**, 221-233 (1997).
78. Aizawa, H., Sutoh, K. & Yahara, I. Overexpression of cofilin stimulates bundling of actin filaments, membrane ruffling, and cell movement in Dictyostelium. *J. Cell Biol.* **132**, 335-344 (1996).
79. Arai, H. & Atomi, Y. Suppression of Cofilin Phosphorylation in Insulin-Stimulated Ruffling Membrane Formation in KB Cells. *Cell Struct. Funct.* **28**, 41-48 (2003).
80. Delorme, V. *et al.* Cofilin activity downstream of Pak1 regulates cell protrusion efficiency by organizing lamellipodium and lamella actin networks. *Dev. Cell* **13**, 646-662 (2007).
81. Sidani, M. *et al.* Cofilin determines the migration behavior and turning frequency of metastatic cancer cells. *J. Cell Biol.* **179**, 777-791 (2007).
82. Li, J., Hsu, H.C. & Mountz, J.D. Managing macrophages in rheumatoid arthritis by reform or removal. *Curr. Rheumatol. Rep.* **14**, 445-454 (2012).
83. Hamilton, J.A. & Tak, P.P. The dynamics of macrophage lineage populations in inflammatory and autoimmune diseases. *Arthritis Rheum.* **60**, 1210-1221 (2009).
84. Ooka, S. *et al.* Proteomic surveillance of autoantigens in patients with Behcet's disease by a proteomic approach. *Microbiol. Immunol.* **54**, 354-361 (2010).
85. Bussone, G. *et al.* Identification of new autoantibody specificities directed at proteins involved in the transforming growth factor beta pathway in patients with systemic sclerosis. *Arthrit. Res. Ther.* **13**, R74 (2011).
86. O' Gradaigh, D., Ireland, D., Bord, S. & Compston, J.E. Joint erosion in rheumatoid arthritis: interactions between tumour necrosis factor alpha, interleukin 1, and receptor activator of nuclear factor kappaB ligand (RANKL) regulate osteoclasts. *Ann. Rheum. Dis.* **63**, 354-359 (2004).
87. Hirayama, T., Danks, L., Sabokbar, A. & Athanasou, N.A. Osteoclast formation and activity in the pathogenesis of osteoporosis in rheumatoid arthritis. *Rheumatology (Oxford).* **41**, 1232-1239 (2002).

88. Schett, G. Cells of the synovium in rheumatoid arthritis. Osteoclasts. *Arthrit. Res. Ther.* **9**, 203 (2007).
89. Wynn, T.A., Chawla, A. & Pollard, J.W. Macrophage biology in development, homeostasis and disease. *Nature* **496**, 445-455 (2013).
90. Guiet, R. *et al.* The Process of Macrophage Migration Promotes Matrix Metalloproteinase-Independent Invasion by Tumor Cells. *J. Immunol.* **187**, 3806-3814 (2011).
91. Hasmann, M. & Schemainda, I. FK866, a Highly Specific Noncompetitive Inhibitor of Nicotinamide Phosphoribosyltransferase, Represents a Novel Mechanism for Induction of Tumor Cell Apoptosis. *Cancer Res.* **63**, 7436-7442 (2003).
92. Holen, K., Saltz, L., Hollywood, E., Burk, K. & Hanauske, A.-R. The pharmacokinetics, toxicities, and biologic effects of FK866, a nicotinamide adenine dinucleotide biosynthesis inhibitor. *Invest. New Drugs* **26**, 45-51 (2008).
93. Olesen, U.H., Thougaard, A.V., Jensen, P.B. & Sehested, M. A Preclinical Study on the Rescue of Normal Tissue by Nicotinic Acid in High-Dose Treatment with APO866, a Specific Nicotinamide Phosphoribosyltransferase Inhibitor. *Mol. Cancer Ther.* **9**, 1609-1617 (2010).
94. Busso, N. *et al.* Pharmacological Inhibition of Nicotinamide Phosphoribosyltransferase/Visfatin Enzymatic Activity Identifies a New Inflammatory Pathway Linked to NAD. *PLoS ONE* **3**, e2267 (2008).
95. Schilling, E. *et al.* Inhibition of nicotinamide phosphoribosyltransferase modifies LPS-induced inflammatory responses of human monocytes. *Innate Immun.* **0**, 1-13 (2011).
96. Van Gool, F. *et al.* Intracellular NAD levels regulate tumor necrosis factor protein synthesis in a sirtuin-dependent manner. *Nat. Med.* **15**, 206-210 (2009).

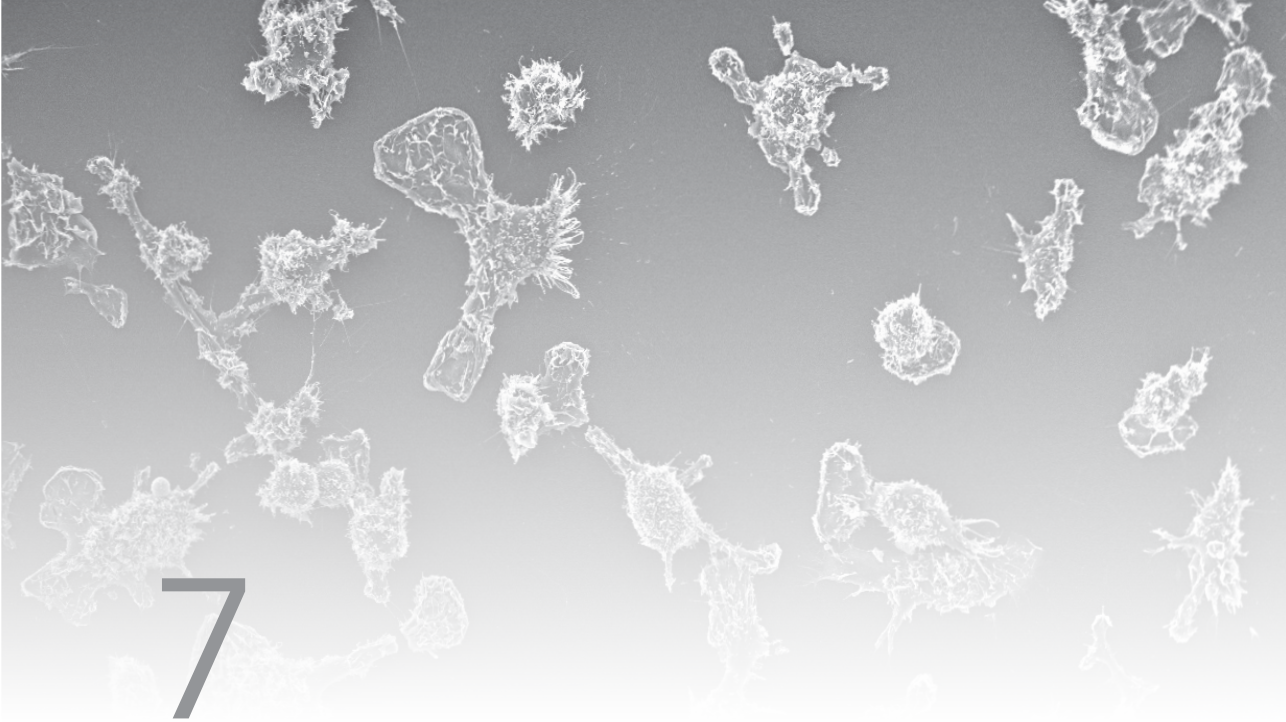

7

Summary

Samenvatting voor de leek (Nederlands)

Lekesamevatting (Afrikaans)

List of abbreviations

Publications

Dankwoord

Curriculum Vitae

Summary

Cell morphology and cell motility are two important characteristics of mammalian cells that contribute significantly to their functionality. The cortical actin cytoskeleton plays an important role herein. Through polymerization and modification of actin filaments, the cell produces protrusive membrane structures that are used to adhere to the extracellular matrix, migrate, probe the extracellular environment, take up fluid, and capture phagocytic targets. These processes are powered by the hydrolysis of significant quantities of ATP. In addition, the properties and functionality of the actin filaments as well as the proteins involved in regulating their assembly/disassembly are controlled by redox state, intracellular pH and, in part, by the physiological state of the cell. Therefore, a close relationship exists between cellular morphodynamics and cellular energy metabolism.

Cells of the immune system, especially macrophages, are morphological hyperactive cells. These cells are involved in the innate immune response against pathogens that enter the body, and in regulating tissue homeostasis by removing apoptotic cells and promoting wound healing. Macrophages continuously probe their environment for signs of infection or tissue damage. When they encounter danger signals, they are activated towards either an inflammatory (M1) or anti-inflammatory (M2) polarization state. Cells with these polarized phenotypes then undergo further different morphological alterations during an immune response. Interestingly, activated macrophages also undergo defined metabolic changes that are characteristic of the polarization phenotype they assume, whereby M1 macrophages undergo the most extensive alterations. Given the many links that exist between actin-based processes and metabolic effects, the question arises whether there is also a coupling between morphodynamic activity and the type and rate of energy-redox metabolism in activated macrophages. The research described in this thesis addresses this issue and provides new insights on the topic.

In the first experimental chapter (**chapter 2**) two mouse macrophage cell lines of different origin (RAW 264.7 and Maf-DKO) were compared with regard to their proliferation rate, morphology, phagocytosis capacity, and carbohydrate metabolism. In line with their tumor background, RAW 264.7 cells had a markedly higher proliferation rate than Maf-DKO cells. In contrast, Maf-DKO cells were morphodynamically more active. These cells formed far more actin-rich membrane ruffles and had a significantly higher phagocytic capacity compared to RAW 264.7 cells. In spite of vast differences in growth rate and morphodynamic activity, the two cell lines did not exhibit significant metabolic differences. Both RAW 264.7 and Maf-DKO cells largely depended on glycolysis while oxidative mitochondrial metabolism was minimal. Maf-DKO cells, therefore, share many similarities with both RAW

264.7 and primary macrophages and provide a suitable alternative model system for further study of the relationship between macrophage morphodynamics and metabolism.

Previous research has shown that the ATP that is required for actin polymerization at, and formation of, the phagocytic cup in macrophages is dependent on local CK-B-mediated ATP-generation from creatine phosphate and ADP. **In chapter 3**, we have demonstrated that CK-B is also physically present and involved in the formation of actin-rich membrane ruffles in macrophages. In addition, the mechanism of CK-B recruitment to the phagocytic cup in activated macrophages was investigated by comparing the translocation of different CK-B-mutants or –homologs with that of wild type CK-B by using live imaging microscopy. From these studies we identified a regulatory role for the C-terminal flexible loop of the CK-B molecule in its translocation to the phagocytic cup. Bioinformatics analysis revealed a number of residues in this region that are available for interaction with other molecules. Substitution of amino acid residues in this region (e.g. Asp326) probably influences the conformation of the loop or even the whole CK-B molecule so that interaction with other molecules is not optimal and CK-B cannot accumulate at specific sites with high actin-based dynamics anymore.

In **chapter 4** the importance of glucose for the morphodynamic alteration of LPS-stimulated macrophages was assessed. Inhibition of glucose metabolism resulted in reduced morphodynamic activity of macrophages (measured as spreading ability and phagocytosis capacity) while inhibition of mitochondrial oxidative phosphorylation did not negatively affect these processes. Interestingly, our results suggested that glucose may also play a non-metabolic role in regulating macrophage morphodynamics of LPS-stimulated macrophages, probably by modifying molecules in pathways that signal to the actin cytoskeleton.

Finally, in **chapter 5** we identified a role for another key compound of cellular energy and redox metabolism, NAD^+, in LPS-induced morphological change. Pharmacological inhibition of the major enzyme involved in NAD^+ salvage synthesis NAMPT (nicotinamide phosphoribosyltransferase) resulted in depletion of cellular NAD^+ levels in both RAW 264.7 and Maf-DKO cells. Under these conditions, cell morphology, spreading, and phagocytosis were significantly disturbed, while proliferation, cell viability and ATP homeostasis appeared unaffected. These findings suggest that NAD^+ also controls macrophage morphodynamics via an ATP-independent mechanism that probably involves the pH- and redox-mediated regulation of actin and actin associated proteins (e.g. cofilin).

In conclusion, the research described in this thesis provides new knowledge with regard to the coupling between macrophage metabolism and morphodynamic behavior and function. A better understanding of the cell biological mechanisms that

drive macrophage activities provides a broader foundation for the development of therapies for diseases in which these cells play a key role, such as cancer and autoimmune disease (e.g. rheumatoid arthritis).

Samenvatting voor de leek

Verandering in celmorfologie en celmotiliteit zijn twee belangrijke processen voor zoogdiercellen. Beide leveren een significante bijdrage tot hun functionaliteit. Het corticale actine cytoskelet speelt in deze dynamiek van vorm en beweging een uiterst belangrijke rol. Door de polymerisatie van monomere actine moleculen vormen zich filamenten die het celmembraan vooruit duwen wanneer ze onder het celoppervlak verlengd worden. Door van de actinefilamenten hele netwerken te vormen vormt de cel smalle uitlopers (filopodia genoemd) of membraanrimpels ('ruffles'). Ook kan het celfront over een groter oppervlak vooruit worden geduwd om een zogenaamde lamellipodium te vormen. De cel gebruikt deze structuren om de extracellulaire omgeving af te tasten of zich eraan vast te hechten, om vloeistof en voedingstoffen op te nemen, of om vooruit of achteruit te bewegen. De opbouw van het actine-netwerk in ieder van de hierbij betrokken membraanstructuren verschilt en wordt gereguleerd door honderden actine-bindende eiwitten (ABPs) en signaleringsmoleculen. De vorming, maar ook het modificeren, van actine filamenten vormt de basis van alle morfodynamische veranderingen van iedere cel. Gezamenlijk vereisen deze processen een aanzienlijke hoeveelheid van de totale chemische energie die een cel herbergt, in de vorm van ATP. Daarnaast worden de eigenschappen en functionaliteit van de actine filamenten zelf, en de daarbij werkzame ABPs, ook nog eens beïnvloed door de intracellulaire pH en de redox status van de cel. Alle drie deze factoren (ATP-productie, pH en redoxstatus) worden op hun beurt weer bepaald door de metabole staat van de cel. Er bestaan dus diverse nauwe banden tussen cellulaire morfodynamica en metabolisme.

Vele types cellen in zoogdieren, en dus ook in het menselijk lichaam, zijn morfologisch actief. Voor met name kankercellen en cellen van het immuunsysteem is morfodynamiek van uitzonderlijk groot belang. Macrofagen horen tot de groep leukocyten (witte bloedcellen) die de eerste lijn van verdediging vormen tegen pathogenen (bijv. bacteriën) die het lichaam binnendringen. Ook reguleren ze de weefselhomeostase door dode cellen te verwijderen en stimuleren ze weefselherstel. Macrofagen komen overal in het lichaam voor en zijn voortdurend bezig om hun omgeving te controleren op indringers of op voortekenen van weefselbeschadiging. Macrofagen bewegen zich daarbij voort door de weefsels, waarbij ze de actine-rijke membraanuitsteeksels gebruiken om veranderingen in de extracellulaire omgeving waar te nemen of om bacteriën en dode cellen te binden en op te nemen via fagocytose. Wanneer gevaarprikkels (bijv. bacteriële componenten zoals lipopolysaccharide (LPS) of signaaleiwitten, cytokines, zoals interleukine 4 (IL-4)) waargenomen worden, worden macrofagen daardoor geactiveerd om een andere status, met nieuwe kenmerken (een ander fenotype) aan te nemen. Het fenotype

dat een geactiveerde macrofaag aanneemt is afhankelijk van de soort prikkel die waargenomen wordt. Op die manier worden macrofagen bijvoorbeeld geactiveerd (of gepolariseerd) tot een M1- of inflammatoire staat door LPS-stimulatie, of tot een M2- of alternatieve (anti-inflammatoire en weefselherstellende) staat door IL-4-stimulatie. Behalve dat macrofagen in deze twee verschijningsvormen verschillende functies hebben tijdens de immuunrespons, ondergaan ze ook verschillende actine-afhankelijke morfologische veranderingen. LPS-gestimuleerde (M1-) cellen spreiden uit en vergroten hun celoppervlak, vormen filopodia en membraanrimpels en fagocyteren pathogenen. Tegelijkertijd vertonen ze een verlaagd migratievermogen, terwijl IL-4-gestimuleerde (M2-) cellen juist een verhoogde migratieactiviteit hebben, maar pathogenen minder goed kunnen fagocyteren.

Opvallend genoeg, ondergaan geactiveerde macrofagen daarbij ook metabole veranderingen die kenmerkend zijn voor het betrokken fenotype. M1-macrofagen die de meest opvallende morfodynamische veranderingen ondergaan, vertonen ook de meest ingrijpende metabolische aanpassingen. Deze kenmerken zich door een verhoogde glucose-opname en -verbruik, een verhoogde flux door het pad van de zogenaamde pentosefosfaat omzettingen en ook een verhoogde nicotinamide adenine dinucleotide (NAD^+-) synthese. Wetende dat actine polymerisatie gedrag beïnvloed wordt door het celmetabolisme, kunnen we dus de vraag stellen of of er een ook een vergelijkbaar verband bestaat tussen de morfodynamische en de metabole veranderingen die plaatsvinden in geactiveerde macrofagen. Het onderzoek dat beschreven is in dit proefschrift levert nieuwe inzichten m.b.t. het beantwoorden van deze vraag.

Voor het bestuderen van macrofagen *in vitro*, kunnen deze cellen geïsoleerd worden uit bloed en gekweekt worden in het laboratorium. Echter, macrofagen die op deze manier verkregen zijn, kunnen niet onbeperkt groeien en vermeerderen en moeten dus na verloop van tijd opnieuw geïsoleerd worden. Het gebruik van geïmortaliseerde macrofaag cellijnen voorkomt dit probleem en biedt dus een goed alternatief. Dit levert weer een ander probleem op. Geïmortaliseerde cellijnen zijn namelijk vaak afgeleid van tumorcellen en bezitten daarom een zodanig gemodificeerd genoom dat ze in vele opzichten niet meer dezelfde eigenschappen hebben als primaire cellen. Het onderzoek dat in dit proefschrift beschreven is, is vooral gedaan op de RAW 264.7 macrofaagcellijn. Aangezien deze cellijn afkomstig is van een Abelson leukemie virus-geïnduceerde ascites tumor van een muis en dus een kankerachtige oorsprong heeft, heb ik in **hoofdstuk 2** een vergelijk gemaakt tussen de RAW 264.7 cellijn en een nieuwe macrofaagcellijn waarvan aangetoond is dat het geen tumorigene eigenschappen heeft. Deze nieuwe cellijn, Maf-DKO genoemd, is afkomstig van muizen met een *MafB/c-Maf* -deficient

hematopoïetische (bloed) systeem. Door de genetische *MafB/c-Maf*-deficientie kunnen deze macrofagen *in vitro* onbeperkt vermeerderen in aanwezigheid van M-CSF (macrofaag colonie-stimulerende factor). Dit in tegenstelling tot normale primaire macrofagen die dit niet kunnen. In de vergelijkende studie is gekeken naar het groeitempo, het koolhydraat metabolisme, en morfodynamische karakteristieken. In overeenstemming met hun tumor oorsprong hadden RAW 264.7 cellen een veel hogere groeitempo dan Maf-DKO cellen. Daarentegen, hadden Maf-DKO cellen veel meer actine-rijke membraanruffels en een veel grotere fagocytosecapaciteit dan RAW 264.7 cellen. Ondanks deze verschillen vertoonden de twee cellijnen echter opmerkelijk genoeg geen significante matabole verschillen. Het glucoseverbruik was hoog en het mitochondriële zuurstofverbruik was minimaal in beide cellijnen. Hieruit concludeerden we dat de metabole uitgangskarakteristieken voor RAW 264.7 en Maf-DKO cellen vergelijkbaar zijn. Dit maakt allebei de macrofaag cellijnen geschikt voor verder onderzoek naar de verbanden tussen morfodynamiek en metabolisme.

ATP (energie)-productie vindt overal in de cel plaats, maar actine-rijke membraanuitsteeksels worden alleen op de buitenrand van de cel gevormd. De energie die benodigd is voor actinepolymerisatie onder en aan (de binnenkant van) het celoppervlak moet dus op de een of ander manier hier terechtkomen. Hiervoor beschikt de cel over een speciaal ATP-productie en -transportsysteem genaamd het creatine kinase-creatinefosfaat (CK-PCr) fosfageensysteem. Voorafgaand onderzoek op ons laboratorium had al aangetoond dat een specifieke CK-isoform (brein-type CK; CK-B) betrokken is bij de nieuwvorming van fagosomen, de actine-rijke structuren waarmee macrofagen soortvreemde partikels binden en opslokken. In **hoofdstuk 3** hebben we aangetoond dat CK-B ook een rol speelt in de vorming van actinerijke membraanruffles en andere uitsteeksels op het membraanoppervlak van macrofagen. Tijdens fagocytose worden een deel van de in de cel aanwezige CK-B eiwitmoleculen gerecruteerd en tijdelijk fysiek gebonden nabij de plaats op de celmembraan waar partikels (in deze geval serum-geopsoniseerde dode gistcellen) zich hechten en waar ze uiteindelijk met membraan worden omhuld en opgenomen worden. Door deze plaats- en tijdgebonden ophoping van aktief CK-B enzyme ontstaat een plaatselijk grote capaciteit voor levering van ATP aan de actine polymerisatie-machinerie. Echter, over hoe CK-B gemobiliseerd wordt en plaatselijk ophoopt onder het membraan is vrijwel niets bekend. In hoofdstuk 3 hebben we ook het mechanisme hierachter verder onderzocht in geactiveerde macrofagen. Hiervoor hebben we de re-localisatie van verschillende CK-B-mutanten of –homologen tijdens fagocytose bestudeerd en vergeleken met het gedrag van wild type (normaal) CK-B enzyme met behulp van merking van de eiwitten met een fluorescente groep en het volgen van deze eiwitten m.b.v. video-

fluorescentiemicroscopie. Hiermee konden we aantonen dat een specifiek domein van het CK-B-molecuul, namelijk de zogenaamde C-terminale buigzame lus, essentieel is voor de migratie naar het fagosoom. Deze lus bevat het aminozuur asparaginezuur op eiwitpositie 326. Wanneer dit aminozuur vervangen wordt door alanine, wordt het CK-B niet meer verplaatst naar de plek op celoppervlak waar zich een fagosoom vormt. Analyse m.b.v. een bioinformatieve aanpak heeft verder aangetoond dat diverse residuen in deze C-terminale lus beschikbaar zijn voor interactie met andere moleculen. Waarschijnlijk beïnvloedt aminozuur substitutie van Asp326 de ruimtelijke oriëntatie van de lus of zelfs van het hele CK-B molecuul. Interactie met andere structuren of moleculen in de celregio nabij het fagosoom is daardoor niet meer optimaal, waardoor het voor CK-B moeilijk wordt op deze specifieke plekken te accumuleren.

In **hoofdstuk 4** is een ander aspect van metabolisme onderzocht. Hierbij heb ik het belang van glucose voor morfodynamische veranderingen van LPS-gestimuleerde macrofagen onderzocht. Remming van het glucose metabolisme met behulp van 2-deoxy-D-glucose (2-DG) leidde tot een afgenomen LPS-geïnduceerde spreiding alsook tot een verlaging van de fagocytosecapaciteit van RAW 264.7 cellen. De globale morfologie van de cel was daarbij echter niet merkbaar aangetast. De glucose-afhankelijkheid van LPS-gestimuleerde morfodynamische processen in macrofagen werd verder bevestigd door glucose in het incubatiemedium te vervangen door galactose. Onder deze omstandigheid was het effect op spreiding en fagocytose veel groter (beide processen werden geremd!) en was ook de celmorfologie zichtbaar aangetast, overigens zonder dat het cellulaire ATP-niveau merkbaar veranderde. Interessant is dat de remmende effecten tegengegaan konden worden door een lage concentratie glucose toe te voegen aan het medium. Deze bevindingen suggereren dat glucose ook een niet-metabole rol speelt in de regulering van morfodynamische veranderingen in LPS-gestimuleerde macrofagen. Een mogelijke verklaring kan zijn dat eiwitten die betrokken zijn bij signaaloverdracht naar het actine cytoskelet o.i.v. aanwezigheid van glucose gemodificeerd kunnen worden en dat hierdoor de dynamiek van de actine-gebaseerde processen anders verloopt.

In **hoofdstuk 5** is het belang van NAD^+, naast ATP de belangrijkste metabole co-factor in de regulatie van de cellulaire energie- en redoxhuishouding, in actine-afhankelijke morfodynamische processen bestudeerd. Door het sleutelenzyme in de NAD^+-herwinningsynthese (NAMPT; nicotinamide phosphoribosyltransferase) te remmen met de drug FK866 werden de cellulaire niveau's van NAD^+ omlaag gebracht in RAW 264.7 en Maf-DKO cellen en werden de effecten hiervan voor en na LPS activering geanalyseerd. Alhoewel de cellulaire NAD^+ niveaus na remming van NAMPT nagenoeg uitgeput was en de niveau's van NADH en NADPH eveneens sterk

gereduceerd waren, was de proliferatie en ATP-productie in kortbehandelde cellen niet aangetast. Andere eigenschappen, waaronder de celmorfologie, het vermogen tot spreiding, en de fagocytosecapaciteit waren echter wel significant veranderd. Wij concluderen uit deze bevindingen dat dat NAD^+ de cellulaire morfodynamica beinvloedt via een ATP-onafhankelijk mechanisme. Op theoretische gronden achten we het waarschijnlijk dat dit gaat via effecten van NAD^+ op de pH- en redox-gestuurde veranderingen die kunnen optreden in actine en in vele daarmee geassocieerde ABPs (bijvoorbeeld cofilin).

Samenvattend, concludeer ik dat morfodynamische veranderingen van LPS-gestimuleerde macrofagen in sterke mate worden gedreven door ATP dat gevormd wordt tijdens de glucose-afbraak in de glycolyse. Het gebruik van deze ATP moleculen wordt lokaal gestimuleerd door ze te produceren via de katalytische werking van CK-B enzymemoleculen die lokaal accumuleren. Bij deze accumulatie is zeer waarschijnlijk modificatie en regulatie van de C-terminale buigzame lus in het CK-B eiwit betrokken. Glucose blijkt echter ook een niet-metabole rol te spelen in het reguleren van morfodynamica door bijvoorbeeld signaalmoleculen te modificeren. Ten slotte is NAD^+, de belangrijkste co-factor in glucose metabolisme en regelfactor van cellulaire pH en redoxstatus, van uiterst groot belang voor de hier bestudeerde morfofunctionele processen in LPS-geactiveerde macrofagen. De in dit proefschrift beschreven nieuwe kennis levert verbeterd inzicht op inzake de koppeling tussen macrofaag metabolisme en morfodynamische functie(s). Een beter begrip van de werking van macrofagen – en de beïnvloeding daarvan door metabole veranderingen – geeft ons naar verwachting een betere uitgangspositie voor het ontwikkelen van therapiën voor ziektes waarbij deze macrofagen een sleutelrol spelen, zoals kanker en auto-immuunziekten zoals reumatoïde artritis.

Lekesamevatting

Selmorfologie en -beweeglikheid is twee belangrike eienskappe van soogdierselle en lewer 'n betekenisvolle bydrae tot hul funksionaliteit. Die kortikale aktien sitoskelet speel hierin 'n belangrike rol. Deur die polimerisasie van monomere aktienmolekules word 'n netwerk van aktienfilamente gevorm wat die selmembraan laat uitstulp soos wat die filamente verleng word. Op hierdie manier vorm die sel uitlopers (ook genoem filopodia) en membraanplooie op die oppervlak, of word die selfront uitgestoot om 'n sogenaamde lamellipodium te vorm. Die sel gebruik hierdie strukture om die ekstrasellulêre omgewing af te tas of daaraan vas te heg, vloeistowwe en voedingstowwe op te neem en voort te beweeg. Die organisasie van die aktiennetwerk in elkeen van hierdie stuwende membraanstrukture verskil en word gereguleer deur honderde aktien-bindende proteïene (ABP'e) en seinoordragsmolekules. Die vorming, maar ook die modifisering, van aktienfilamente vorm die basis van alle morfodinamiese veranderinge wat in selle plaasvind en vereis 'n aansienlike hoeveelheid energie in die vorm van ATP. Daarnaas word die eienskappe en funksionaliteit van die aktienfilamente asook die ABP'e beïnvloed deur die intrasellulêre pH en die redoksstatus van die sel. Al drie hierdie faktore (ATP-produksie, pH en redoksstatus) word bepaal deur die metaboliese status van die sel en daarom bestaan daar 'n noue verband tussen sellulêre morfodinamika en metabolisme.

Alhoewel baie seltipes morfologies aktief is, is die aktiwiteit van kankerselle en selle van die immunsisteem van uitsonderlike belang. Makrofage is tipe leukosiete (witbloedselle) wat 'n eerste linie van verdediging vorm teen patogene (bv. bakterieë) wat die liggaam binnedring en weefselhomeostase reguleer deur dooie selle te verwyder en weefselherstel te bevorder. Hierdie selle kom oral in die liggaam voor en is voordurend besig om die ekstrasellulêre omgewing te observeer vir indringers of vir tekens van weefselbeskadiging. Om dit te doen, kan makrofage in die weefsel voortbeweeg en aktien-ryke membraanuitstulpings vorm om veranderinge in die ekstrasellulêre omgewing waar te neem en bakterieë of dooie selle op te neem d.m.v. fagositose. Wanneer gevaarprikkels (bv. bakteriële komponente soos lipopolisakkariede (LPS) of sitkiene soos interleukiene 4 (IL-4)) waargeneem word, word makarofage daardeur geaktiveer om 'n sekere kenmerkende status (fenotipe) aan te neem. Die fenotipe wat 'n geaktiveerde makrofaag aanneem, is afhanklik van die prikkel wat waargeneem word. So word makrofage byvoorbeeld geaktiveer (of gepolariseer) tot 'n M1- of inflammatoriese status deur LPS-stimulasie, en tot 'n M2- of alternatiewe (anti-inflammatoriese en weefselherstellende) status deur IL-4-stimulasie. Behalwe dat hierdie twee fenotipes verskillende funksies het tydens die immuunrespons, ondergaan die selle ook verskillende aktien-afhanklike

morfologiese veranderinge. LPS-gestimuleerde (M1-) selle sprei uit en vergroot hul seloppervlak, vorm filopodia en membraanplooie, fagositeer patogene, maar vertoon verlaagde voortbeweging, terwyl IL-4-gestimuleerde (M2-) selle beter voortbeweeg maar patogene minder goed fagositeer.

Opvallend genoeg ondergaan geaktiveerde makrofage ook gedefinieerde metaboliese veranderinge wat kenmerkend is van die betrokke fenotipe. M1-makrofage, wat die mees opvallende morfodinamiese veranderinge ondergaan, vertoon ook die mees treffende metaboliese aanpassings. Hierdie aanpassings sluit in verhoogde glukose-opname en -verbruik, verhoogde fluks deur die pentosefosfaatweg en verhoogde nikotienamied adeniendinukleotied (NAD^+)-sintese. As in ag geneem word dat aktienpolimerisasie en -modifikasie beïnvloed word deur selmetabolisme, ontstaan die vraag dus of daar 'n verband is tussen die morfodinamiese en die metaboliese veranderinge wat plaasvind in geaktiveerde makrofage. Die ondersoek wat in hierdie proefskrif beskryf is, bied nuwe insigte in die beantwoording van hierdie vraag.

Vir die bestudering van makrofage *in vitro* kan hierdie selle geïsoleer word uit bloed en gekweek word in die laboratorium. Makrofage wat op hierdie manier verkry is, kan egter nie onbeperk groei en vermeerder nie en moet dus na verloop van tyd opnuut geïsoleer word. Die gebruik van geïmortaliseerde makrofaagsellyne oorkom hierdie probleem en bied dus 'n goeie alternatief. Alhoewel, sellyne is dikwels afgelei van geïsoleerde tumorselle en daarom geneties so gemodifiseer dat dit in vele opsigte nie altyd meer dieselfde eienskappe vertoon as primêre selle nie. Die ondersoek wat in hierdie proefskrif beskryf is, is gedoen op die RAW 264.7-makrofaagsellyn. Aangesien hierdie sellyn afkomstig is van 'n Abelson leukemie virus-geïnduseerde askitestumor van 'n muis en dus 'n kankeragtige oorsprong het, is dit in **hoofstuk 2** vergelyk met 'n nuwe makrofaagsellyn waarvan aangetoon is dat dit nie kankeragtige eienskappe besit nie. Hierdie nuwe sellyn (Maf-DKO) is afkomstig van muise met 'n *MafB/c-Maf*-gebrekkige hematopoïetiese (bloed) sisteem. Deur die *MafB/c-Maf*-gebrek kan hierdie makrofage *in vitro* onbeperk vermeerder in die teenwoordigheid van M-CSF (makrofaag kolonie-stimulerende faktor) in teenstelling met normale primêre makrofage. In die vergelykende studie is gekyk na groeitempo, morfologie, fagositose kapasiteit, en koolhidraatmetabolisme. In ooreenstemming met hul kankeragtige oorsprong, het RAW 264.7-selle 'n veel hoër groeitempo gehad as Maf-DKO-selle. Daarenteen het Maf-DKO-selle veel meer aktien-ryke membraanplooie gevorm en 'n veel groter fagositose kapasiteit gehad as RAW 264.7-selle. Ten spyte van hierdie verskille het die twee sellyne geen betekenisvolle metaboliese verskille getoon nie. Glukoseverbruik was hoog, maar mitochondriale suurstofverbruik was minimaal in albei sellyne. Hieruit lei ons af dat die basiese metaboliese

kenmerke van RAW 264.7- en Maf-DKO-selle vergelykbaar is. Dit maak albei hierdie makrofaagsellyne geskik vir verdere ondersoek na die verband tussen morfodinamiek en metabolisme.

ATP (energie)-produksie vind verspreid deur die hele sel plaas, maar vorming van aktien-ryke membraanuitstulpings vind slegs op die buiterand van die sel plaas. Die energie wat benodig word vir aktienpolimerisasie onder die selmembraan moet dus op die een of ander manier hier teregkom. Hiervoor beskik die sel oor 'n spesiale ATP-transportsisteem genaamd die kreatienkinase-kreatienfosfaat (CK-PCr) fosfageensisteem. Voorafgaande ondersoek in ons laboratorium het al aangetoon dat 'n sekere CK-isoform (brein-tipe CK; CK-B) betrokke is by die vorming van die aktien-ryke fagositiese kelk in makrofage. In **hoofstuk 3** het ons aangetoon dat CK-B ook 'n rol speel in die vorming van aktien-ryke membraanplooie in makrofage. Tydens fagositose word CK-B fisies aangetrek na die plek op die selmembraan waar die teiken (in hierdie geval serum-geopsoniseerde gisdeeltjies) vasheg en opgeneem word. CK-B versamel onder die membraan en kan dus hier ATP lewer aan die aktienpolimerisasie-masjinerie. Hoe CK-B egter hier teregkom, is onbekend. Dus het ons verder in hoofstuk 3 ook die meganisme hieragter ondersoek in geaktiveerde makrofage deur die lokalisering van verskillende CK-B-mutante of -homoloë tydens fagositose te vergelyk met wilde tipe (normale) CK-B m.b.v. video-fluorisensiemikroskopie. Hieruit kon ons aantoon dat 'n spesifieke area in die CK-B-molekule essensieel is vir die verplasing daarvan na die fagositiese kelk, naamlik die C-terminale buigsame lus. Hierdie lus bevat die aminosuur aspartiensuur op posisie 326 en wanneer hierdie aminosuur vervang word met alanien, kan CK-B nie meer verplaas word na die fagositiese kelk nie. Bio-informatika-analise het aangetoon dat verskeie residu's in hierdie C-terminale lus beskikbaar is vir interaksie met ander molekules. Waarskynlik beïnvloed aminosuursubstitusie van Asp326 die ruimtelike oriëntasie van die lus of selfs van die hele CK-B-molekule, sodat interaksie met ander molekules nie meer optimaal is nie en CK-B dus nie meer op 'n spesifieke plek kan versamel nie.

In **hoofstuk 4** is die belang van glukose vir morfodinamiese veranderinge van LPS-gestimuleerde makrofage ondersoek. Inhibering van glukosemetabolisme m.b.v. 2-deoksi-D-glukose (2-DG) het gelei tot 'n beperkte LPS-geïnduseerde spreidingsvermoë asook 'n verlaagde fagositosekapasiteit van RAW 264.7-selle, alhoewel selmorfologie nie merkbaar geaffekteer was nie. Die glukose-afhanklikheid van LPS-gestimuleerde morfodinamiese prosesse in makrofage is bevestig deur glukose in die inkubasiemedium te vervang met galaktose. Onder hierdie kondisie was die remmende effek op spreiding en fagositose veel groter en was ook die selmorfologie geaffekteer, sonder dat sellulêre ATP-vlakke verander het. Interessant genoeg kon die remmingseffek omgekeer word deur 'n lae konsentrasie glukose

toe te voeg aan die medium. Hierdie bevindinge suggereer dat glukose ’n nie-metaboliese rol speel in die regulering van morfodinamiese veranderinge in LPS-gestimuleerde makrofage. ’n Moontlike verklaring kan wees dat molekules wat betrokke is in seinoordrag na die aktiensitoskelet deur glukose gemodifiseer word en dat die dinamiek van die aktine-gebaseerde prosesse hierdeur anders verloop.

In **hoofstuk 5** is die belang van NAD^+ (naas ATP die belangrikste metaboliese ko-faktor in die regulering van sellulêre energie- en redokshuishouding) in aktien-afhanklike morfodinamiese prosesse bestudeer in LPS-geaktiveerde makrofage. Deur die sleutelensiem in NAD^+-herwinningsintese (NAMPT; nikotienamied-fosforibosieltransferase) te inhibeer, kon die sellulêre vlakke van NAD^+ omlaag gebring word in RAW 264.7- en Maf-DKO-selle. Alhoewel NAD^+ nagenoeg uitgeput was en die vlakke van NADH en NADPH ook gereduseer was, was selgroei en ATP-produksie nie geaffekteer nie. Selmorfologie, spreiding, sowel as fagositose was egter wel opmerklik aangetas. Hieruit kan afgelei word dat NAD^+ sellulêre morfodinamika reguleer deur ’n ATP-onafhanklike meganisme. Waarskynlik behels hierdie meganisme die pH- en redoksbemiddelde regulering van aktien en ander ABP’e (byvoorbeeld cofilin).

Om op te som, morfodinamiese veranderinge van LPS-gestimuleerde makrofage word aangedryf deur ATP hoofsaaklik afkomstig van glukose-afbraak deur glikolise. Hierdie ATP word lokaal besorg deur CK-B wat hier versamel d.m.v. die C-terminale buigsame lus. Glukose blyk egter ook ’n nie-metaboliese rol te speel in die regulering van morfodinamika deur byvoorbeeld seinmolekules te modifiseer. Ten slotte is NAD^+, ko-faktor in glukosemetabolisme en reguleerder van sellulêre pH en redoksstatus, van kardinale belang vir morfofunksionele prosesse in LPS-gestimuleerde makrofage. Die ondersoek wat in hierdie proefskrif beskryf is, lewer nuwe kennis aangaande die koppeling tussen makrofaagmetabolisme en morfodinamiese funksie. ’n Beter begrip van die werking van makrofage verskaf ’n breër fondament vir die ontwikkeling van terapieë vir siektetoestande waarby hierdie selle ’n sleutelrol speel, bv. kanker en outo-immuunsiektes soos rumatoïede artritis.

List of abbreviations

2-DG	2-deoxy-D-glucose
ABP	Actin binding protein
ACMS	α-amino-β-carboxy-muconate-ε-semi-aldehyde
ADP	Adenosine diphosphate
AMP	Adenosine mono-phosphate
AMPK	AMP-activated protein kinase
ANT	Adenine nucleotide translocator
Arp2/3	Actin related protein 2/3
ATGL	Adipose triglyceride lipase
ATP	Adenosine triphosphate
BCG	Bacillus Calmette–Guerin
CARKL	Carbohydrate kinase-like protein
CD38	Cluster of differentiation 38
Cdc42	Cell division control protein 42 homolog
CFU-GM	Granulocyte/macrophage colony-forming units
CK	Creatine kinase
CK-B	Brain-type creatine kinase
CM	Conditioned medium
COZ	Complement opsonized zymosan
Cr	Creatine
CR3	Complement receptor 3
CSF-1	*See M-CSF*
CxCL2	Chemokine (C-X-C motif) ligand 2
DAD	Dia autoinhibitory domain
DMEM	Dulbecco's modified Eagle's medium
DTT	Dithiothreitol
ECM	Extracellular matrix
ETC	Electron transport chain
F6P	Fructose-6-phosphate
FA	Fatty acid
F-actin	Filamentous actin
FBS	Fetal bovine serum
FCCP	carbonyl cyanide-*p*-trifluoro-methoxyphenyl-hydrazone
FcγR	Fcγ-receptor
FH-1/2	Formin homology ½
FITC	Fluorescein isothiocyanate
FOXO	Forkhead box
G3P	Glyceraldehyde-3-phosphate
G6P	Glucose-6-phosphate
GAA	Guanidinoacetate
G-actin	Globular actin
GBD	GTPase binding domain
GLUT	Glucose transporter
GSH	Glutathione
GSSG	Reduced glutathione
HIF	Hypoxia-inducible factor
HSC	Haematopoietic stem cell
HXK	Hexokinase
IDO	Indolamine 2,3-dioxygenase
IFN-γ	Interferon gamma
IgG	Immunoglobulin G
IL-1/4/6/10/13	Interleukin-1/4/6/10/13
iNOS	Inducible nitric oxide synthase
ITAM	Ig gene family tyrosine activation motive
KLF4	Krüppel-like factor 4
LDH	Lactate dehydrogenase
LDH	Lactate dehydrogenase
LDL	Low density lipoprotein
LPL	Lipoprotein lipase
LPS	Lipopolysaccharide
Mac-1	Macrophage-1 antigen (complement receptor 3)
M-CSF	Macrophage colony stimulating factor
MCT1	Monocarboxylate transporter 1
mDia	Mammalian Diaphanous-related formin

MPC	Mitochondrial pyruvate carrier
MPS	Mononuclear phagocyte system
Mrc-1	Macrophage mannose receptor 1
MtCK	Mitochondrial creatine kinase
MyD88	Myeloid differentiation factor 88
NA	Nicotinic acid
NAAN	Nicotinic acid adenine dinucleotide
NAD^+	Nicotinamide adenine dinucleotide
NADH	Reduced nicotinamide adenine dinucleotide
NADK	NAD kinase
$NADP^+$	Nicotinamide adenine dinucleotide phosphate
NADPH	Reduced nicotinamide adenine dinucleotide phosphate
NADS	NAD synthase
NAM	Nicotinamide
NAMN	Nicotinic acid mono-nucleotide
NAMPT	Nicotinamide phosphoribosyltransferase
NAPRT	Nicotinic acid phosphoribosyltransferase
NMN	Nicotinamide mono-nucleotide
NMNAT	NAM mononucleotide adenylyltransferase
NO	Nitric oxide
NOX	NADPH oxidase
NPF	Nucleation promoting factor
NR	Nicotinamide riboside
NRK	Nicotinamide riboside kinase
N-WASp	Neuronal isoform of WASp
OXPHOS	Oxidative phospho-rylation
PAMP	Pathogen-associated molecular pattern
PARP	Poly-ADP-ribose-polymerases
PBMC	Peripheral blood mononuclear cell
PBS	Phosphate-buffered saline
PBS-G	Phosphate-buffered saline and glycine
PBS-T	Phosphate-buffered saline and Tween
PCr	Phosphocreatine
PDGF	Platelet derived growth factor
PFK2	Phosphofructokinase 2
pHi	Intracellular pH
P_i	Inorganic phosphate
PP_i	Pyrophosphate
PI3K	Phosphoinositide 3-kinase
PIP_2	Phosphatidylinositol 4,5-biphosphate
PIP_3	Phosphatidylinositol 3,4,5-triphosphate
PKM	Pyruvate kinase (muscle isozyme)
PMA	Phorbol 12-myristate 13-acetate
PPAR	Peroxisome proliferator-activated receptor
PPP	Pentose phosphate pathway
PRR	Pattern recognition receptor
PtdIns(3,4,5)P_3	Phosphatidylinositol 3,4,5-triphosphate
PtdIns(4,5)P_2	Phosphatidylinositol 4,5-biphosphate
QPRT	Quinolinate phosphoribosyltransferase
R5P	Ribose-5-phosphate
RA	Rheumatoid arthritis
ROS	Reactive oxygen species
Ru5P	Ribulose-5-phosphate
S7P	Sedoheptulose-7-phosphate
Scar/WAVE	Suppressor of cAMP

	receptor /WASp family verprolin homolgous
SDS	Sodium dodecyl sulphate
SDS-PAGE	SDS-polyacrylamide gel electrophoresis
SEM	Scanning electron microscopy
SGLT	Na^+-dependent glucose co-transporters
SRB	Sulforhodamine B
SSH-1L	Slingshot-1L
STAT6	Signal transducer and activator of transcription 6
TAMs	Tumor associated macrophages
TBS-T	Tris-buffered saline and Tween
TCA	Tricarboxylic acid
TCA	Trichloroacetic acid
TDO	Tryptophan 2,3-dioxygenase
TEPM	Thioglycollate elicited peritoneal macrophages
TG	Triglyceride/ Triacylglycerol
TGFβ1	Transforming growth factor β1
TGL	Triglyceride lipase
TLR	Toll-like receptor
TNF	Tumor necrosis factor
Tris	Tris(hydroxymethyl)-aminomethane
TSAC	Transition state analog complex
UDP-GlcNAc	Uridine diphosphate N-acetyl-glucosamine
VDAC	Voltage-dependent ion channel
WASp	Wiskott-Aldrich syn-drome protein
WAVE	WASp family verprolin homolgous
WIP	WASp interacting protein

Publications

Venter, G., Oerlemans, F. T. J. J., Wijers, M., Willemse, M., Fransen, J. A. M., and Wieringa, B. (2014) Glucose Controls Morphodynamics of LPS-Stimulated Macrophages. *PLoS ONE* **9**, e96786

Venter, G., Oerlemans, F. T. J. J., Willemse, M., Wijers, M., Fransen, J. A. M., and Wieringa, B. (2014) NAMPT-Mediated Salvage Synthesis of NAD^+ Controls Morphofunctional Changes of Macrophages. *PLoS ONE* **9**, e97378

Dankwoord

Wie had dat nou gedacht? Er kwam toen toch nog een proefschrift uitrollen!! Maar ja, dat kwam niet zomaar - daar moest wel héél veel voor gebeuren! Zo veel, dat ik het in mijn eentje écht niet zou hebben gered. Om zover te komen, heb ik de hulp en ondersteuning van zoveel mensen gehad. Aan jullie wijd ik dit laatste subhoofdstuk van mijn proefschrift. God bracht jullie, met en zonder jullie medeweten, op mijn pad en daar ben ik ontzettend dankbaar voor! Lang heb ik er naar uitgekeken om dit stukje te gaan schrijven, maar nu het zover is vind ik het toch lastig, want het is voor een groot deel ook mijn afscheidsrede en na zes en een half jaar vind ik het nog steeds moeilijk om mijn emoties in het Nederlands uit te drukken!

Ruim negen jaar geleden, in mei 2005 toen ik nog bezig was met mijn Masteropleiding, begon ik er al van te dromen mijn promotieonderzoek in Nederland te gaan doen en heb ik voor het eerst contact opgenomen met Bé. In de twaalf maanden erna werden veel e-mails heen en weer gestuurd en probeerde ik een PhD-scholarship te krijgen voor een promotiestudie in het buitenland. Omdat dat helaas niet lukte, ben ik in 2006 toch maar begonnen als PhD op het lab waar ik was afgestudeerd. En toen, een jaar later, kreeg ik ineens een e-mail van Bé waarin hij me uitnodigde te solliciteren voor een aio-functie bij de afdeling Celbiologie...! Na nog een paar e-mails en een bezoek aan het lab, hebben we de knoop doorgehakt en ben ik eindelijk in januari 2008 begonnen als aio bij de afdeling Celbiologie. Bé en Jack, allereerst wil ik jullie bedanken voor de kans die jullie me gaven om mijn droom te verwezenlijken! Ten tweede wil ik jullie bedanken voor jullie inzet - zonder jullie harde werk was dit proefschrift nooit geworden wat het nu is! Alhoewel ik in totaal ruim zes jaar bezig was met mijn onderzoek, heb ik in de laatste twee jaar zeker het meest geleerd. Dit was de tijd waarin ik begon te schrijven, waarin de 'laatste' proeven gedaan moesten worden en dat we steeds vaker moesten overleggen. Soms zonk me de moed in de schoenen als ik een werkstuk van jullie terugkreeg en ik bij de eerste oogopslag alleen maar groen/rood/paars-gemarkeerde tekst zag! Maar als ik er eenmaal doorheen was viel het altijd mee en was ik zelf ook meer tevreden met het eindresultaat. Bé, de nuchtere manier waarop je alle soorten problemen benaderde zorgde ervoor dat de stressniveaus bij mij niet regelmatig de hoogte in schoten en dat ik perspectief behield. Bedankt voor jullie tijd, geduld en aanmoediging de afgelopen jaren!

Frank, mijn rechterhand, bedankt voor al de spreading assays die je gedaan hebt, de pilot-proeven die je hebt ingezet, en alle cellen die je voor me hebt doorgezet als ik er niet zelf kon zijn. Dankzij jou was ik ook niet de enige die op de kweek hardop met de radio zat mee te zingen! Fijn dat je ook nog mijn paranimf wil zijn! Marieke W, ook jij hebt een grote bijdrage geleverd aan de resultaten die in

dit proefschrift zijn opgenomen. Bedankt voor alle 'laatste proefjes' die je voor me deed! Nooit was het te veel moeite om 'even' een blotje te draaien, cellen te fixeren en te imagen, of zelfs te TIRFen! Van jou heb ik op het lab echt heel veel praktische dingen geleerd. Super dat ook jij mijn paranimf wil zijn! Mietske, als co-auteur van alle vier experimentele hoofdstukken wil ik jou bedanken voor alle SEM-plaatjes. Uren heb je achter de SEM doorgebracht om plaatjes te schieten van mijn celletjes, en zoals je kunt zien, kun je ze overal terugvinden in dit boekje – super bedankt!

Tijdens de eerste acht maanden van mijn onderzoek had ik ook nog een derde begeleider: Helma. Dankzij jou vond ik snel mijn weg op het lab, heb ik geleerd ieder experiment tot in de details te plannen en het protocol volledig uit te schrijven. Ook wil ik jou, Saskia en Hanka bedanken voor jullie grote bijdragen aan het CK-B- hoofdstuk. Hopelijk wordt dat nu ook snel geaccepteerd en gepubliceerd!

Huib en Jan, bij jullie kon ik terecht voor alle andere algemene lab-dingen die ik niet wist. Altijd waren jullie bereid me te helpen, dus ook aan jullie heel erg veel dank! Dan mijn kweek-buddies: Walther, Rinske, Anke, Anchel, Susan en Ingeborg, samen met jullie was het altijd gezellig op de kweek! Bedankt voor al de keren dat jullie tijdens een weekend mijn cellen doorzetten en 's middags laat of 's ochtends vroeg medium wilden verversen of LPS bij de cellen wilden doen, omdat ik er vanwege Stephan niet zelf kon zijn. Nogmaals: promoveren doe je niet alleen! Ook mijn U-genoten: Remco, Stefi, Claire en Michiel wil ik bedanken voor de gezellige sfeer op het lab, informatieve discussies en de praktische tips die ik van jullie kreeg. Hetzelfde geldt voor mijn mede-aio's: Lieke, Mirthe, Irene, Annika, Marieke dV, Monique, Samuel, Bettina, Olga, Pavel en Antoine. Het was fijn om af en toe frustraties te kunnen delen met andere 'lotgenoten' en tips te geven en te krijgen over allerlei praktische en logistieke kwesties! *Also Ganesh from upstairs, thanks for your help with the O_2 assays!* Behalve Bé en Jack zijn er ook drie andere 'belangrijke mensen' die ik wil bedanken: Rick, Wiljan en Ineke. Alhoewel jullie niet mijn directe begeleiders waren, heb ik van jullie ontzettend veel geleerd tijdens de literatuurpresentaties en werkbesprekingen en kon ik bij jullie ook terecht voor vragen en advies. Magda, onze lieve secretaresse, dank je wel voor je vriendelijkheid, de administratieve ondersteuning, dat je een paar keer oma wilde spelen voor Stephan en dat ik jouw koffiemok mocht 'lenen' voor 5 jaar...! Alle andere collega's: Mariska, Katarina, Linda, Cindy, Marina, Anna, Gert-Jan, Esther, Julia en de Moldiertjes, met elk van jullie had ik op een andere manier contact en dat was ook wel belangrijk om me helemaal thuis te voelen op de 6e verdieping. Dank daarvoor!

Ook buiten het lab had ik heel veel mensen die om me heen stonden en zonder wier hulp en ondersteuning promoveren niet mogelijk was. Allereerst, Stephans

lieve oppassers: Stynie, Arieke, Carin, Martine en Jan-Douwe, ik kan jullie niet genoeg bedanken voor de maanden die jullie vrijwillig (!) op Stephan hebben gepast zodat ik zorgeloos achter mijn computer kon gaan zitten schrijven! Zonder jullie had ik dit boekje nooit af kunnen maken! Johan Dirk, Bouwien en kinderen, van jullie hebben we de afgelopen jaren heel veel steun gekregen, praktisch en emotioneel. Bedankt voor jullie onbaatzuchtige liefde en alle gezellige sinterklaasavonden! Onze Bijbelkring, bedankt voor jullie belangstelling, medeleven en de geestelijke ondersteuning. Yvonne, jij in het bijzonder bedankt voor het schrijven van mijn CV en het nakijken van dit stuk! *Roema, vir jou wil ek dankie sê vir die aanmoediging wat ek van jou gekry het (via Skype) en van al die besoekies elke keer as jy vir jou eie PhD-navorsing na België toe moes gaan. Hopelik sal ons mekaar nou weer meer gereeld sien!*

Mijn lieve (Nederlandse) familie, Jan en Joke, Pieter en Gerda, Johan en Elly, jullie vingen me op toen ik naar Nederland kwam en werden hier mijn pleegouders! Ik ben jullie erg dankbaar voor alle liefde, telefoontjes en bezoekjes die ik (wij) van jullie kreeg (kregen). Het was soms lastig om uit te leggen waarom het maar niet opschoot met mijn studie, maar jullie bleven altijd geïnteresseerd en hadden altijd een bemoedigend woord. Ik zal jullie gaan missen!

Na zes en een half jaar is het tijd om terug te keren naar Zuid-Afrika, naar onze andere familie die we heel erg hebben gemist! *Al my boeties en sussies, julle wag al lank dat ons moet terugkom en sodat julle Stephan kan sien en hy met sy nefies en niggies kan speel. Uiteindelik is dit sovêr - dankie vir julle begrip, belangstelling en geduld! Evette, dankie vir jou harde werk om hierdie boekie so mooi te maak en ook vir al die kere wat jy kom kuier het en jou nefie vermaak het sodat ek kon werk!*

Pa Evert en Ma Elsie, dankie vir julle vertroue, liefde, gebede, aanmoediging en al die kuiers hier in Nederland! By julle kom ek altyd tuis en kan ek ontspan en net myself wees. Ek is dankbaar vir alles wat ek by julle geleer het, maar veral dat ek in alles op God moet vertrou. My skoonouers, Pa Fanie en Ma Lorraine, dankie dat julle nie vir 'n oomblik in my getwyfel het nie en enduit in my bly glo het! Julle was vir my 'n groot bron van bemoediging!

Liewe Pieter, ek kom woorde kort as ek wil sê hoe ongelooflik lief ek vir jou is en hoe ontsettend dankbaar ek is dat die Here jou vir my gegee het as man! Jy het baie opgeoffer om saam met my Nederland toe te kom en my te help om my droom te verwesenlik. Elke keer as ek van frustrasie, moedeloosheid, of telleurstelling in trane was, het jy my weer gerusgestel, perspektief gegee en herinner dat niks buite God omgaan nie. Dankie vir al die vrolike toebroodjies, die (onverwagse) besoekies in die lab en al die ander klein bederfies waarmee jy my altyd weer opgebeur het! Ek is baie lief vir jou!

Gerda

Die mense wat ek lief het
Kom groei op my soos mos
Daar laat ek hul na hartelus gedy
En loop ek deur die wêreld
- beskut teen die koue -
Die snoesigheid self:
Ek met my moskombersie
En as daar 'n oorlog kom
Word die mense wat ek lief het
'n Ekstra liefdeslaag om my
So marsjeer ek deur die wêreld
Gepantser teen die vuur
Die onaantasbaarheid self:
Ek met my menskombersie
....

Stephan Bouwer

Curriculum Vitae

Gerda Venter is op 11 april 1982 geboren te Krugersdorp in Zuid-Afrika. Met haar ouders verhuisde zij naar Vereeniging, waar zij zowel de basis- als de middelbare school doorliep. In 2000 behaalde Gerda haar *Matrieksertifikaat* (diploma middelbare school) aan de Drie Riviere Hoërskool in Vereeniging. Van 2001 tot en met 2003 studeerde zij Biologische Wetenschappen aan de Potchefstroomse Universiteit vir Christelike Hoër Onderwys, nu de Noordwes Universiteit (NWU). Daar behaalde zij cum laude haar Bachelor of Science diploma. Aansluitend volgde zij een Bachelor of Science honours studie aan de afdeling Biochemie van de NWU, onder begeleiding van prof. Harry Kotzé en prof. Piet Pretorius. Zij liep hier ook stage en haalde haar diploma hier eveneens cum laude. Vervolgens begon Gerda aan haar Master opleiding en liep bij de afdeling Biochemie weer stage onder begeleiding van de eerder genoemde leraren. In 2006 behaalde zij haar Master of Science diploma. Tijdens haar Bachelor en Master opleiding maakte Gerda kennis met de wereld van de cellulaire energie en redox metabolisme en wist zij dat ze in deze richting verder wilde met een promotiestudie, het liefst in Nederland. Omdat dat niet meteen lukte is zij later in 2006 aan een promotiestudie begonnen op het Mitochondrieel Research Laboratorium van prof. Francois van der Westhuizen, opnieuw aan de afdeling Biochemie van de NWU. Daarnaast werkte zij tijdelijk als docent Biochemie en gaf college aan tweedejaars farmacie- en verpleegkundestudenten. In 2007 kreeg Gerda wél de gelegenheid om in Nederland als junioronderzoeker aan een promotieproject te beginnen. Nadat alle onderwijstaken in Zuid-Afrika waren afgerond startte zij in 2008 in Nijmegen met haar promotieonderzoek aan de afdeling Celbiologie van het Radboud UMC, onder begeleiding van prof. dr. Bé Wieringa en dr. Jack Fransen. De resultaten van dit onderzoek worden in dit proefschrift beschreven.